NEW TECHNIQUES AND MEASUREMENTS IN GROUND-BASED INFRA-RED ASTRONOMY

by

Paul Richard Jorden B.Sc., A.R.C.S.

A thesis submitted for the degree of Doctor of Philosophy of the

University of London and for the Diploma of Imperial College.

Astronomy Group,
Blackett Laboratory,
Imperial College,
London, S.W.7.

August, 1977

ABSTRACT

The research described in this thesis has been done in the Infra-red Astronomy Group of Imperial College; astronomical observations have been made on the 60-inch telescope in Tenerife. The first chapter contains a discussion of the infra-red photometry system that has been employed for this work. Chapter two describes the testing and operation of detectors and pre-amplifiers, for 1-10 μm measurements. The following chapter deals with the control instrumentation, particularly a new sample control and computer system, as used in Tenerife.

Chapter four describes a study of H II regions and some new results on two areas (Sharpless 54, G45.5 + 0.1) are presented. The last section of this thesis contains a description of a compact helium-cooled Fabry-Perot spectrometer. The design and construction, control and usage of the device are discussed. Some preliminary test results of this instrument are given as well as future plans for 10 μm spectroscopy.

Preface

This thesis is a description of some of my research since 1972 in the Infra-Red Astronomy Group. The two main themes have been a study of infra-red emission from H II regions and the development of a novel infra-red spectrometer. The work has inevitably included many other aspects of infra-red astronomy, particularly those with an instrumental bias. Electronics as related to detector pre-amplifiers, a photometry control system and computing are also discussed.

The work on H II regions was done in collaboration with Dr. P.A. Whitelock, with the aim of studying possible protostellar objects in the infra-red. At first this project was not very effective (due to detector problems) but results have been obtained for Sharpless 54 and G45.5 + 0.1 regions. These H II regions give good examples of the type of information that can be gained from infra-red studies; further work is planned in this field. The cooled spectrometer project has suffered from problems due to faulty cryostats and has not yet been fully developed to the stage initially anticipated. The additional demands of operation under cryogenic conditions have proved very time-consuming during the testing stages, although some very useful astronomy is anticipated after further work.

Primarily I should like to thank my supervisor, Dr. Mike Selby, for his guidance and encouragement. I am glad to acknowledge the friendship and help of other colleagues, particularly Patricia Whitelock and Andrew MacGregor. Thanks also to Professor Jim Ring, and to Richard Wade for useful discussions.

CONTENTS

List of Tables

List of Plates

List of Figures

CHAPTER 1

INTRODUCTION, THE PHOTOMETRY SYSTEM

Much of the work described in this thesis is related to the use of

the 60-inch telescope at Izaña in Tenerife. Some equipment has been built

and used successfully there and some new results are presented here. This

chapter gives some details of the telescope and describes the photometry

system used on it.

1.1. The 60-inch Tenerife Flux Collector

The telescope is situated at a height of about 2500 metres with a

position of : 28° $17'$ $32"$ latitude, 1^h 05^m 48.1^s longitude. The amount of

precipitable water vapour can be as low as 1 mm at this high, dry mountain

site. The maximum available zenith angle of about 67° corresponds to an

air mass of 2.6. The 60-inch diameter primary has a design focal ratio of

13.5 and the photometer used by the Imperial College group is built to

operate with it's detectors at the design focus in a Cassegrain configuration.

Figure 1.1 shows the optical system of the telescope.

The resulting plate scale of the telescope is $10"$ mm^{-1} and a focal

plane detector aperture of 1 mm diameter defines a $10"$ beam size on the

sky (if no field optics are used). The focal-plane Airy pattern at 10 μm

has a diameter of $3.3"$ between the first minima (where 84% of the energy

is collected). The mirror surface gives an optical image size of about $2"$

and so a total beam size of less than $5"$ is not useful. In practice, for

good photometry under most conditions, a $10"$ beam is used.

The "resolution limit" at 10 μm is $1.7"$ and work by P.A. Whitelock(1976)

has indicated that size estimates of this order are possible under good

conditions (with adequate signal to noise). In good conditions seeing of

$2"$ is obtained although $3-4"$ is more normal. Photometry can be done with

$5"$ seeing but its accuracy deteriorates rapidly if the seeing exceeds $5"$.

The 60 inch Tenerife Telescope

Primary Mirror

Black Annulus
(I/D = 15 inches)

Secondary Mirror

Instrument Flange

Cassegrain Focus

45   135 $22\frac{1}{4}$ $49\frac{3}{4}$

207
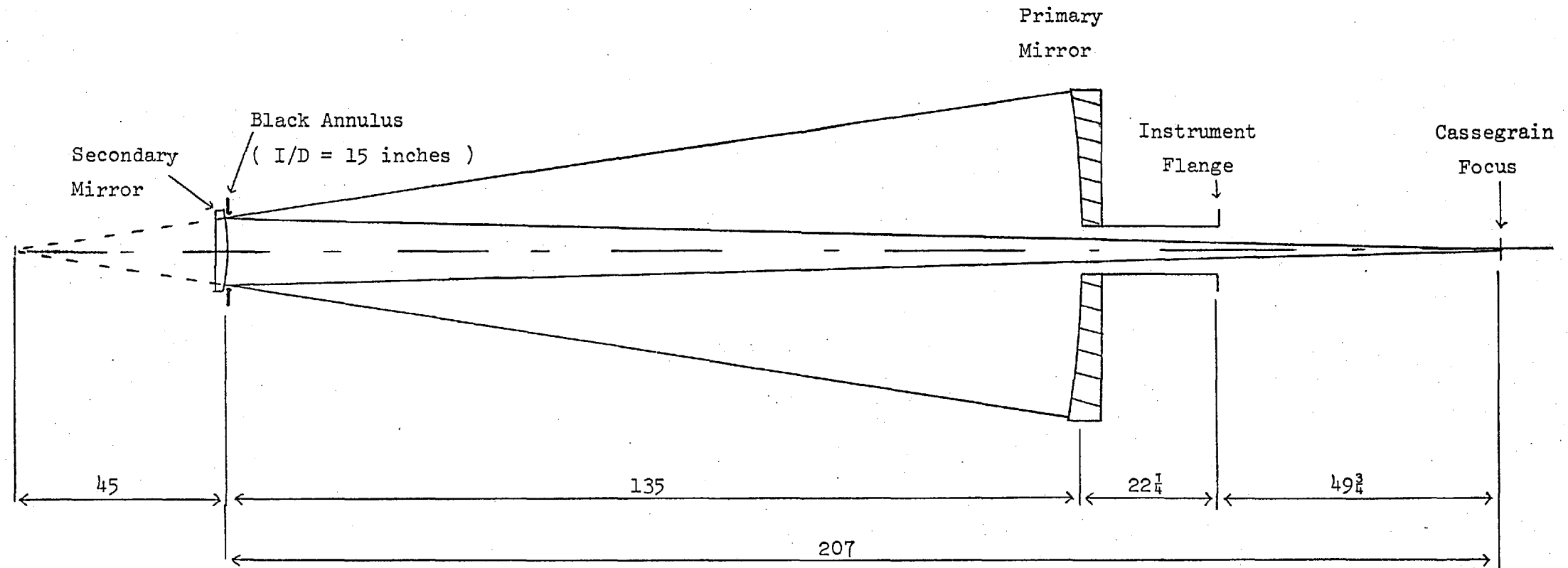
all dimensions in inches

Figure 1.1

Good observing conditions can be obtained in winter but the number of
nights that are clear of possible cloud or snow is less. From experience
of the last three years the Summer months usually are the most profitable,
although of course they are shorter and are invariably warmer. Depending
on the conditions, dust blown from the Sahara can cause problems; it can
make the sky much brighter visually and in the near infra-red. The
extinction caused by the dust in the infra-red is small compared to its
visual absorption. Since the telescope is situated on a ridge, wind
blowing particularly from the North is occasionally a restricting influence.
The particularly light telescope structure can be prone to a few arc secs
of wind bounce in declination which has been known to limit photometric
measurements under otherwise good conditions.

The drive system of the telescope, built by the Royal Observatory Edinburgh,
generally performs well. Various modes of offsetting and guiding have been
utilised and are described later. Some problems of intermittent natures
have been caused partly by the dry, dusty environment and the loose or poor
contacts of many drive rack boards; careful maintenance usually prevents
anything serious.

The telescope is moved manually over large distances or can be moved
by a degree of so at the fast setting rate of $1' \, s^{-1}$. It also has a slower
guiding rate of about $1''5 \, s^{-1}$. The position can be determined by electronic
displays driven by digital encoders with a maximum resolution of $5''$. In
practice the accuracy is a lot less due to systematic errors in the encoder
drive system and slight telescope flexure. However, when offsetting short
distances and with care, the telescope can be moved precisely; for example,
an accuracy of about $10''$ over a $30'$ motion would be possible.

1.2. The Photometer

The Photometer frame, as used on the 60-inch F.C., is shown in Figure 1.2.

It consists of a light framework which supports a baseplate under the

instrument flange of the Cassegrain focus. A focal plane chopper and beam

splitters underneath the base reflect the beam twice so that it passes up

into a detector cryostat. Cryostats for use on this system are designed

with windows at their base.

Two eyepieces are also fitted to the photometer. The main guide eye-

piece is fed with a visual image of the star field (of about 3') via the

dichroic chopper mirror. The secondary eyepiece views the field after it

has been reflected by the first chopper mirror, thus it is used to give

a visual estimate of the chop amplitude, but only receives about 25% of

the visual light.

When the Photometer and cryostat are secured to the telescope, it is

necessary to allow for their weight by removing various balance weights.

A grid of 5 lb weights underneath the primary mirror is available for this

purpose; the weights are systematically removed until the total weight is

correct and also the distribution must be such as to give zero moments in

both coordinates. Experience has shown that careful balancing is a very

necessary preliminary to any raster scanning programme since any unbalance

causes tracking errors during scan lengths of 1', or more. A record is

kept of the balance weight configuration to facilitate changes when a

different cryostat is fitted. The pre-amplifier and amplifier for the

detectors are usually secured to the photometer frame; in addition the

chopper control is also kept nearby for ease of adjustment.

PHOTOMETER AS USED ON 60" FLUX COLLECTOR

≃¼scale

156" to
Secondary
Mirror

Telescope
Instument Flange

Cryostat

Pre-
Amp.

Telescope
Focus

Artificial
Star fits
here

Photometer
Base

Secondary
Eye-
piece

Fixed or
Rotating Mirror

Chopper Mirror
(Beamsplitter)

Guide
Eyepiece

Base Cover

X-Y Slides
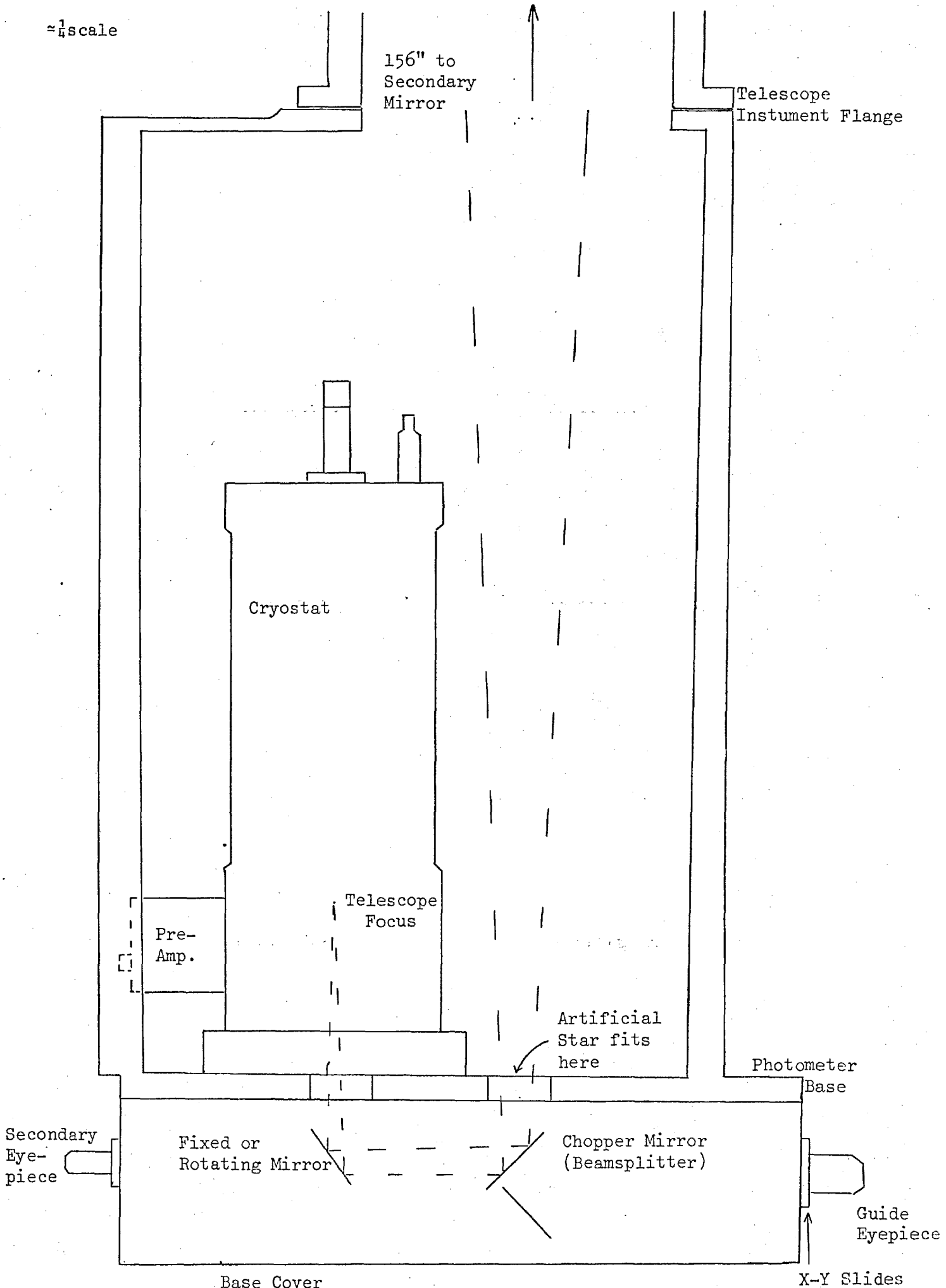
The cryostats that we use on the photometer vary in weight from about 15 kg to over 30 kg. Two cryostats are shown in Figure 1.3; the BOC Helium cryostat holds 1.5ℓ of Helium and 2ℓ of Nitrogen, and is now used mainly for tests. The Oxford Instruments cryostat holds 2ℓ of Nitrogen with a hold time of about 20 hours and is routinely used on the telescope with an In Sb detector and 1-5 μm filter wheel. For use on the telescope a lightweight cryostat with a long hold time is desirable, the nitrogen-cooled cryostat being particularly convenient since it can keep a good vacuum for a week without re-pumping and is readily topped up without removal from the photometer.

1.3. Alignment

Figure 1.4 shows the photometer optical layout; careful adjustment is needed prior to operation. The alignment procedure is usually only necessary once, at the beginning of an observing period, unless the chopper is changed. After setting up, a blackened cover is normally fitted over the photometer base optics.

At 10 μm in particular, careful alignment is required in order to prevent serious "chopping signals" which would give a large, possibly variable output signal. This chop signal results when the detector beams, in each half·of the chop-cycle, receive different radiation signals from their surroundings. Detector beam effects and chopper motions are discussed· further in Section 1.5

At shorter wavelengths ($\lambda < 2$ μm) sources such as lamps are a potential risk, rather than "room-temperature" sources. Varying dome illumination has been found to change the detector resistance (with say, a 1.2 μm filter) and so only minimal illumination is now used. There is a risk of increased noise or even a spurious signal being produced by stray radiation being scattered into the photometer.

"BOC" HELIUM CRYOSTAT
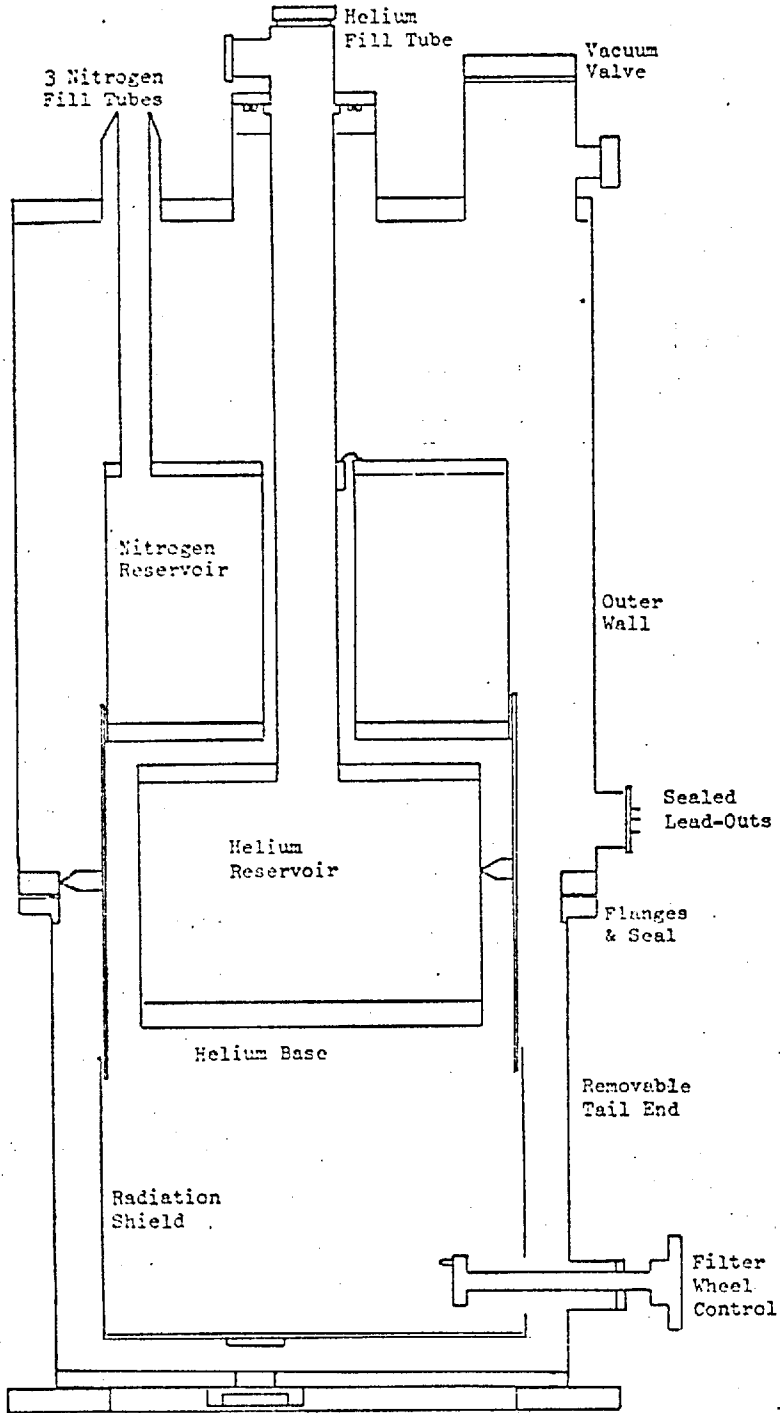
"OXFORD INSTRUMENTS" NITROGEN CRYOSTAT

Helium Fill Tube

Vacuum Valve

3 Nitrogen Fill Tubes

Nitrogen Reservoir

Outer Wall

Sealed Lead-Outs

Helium Reservoir

Flanges & Seal

Helium Base

Removable Tail End

Radiation Shield

Filter Wheel Control

Evacuation & Pressure Relief

3 Nitrogen Fill Tubes

Demountable Top Plate

Nitrogen Vessel

≈¼ size

Nitrogen Base for Detectors etc.

Radiation Shield

Pre-amp Box And Sealed Lead-Outs

Aperture Holder

Demountable Base

Sealed Window

Figure 1.3

PHOTOMETER OPTICS – ALIGNMENT
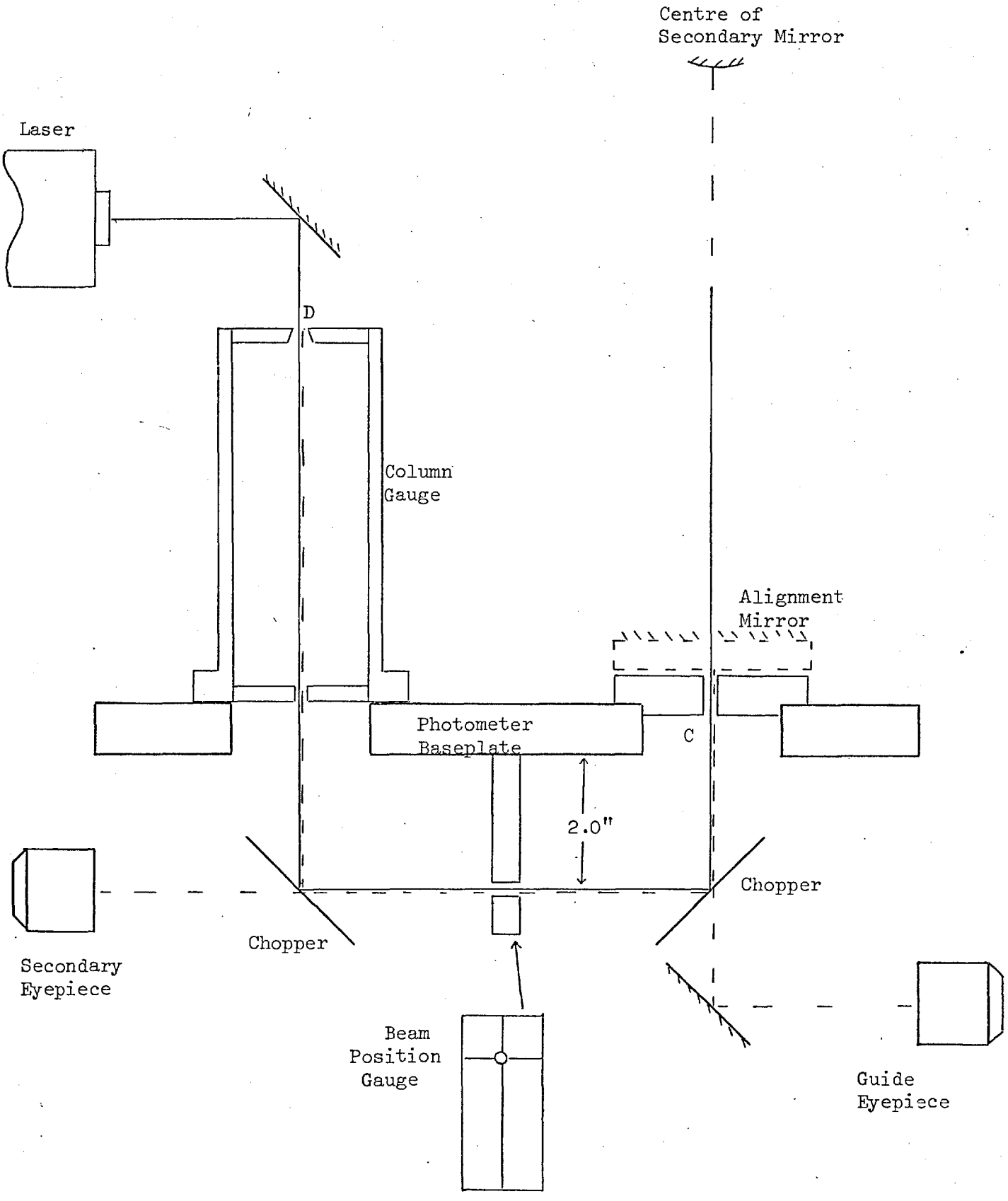
Figure 1.4

As shown in Figure 1.4, a beam from a He : Ne laser is reflected down into the detector position through a vertical column gauge. This gauge has a small top aperture at the normal position of the detector (D) and another at the base. Thus, a vertical beam as it would emerge from the detector is defined. The beam is then reflected in turn by two beam-splitters until it is directed towards the secondary mirror.

A gauge plate is used to check that the "horizontal" beam is the correct distance from the base, as a check that the total path length is correct. The beam passes through a central hole in the aperture at C. The chopper mirror is adjusted so that the beam strikes the centre of the secondary mirror. When this is done, an axial ray from the telescope would then be brought to an exact focus at the detector position D, at a fixed height of 5.4 inches above the baseplate in our system.

An alignment mirror is then placed over the aperture C in order to reflect the beam back along its own path. This gives reflected beams which pass to both eyepieces, which can then be adjusted on X, Y slides until their central cross-wires are aligned with the optical path.

The laser, aperture C and mirror are then removed and an "artificial star" is positioned over the hole at C. This serves to give a 10" wide, f/13.5 beam which should focus at D. The alignment and focus of the eye-pieces can also be checked at this stage.

The cryostat is then fitted on the photometer and moved until it is precisely over the beam position, a maximum signal is then received from the detector. The final test is performed at night when a star is viewed, the detector beam position is usually found within about 10" of the expected position in the eyepiece.

The accuracy of the alignment is such that the laser beam can be aligned to within 1 mm or so of the secondary centre, this corresponds to an angular error of about 40". A displacement of the beam by 1 mm on the secondary results in a 3.3 mm movement on the primary. (The secondary has a radius of curvature of 292 cm, the primary-secondary separation is 343 cm).

1.4. Observing Procedure

1.4.1. First observing night

When the cryostat has been positioned on the photometer a bright star is brought into the field. The telescope is moved until a maximum signal is obtained and the guide-position of the cross-wires is set; the telescope focus is also adjusted if necessary to give a maximum signal. The chop amplitude is set, normally to 10", and thereafter monitored occasionally. The scan rate of the telescope is measured and profiles of the scan are obtained by scanning in dec. and R.A., if any mapping is to be performed.

Whenever possible it is preferable to observe a sequence of standard calibration stars over the widest range of magnitudes (e.g. at 2.2 μm, $m_K = -2$ to +10). Ideally this would be done at several air-masses and with each filter. The linearity and sensitivity of the detector can then be determined.

In practice it is found that the best way to determine sensitivity is by trying to detect a faint star during a slow scan. Extrapolating from signal/noise measurements on a bright star can only give a guide to the limiting sensitivity. The noise fluctuations in the signal of a bright star are often larger than the detector noise due to guide position changes etc; however, the signal level on a bright star and the noise level on clear sky can be used to give the limiting S/N – provided the system is linear of course.

1.4.2. Subsequent observing nights

The cryostat need only be re-aligned if it had been removed. A calibration star can be observed directly; beam position and chop amplitude are briefly checked. Signal levels on a calibration star can be compared with previous values. Some typical signal records are shown in Figures 1.5, 1.6 and 1.7. Various "standardised" record sheets are used to help us keep good records of observing details, particularly amplifier gains, etc.

A "General" sheet is filled in for each night's work. This includes details of weather, detector conditions and general electronic settings. A "Photometry" sheet is used to record details of observations on a particular object, each one is given a unique reference number. For each filter used, the sidereal times, amplifier gains, sample intervals, etc. are recorded. A "Scan/Raster" sheet records parameters that are relevant when a scan of a region is performed, e.g. wavelength, scan rate, co-ordinates, gain settings are included.

Other sheets have been used to aid recording of new sources that are found during raster searches. Another is used to lay out details of a finding procedure for observations of new or difficult objects. The careful use of these items is found to save time when observing and to simplify analysis of the results.

1.4.3. Calibration

When observing, it is normal to first observe a suitable cali-bration star (at each wavelength), and then to observe the object to be studied. This is followed by another calibration star, then a new object, and so on. Up to 50% of the time could be spent on calibration stars, although 20-40% is more common, since fainter study objects would be measured for rather longer.

PHOTOMETRY OBJECT SHEET

REF. NO: *0116*
(Must go on <u>all</u> related
records, eg. Chart, Tape
etc.)

DATE : 21/22 April

GUIDE OBSERVER : R Wade

SHEET FILLED IN BY : PRJ

SEEING/WEATHER COMMENTS : 3-4" . Steady

OBJECT NAME (+ DESCRIPTION) :

CALIBRATION/STUDY   ζ Mon

CHARTS USED + CO-ORDS. : (1950/197)

R.A.: HR.   MIN.   SEC. / DEC.:   °   '   "

OBSERVATION RECORD

FILTER (Specify)	J	H	K	L	M		
START S.T.	09^h26^m	09^h30^m	09^h35^m	09^h39^m	09^h43^m	h	m
END S.T.	h m	h m	h m	h m	09^h46^m	h	m
R_L (MΩ)							
R_{L+D} (MΩ)							
DET. BIAS (V)							
OP. AMP. $O/_P$ $V_{D.C.}$							
AMPLIFIER GAIN	10	10		30	30		
CHART GAIN	5 v	5 v		5 v	5 v		
FILTER GAIN?	1	1		1	3		

(p constant possible)

(∴ odd no. of sets)

DVM RANGE   : 1 v   AMPLIFIER USED   :

INTEGRATION TIME : 1   SEC.   PSD FILTER   : IN/OUT

NO. OF PRINTS   : 10   OTHER FILTER USED? : C.F.

PRINT INTERVAL : 2   SEC.   FET BIAS   :   VOLTS

CHART SPEED   : 30 mm   DET. BIAS (If constant):   VOLTS

TICK IF OPERATIONAL: PRINTER ✓ | PUNCH | CHART ✓ | COMPUTER ✓ | OBSERVERS ✓

COMMENTS   Figure 1.5

```
R.A.? 08? 46
DEC.? -00? 53
S.T.? 00? 06


RUN REF.  J


S/N=-108.384
S/N=-165.787
S/N=-214.914
S/N=-217.027


S.T.? 00? 30
MEAN AIR MASS = 1.24937
TOTAL AMP. GAIN? 10
INTENSITY =-.009747  S.E. = 4.59607E-4
 'MAG.' =   2.50336


1 FOR COMPARISON? 0
1 FOR NEW OBJECT? 0

RUN REF.  H


S/N=-58.3287
S/N=-60.8729
S/N=-66.6875
S/N=-80.2572
S/N=-93.0183


S.T.? 00? 34
MEAN AIR MASS = 1.23529
TOTAL AMP. GAIN? 10
INTENSITY =-.106942   S.E. = 1.14969E-3
 'MAG.' =   2.42772


1 FOR COMPARISON? 0
1 FOR NEW OBJECT? 0

RUN REF.  K


S/N=-136.242
S/N=-167.303
S/N=-135.493
S/N=-147.693


S.T.? 00? 38
MEAN AIR MASS = 1.26723
TOTAL AMP. GAIN? 10
INTENSITY =-.00298   S.E. = 5.61842E-4
 'MAG.' =   2.70323


1 FOR COMPARISON? 0
1 FOR NEW OBJECT? 0

RUN REF.  L


S/N=-996.249
S/N=-84.1948
S/N=-90.3136
S/N=-102.377


S.T.? 00? 42
MEAN AIR MASS = 1.25361
TOTAL AMP. GAIN? 1+30
INTENSITY =-.031677   S.E. = 3.09416E-4
 'MAG.' =   3.74995
```
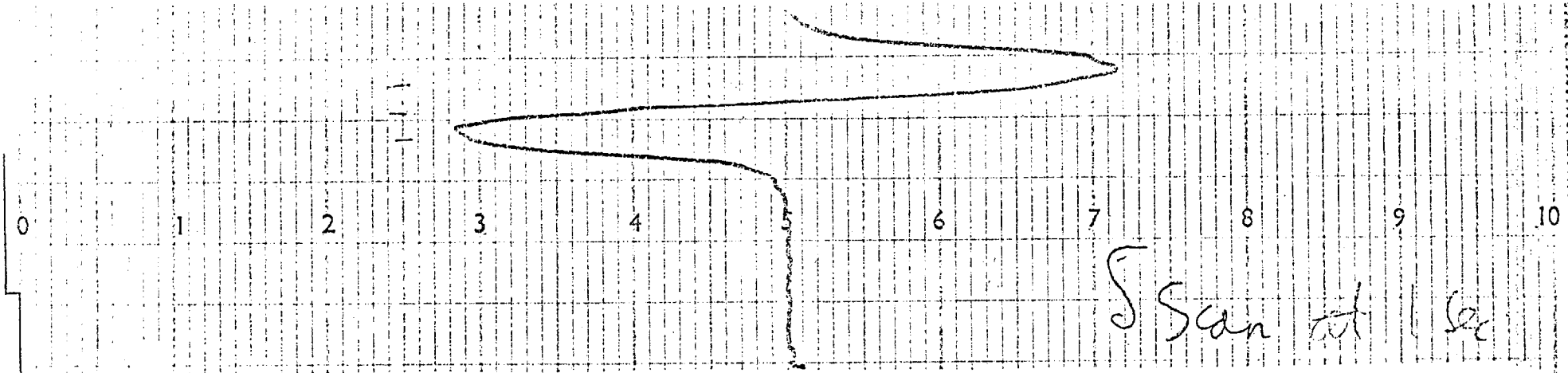
Figure 1.6

Part of 0104 Record

Typical Chart Record

Figure 1.7

14
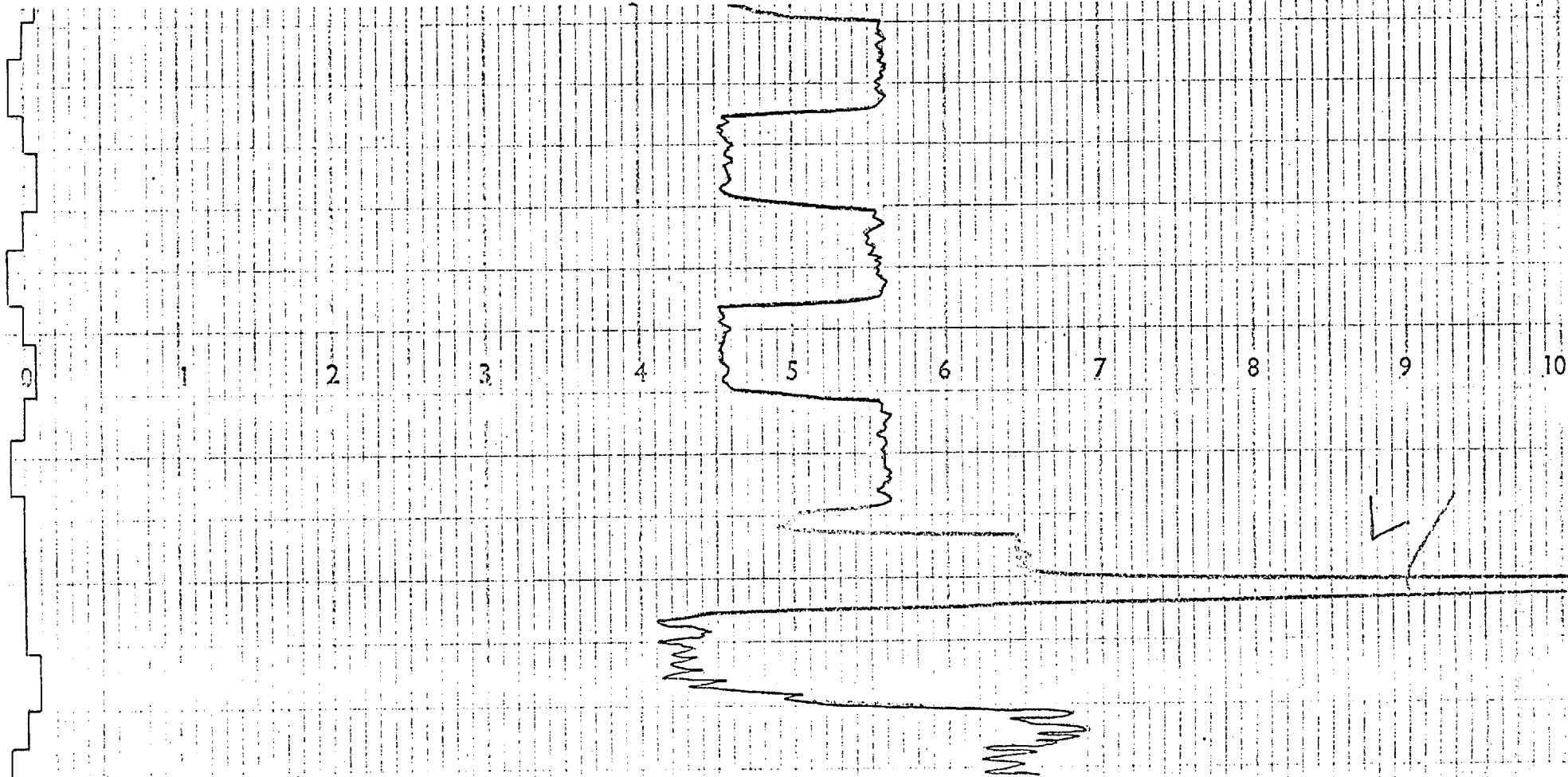
The calibration star is often used to check that the detector beam position is correct. For example, at 10 µm and 1.5 air masses the infrared image suffers a refraction of 1.2" with respect to the visual image. If this were not corrected, a significant error could occur in going from one region of the sky to another. (A.D. MacGregor (1974 Thesis) shows that a sinusoidal chop of 10" has a $\sim$ 15% signal loss for a 1.2" guide error).

Differential refraction curves are indicated in Figure 1.8. Numerical data can be found in Allen (1973). Basically, refraction $R_\lambda \sim (n-1) \tan Z$ where Z = zenith angle; n = refractive index of air, a function of wavelength λ. For λ = 0.55 µm, Z = 45° we find Refraction, R $\sim$ 60".

The calibration star observations are typically made at several different zenith angles in order to assess the mean extinction per air mass. However, it is best to observe standard stars as near to the object of study as possible. This is convenient in most cases and it helps to reduce the effects of variable extinction. (Some typical figures are given in Section 2.2).

1.5. Chopping Methods

1.5.1. Introduction

In order to detect weak infra-red signals by using a PSD system (see Chapter 2), it is necessary to modulate the radiation in a periodic way. This "chopping" can be performed by interrupting the beam to the detector or by oscillating the detector beam on and off the source. Various chopping alternatives are discussed by Low and Rieke (1974), and papers on different chopper systems are to be seen occasionally in the literature.

An ideal chopper should alternately allow the detector to see different fields of view on the sky, without changing the level of

Infrared Beam Displacement with respect to Visual Image

as a function of Air Mass
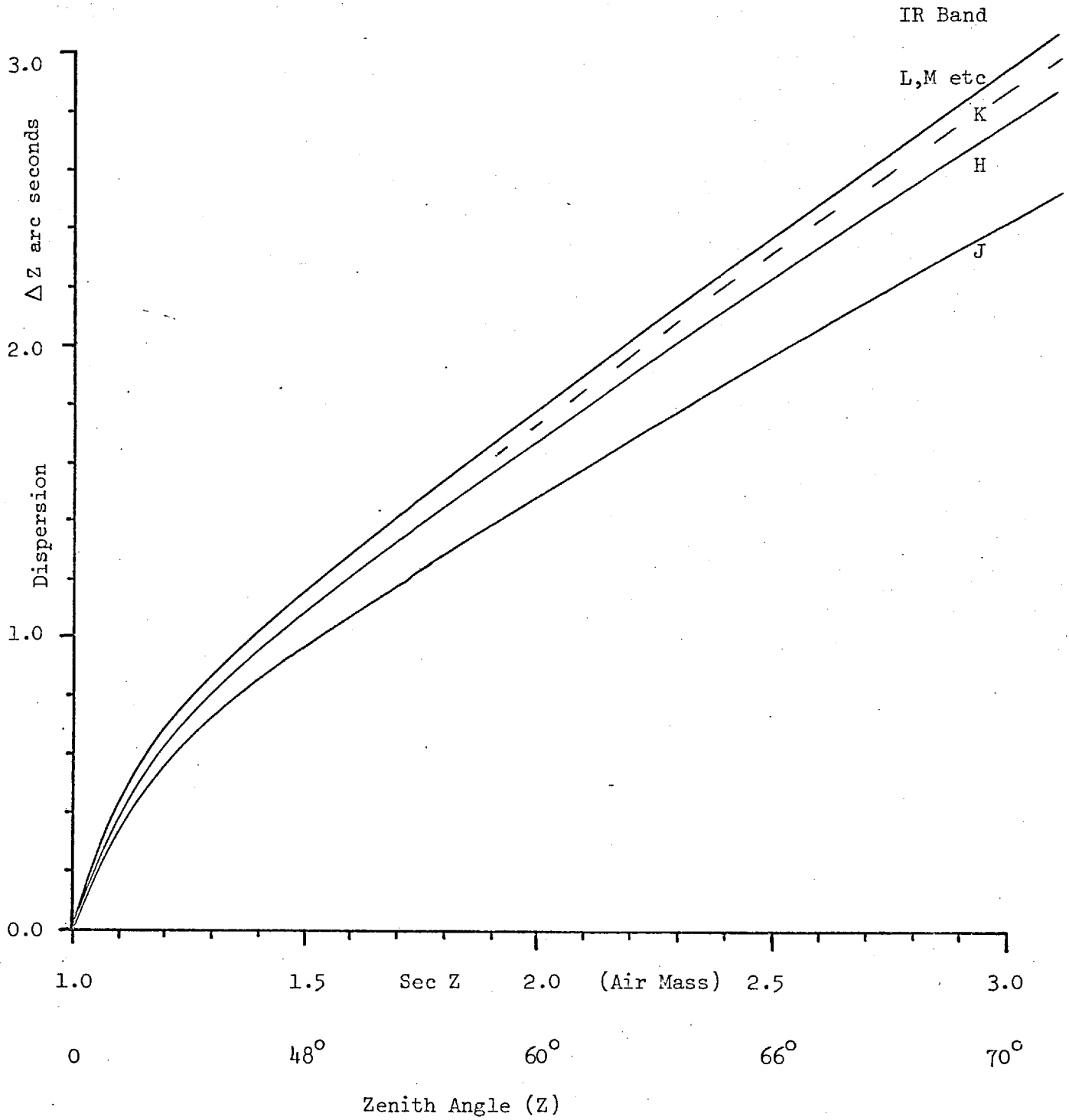
Figure 1.8

background radiation. For example, at 10 µm, where the sky background is $\sim 10^{-8}$ W and the shot noise $\sim 10^{-14}$ W it is necessary that the modulation of the background is less than 1 part in 10^6 if no extra noise is to be introduced.

Movement of the whole telescope or primary mirror is not practical; on large telescopes this would be too slow for useful background cancellation. It seems that oscillating the telescope secondary mirror at a rate of 5-10 Hz is very effective, but can only be done on telescopes that have been designed or adapted for this purpose.

An alternative chopping method is to introduce a modulator near the focal plane of the telescope, this is convenient in practice and is done by many infra-red workers. In the case of the Tenerife telescope a 10" chop amplitude requires a beam displacement of 1 mm.

A very simple chopper consists of a rotating disc, with sections cut out to interrupt the beam, or offset mirror segments to alternately displace the beam. In practice, except for laboratory tests, this system is not used because of the large differences in radiation seen during a chop cycle. A large, and often variable, output offset is the result - this is particularly serious at wavelengths near 10 µm, where room temperature (and sky) emission is most strong.

The main advantage of the secondary mirror chopper is directness; that is, no extra mirrors need be used with an "upward-viewing" cryostat. This is offset by the fact that no fixed image is available for guide purposes, and large F/numbers are required (these make alignment within the cryostat more difficult). The focal-plane chopper has the advantages of low cost, easier adjustment, and higher chop frequencies.

1.5.2.   Practical choppers

The most effective way of sky background cancellation is to use an oscillating mirror near the focal plane, this causes the detector to alternately view (sky and source) and (sky). We have used two types of chopper for this purpose. The simplest type uses a displacement of a plane mirror in a direction parallel to the detector beam. The other uses two rotating mirrors to give the same final displacement of the beam. These two systems are shown in Figure 1.9,

The Single-mirror type

A square-wave low frequency chopper of the first type has been built and used for some time (Fig.1.9a). This was based on a design by Fahrbach et al.(1974). It is used at 5-20 Hz and has a displacement sensor and feedback system to maintain a precise motion. A square-wave modulation is used for maximum efficiency; the detector spends 50% of the time on the source compared with a lower fraction in the sinusoidal case. The system is less sensitive to guide position errors or to image size changes (some numerical estimates of the errors were given by MacGregor, 1974).

The mirror frame is supported by a simple bearing, but this does not give a precisely parallel motion and is also prone to friction. A chopper throw of 1 mm has been measured to give several mms movement on the secondary during alignment tests. A more sophisticated mounting system, using perhaps a parallel spring carriage, would be an improvement. Molybdenum Disulphide powder has been found to be better than oil as a lubricant for the bearing, mainly because it does not suffer in the dry atmosphere.

A low frequency chop at 5 Hz was found to be optimum for the PbS detector. More recently a chop frequency of 10-15 Hz has been used with

(a) Low Frequency Square-wave Chopper
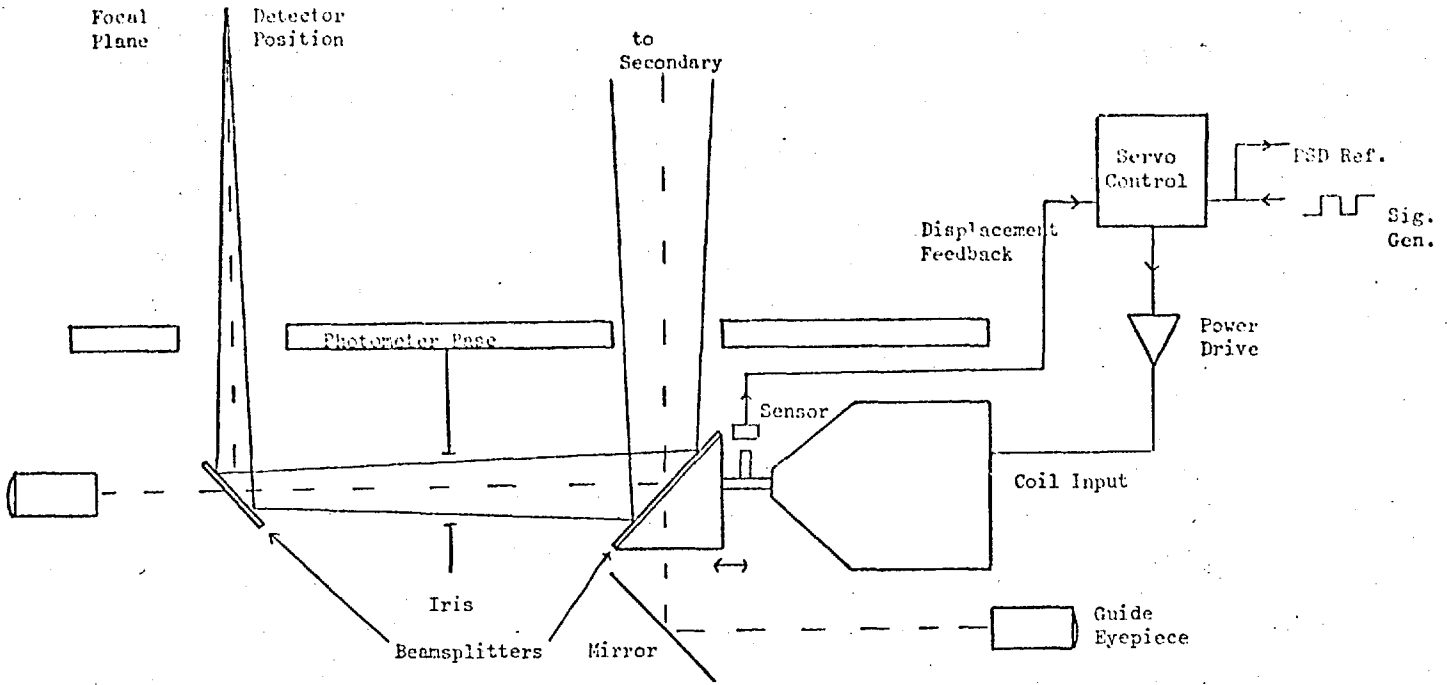
(b) High Frequency Resonant Double Chopper

Figure 1.
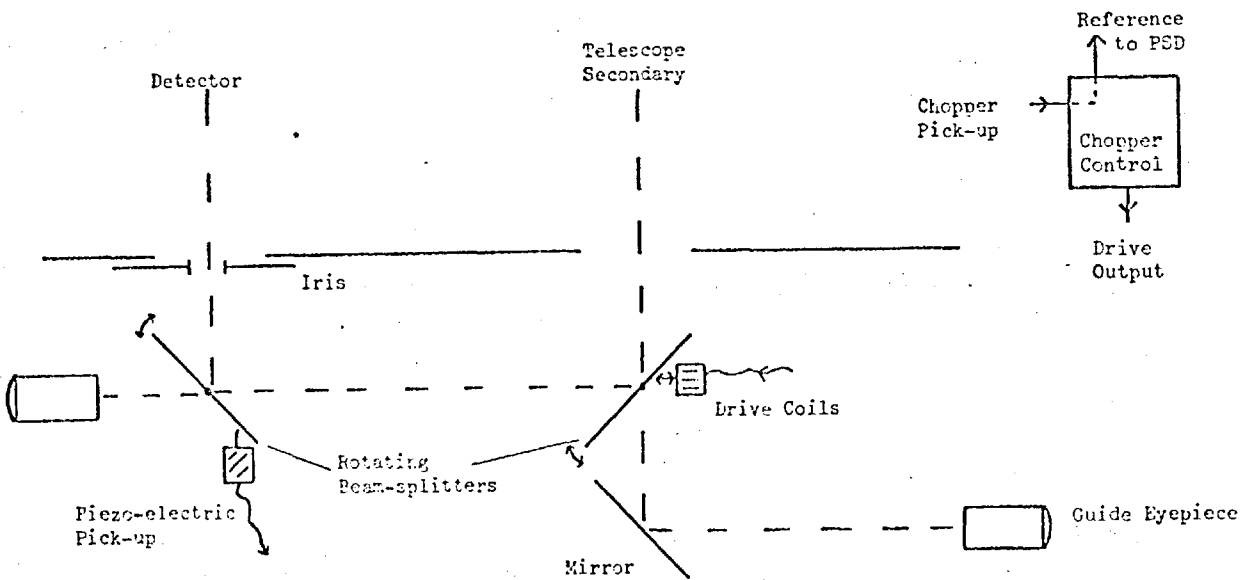
an InSb detector. The detector response falls with frequency and this mainly determines the operating frequency; this type of chopper cannot be driven to give a "good" square-wave at frequencies much above 20 Hz.

The Double-mirror type

From measurements of S/N on a 10 µm Cu:Ge detector a chop frequency of 300 Hz was found to be optimum. A double-mirror chopper operating at this frequency has been constructed and is described more fully in a paper (see Appendix 1). The chopper, using a pair of rotating mirrors, acts effectively as a "cube-corner". A diagram is shown in Figure 1.9b.

The advantage of this is that it is a balanced resonant system and introduces very little microphonic vibration to the photometer. It needs little power for operation but does however only give a sinusoidal motion; it also produces a negligible focus error compared to the single mirror type. The stability of oscillation that is obtained is particularly important, for 10 µm use, in order to maintain a constant radiation beam on the detector.

The two mirrors need to be carefully set to give a total 180° beam reflection. The whole chopper is aligned to give a beam path close to the centre of the secondary. In operation there is negligible error (less than 1 mm at the secondary) for a 10" throw.

The chopper has a mirror separation of $D = 15$ cm, and a throw of $d = 1$ mm requires rotation of each mirror by an amount $\theta = \pm d/(4D) = 0.0016$ rad $= 5'.6$. (This results in a movement at the edge of each mirror of $\pm .04$ mm). The optical path change, or focus error, of this system is, $\Delta x \sim \pm \theta d/2 = 0.8$ µm compared to a 1 mm change with the single mirror chopper.

1.5.3. An improved chopper

A chopper with the advantages of the double-mirror action and a square-wave motion has recently been constructed. The assembly is similar in size to that of the double-mirror chopper described, but uses strip-spring pivots instead of torsion bar supports. The drive is provided by a single coil (Model 200, Ling Dynamic Systems Ltd) which can give a square, sinusoidal or triangular motion. A magnetic displacement sensor is used.

The chopper is symmetrically constructed for minimal vibration but does not have a strong design resonance as before. It has been found to give a good square-wave motion at 20 Hz, with a modulation efficiency of 90% (i.e. out of a 50 ms period, the two movements take $2\frac{1}{2}$ ms each). Sinusoidal motion at any frequency up to at least 100 Hz could readily be obtained. The chopper has a resonance of $\sim$ 50 Hz, which is due to the Ling Coil suspension primarily.

With a "simple" chopping system the beam from the detector moves across the secondary and primary and any differences of emitted radiation result in an PSD output offset. It is, in principle, possible to arrange that the motion is kept to zero at the secondary or the primary. This is done by causing the angle of the emergent beam to change during the chopper throw so that its position at the primary mirror (for example) is constant.

This technique is shown in Figure 1.10. The chopper has a total throw of $\pm$ d/2 and all beams are directed towards point I (this is the image of the primary mirror in the secondary).

Primary

Focal
Plane

$\frac{d}{2}$

uncorrected beam

Secondary

I

chopper
throw

$\longleftarrow$ Y $\longrightarrow$ | $\longleftarrow$ R $\longrightarrow$ | $\longleftarrow$ X $\longrightarrow$
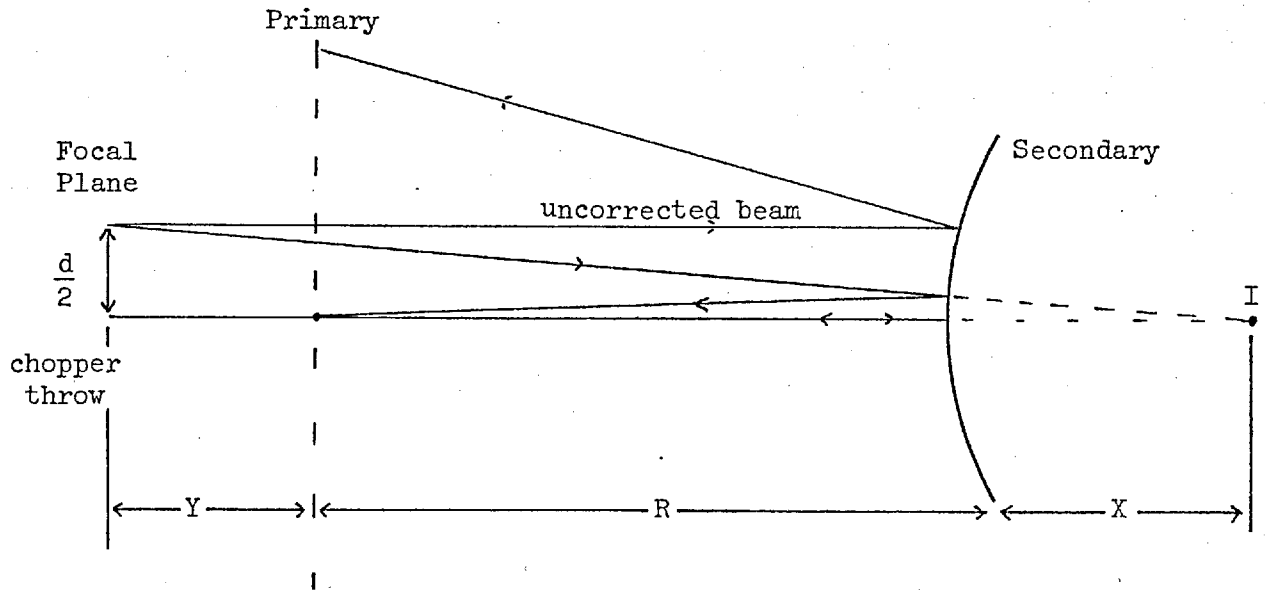
(a) Corrected and uncorrected chopper beams

θ_2

θ_1

D

L_2

L_1
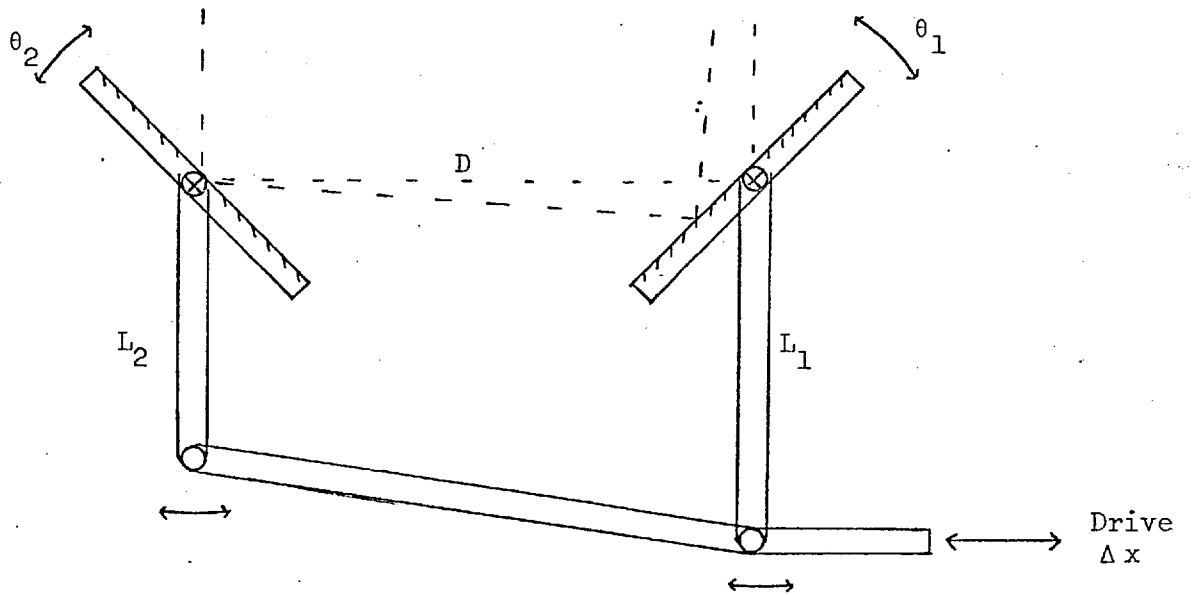
Drive
Δx

$$\Delta x = L_1 \cdot \theta_1 = L_2 \cdot \theta_2 \qquad \text{or} \quad \frac{\theta_1}{\theta_2} = \frac{L_1}{L_2}$$

(b) A drive method for differential mirror rotation

Figure 1.10

The distance of I from the focal plane is $Z = X + R + Y$

$R = 343$ cm, $Y = 183$ cm, secondary radius $= 292$ cm

it is easily shown that $X = 102$ cm . Hence $Z \sim 627$ cm

The angular beam adjustment required is therefore $\alpha = (d/2)/Z$

This is accomplished by turning one mirror through $\delta\alpha = \alpha/2 = (d/2)/2Z$

However, the chop angle $\theta = {}^{(d/2)}/2D$, D = mirror separation ~ 15 cm

$\therefore$ The correction needed $= \dfrac{D}{Z} = \dfrac{6}{247} \sim 2\frac{1}{2}\%$

that is, one mirror must be rotated $2\frac{1}{2}\%$ more than the other. One method of accomplishing this, by using drive arms of different lengths, is shown in Figure 1.10b.

A useful consequence of compensation on the primary mirror is that motion on the secondary is reduced by a factor of 6 ($\alpha x \sim 0.08$ mm, instead of 0.5 mm previously). The Tenerife telescope has a blackened annulus around the secondary to prevent the outer edge of the primary from being visible at the detector. We use an f/12 or similar detector beam which ensures that even when chopped the whole of this ring is always included in the beam and therefore no changing signals should be generated. However, a 3% angular correction of the chopper throw would allow the detector beam to be fixed at the position of the secondary. This does in fact simulate the motion of a secondary mirror chopper; the same final motion on the primary is produced (0.65 mm for a 10" throw).

1.6.   Filters, Windows and Beam-Splitters

The cooled filters that are used are purchased from firms such as Grubb-Parsons and OCLI Ltd. They typically have 70-80% transmission, which is rarely completely uniform in the pass band. Low and Rieke (1974) have mentioned that it is possible to get different beam displacements from non-parallel surfaces of different filters, this should be checked but does not seem a problem with modern filters.

Quite sharp cut-on and cut-off edges can be obtained and blocking of other wavelengths to < 0.1% is also common. Filters have generally been chosen so that their transmission characteristics match those of the atmospheric windows (see Section 2.2 also). However, with the high sensitivity of present and future detectors it seems that rather narrower filters would be advantageous; the signal, although slightly less, would suffer much less from extinction effects caused by variable atmospheric transmission – which mainly affects the edges of the bands.

Dielectric filters suffer a reduction in effective wavelength of $\delta \lambda \sim 1\frac{1}{2}$ or $2\frac{1}{4}$% as the temperature drops from room temperature to 77K or 4.2K respectively. This effect should be allowed for, when designing a cooled filter system. (OCLI Technical Report 1967). The transmission of the filter can also improve when cooled.

The vacuum sealed cryostat windows that we commonly use are Calcium Fluoride and KRS5 (Thallium Bromo-iodide, a synthetic crystal). These give reasonably flat transmission of 70-80% over quite a wide range. CaF_2 has a refractive index ~ 1.4, and a reflection loss of 6%; KRS5 has a refractive index ~ 2.4, with a reflection loss of 30%. Anti-reflection coating of KRS5, for 8-13μm, can enhance the transmission to over 90% in the wavelength band of interest.

1.6.1. Beam-Splitters

The beam splitters that are used, for example in the chopper, consist of a polished glass plate coated with a thin layer of gold to give a visible transmission of close to 50%. This results in an infra-red reflectivity of at least 90% at 2.2μm, and 98% at 10μm. For a maximum reflection at J(1.2μm) it is best in fact to have a visible

transmission of 30-40%, resulting in a rather fainter image for guide purposes.

Some theoretical curves and practical results are shown in Figure 1.11. The theoretical curves (derived from a program by R.J. Scaddan) show reflectivity and transmission for various thicknesses of gold deposited on a substrate of refractive index 1.4. The measured transmission of an actual beam-splitter is also given. (However, the absorption of glass for $\lambda > 1\,\mu m$ is not included in the theoretical calculations). The cleaning and coating process (for 5-cm chopper mirrors) is now described. A perfectly clean glass substrate and the thin chrome layer are important for a good gold coating. It is not clear exactly how many of the stages of cleaning are essential but the combination gives good results; the coatings are the result of Bob Airey's careful work.

Gold Coating

The glass is scrubbed with cotton wool in a solution of 10% "Decon 90" with a small amount of chalk as a fine abrasive. It is then rinsed in tap water, preferably in an ultrasonic bath. The glass is left in chrome sulphuric acid for 10-15 minutes, then all traces of acid are removed by rinsing in running water for $\frac{1}{2}$-hour and using 3 changes of distilled water. Drying is best performed in an isopropyl alcohol vapour bath (with polishing as an alternative).

The plate is then mounted in a vacuum chamber (an oil diffusion pump and cold trap). It is cleaned by an AC glow discharge for about 15 minutes, with a slight air leak as required. The chamber is pumped to a good vacuum and then a thin layer of pure chromium is evaporated so as to give 90% visible transmission. Transmission is measured with a simple lamp, green filter and detector.

REFLECTION & TRANSMISSION OF THIN GOLD FILMS ON GLASS
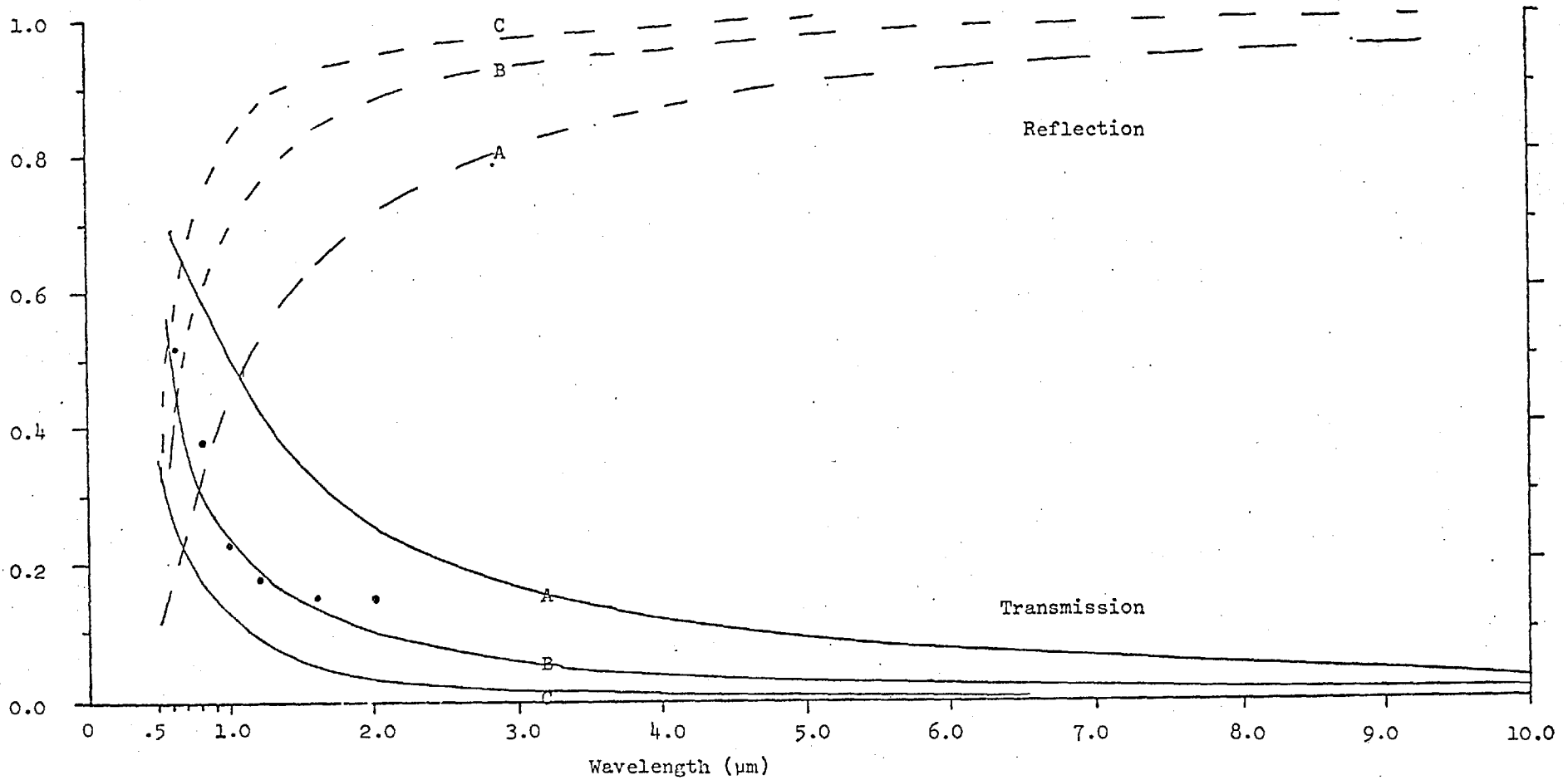
The Dots show measured values of Transmission of a sample with 55% Transmission @ 5500 Å

Theoretical Curves
$\begin{cases} A & 0.009\mu m \text{ layer of Gold on glass (absorption beyond 1} \mu m \text{ is not shown),} & T=70\% @ 5500 \text{ Å} \\ B & 0.016\mu m \text{ layer} & T=50\% @ 5500 \text{ Å} \\ C & 0.023\mu m \text{ layer} & T=35\% @ 5500 \text{ Å} \end{cases}$

Figure 1.11

Finally, a gold layer is evaporated until the required visible transmission is obtained, typically 40%. A final test is to measure the resistance of the coating; a resistance of less than 10Ω across a 5-cm plate indicates a good coating. Measured resistances of more than 100Ω have always corresponded to a coating of low reflectance (and also to much less abrasion resistance). A good beam-splitter with a visible transmission of 42% gave a measured $10\mu m$ reflection of 98%, it could be easily cleaned and would not wipe off with light contact.

Aluminium is not suitable for partially transmitting mirrors since it exhibits strong absorption. A thick layer is of course used for other beam directing mirrors such as are used to reflect the beam into the guide eyepiece. Experience has shown that thick (> 6mm) glass mirrors and careful securing in their frame is necessary to prevent bending or cracking of the coated chopper mirrors.

The guide eyepiece

For the guide eyepiece it is found convenient to have a grid of crosswires at 10 arcsec intervals covering the whole field; this is particularly useful when mapping or defining positions of sources in new star fields. The second eyepiece only has a few sets of crosswires near its centre, which are adequate for checking the chopper motion. We have found it reasonably convenient to position fine ($\sim$ 0.025mm) nylon wires on an annulus and secure with adhesive. These wires are strong, stretch slightly, and seem to work well when illuminated by a ring of four red light-emitting diodes.

CHAPTER 2

INFRA-RED DETECTORS AND PHOTOMETRY

2.1. Detection System, PSDs

The general system used for infra-red photometry is based on similar

principles to that of most infra-red groups and is shown in Figure 2.1.

It consists of a cooled detector element with an associated load/feedback

resistor which feeds a field-effect transistor (FET) as an impedance

converter. Typical IR detectors have impedances which range from

$10^6 - 10^{12}$ Ω and junction FET's or MOS FET's (rather than bipolar

transistors) are therefore used.

The detector and load resistor are cooled to reduce thermodynamic

noise (Resistor Johnson noise voltage $V_n = (4kTR\Delta f)^{\frac{1}{2}}$). The FET is cooled

in order to reduce gate current leakage and noise, and also because this

enables it to be situated close to the detector to reduce microphonic

pick up (at the high impedance input). The pre-amplifier and detector

bias facilities are contained in a box mounted on the side of the cryostat.

The signal passes into an AC amplifier in order to increase the signal

level to about 1 volt peak-peak (a detector resistance measuring circuit

is also included in our amplifier). The amplified signal is then fed via

an optional tuned filter into a phase sensitive detector (PSD).

2.1.1. Phase sensitive detection

The PSD acts as a synchronous switch and serves to provide a DC

output which is proportional to those elements of the input signal with

the same frequency and phase as the reference (derived from the IR beam

chopper). This can be considered as a multiplication of the input signal

INFRA-RED DETECTION SYSTEM

(NOTES)

Modulator — reference

D   R

Cooled FET

Pre-amplifier

Main Amplifier

Optional Filter

Oscilloscope

Phase Sensitive Detector

Reference Unit

Digital Voltmeter

Chart Recorder

Data Recording System
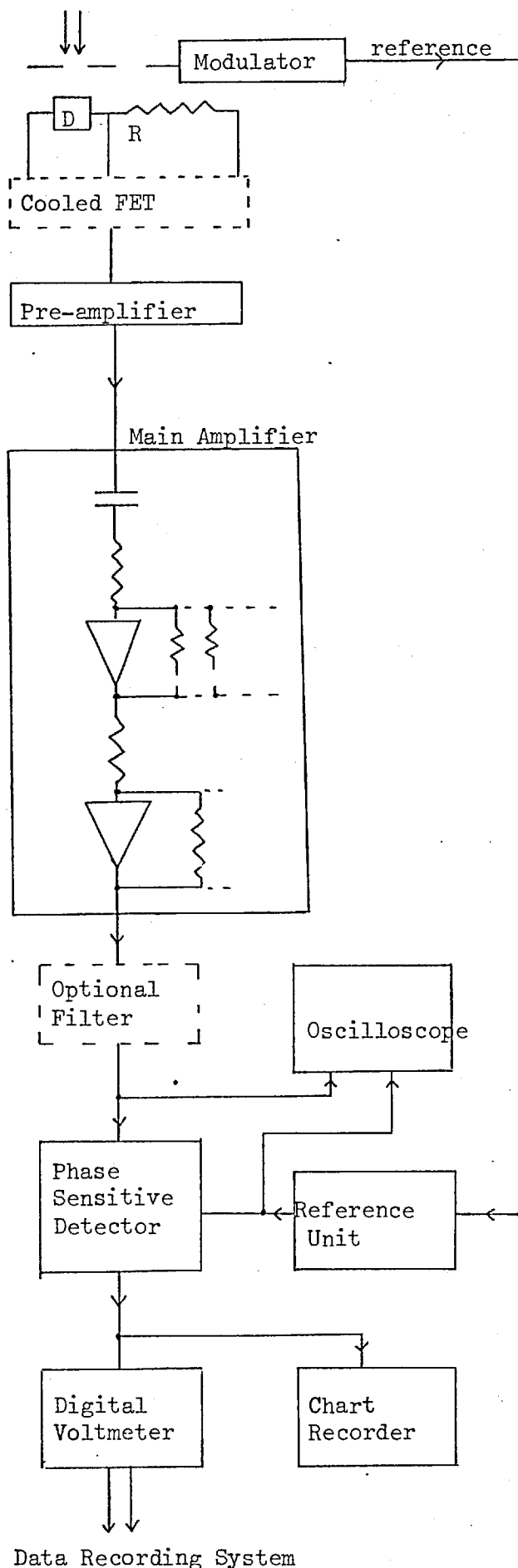
Vibrating(or rotating)mirror chopper normally used

Cooled Detector & Load/Feedback Resistor,with cooled Field Effect Transistor as an impedance converter

Pre-amp. - on outside of cryostat

Home-made (ADM) amplifier with variable switched gains

Coherent filter or other tuned filter used when needed

Oscilloscope monitors signal and reference waveforms

A standard "Brookdeal" PSD & Phase shifter are used

The "Hewlett-Packard" DVM digitises the data before recording

by the square-wave reference. In the case of a square-wave signal the PSD acts as a "matched filter", this gives optimum detection of the signal, e.g. for an input signal (sinusoidal) $= V_s.\cos(\omega t + \phi)$ and a reference square-wave $= V_R . \frac{4}{\pi} (\cos\omega t - \frac{1}{3} \cos3\omega t .....)$. The output of the PSD is $V_o \alpha V_s V_R (\cos\phi + \cos(2\omega t + \phi) .....)$. See, for example, Blair & Sydenham (1975). In our case $V_R = $ constant, where ϕ is the phase difference between signal and reference; in practice this is set to zero before each observing session. A low pass filter is used at the output of the PSD so that a "DC" output is obtained which is proportional to the input signal amplitude. The "gain" of our commercial Brookdeal -411 PSD is such that a 1 V r.m.s. input gives a 10 V DC output.

A simple RC low pass filter is used at the output; a time constant of $\tau = RC = 1$ second is useful in practice, giving a reasonable response time and a suitably small bandwidth in order to reduce the noise seen at the output. The noise bandwidth of this filter is $\Delta f_n = (4RC)^{-1}$, and the full "half-power" bandwidth (usually applied to the signal) is $\Delta f = 2.(2\pi\tau)^{-1}$.

The PSD is a linear detector with an output voltage proportional to the input signal. For white noise (of constant power per unit bandwidth) the noise voltage $V_N \alpha (\Delta f)^{\frac{1}{2}}$. The signal/noise ratio at the output of the PSD is therefore proportional to $(\Delta f)^{-\frac{1}{2}} \alpha \tau^{\frac{1}{2}}$, giving a large reduction in noise as bandwidth is reduced.

The PSD also has contributions to the output which result from input components at odd harmonics of the reference frequency (ω_o). In the case of "white" noise these uncorrected noise components increase the noise by $\sim$ 10%. (The odd harmonic contributions, from white noise, give $V_n^2 \alpha 1 + ^1/3^2 + ^1/5^2 ..... = \pi^2/8$, compared with the first harmonic of 1; the increase is $\therefore (\pi^2/8)^{\frac{1}{2}} -1 = 0.11$). Chopper induced microphonic noise at say $3\omega_o$ could be more serious (up to 30%).

The use of a narrow-band coherent filter or a wide band tuned filter (centred on ωo) at the PSD can virtually eliminate these signals if required. This facility could also be useful in the presence of strong line frequency noise or other discrete frequencies which might overload the PSD input; this has not proved to be the case and modern PDSs usually have a large dynamic range.

The single low pass filter, which determines the bandwidth of the PSD system, has a response time $t \sim 2.2$ RC (defined as the time taken to approach within 1dB of a "step" level). The use of two such filters at the PSD output could give a response time of $t = 2.9$ RC with a noise bandwidth of $\frac{1}{2}(4RC)^{-1}$. Two filters of RC = 0.75 s should have the same response time as a single filter (with RC = 1 s) and a narrower bandwidth. The gain in signal to noise is small however ($\sim 10\%$ at best), and the instrumental profile (the response to a scan through a source) may be degraded.

2.1.2. Operating practice

The signal information is recorded by digitally sampling the DVM every one or two seconds. At low chopping frequencies (5-20 Hz) a time constant of about 1 second is needed to filter out any "reference ripple" in the output. At higher frequencies a shorter time constant could be used but the data would then need to be sampled more frequently. In practice we use a 1 second time constant for most occasions.

Following normal infrared practice the telescope is "nodded" every 20 seconds or so, this places the detector beam in an "upper" or "lower" position. These alternating signals, of opposite phases, are then algebraically added to give a final measure of the IR source strength. The total data record may then be integrated for as long as necessary to obtain the required signal to noise.

This nodding procedure is an efficient means of determining the signal level without having to measure the absolute DC zero level of the PSD which can drift slowly. The beam-switching process is in fact another level of phase-sensitive detection which eliminates the effects of instrumental drifts and sky gradients, in the same way as sky-chopping removes the effect of a constant sky emission. It is of course important to nod at a rate which is high compared to rates of drift.

Chopping of the detector beam causes at least a $2^{\frac{1}{2}}$ loss of signal/noise since the detector only views the source for less than half of the time. Provision of an extra detector would overcome this disadvantage, but the extra complexity of closely matching two signal channels does not make this worthwhile at present.

2.2. Photometry and Analysis

Our normal mode of photometry consists of integrating for 20 seconds in one beam and then nodding to the other beam for a similar set of data samples (10 values at 2 second intervals). A signal/noise of 50 (or $\Delta M = 0.02$) magnitude is adequate for one observation of a standard star at a given wavelength. It is however necessary to make several measurements of a calibration star in order to accurately assess any extinction and other "systematic" errors, including beam-centering, guide errors,etc.

Calibration stars are usually observed for two to five minutes at each wavelength, this gives an adequate estimate of the signal ($\leq 1\%$). An object would be measured for two minutes to several hours, depending on its intensity. The use of the computer enables us to make an "on-line" estimate of signal to noise.

Results are recorded on a chart recorder, a digital printer, sometimes an 8-hole tape punch in BCD code, and also by the computer. If the computer is used, an immediate output of the signal intensity is available; if not, the recorded data would be analysed later, often at the end of the observing period.

The atmosphere

As mentioned before (Sec.1.6), the filters that we use are designed to match the "windows" of high atmospheric transparency. Figure 2.2 shows examples of some filters and the atmospheric transmission from 1 - 15 μm (derived from Ridgeway and Capps 1974, $\lambda < 3\mu m$; and Low and Rieke 1974, $\lambda > 3\mu m$). Most IR groups to date have used "standard" filters for each window to allow good comparison between results, particularly useful when common calibration-star lists are used.

The transmission of the atmosphere varies mainly due to the amounts of H_2O, CO_2, O_3, N_2O, etc. (see Wolfe 1965). The extent of variation was shown by a dotted line in Figure 2.2. These components cause absorption which can vary with the weather or the time of day; a high, dry observatory site is chosen to minimise these variations.

Some typical measurements of sky intensity and extinction are given in Table 2.1. ·The sky brightness levels were measured with the In Sb detector, on the 60-inch telescope in a 10" beam. The DC output level from the detector pre-amplifier gave a measure of the background radiation level (compared to a 77K blank disc in the cryostat which emitted virtually zero radiation). These levels were then converted to magnitude by comparison with standard star measurements.

ATMOSPHERIC TRANSMISSION AND FILTER BANDS
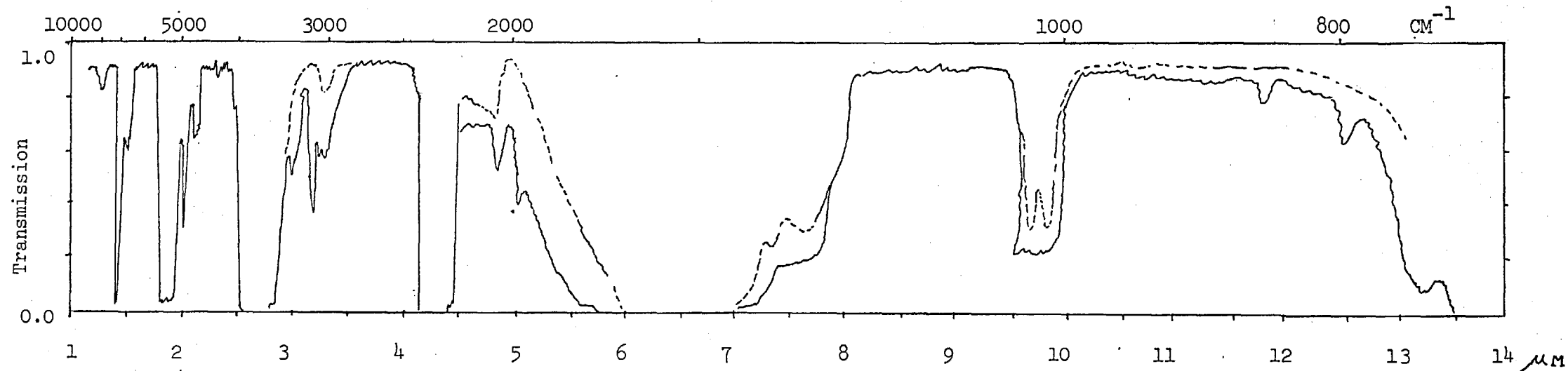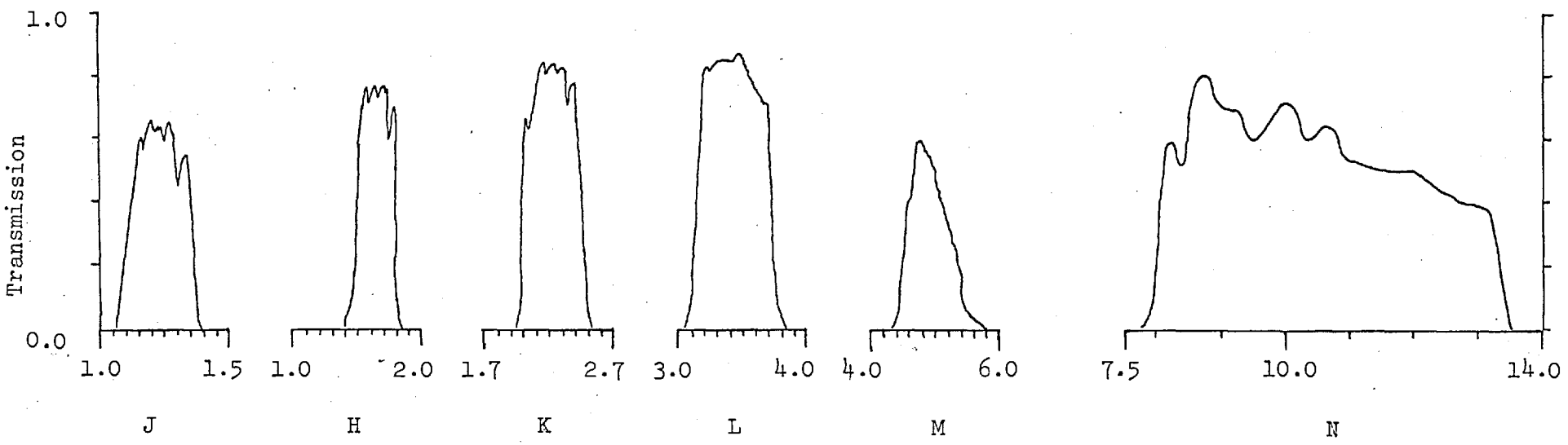
Figure 2.2

The equivalent background radiation and corresponding shot noise are derived from the measured sky brightness. The flux levels taken to correspond to a zero magnitude star are given. These figures, derived from Johnson's (1966) data, are used for flux conversions for the IR photometry of Chapter 4.

TABLE 2.1: Sky Measurements

Filter Band	J	H	K	L	M
Wavelength (μm)	1.2	1.65	2.2	3.5	4.9
Extinction/Air Mass (typical)	0.1	0.05	0.05	0.1	0.2
Extinction/A.M. (average range)	0-0.25	0-0.15	0-0.2	0-0.3	0-0.4
Sky Brightness (theory)		$7\frac{1}{2}$	$6\frac{1}{2}$	0	-7
Sky Brightness (measured magnitude)	+3	> 10	+6	-1.5	-6
Zero Mag. Flux ($Wm^{-2}\mu m^{-1}$)	$3.4\ 10^{-9}$	$1.2\ 10^{-9}$	$3.8\ 10^{-10}$	$7.6\ 10^{-11}$	$2.3\ 10^{-11}$
Sky Background ($Wm^{-2}\mu m^{-1}$)	2.10^{-10}	$<10^{-13}$	2.10^{-12}	3.10^{-10}	6.10^{-9}
Corresponding Shot Noise ($W\ Hz^{-\frac{1}{2}}$)	4.10^{-15}	$<10^{-16}$	3.10^{-16}	4.10^{-15}	2.10^{-14}
Filter Bandwidth $\Delta\lambda$ (μm)	0.24	0.3	0.4	0.55	0.8
Photon Energy hν (Joules)	10^{-20} x 17	12	9.1	5.7	4.1

NOTES: (1) The Theoretical Sky Brightness comes from A.D. Macgregor(1974 Thesis), data was based on that of Wolfe (1965).

(2) The Sky Background at 1.6 μm was too small to measure.

(3) The extinction measurements are the mean of a few good nights in April 1976.

(4) The Telescope has an area = 1.7 m^2 (used with $\Delta\lambda$ to derive total flux, and hence Shot Noise).

2.3. Notes on Detector Operating Characteristics

The linearity of detector response is important, especially if
measurements are to be made over a wide magnitude range. Early work with
a PbS photoconductor was complicated by a non-linear response, although
it was found to be very sensitive (limiting magnitude, $m_K \sim 9.5$). Figure 2.3
shows the form of the response we obtained and also the measured variation
of detector impedance on stars of various magnitudes (at 2.2 µm).

It seemed that on faint sources ($m_K > 6$), where the sky background was
the dominant radiation, the sensitivity was constant (and the detector
impedance did not change). It was necessary to operate this detector at
5 Hz, with a square-wave chop, for best results.

The new InSb detector, with a more sophisticated pre-amplifier circuit,
has shown good linearity. Tests on the telescope covering a magnitude
range of at least 8^m have shown no detectable non-linearity. The detector
should be able to measure over a range of 15 magnitudes and a linear response
is anticipated (the photovoltaic detection process should generate a
current in proportion to the incident radiation).

More tests are in progress but calibration against very faint stars
is limited by the accuracy to which standards are known. We have used some
stars down to $m_K = +10$, from measurements made by Allen (1973). We
currently use the InSb detector at ~ 20 Hz.

At 10 µm our sensitivity (using an 8-13 µm filter) is apparently
limited by the emission from the ring surrounding the secondary. This ring
(if included in an f/12 detector beam) has an area of 155 cm^2 and an
emissivity ~ 1; the reflecting secondary has an area of 1122 cm^2 with an
emissivity $\lesssim 0.1$. The ring thus emits at least as much "300K" radiation

PbS Detector Non-Linearity at 2.2μm
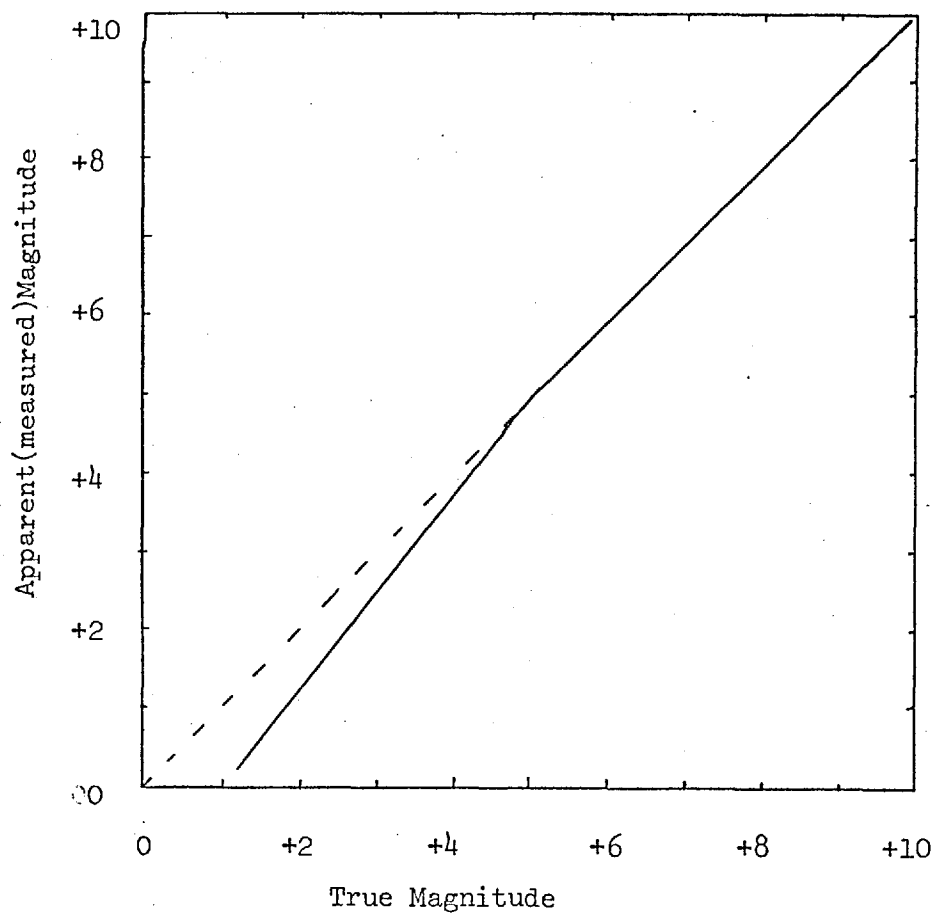
Notes:
Detector response
seems linear for
magnitudes fainter
than about +5.
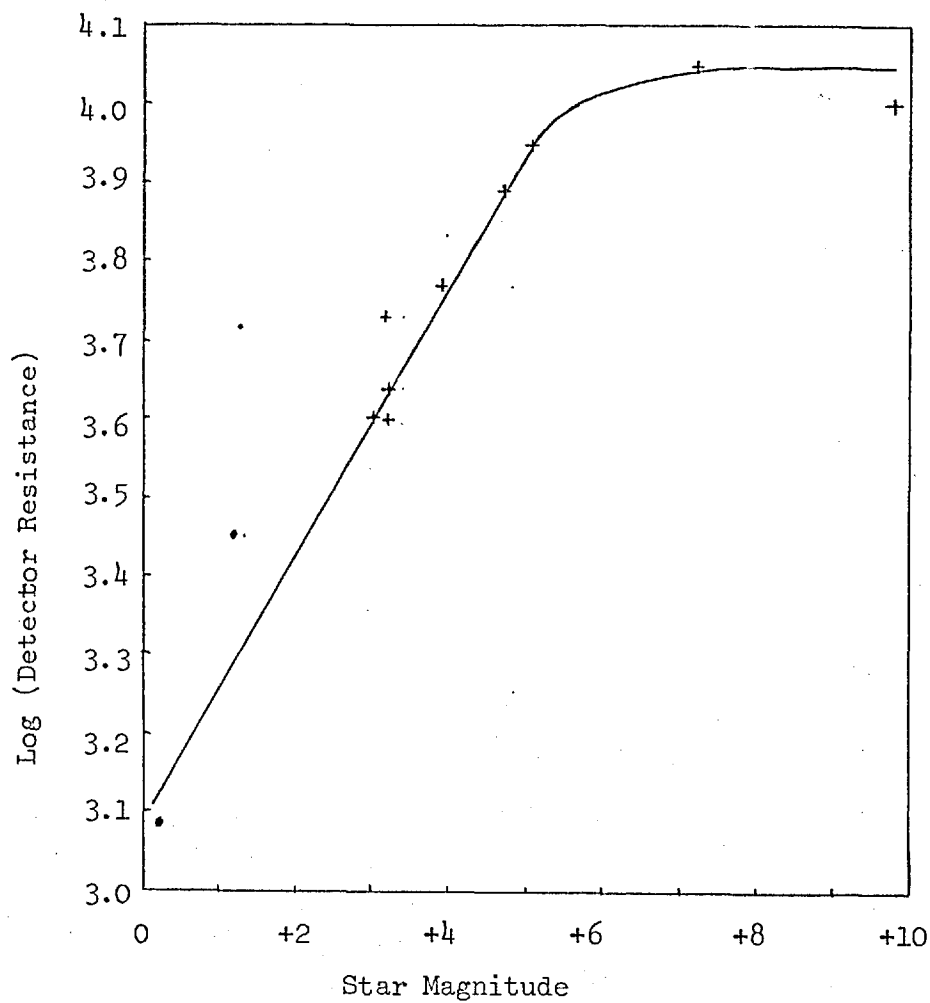
crosses are a mean
of measurements made
on several nights,
dots are single
measurements.

Figure 2.3

as the sky and mirror. Various solutions exist, the best is to cut the secondary down to a 38 cm diameter and remove the secondary stop.

The background falling on the detector can be reduced by using narrower (cooled) filters and thus better detection sensitivity (NEP's, see later) can be achieved. Previous work has mainly been done at 10 μm using Cu:Ge detectors but the superior As:Si ones are being adopted, although large improvements are not possible when "sky" emission (i.e. background shot noise) is dominant.

At 10 μm the background radiation on the detector is always dominant and even stars of $m_N = -5$ only impose a small addition to the normal radiation level. Thus linear response is expected and has been obtained in practice.

Detector properties are not necessarily stable. The PbS detectors had an impedance (and therefore sensitivity) which varied considerably, particularly if they were dried out by heating. Their performance deteriorated over a period of a few years. An InSb detector should exhibit a constant sensitivity, a variation in impedance only changes the noise level.

When first installed an InSb detector appeared to take over one hour to settle after cooling, however, this was later found to be a result of inadequate cooling of a filter blank. A Cu:Ge detector currently in use in the "Mullard" cryostat takes up to 12 hours after cooling, before its impedance reaches a stable level (2000 MΩ). This behaviour appears intrinsic to the detector rather than a result of very slow cooling.

2.4. Detector Electronics and Amplifiers

2.4.1. Photoconductor pre-amplifiers

The simplest method of using a photoconductive detector (e.g. PbS, Cu:Ge) is shown in Figure 2.4. A bias voltage is applied across the detector and load resistor, the signal voltage (a result of a radiation-induced conductivity change) is applied to the FET gate. An output signal from the source resistor is then taken to the main amplifier.

The arrangement in Figure 2.4 suffers from the fact that a change in detector impedance (from background radiation changes or otherwise) results in a change in the effective bias voltage. The sensitivity therefore is not constant. An improved pre-amplifier (based on a paper by Wyatt et al. 1974) has been recently adapted for use and is shown in Figure 2.5.

The circuit of Figure 2.5 (known as a "Trans-Impedance Amplifier") uses the virtual-earth property of an operational amplifier to maintain one side of the detector at 0 volts. A constant detector bias is thus ensured and the output is a direct measure of the signal current induced by the radiation. Note that in this circuit, mode A is the feedback configuration, and mode B is equivalent to the circuit of Figure 2.4, this facility is useful for test purposes.

This type of pre-amplifier has been used with a PbS detector and is now in use with an As:Si detector.

The detector is considered as a current source for purposes of analysis.

Incident Radiation P (W) generates a current, $i = P \cdot R_i$

where, the Current Responsivity (a function of bias voltage) $= R_i \; (AW^{-1})$

the Output Voltage, $V_o = R_i \cdot R_f \cdot P$

Typical values of R_i would range from 1mA − 1A per watt.

"SIMPLE" DETECTOR PRE-AMPLIFIER

Helium Temp.   Nitrogen Temp.
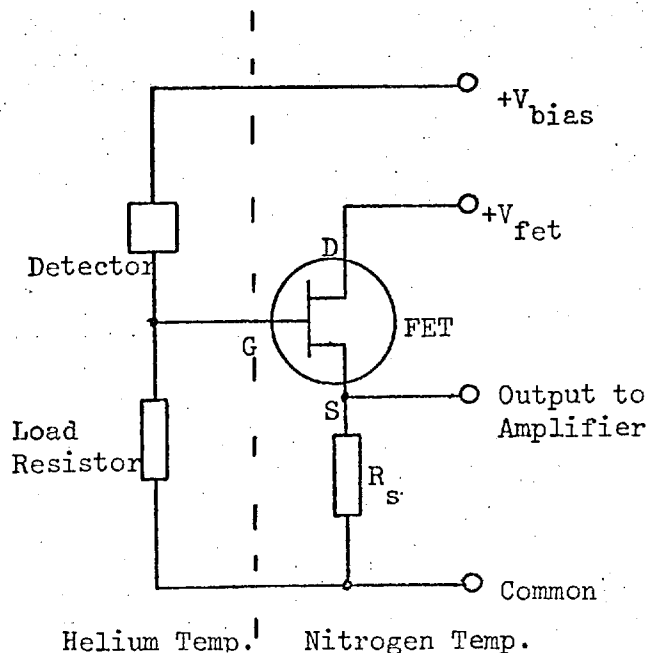
Sensitivity of Simple Preamplifier and Detector

Effective bias voltage across detector $= V_{bias} - V_G$

FET gate voltage $V_G \simeq V_o$ (source follower configuration)

V_o = output voltage for a radiation signal W

R_L = Load resistance , R_D = effective detector impedance

Sensitivity $S = \dfrac{dV_o}{dW} \propto V_{bias} \cdot \dfrac{R_L \cdot R_D^2}{(R_L + R_D)^2}$

Johnson noise voltage $V_N = (4kTR_p)^{\frac{1}{2}}$ (in a 1Hz bandwidth)

where $R_p^{-1} = R_D^{-1} + R_L^{-1}$.

Maximum sensitivity requires $R_L = R_D$

Maximum signal/noise , $\dfrac{dS}{dV_N} = 0$, requires $R_L = R_D/2$
(if Johnson noise limited)

Constant sensitivity is obtained if $R_L \ll R_D$
at the expense of lower sensitivity

Figure 2.4

FEEDBACK PRE-AMPLIFIER USED FOR A HELIUM COOLED IR DETECTOR

| Helium cooled | Nitrogen cooled | Room temperature |

Feedback Resistor R_F

Dual FET

+V_{cc}

Output B

A B

Normal Output A

Detector

R_D

-Vcc

Common

+V_{bias}
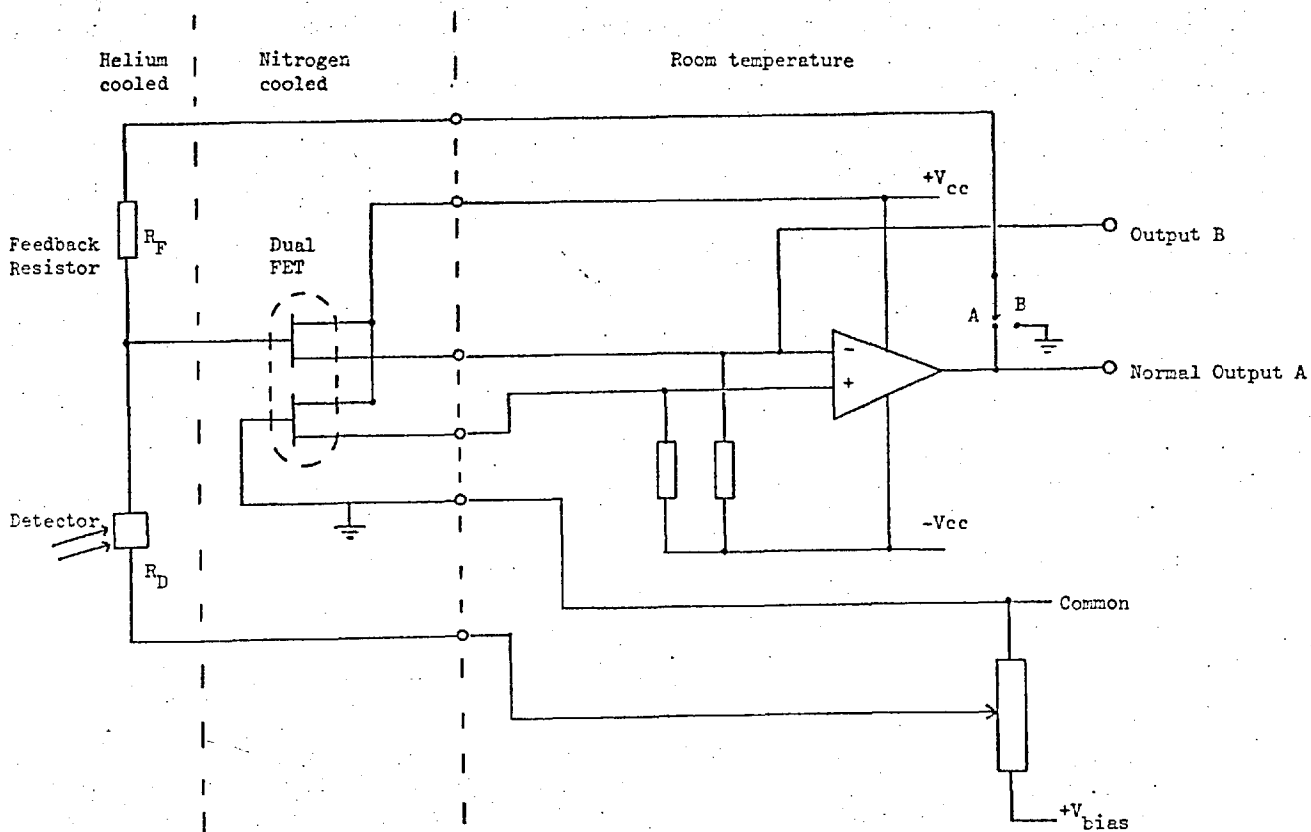
Noise-equivalent Circuit

C_f

R_f

R_c

Δi

R_d

C_d

i_n

v_n

C_c

A

V_o

Common
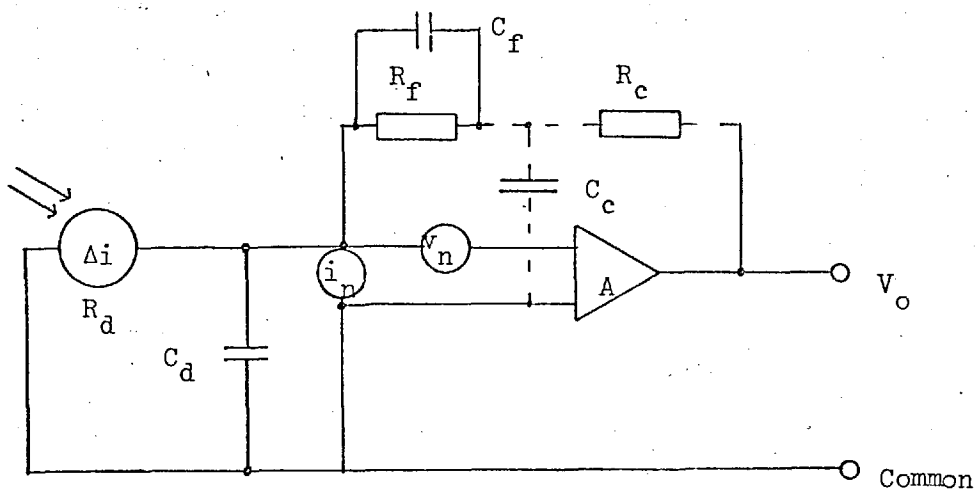
R_c & C_c are (optional) frequency compensation components,

where $R_c \cdot C_c = R_f \cdot C_f$, and $R_c \ll R_f$ normally.

Figure 2.5

The detector has a Johnson current noise $i_{DN} = (4kT/R_D)^{\frac{1}{2}}$ A Hz$^{-\frac{1}{2}}$

this results in an output voltage noise $V_{DN} = (4kTR_F^2/R_D)^{\frac{1}{2}}$ V Hz$^{-\frac{1}{2}}$

the feedback resistor also contributes $V_{FN} = (4kTR_F)^{\frac{1}{2}}$ V Hz$^{-\frac{1}{2}}$

The total Johnson noise at the output is therefore,

$$V_{JN} = (V_{DN}^2 + V_{FN}^2)^{\frac{1}{2}} = (4kT\, R_{Eff})^{\frac{1}{2}} \quad \text{V Hz}^{-\frac{1}{2}} \quad \ldots\ldots\ldots \quad (2.1)$$

For example, at 4.2K, if $R_F = 10^9$ Ω, $R_D = 10^{10}$ Ω,

$\therefore V_{JN} = 0.5\ \mu V\ Hz^{-\frac{1}{2}}$. See Figures 2.6 and 2.7 for graphs of R_{Eff} and

V_{JN} respectively. Here $R_{eff} = R_F (1 + R_F/R_D)$.

The radiation background (P_c) generates a current $i_c = R_i \cdot P_c$

this has a shot noise fluctuation, $i_N = (2\ e\ i_c)^{\frac{1}{2}}$

output voltage shot noise, $V_{SN} = R_F\ i_N = (2\ e\ V_c\ R_F)^{\frac{1}{2}}$ .... (2.2)

V_c, the DC output produced by the background $= i_c\ R_F = R_i\ P_c\ R_F$

The above relations may be combined to show that the shot noise will

exceed the Johnson noise (for $R_D > R_F$)

when $V_c > \dfrac{2kT}{e} = 0.7$ mV

(from equations 2.1, 2.2 we require $V_{SN} > V_{JN}$, hence $2\ e\ V_c\ R_F > 4kT\ R_F$)

There are, in practice, other contributions to the output noise. The detector may exhibit excess noise (see Section 2.5) and the pre-amplifier input noise must be considered. The input noise voltage of the FET is an important parameter and values of < 10 nV Hz$^{-\frac{1}{2}}$ are quoted for the 2N 6484 N-channel J FET (at 300K, 10 Hz).

This input noise is amplified if the operating frequency is $(2\pi f) > (R_F\ C_T)^{-1}$; the maximum amplification of noise is by a factor $(C_F + C_T)/C_F$, when $(2\pi f) \geq (R_F\ C_F)^{-1}$. C_T is the total input capacitance, typically ~ 10 pF; C_F is the feedback capacitance, typically ~ 0.5 pF $\therefore$ Maximum noise amplification should not exceed $^{10}/0.5 = 20$.

TIA Amplifier - Johnson Noise Effective Impedance $R_{Eff}=R_F(1+R_F/R_D)$
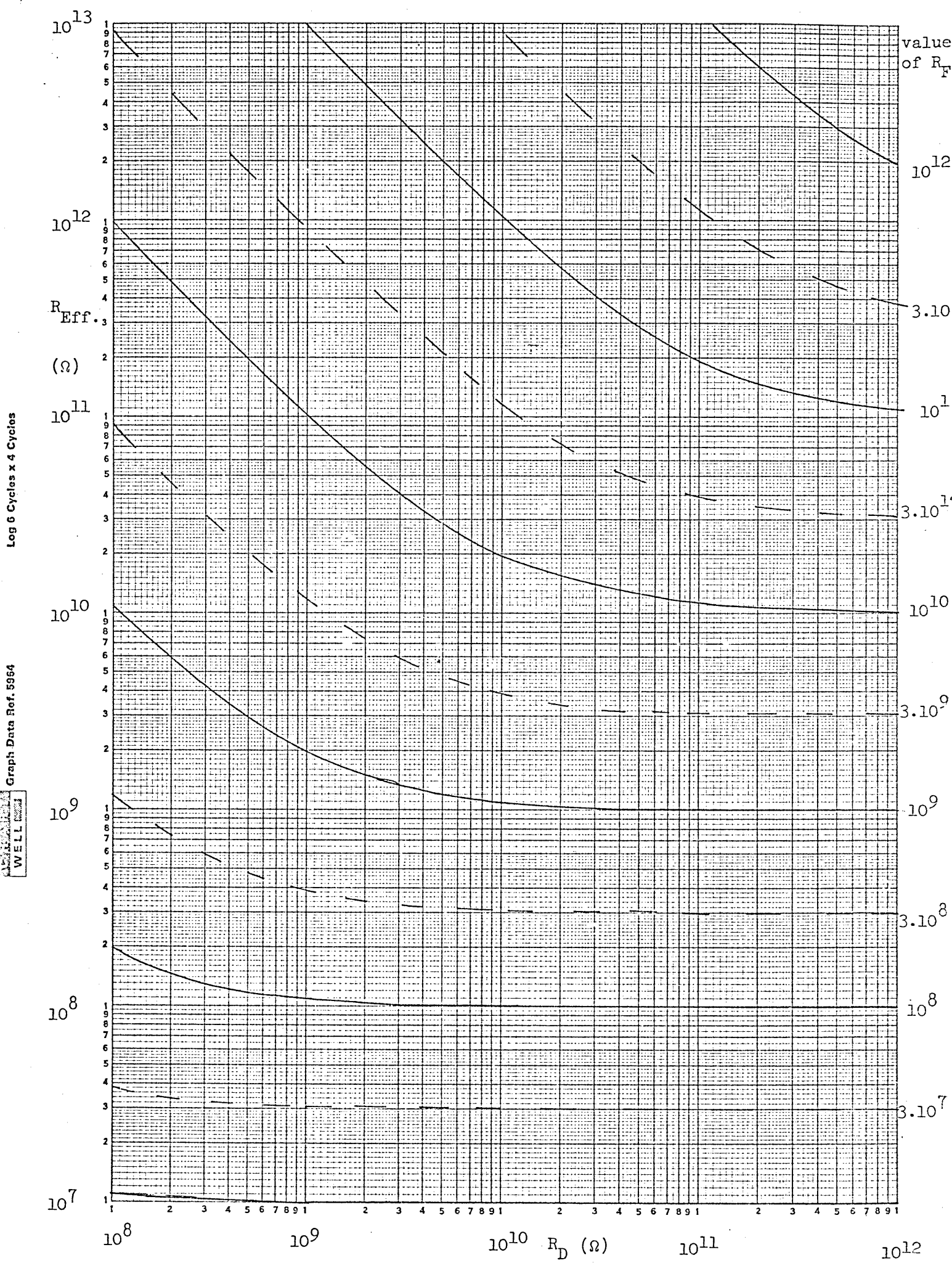
Figure 2.6

44
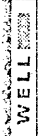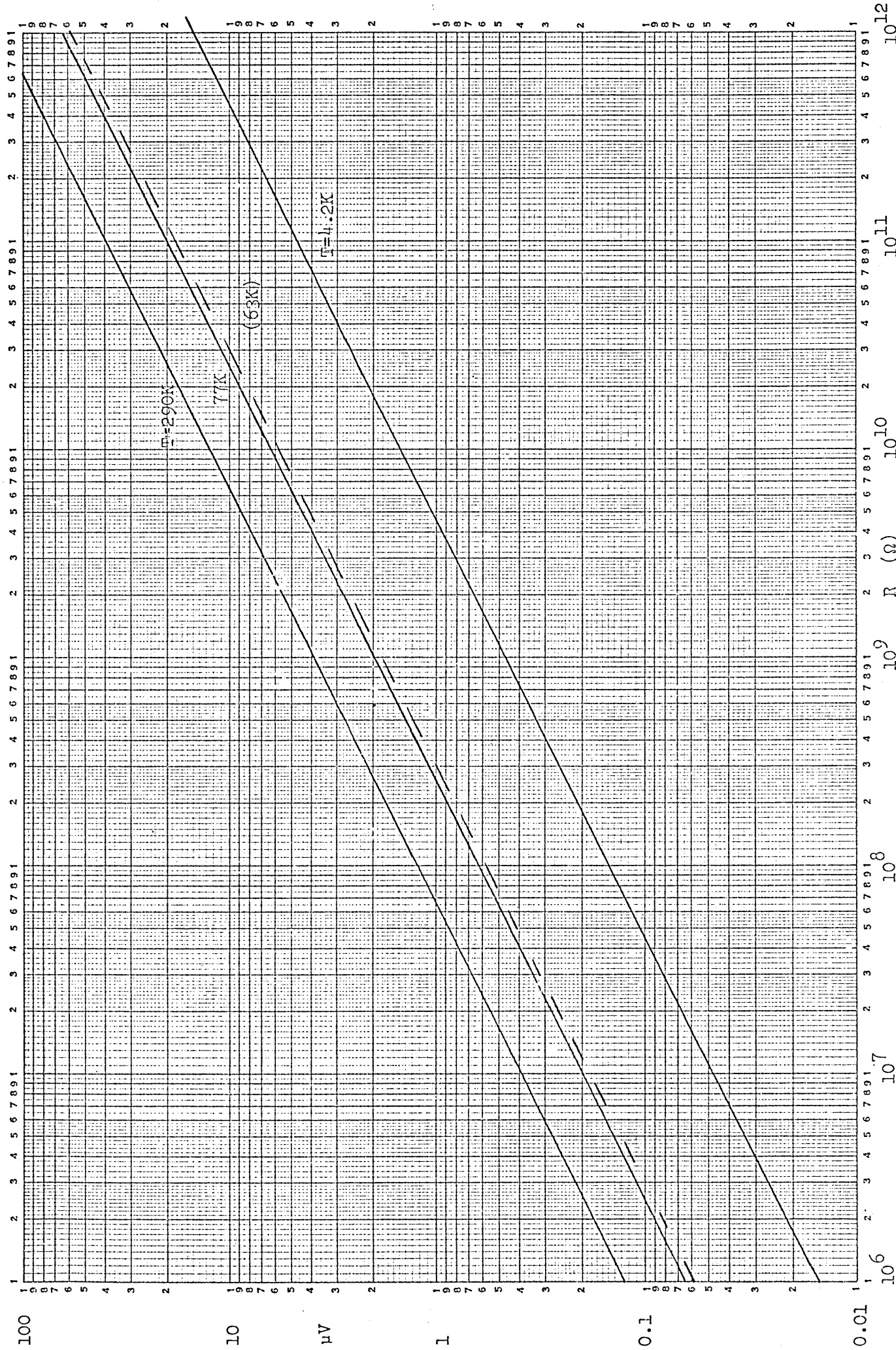
Figure 2.7

The simple bias arrangement gave a "fall-off" in frequency response as a result of input capacitance (e.g. across the detector), the corresponding time constant was $\tau = R_p C_D$. R_p is the parallel resistance of R_D and R_L. For $R_p \sim 10^{10} \Omega$, $C_D \sim 10$ pF, $\therefore$ $\tau \sim 100$ mS.

The negative feedback of the TIA pre-amplifier reduces the effect of input capacitance by a factor A, where A is the open-loop gain (typically $\sim 10^5$). It can be shown that this gives a time constant $\tau = R_F (C_F + C_T/A) \sim R_F C_F$. For $R_F \sim 10^{10} \Omega$, $C_F \sim 0.5$ pF. $\therefore$ $\tau \sim 5$ mS.

By means of frequency compensation components R_c, C_c it is possible to compensate for the effects of the capacity across the feedback resistor. If values of these components are chosen such that $R_c . C_c = R_F . C_c$, then $\tau = R_F (C_F + C_T)/A$, (theoretically, if $R_F \sim 10^{10}$, $C_p \sim 10^{-11}$F, $\therefore$ $\tau \to 1\mu s$).

It is therefore possible to get a large improvement in operating frequency range. However, in the fully compensated circuit, the input noise is amplified by a factor of $R_F (C_F + C_T) 2\pi f$, at an operating frequency f. If we operated at a maximum frequency $f \sim \frac{1}{2\pi \tau}$, then the input noise could be multiplied by a factor = A. This increase in noise limits the operating frequency in practice.

Further details of the circuit analysis are given by Wyatt et al. (1974), and examples of its use with an As:Si detector are given in Section 2.5. In summary, this pre-amplifier allows useful operation up to ~ 100 Hz (for typical values of R_F, C_F); the output response is linear, although optimum values of detector bias need to be chosen.

Under very low background conditions the Johnson noise of the feedback resistor may control the NEP ($= (4kT \Delta f)^{\frac{1}{2}}/R_i (R_F)^{\frac{1}{2}}$, if $R_F < R_D$). A high value of R_F is optimum. At larger background levels shot-noise

limited operation should be possible. (For example, with $R_F = 10^9 \Omega$, $R_i \sim 30$ mA W^{-1}, background $\sim 10^{-8}$ W, equation 2.2 gives : output shot-noise ~ 10 μV).

2.4.2. The Indium Antimonide detector pre-amplifier

The present use of an InSb photovoltaic detector has required the use of a modified circuit as shown in Figure 2.8. A similar pre-amplifier was fully described by Hall et al.(1975).

The circuit maintains a zero voltage bias across the detector and the output is a direct measure of the current generated by the radiation falling on the InSb junction. A summary of the relevant equations, which describe the operation of the detector, are given in Figure 2.8.

It is important that the circuit is adjusted so that the voltage across the detector is zero. This ensures that the detector can only generate Johnson noise (in the absence of radiation, any excess noise violates thermodynamic principles). With high backgrounds it is possible for the photon shot noise to be dominant. At low backgrounds, if the bias exceeds ~ 10 mV an increase in noise is evident (the noise nearly doubles when bias is ~ 10 mV).

The detector response is linear over a wide range of intensity when operated in the mode described, the sensitivity should not vary with background level or detector impedance. However, the voltage response is proportional to the value of feedback resistance (R_F), and it is important that this has a linear voltage-current characteristic. At high frequencies the response is reduced mainly by the effects of stray capacitance across R_F.

Photovoltaic Detector Preamplifier
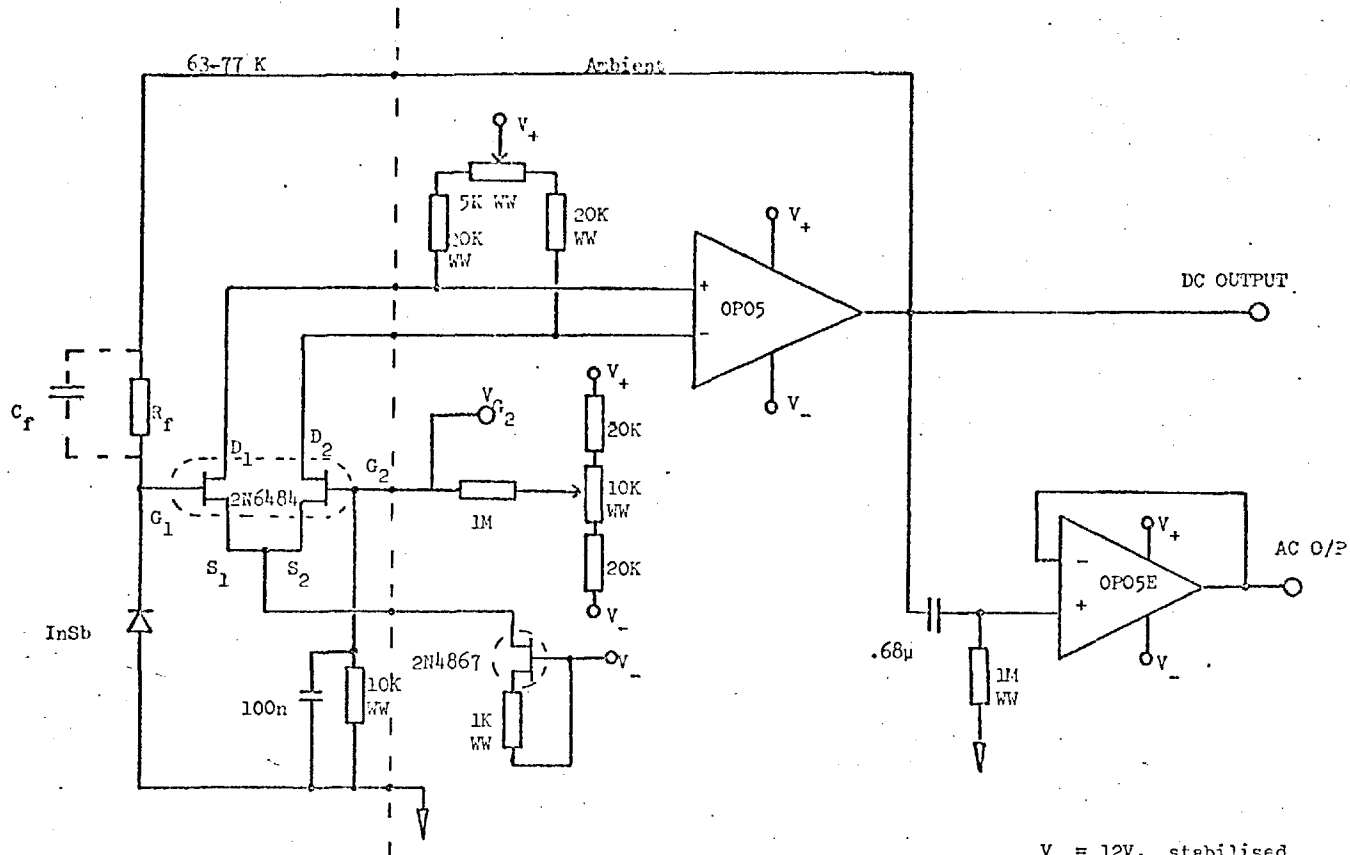
V_+ = 12V. stabilised
V_- = -12V. stabilised

N.B. The detector bias, V_{G2} can be switched to 0 Volts.

Operating Theory

Signal Current I_s = ηeN , Output Voltage $V_o = R_F \cdot I_s$

where N = total no. of photons/sec. = $\int \frac{F_\lambda}{h\nu} d\lambda = \lambda P_\lambda /hc$

F_λ = Incident Radiation (W μm^{-1}) , P_λ = Monochromatic Power (Watts)

Johnson Noise Current from Detector $I_n = (4kT\Delta f/R_D)^{\frac{1}{2}}$

Hence, the Noise Equivalent Power - NEP= $\frac{P_\lambda}{(I_s/I_n)} = \frac{(4kT)^{\frac{1}{2}} hc}{e\eta\lambda R_D^{\frac{1}{2}}}$ (Δf=1 Hz)

The above result applies for Johnson noise limited operation,

the output signal is detector Johnson noise limited if $R_F \gg R_D$.

The NEP is the power(P_λ) for which the signal equals the noise in a 1 Hz

bandwidth. η = Quantum Efficiency (~constant from 1-5 μm)

e = Electronic Charge

Figure 2.8

Some typical values for the various parameters are given in Section 2.5.2. In addition to the points made earlier (and the analysis given by Hall et al.1975), there are a few additional points which are relevant.

A large radiation flux (background on signal) will cause a large output voltage; the dynamic range may be limited by the available output voltage of the circuit which is typically ± 9V. It is possible to compensate for the background by introducing extra feedback to cancel the background-induced DC current (without changing the signal-induced output). However, this technique can increase the Johnson noise at the output and this becomes a disadvantage under low background levels.

At present we find it convenient to change the value of R_F, thus changing our sensitivity, for different background levels. We use one value (e.g. $10^{10}\Omega$) for J, H, K filters and another ($5.10^8\Omega$) for L, M; this eliminates the problem of saturation at large backgrounds. It is possible to have several cooled resistors and a selector switch at room temperature, but the long leads that are required from the high impedance input are very susceptible to microphonic pick-up. A better solution is the use of a miniature latching relay which can be cooled to 77K in close proximity to the detector and resistors; it is activated by low impedance coils and only dissipates a small amount of power when it is changed over.

The pre-amplifier is set up by operating the detector under "zero" background (a 77K cooled blank); with $V_{G2} = 0$ the drain voltages are trimmed so that the output is zero (see Figure 2.6). A constant current source, or a regulated supply voltage, is used to ensure stable conditions.

The detector impedance is measured by recording the change in output current (V_{out}/R_F) as the voltage across the detector is changed. The detector bias (V_{G1}) follows the gate voltage of the other FET (V_{G2}) and this voltage can be adjusted over a range of about ± 100 mV. The detector impedance is therefore given by

$$R_D = \frac{\Delta V_G}{(\Delta V_{out} - \Delta V_G)/R_F}$$

2.4.3. Amplifiers

The signal from the detector pre-amp passes into a wide-band (1 Hz – 2 kHz) amplifier with a variable gain of $1-10^5$ (designed by A.D. Macgregor). The amplifier must have a constant gain over the range of frequencies used, especially when low frequency chops at 5 Hz are used. The relative gains must be accurate to better than 1% for precise photometry.

These requirements can be met by careful choice of components and 'normal' design procedure. The stability of the components is one of the most important considerations. The amplifier does not contribute to the noise normally although 50 Hz line pick-up can occur if the box is not well earthed.

The pre-amplifier and main amplifier are powered by batteries and it is particularly important that the bias voltage to the detector should not drift. Best performance has been achieved by the use of Manganese batteries (e.g. MN1604, 9V), these have a capacity which is roughly 3 x that of normal batteries. Mercury batteries have an even larger nominal capacity but they exhibit a serious drop in output voltage when cold (especially below 10°C).

2.5. Detector Tests

Introduction

Many parameters of the detector and circuitry need to be measured and optimised for maximum sensitivity, linearity and reliability. Some tests are made in the laboratory on a test arrangement as shown in Figure 2.9, but the final performance on the telescope is particularly important.

Absolute calibration can be performed using the black-body, although a more direct arrangement than that shown is sometimes used. Noise measurements are usually made using a Hewlett-Packard Spectrum Analyser. The cryostat stand can also be mechanically vibrated in a vertical plane to test for microphony.

2.5.1. Tests on a copper-doped germanium detector

A Cu:Ge helium-cooled photoconductor has been used for some time, mainly at 10 μm. It has been operated with the classic bias circuit as shown in Figure 2.4, a helium-cooled load resistor has been used. ("MOX" – 200 MΩ). Some measurements of signal and noise as a function of frequency are shown in Figure 2.10 – for an SBRC detector.

The detector response is found to fall off gradually with frequency (-3dB point $\sim$ 500 Hz), whereas the noise falls off sharply in a $^1/f$ form; this results in a peak signal/noise at around 300-500 Hz. These tests were performed when $R_D \sim 200$ MΩ (although the detector resistance attains a value of ~ 2000 MΩ six to ten hours after cooling).

Further tests were performed on a similar (Quist) detector, of area 2 x 4 mm^2 (in a Thor cryostat). Figure 2.11 shows spectrum analyser measurements of detector noise versus frequency for various bias voltages.

OPTICAL TEST FACILITY

PLAN
VIEW

Cryostat Stand

Iris

Concave Mirror

Monochromator

Flat Mirror

Filter Holder

Chopper

Black Body

PARTIAL

SIDE

VIEW

Detector Position

Cryostat Stand

TEST ELECTRONICS

IR Detector

Amplifier

Chopper

Scope

P.S.D.

Phase Shifter

reference

DVM

Chart Rec.
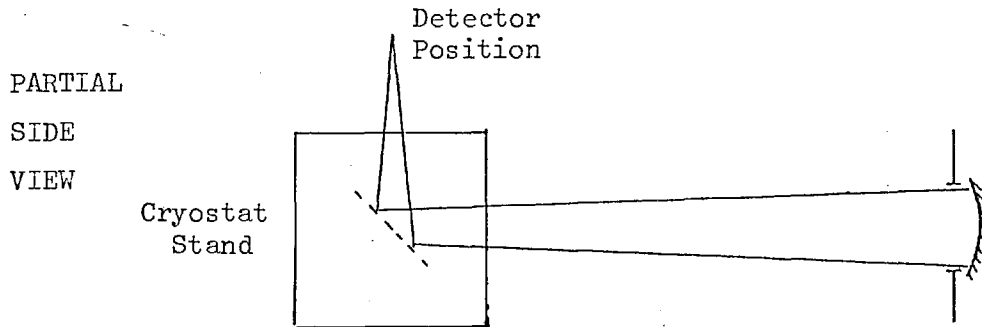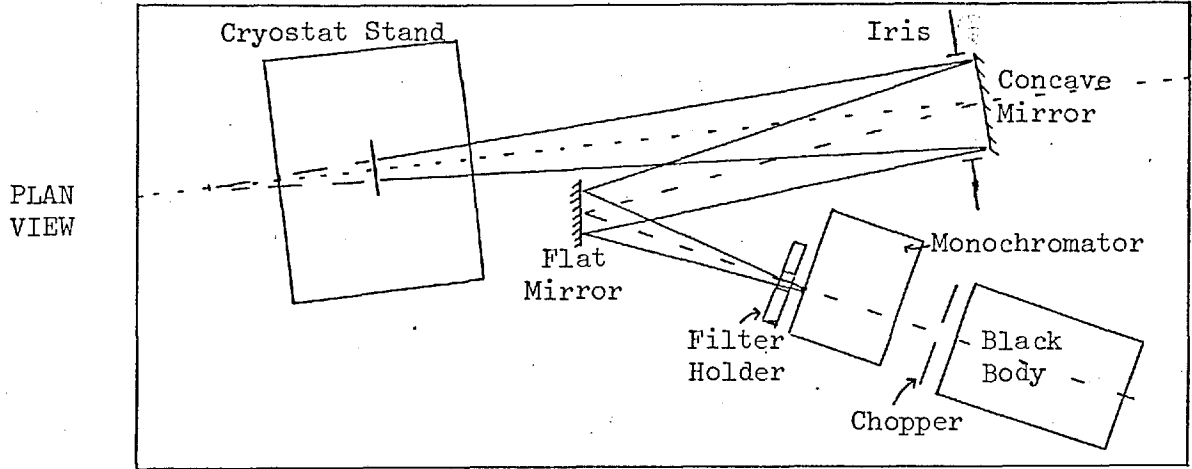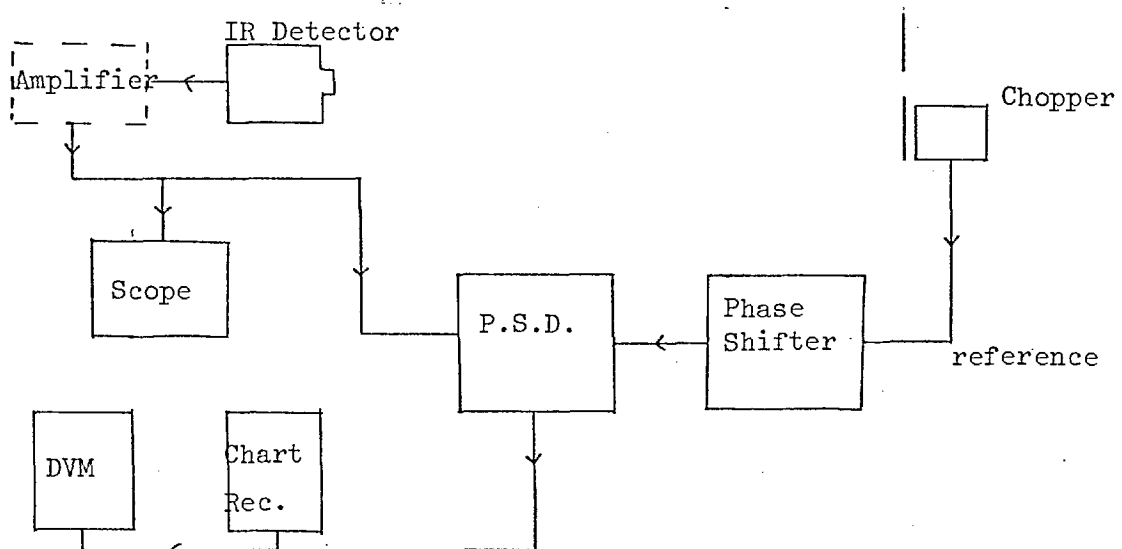
Figure 2.9

SIGNAL & NOISE TESTS ON Cu:Ge DETECTOR IN "MULLARD" CRYOSTAT

Figure 2. 0

52
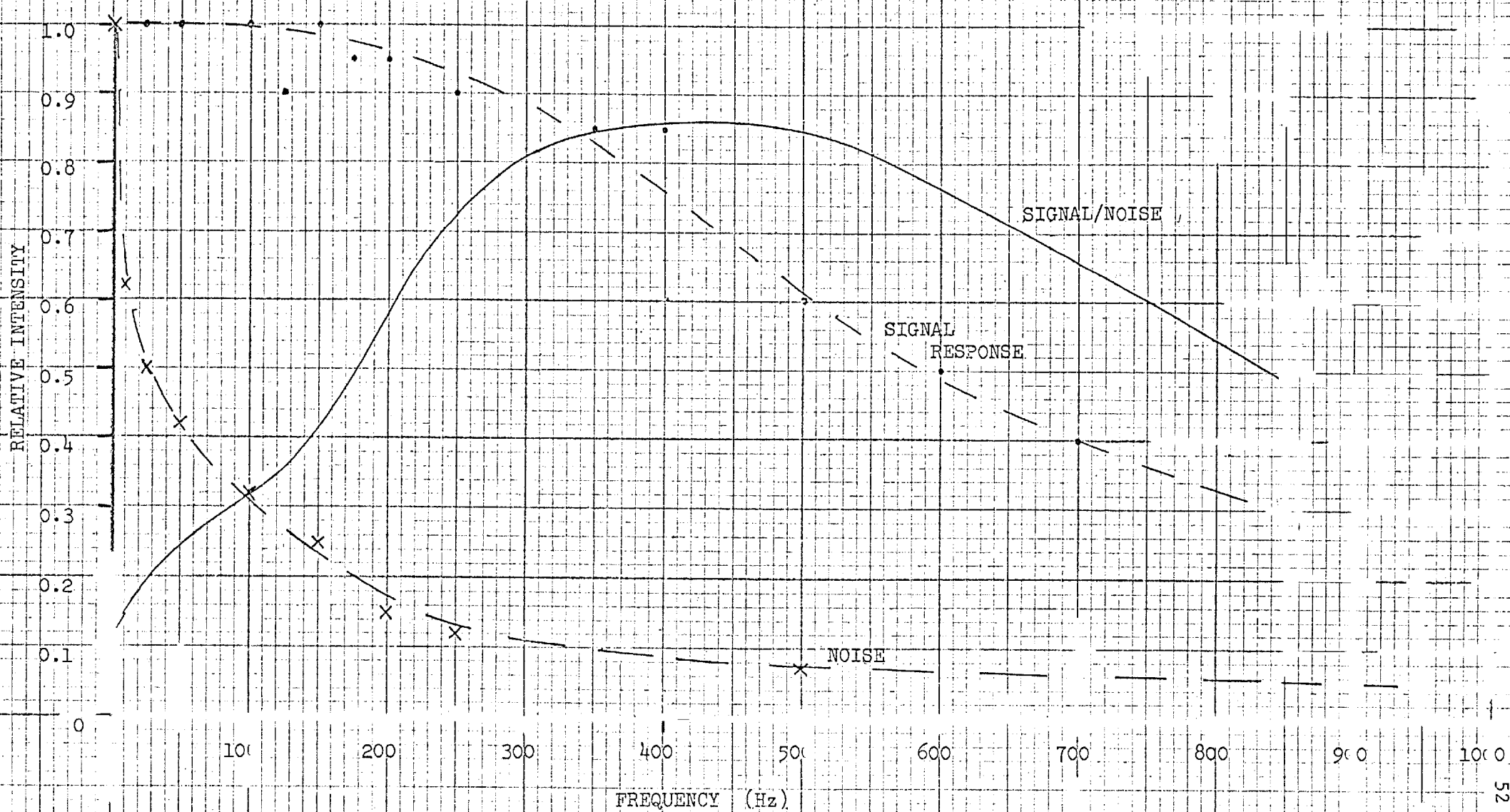
Cu:Ge Detector Response as a function of frequency

Detector
Noise
(for Detector
bias= 0-5V.)

Detector
Noise

(bias=0-13V.)

(30 Hz bandwidth)

Relative
Signal
Response
&
S/N Ratio

(at 5V. bias)
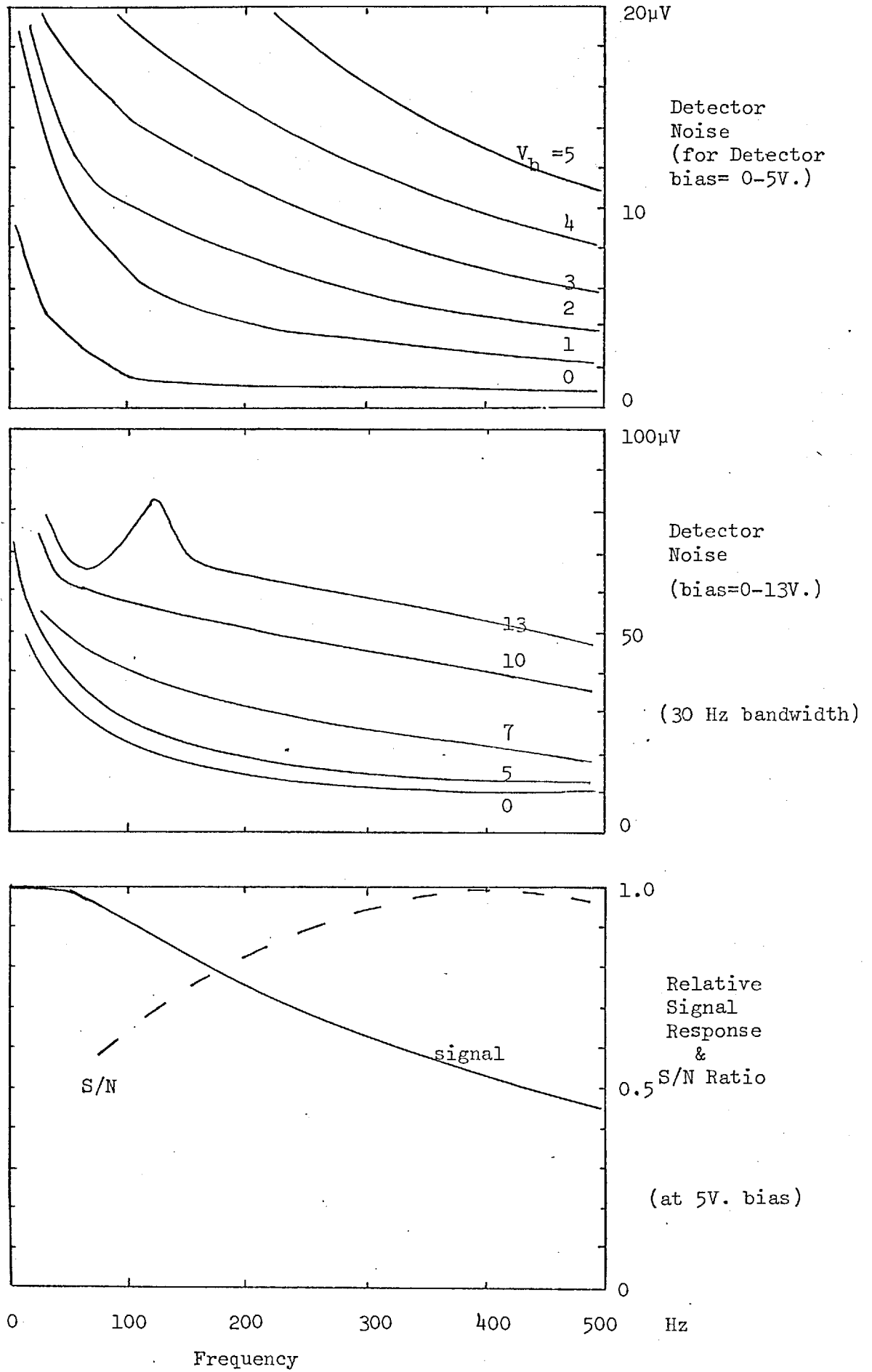
Frequency

Figure 2.11

The signal response as a function of frequency is also shown, together with the signal/noise ratio. (The rise of the noise curves for frequency < 50 Hz is mainly artificial, as a result of the spectrum analyser response).

In Figure 2.12a the variation of detector resistance with bias voltage is shown; the total effective impedance of the detector in parallel with the load is also shown. The load resistance was 100 MΩ (Eltec model 102) in this case. A reduction in the effective impedance gives a lower time constant and therefore an increase in response at a given frequency; for this detector a change in bias from 1-5V only reduced R_p slightly (as in Figure 2.12a).

In Figure 2.12b the signal response, detector noise and S/N ratio are plotted as functions of bias voltage, at 300 Hz. It is seen that a detector bias of 2-3 volts and a chop frequency of 300-500 Hz give best results. (A bias of 2 volts corresponds to a field of 5 Vcm^{-1} across the detector). It was also found that a 9V FET bias gave less noise than an 18V bias (due to reduced gate reverse current with a lower drain voltage). A U184 FET was used with a 51KΩ source resistor.

2.5.2. Indium Antimonide detector performance

The InSb photovoltaic detector operates well at 77K with a wavelength response out to $\sim$ 6 μm. As shown earlier (Figure 2.6) an operational amplifier and feedback resistor R_F maintain a zero bias voltage. The feedback resistor(s) are mounted as close to the detector, and as rigidly as possible. Matched JFETs (also mounted nearby at 77K), together with a constant current source, give drift-free operating conditions when carefully set up. The use of value of R_F > R_D results in an output noise which is dominated by the detector Johnson noise contribution.

Cu:Ge Parameters as a function of Bias Voltage

(a)

Effective
Parallel
Resistance

$$R_p^{-1} = R_D^{-1} + R_L^{-1}$$

(b)

Signal response
Detector noise,
& S/N ratio

versus Det. bia

(arbitrary
linear
scale)
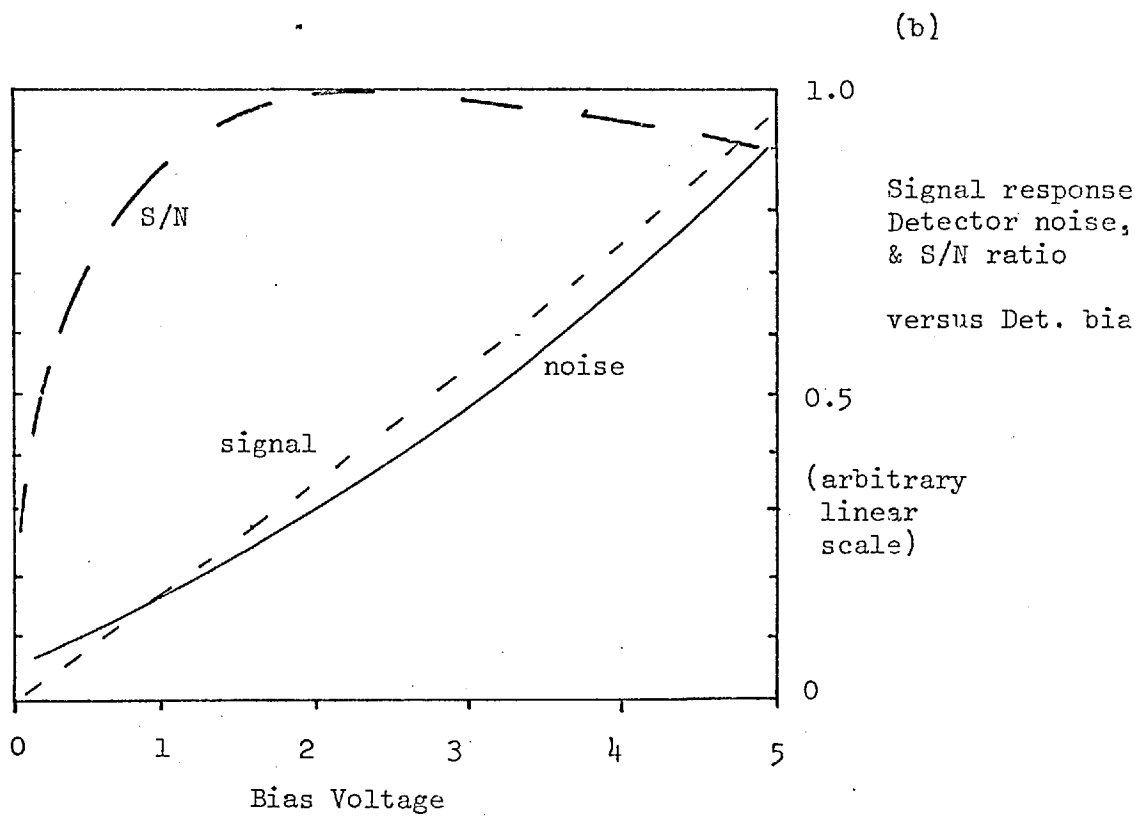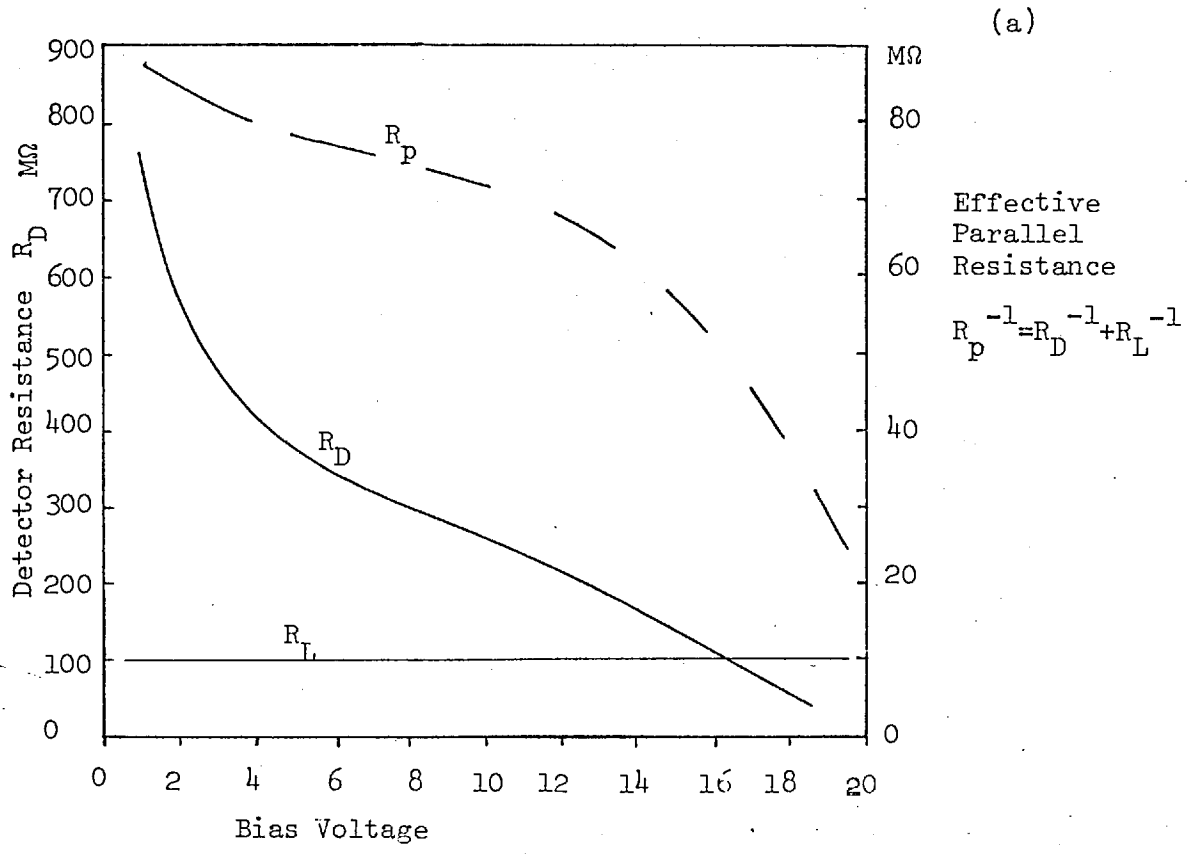
Figure 2.12

Some characteristics of an SBRC 0.5 mm square detector, as measured (February 1977) by A.D. MacGregor, are given below.

Load Resistance, R_F	=	7500 MΩ
Detector Resistance	=	500 MΩ @ 77K
Measured Output Voltage Noise, V_N	=	20 μV $Hz^{-\frac{1}{2}}$
Theoretical Johnson Noise	=	20 μV $Hz^{-\frac{1}{2}}$
Measured Voltage Responsivity, R_V	=	5.7×10^9 V W^{-1} @ 2.2 μm
Corresponding Current Responsivity, R_I	=	0.76 A W^{-1}
Theoretical Maximum Response	=	1.8 A W^{-1} (from Fig. 2.8)
Derived Operating NEP, ($^{V_N}/R_V$)	=	4×10^{-15} W $Hz^{-\frac{1}{2}}$
(Signal level used	=	6×10^{-12} W)

When cooled to 63K and hypersensitised (Section 2.5.5.),

Detector Impedance	=	10^{11} Ω (R_F = 7500 MΩ)
Theoretical Johnson Noise	∿	5 μV $Hz^{-\frac{1}{2}}$
Measured Output Noise	∿	15 μV $Hz^{-\frac{1}{2}}$
∴ Measured Minimum NEP	∿	3.10^{-15} W $Hz^{-\frac{1}{2}}$
With $R_F \geq 10^{11}$ Ω, an NEP	∿	3.10^{-16} W $Hz^{-\frac{1}{2}}$ should be possible.

2.5.3. Arsenic-doped silicon detector tests

This photoconductor (supplied by SBRC) is used with a T1A pre-amplifier (Figure 2.5). The detector and feedback resistor are cooled to 4.2K; helium cooled MOSFETs and Nitrogen-cooled JFETs have been tested.

Early tests were made with a Siliconix 2N5197 dual JFET, cooled to 77K; a feedback resistance of 26,000 MΩ was used. A narrow band (8-9.5 μm) filter was used to restrict the room temperature radiation falling on the detector to 2×10^{-9} W (with a shot noise of ∿ 6×10^{-15} W $Hz^{-\frac{1}{2}}$). Some results are presented below.

5V bias, 300K background; Detector Resistance $= 2 \times 10^{11} \, \Omega$

(this value varied from 2.8-1.5 $\times 10^{11}$ as bias changed from 1-10 volts)

5 Hz, 20V bias, 4.5×10^{-10} W signal; Voltage Response $= 3 \times 10^{8} \, V \, W^{-1}$

$R_F \sim 2.6 \times 10^{10} \, \Omega$, $\therefore$ Current Responsivity $\sim 10 \, mA \, W^{-1}$

Expected Photon Shot Noise, $3 \times 10^{8} . 6 \times 10^{-15}$ $\sim 2 \, \mu V \, Hz^{-\frac{1}{2}}$

Expected Johnson Noise from R_F $\sim 2.5 \, \mu V \, Hz^{-\frac{1}{2}}$

Measured Output Noise $= 2 \, 5 \, \mu V$

$\therefore$ Derived NEP, $2.5 \times 10^{-6}/3 \times 10^{-8}$ $\sim 10^{-13} \, W \, Hz^{-\frac{1}{2}}$

Graphs of signal response and noise, at 5 Hz, are shown for mode A (T1A) in Figure 2.13. The measured frequency responses, mode A and mode B (non-feedback method), are given in Figure 2.14. It was found that $\sim$ 10V bias and 20 Hz operating frequency gave minimum NEP, although the excess noise prevented a lower NEP from being attained. The signal and noise varied non-linearly with bias voltage, the effect is not explained, but has not been found in more recent tests by A.D. MacGregor.

Further work has been done with a helium-cooled MOSFET (to replace the JFET). This should have the advantage of less gate leakage, higher input impedance, and close proximity to the detector (which greatly reduces microphone problems). A pre-amplifier (recommended by "Rockwell") is shown in Figure 2.15, a Siliconix M103 MOSFET is used.

Tests were performed with this arrangement and similar results to the previous ones were obtained. An NEP $\sim 10^{-1.3} \, W \, Hz^{-\frac{1}{2}}$ was measured. Noise in excess of the Johnson Noise or background shot noise was again obtained, this can be attributed to detector "contact" effects or pre-amplifier noise. Substitution of a larger value of feedback resistor gave a larger output noise than should have been obtained.

As:Si Detector Signal & Noise versus Bias Voltage

Signal & Noise measured at 5Hz

Figure 2.13

As:Si Detector Frequency Response
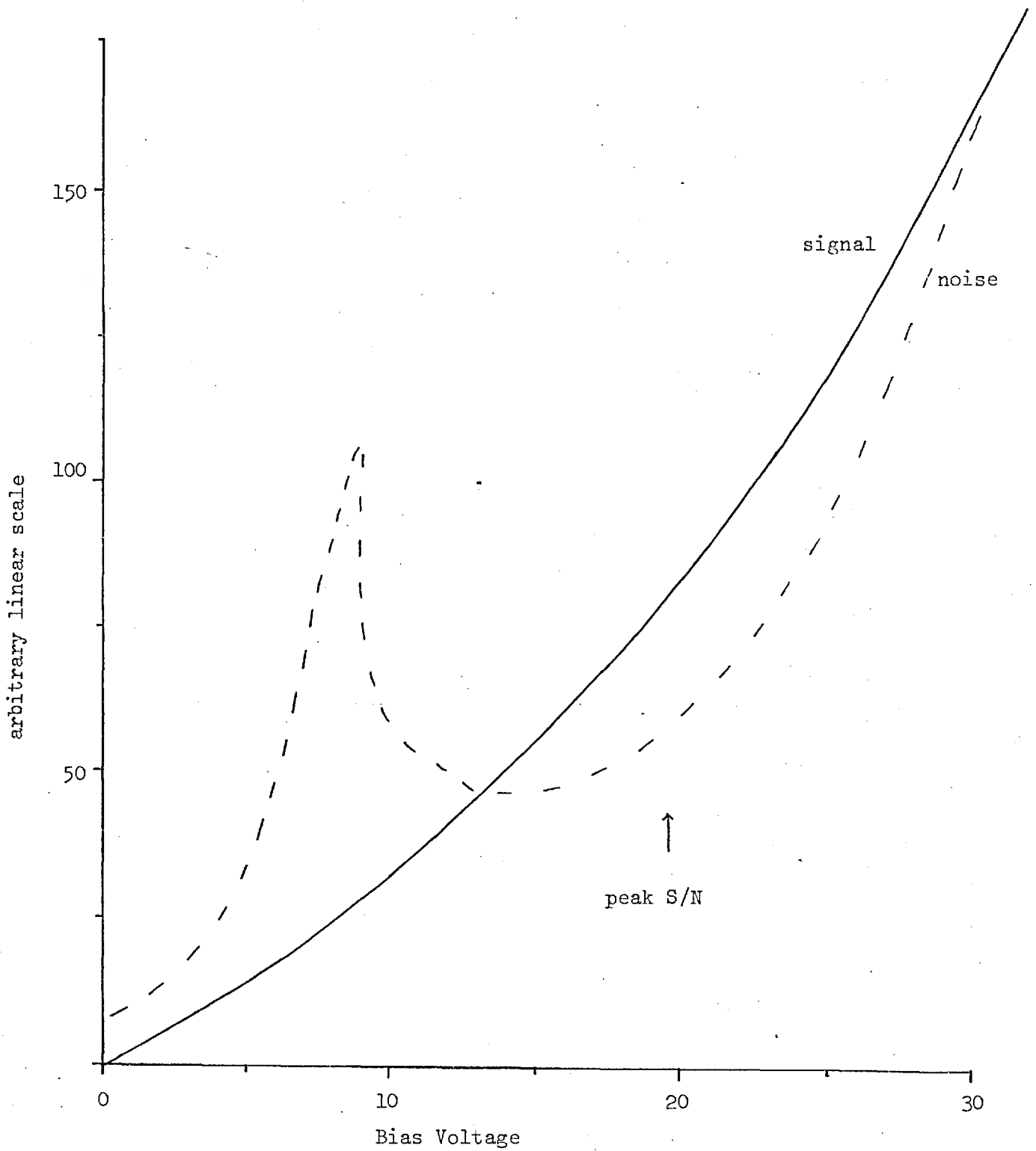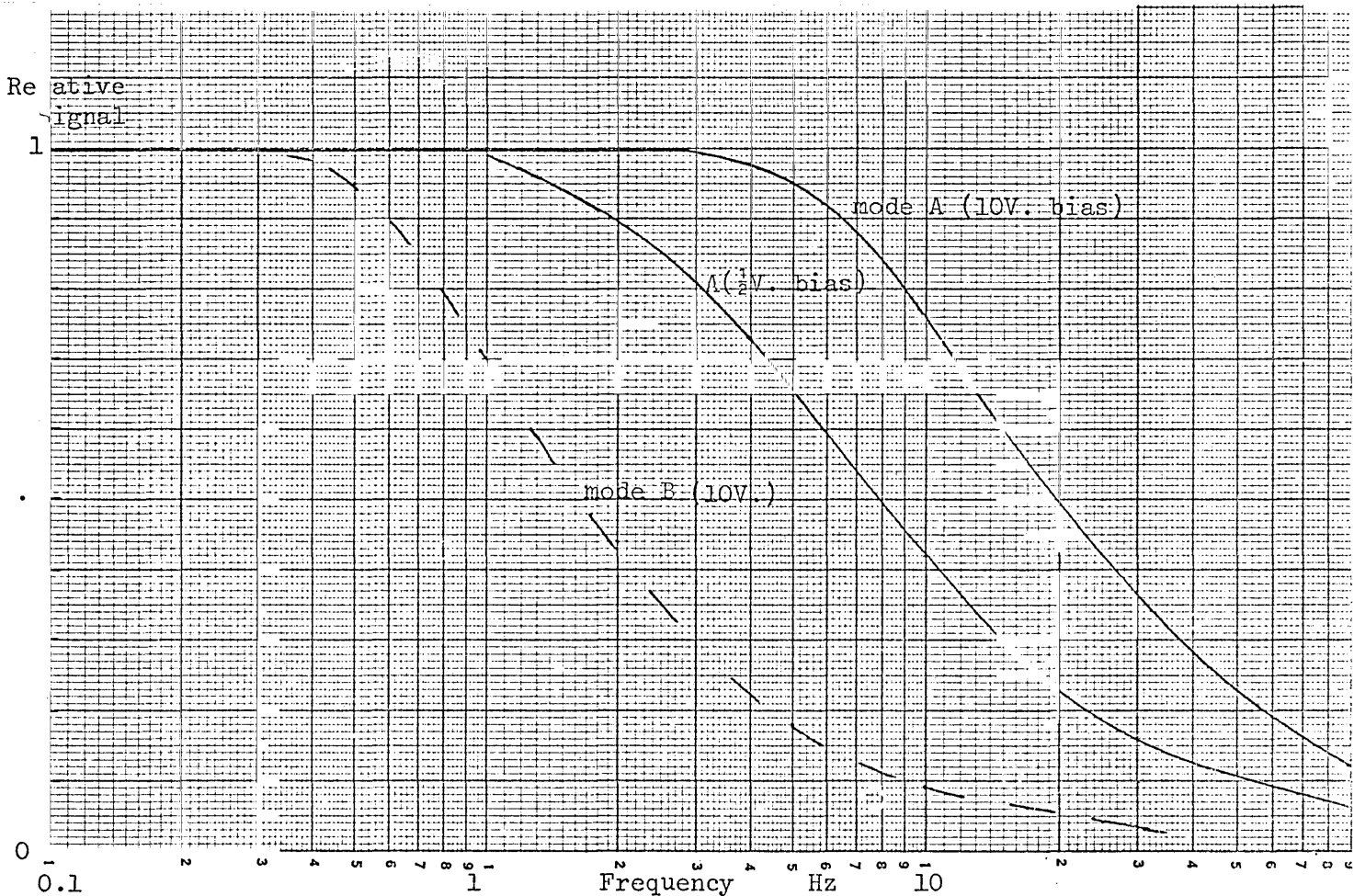
mode B (simple bias circuit) $\tau = R_p(C_T + C_F)$, $R_p^{-1} = R_D^{-1} + R_F^{-1}$

$R_F = 2.6 \ 10^{10} \ \Omega$, $R_D = 1.5 \ 10^{11} \ \Omega$ (load & detector impedances, @ 10V. bias)

measured frequency response indicates a time constant(τ) of ~ 0.16 s ,

hence total input capacity $\sim 7pF$ - approximately as expected(from FET mainly).

mode A (feedback TIA circuit) $\tau = R_F(C_F)$

measured frequency response shows a time constant $\tau = 13$ ms ,

hence capacitance of feedback resistor $C_F \sim 0.5pF$

The feedback resistor had an impedance which varied with voltage and

therefore the time constant changed somewhat as the bias voltage was changed.

Figure 2.14

The "Rockwell" Preamplifier

4.2 K   Room temperature
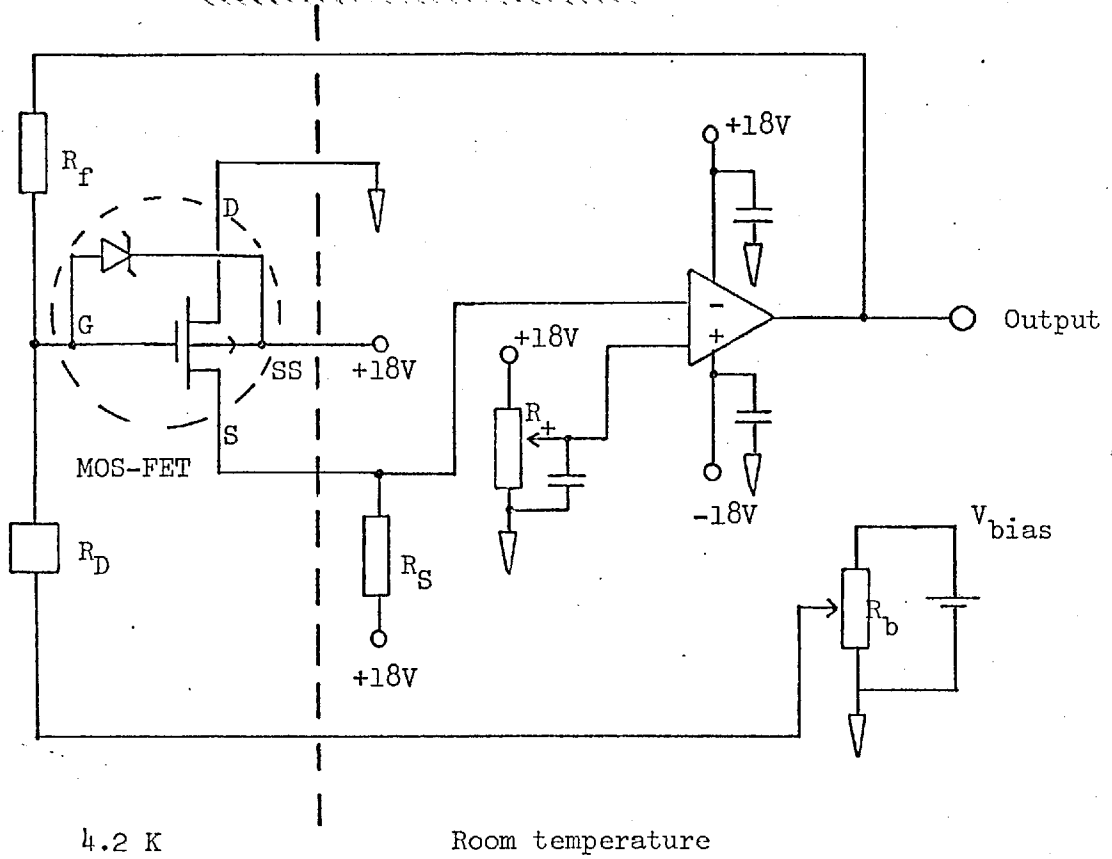
Operating Conditions

MOS FET : P channel M103 (with gate protection diode)

gate-source capacitance = 4pF

drain current I_D = ½ mA , V_{DS} ∿ -6V

hence, heat dissipation (at 4.2K) is 3mW .

R_S = 20 K WW , R_b = 100 K   , R_+ = 100 K

Figure 2.15

A non-linear variation of signal (and noise) with bias voltage was obtained again. The output noise varied from $\sim$ 20 μV (@ 20V bias) to 10 μV (@ 0V bias); this compares with an expected Johnson + background noise $\sim$ 2 μV. The current response was similar to previous values.

Further tests are still in progress on these detectors to determine precisely the optimum operating conditions. The main problem to solve is the excess noise production. Leakage current through the gate protection diode has been suggested as a possible noise source, although at 4.2K leakage should be negligible. A leakage current of 10^{-15} A has a noise of $\sim$ 2 x 10^{-17} A Hz$^{-\frac{1}{2}}$, which gives 2 μV Hz$^{-\frac{1}{2}}$ with a value of $R_F = 10^{11}\Omega$). A.D. MacGregor has tested an Intersil IT 1700 MOSFET (without protection diode) but still finds excess noise that appears to increase as the value of feedback resistor increases.

2.5.4. Component data

High value, compact load resistors are required for the detector circuits and two types are in use at present. Victoreen "MOX-400" resistors are available in values up to $10^{10}\Omega$ with lengths of 1-3 cm; Eltec "types 102, 104" semiconductor-glass resistors have values up to $2 \times 10^{11}\Omega$ and sizes as small as 3 mm. These resistances increase in value when cooled from 300K to 4.2K, by factors of 2 and 3 respectively.

A serious problem is that the Eltec resistors can have appreciable voltage coefficients; at 4.2K one resistance changed from 3300-1600 MΩ as V changed from 1-15 volts. At room temperature the voltage coefficient appears to be $\leq$ 0.3% V^{-1} for values < 100 MΩ although higher values exhibit larger changes. A "MOX-400" resistor (100 MΩ nominal at 300K) only changed by 4% as V changed from 1-10 volts at liquid helium temperatures. More tests need to be done to check the variation of voltage

(and to measure the noise) of these resistors when cooled; it appears that the "MOX-400" types may be superior if values of $R \leq 10^{10} \Omega$ are needed. R_F must be sufficiently high that detector noises exceed amplifier input noise sources.

The Field-Effect-Transistors that are used with the pre-amplifiers need to be chosen for low noise characteristics. The Siliconix 2N3089A or Intersil 2N6484 dual FET both have input noise values ~ 10 nV $Hz^{-\frac{1}{2}}$ (these are junction-FETS). The Intersil IT1700 MOSFET (without gate protection diode) is used at present, its noise is quoted as 150 nV $Hz^{-\frac{1}{2}}$ although ~ 1 µV $Hz^{-\frac{1}{2}}$ is typical for many MOSFETS (from A.D. MacGregor).

2.5.5. Future Developments

InSb - Hypersensitisation

The InSb detector has an NEP which is detector Johnson noise limited at 77K, for $\lambda \sim 2$ µm, in most cases. From Figure 2.8, the NEP $\alpha \; T^{\frac{1}{2}}/R_D^{\frac{1}{2}}$, if $R_F > R_D$; thus a reduction in temperature and an increase in detector resistance should give improvements. It has been found that the following procedure improves the NEP:

(a)   when cooled to 77K illuminate the detector with a bright radiation source (e.g. 100W lamp, through J filter, for about 5 minutes).

(b)   pump on the nitrogen until it freezes at $\sim$ 63K.

(c)   Repeat step (a).

The detector resistance can be measured at each stage (the preamp. is switched off whilst being "flashed"). An increase in detector impedance by a factor ~ 100 is possible although the effect of flashing cannot be fully explained at present. Tests (as mentioned earlier) have indicated a distinct improvement after the procedure, but the full theoretical drop in Johnson noise has not yet been achieved.

Electro Optical Feedback

The very large values of feedback resistor, with their corresponding shunt capacitances, are rather inconvenient to use. A light-emitting diode and Silicon photodiode can be used to provide an efficient method of feedback coupling, with a high effective impedance.

An example of this technique is shown in Figure 2.16a; this high speed pre-amplifier utilises the low capacitance of Si diodes to enable relatively high frequency operation with high impedance InSb detectors (the circuit is from KPNO). A 90/10% beam splitter gives a gain of x 10 in this circuit, allowing the use of smaller load resistors.

It is also possible to apply this method in order to compensate for the sky background radiation. An example of this is shown in Figure 2.16b; the circuit is used by Caltech at present. It should be noted that any background compensation contributes extra noise to the output (an amount equal to the background shot noise).

The main advantage of this feedback technique would seem to be the convenience of small size in some cases and low associated capacitance. A high linearity is also anticipated with the use of photodiodes, unlike the case with some high value resistors. The background compensation allows use of a constant high sensitivity without the need to reduce the feedback resistor to prevent saturation. The use of these circuits is under investigation at present.

Electro-optical Feedback

(a) KPNO Circuit
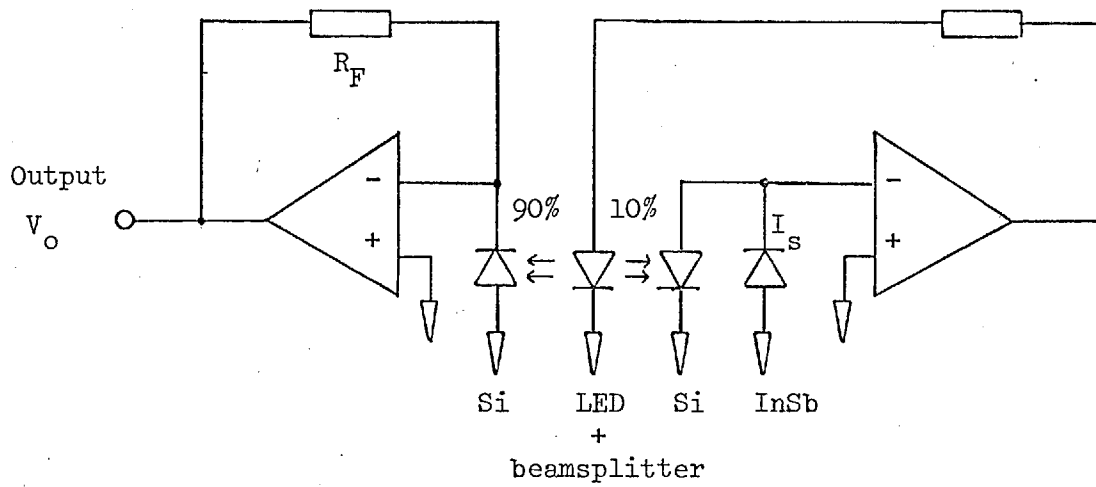
In the above circuit, with a 10/90 % beamsplitter

$$V_o = \frac{0.9}{0.1} \cdot R_F \cdot I_s$$, where I_s = signal current from InSb detector

(b) CALTECH Circuit

(low pass filter, $RC \sim 1$ sec.)
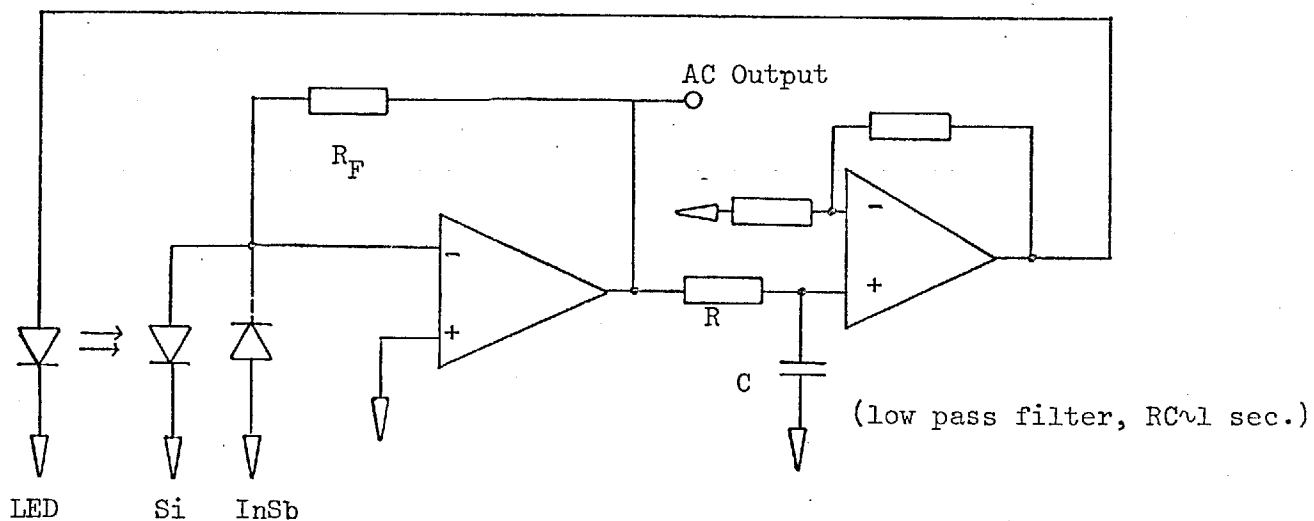
Figure 2.16

CHAPTER 3

CONTROL ELECTRONICS FOR OBSERVING

3.1. Introduction, General Description of Electronics

For infra-red observing careful consideration of the electronic systems is important. At one extreme we have the sensitive detectors requiring low noise amplification and optimum analog signal processing in order to extract the final signal with highest accuracy and signal to noise. Also the telescope control and data sampling systems with which I have been concerned present many problems and demand a design of control logic which is flexible and allows most effective use of observing time.

The general layout of the electronics, as presently used in Tenerife, is shown in Figure 3.1. Some of the signal processing has been described in Chapter 2; here we are mainly concerned with those elements which control the sampling operations, movements of the telescope, and handle the digitised data recording. The system is continually being improved as new requirements are demanded and as financial and other considerations allow. The recent availability of a Nova computer system has already given us the capability of some on-line data analysis which improves our efficiency considerably. Further developments of this, and also perhaps use of it for telescope control should give further advances.

Power Supplies

The available 240V electricity supply is of course suitable for most of our instruments, but the lack of a very adequate earth at this dry observatory site causes many problems due to noise and pick-up which would not otherwise be encountered. The physical and electrical separation of
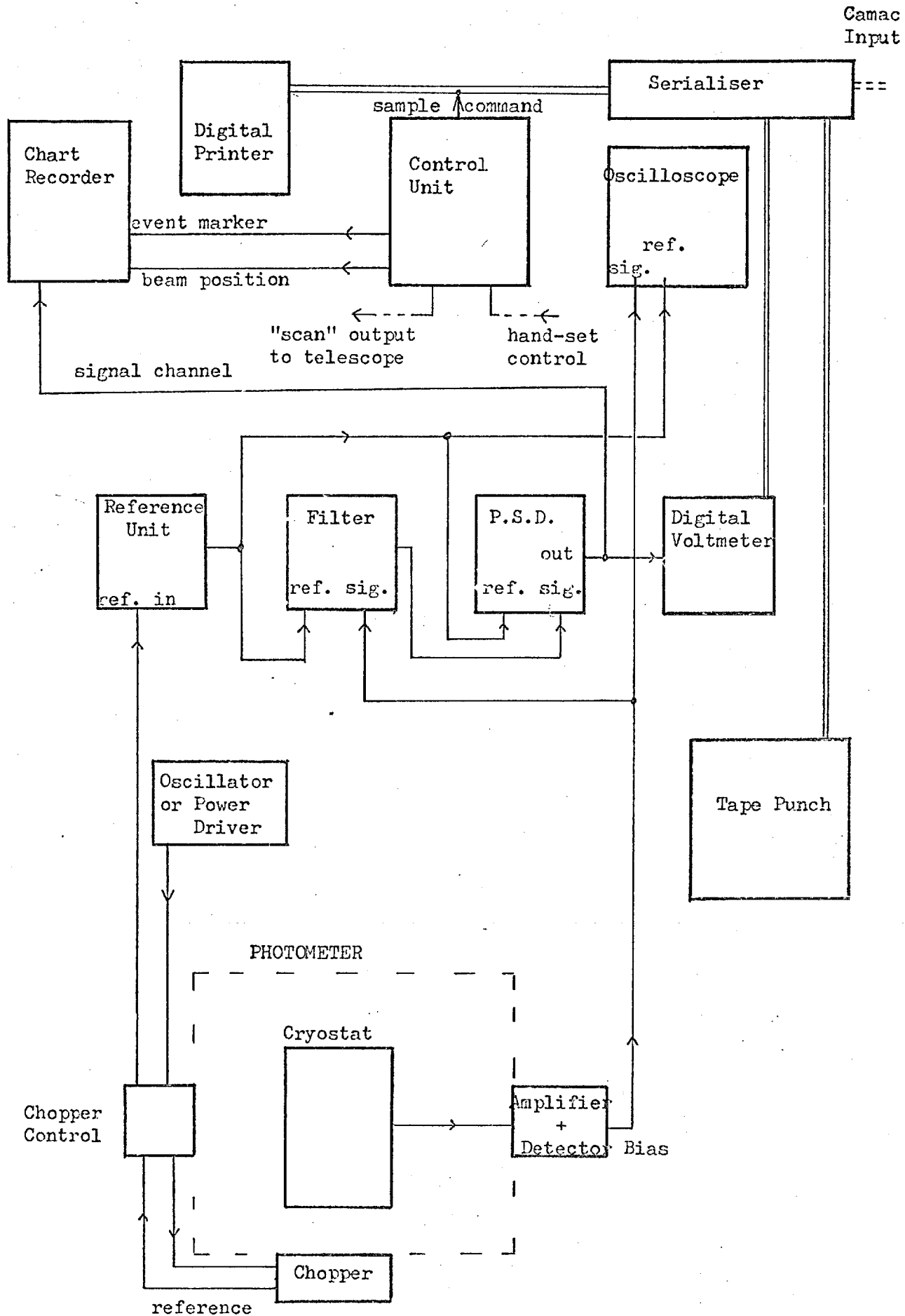
Figure 3.1

different parts of the system helps to reduce these problems. The sensitive parts of the signal processing chain, including the PSD and DVM are fed via an isolated, stabilised mains unit. The larger power-consuming Tape-punch and Printer are fed separately. Radio-frequency line filters have been fitted to a few devices.

False triggering of the Printer or Tape;punch can be a problem unless care is taken with the earth returns. A few devices which take little power or are "hung" on the telescope are conveniently powered by batteries. Checking and replacing of batteries is important to reduce the possibility of drifts occurring as the power drops - the possibility of using regularly recharged nickel-cadmium cells is being considered.

Noise

Several sources of unwanted "noise" are present and present problems of varying degrees. 50 or 100 Hz mains pick-up is often evident on signal channels but is fairly effectively removed by the PSD system (although it is necessary to avoid reference frequencies which are sub-harmonics of 50 or 100 Hz). Higher frequency "TV carrier" pick-up also appears but causes few problems.

Other noise sources, at the chop frequency are more serious. "Chopping signals" due to a modulation of the radiation background need to be minimised by careful alignment (these should not increase the noise above the normal sky noise which is present with the chopper off). Microphonic pick-up, especially when excited by the chopper, can be removed in most cases by careful mechanical and electrical design.

3.2. Sample Control Unit

In the normal modes of observation,including point photometry and area scanning, there are many functions that have to be regularly performed and can usefully be controlled automatically, the most important

of these being control of the data sampling. When the first infra-red

system was constructed in Tenerife a motor driving cam-operated micro-

switches performed the function of giving a series of "contact-closures"

to cause a Printer to record the data. This system, although "simple",

was limited in its flexibility and it was seen that a more sophisticated

system was needed.

3.2.1. Controller design

The controller that I designed using digital TTL elements was

built to perform two basic functions necessary for our photometry; that

is, to provide regular groups of "record" pulses and also "nod" control

signals to cause telescope motion between two beam positions (see

Chapter 2). It was relatively easy to include a few extra facilities

such as a 'pause' control (and warning light) and chart record outputs

to indicate the status of the recording sequence.

A block diagram of the controller is shown in Figure 3.2. An

internal clock oscillator provided basic timing pulses and "thumb-wheel"

switches enabled various counters to divide the clock rate as required

to give different recording intervals. The device provides sample commands

during one half of its cycle and then has a pre-set pause before

continuing its cycle.

A control box based on these principles was built and used

successfully in Tenerife for some time (occasionally known as the "blue

box" for obvious reasons). Whilst in use its usefulness was increased

several times by adding extra counters to enable more recordings than

originally anticipated to be done. Also, additional outputs were

obtained by wiring relays which now allowed more control of the telescope;

in particular, enabling scans and rasters of up to 1000 sample points,

which were done automatically and in synchronism with the data recording.

Block Diagram of Sample Controller Elements
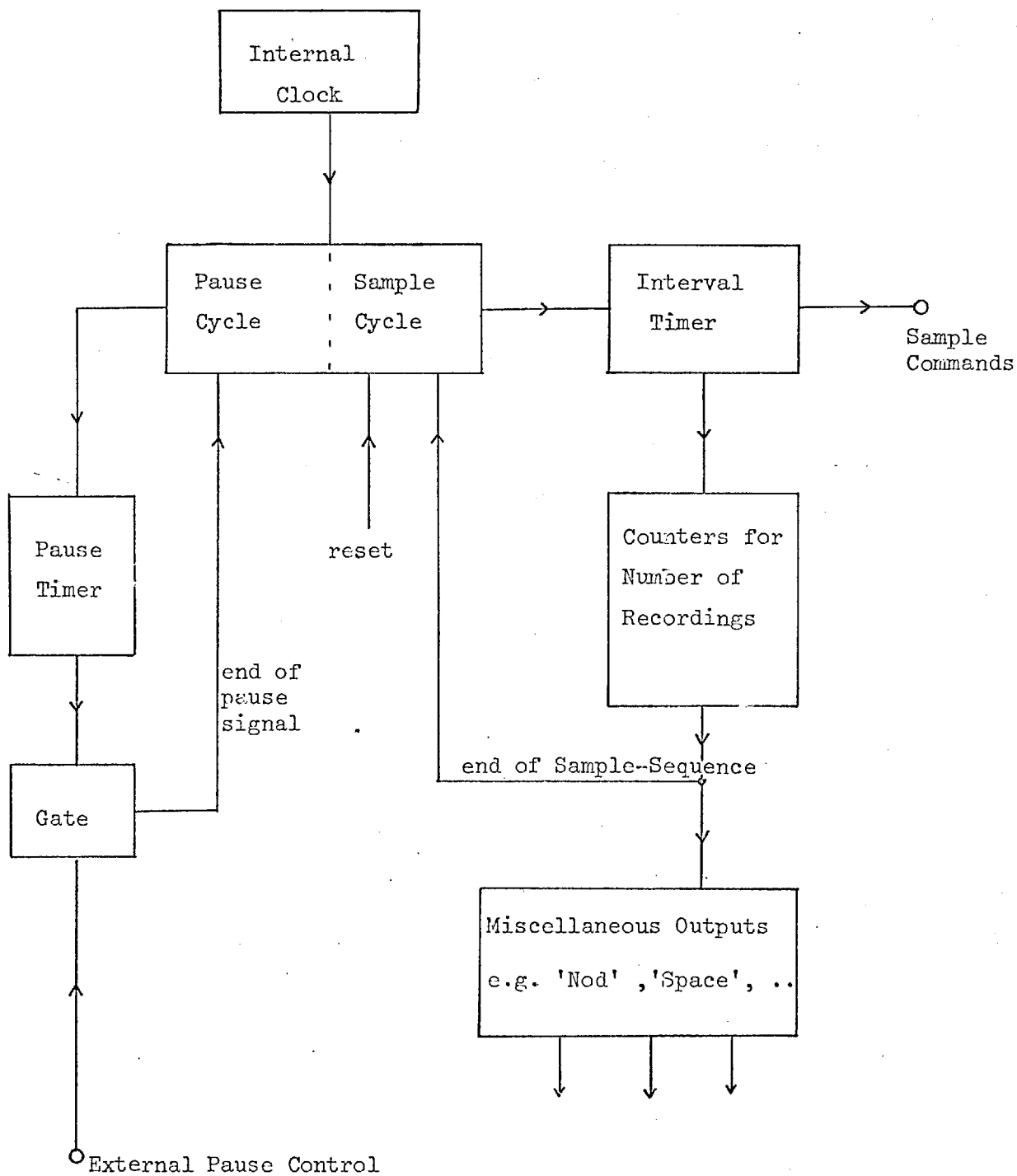
Figure 3.2

3.2.2. The Mark II Controller

After various extensions to the control box further changes were impractical and the box was physically rather crowded and difficult to service. A second control box (to become known as "Paul's Box" usually) was designed on similar principles to include all the previous features and also provision for many future applications. This Mark II Controller was also modified in various aspects for more flexibility and ease of use. The whole of the control logic is shown in Figure 3.3, and the various elements of the device are now described in detail.

A clock oscillator at 1024 Hz and following binary dividers can select many basic operating periods — usually 1.0 seconds is used but the maximum rate of 1 kHz can be useful for setting up and testing. The main control logic and various counters serve to count a set number of pulses (from 1 - 1000) which can be divided to have long delays between them. These are the basic "record" pulses used to initiate a data sample on the DVM/Printer.

Following this recording sequence is a pre-set pause, and then the cycle re-starts if required. Many different logic levels and pulses are generated and used to control miniature relays. These relays are used to supply "contact-closures" or various output voltages for most of the control functions required by the external devices; in addition, some direct TTL (0 - 5.0 V) logic levels are used as outputs.

The device provides "record" pulses for primary data sampling by DVM and/or computer, and also chart-recorder outputs for "event-mark" indication. Control signals are also available for control of the telescope, for "nodding" or scanning — as described later. Additional control outputs are used to change colour and spacing of a printer — for ease of reading later. The control box also provides status signals for use with computer control.

LOGIC DIAGRAM OF MARK II SAMPLE CONTROLLER
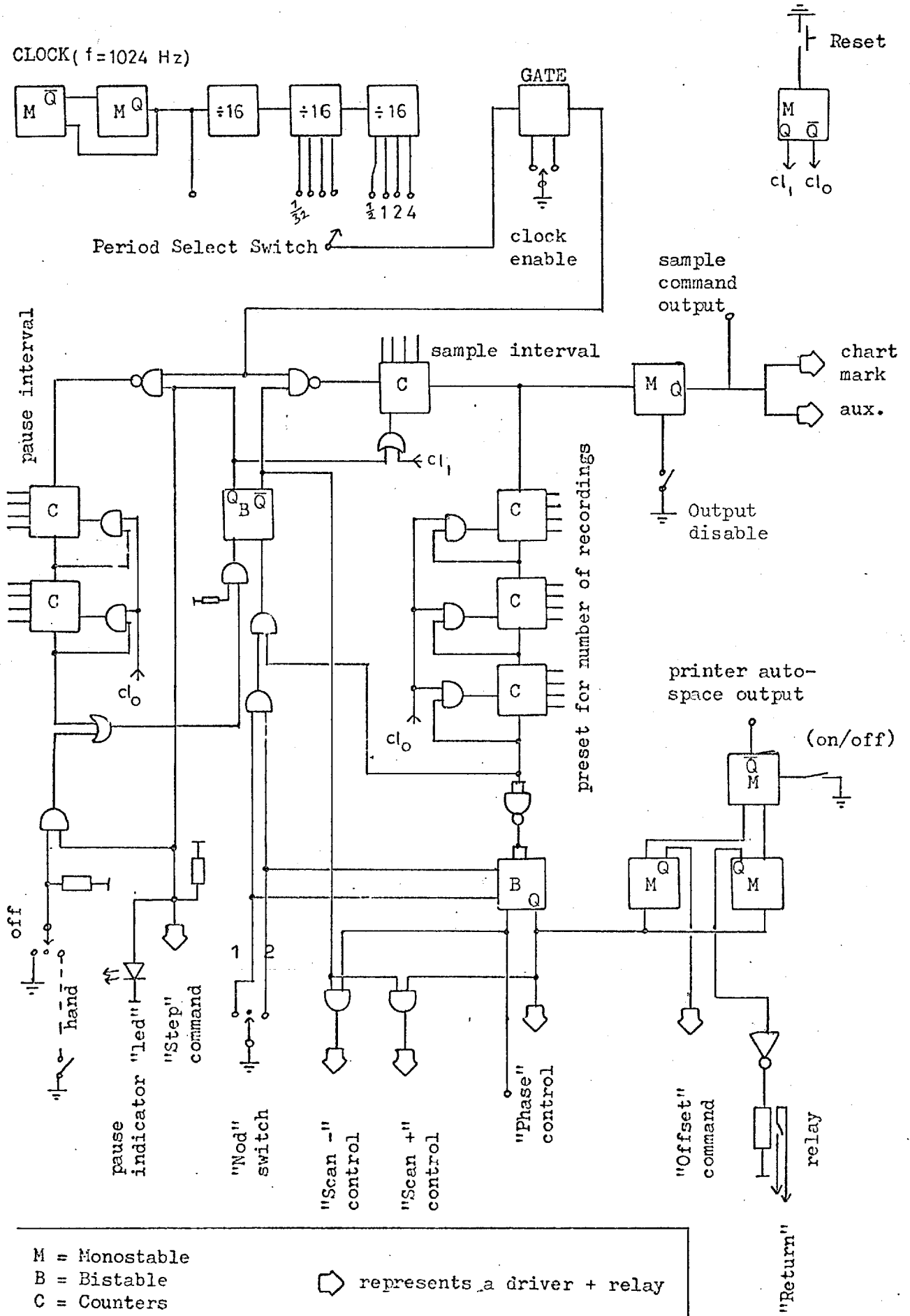
Figure 3.3

Provision is made for control of a synchronised up/down counter

used as a digital phase-sensitive detector. An output level which

alternated with each set of recordings (the "phase" output) could be

used to control the direction of an up/down counter. If the detector

signal is digitised and fed into this counter the action of a digital

PSD is thus performed by alternate addition or subtraction of the signal.

This technique, when incorporated into an instrument, would give precise

results and be capable of accurate "integration" of any length. However,

it has now been superseded by the availability of a computer.

Sample
Commands

"Phase"
Control.

"Offset"
·Command

"Return"

Auto-space
Output

"Scan+"

"Scan-"

Pause
State
(also
"Step"
Command)

↑record   pause
phase   phase

↑

Start of   start of
1st cycle   2nd cycle

SAMPLE CONTROL UNIT
OUTPUT SEQUENCE
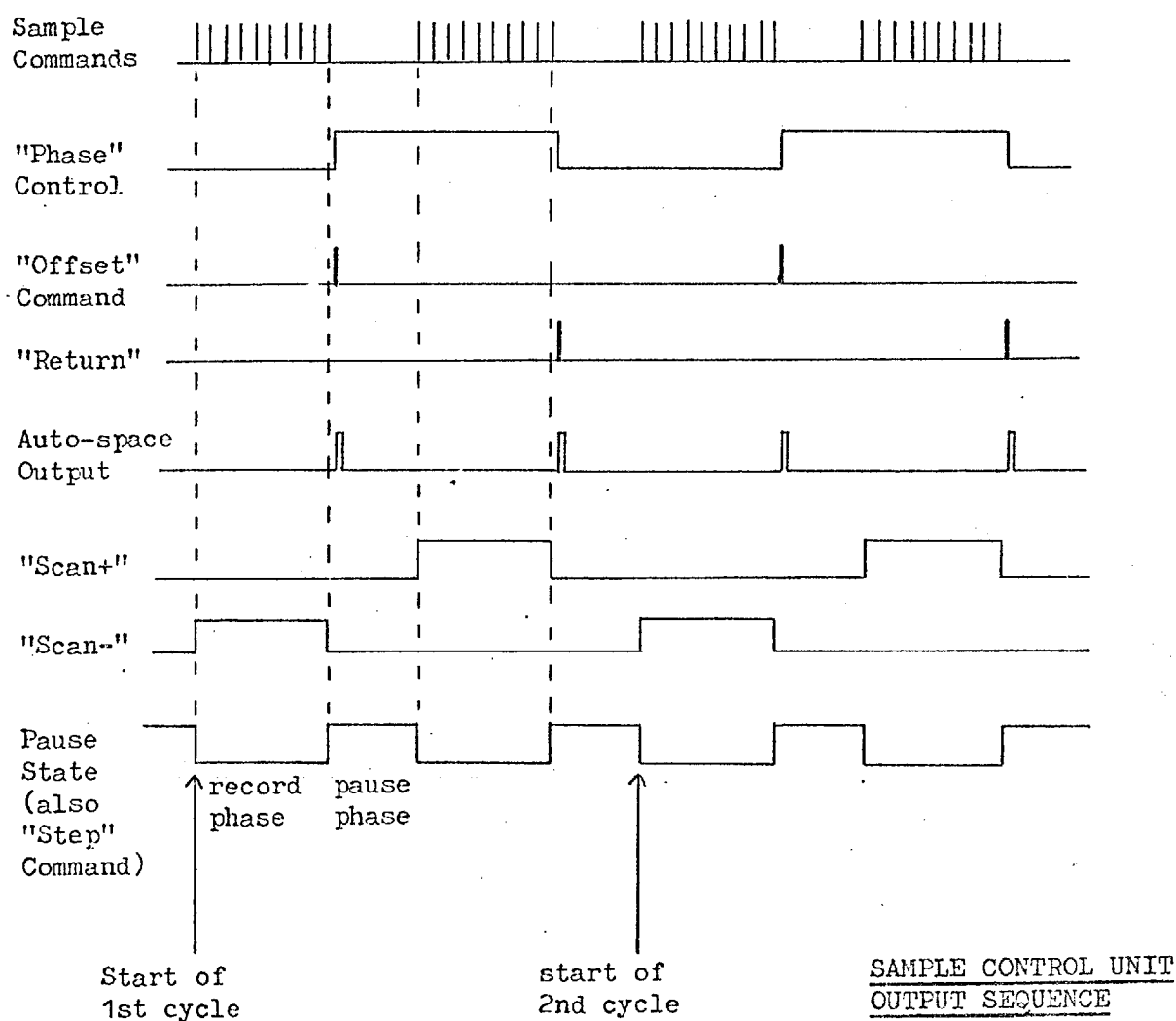
Figure 3.4

Control Sequence

The following controls and settings are available, see Figure 3.4

for details of some of the output signals in sequence. The number of

record pulses, and intervals between them, can readily be pre-set and

adjusted when required. At the end of a record sequence an adjustable pre-set pause period is initiated. Continuation of recording can be automatic, manually controlled, or initiated by computer as desired.

The output used for sample control can be readily disabled if an error occurs or for convenience of testing; the record sequence can be reset and started at any time or merely "paused" on completion of the set number of samples. A further "nod" control enables the telescope to be offset and returned with ease - this is normally done automatically by the control box at the end of one set of recordings.

Construction and Operation

The controller is constructed on 6 boards fitting in a standard 'Vero' module. It operates from a single 5V regulated supply and consumes 4 watts. The digital logic elements are found to be reliable in use and with suitable drivers adequately operate the various relays used. Most care is needed when logic outputs or inputs are used directly, suitable buffers are required to ensure that the operation is not impaired by external noise or poor voltage levels; for example, an appropriate inverter-driver is required to send a control output to the computer which is situated 15 metres away, but standard TTL devices are sufficient for all logic purposes. The clock oscillator can be set to 0.1%, i.e. 1 sec. in 1000, and its stability is better than this for all operating conditions. The most precision is required in order to obtain repeatable scans when these last for several hundred seconds, the timing error proves to be negligible in practice.

3.3. Telescope Control

The 60-inch Flux-collector drive system has a control rack built by ROE which enables manual, semi-automatic, or external operation of many different drive modes. It has proved most convenient to control

several motions externally in synchronism with our data recording by using my control box. More details of the scanning procedures are given in a later chapter but here I shall describe the interfacing of my control box with the control console and some aspects of offset control as used for photometry. The provision of suitable interfaces by ROE, which has enabled external control of RA and Dec. motions, has been vital to the implementation of the various control modes which we have found useful. Output signals which indicate the telescope position and drive rack status have not been utilised, but may prove useful in future if more sophisticated controls are used, particularly perhaps with the help of the computer, should this become practicable.

The "Scan Control" Box

A simplified diagram of the control wiring is shown in Figure 3.5. My control box basically provides 5 control signals (relay contact-closures) which are fed into a "scan-control" box which performs various switching combinations for the modes of use required. The controls generated are: offset, return, scan +, scan -, and step; the actual function they perform varies depending on usage.

The "scan box" is linked to various inputs of the drive console: RA+, RA-, DEC+, DEC-, DEC Reset (RA Reset), DEC Return, DEC Offset (RA Offset). The first four cause a scanning motion at the "Slow-Guide" rate whilst they are maintained, the others result in an offset, return, or reset command when a pulse is applied. The actual usage of the "scan-box" depends on whether we wish to do photometry or scans/rasters as described below.
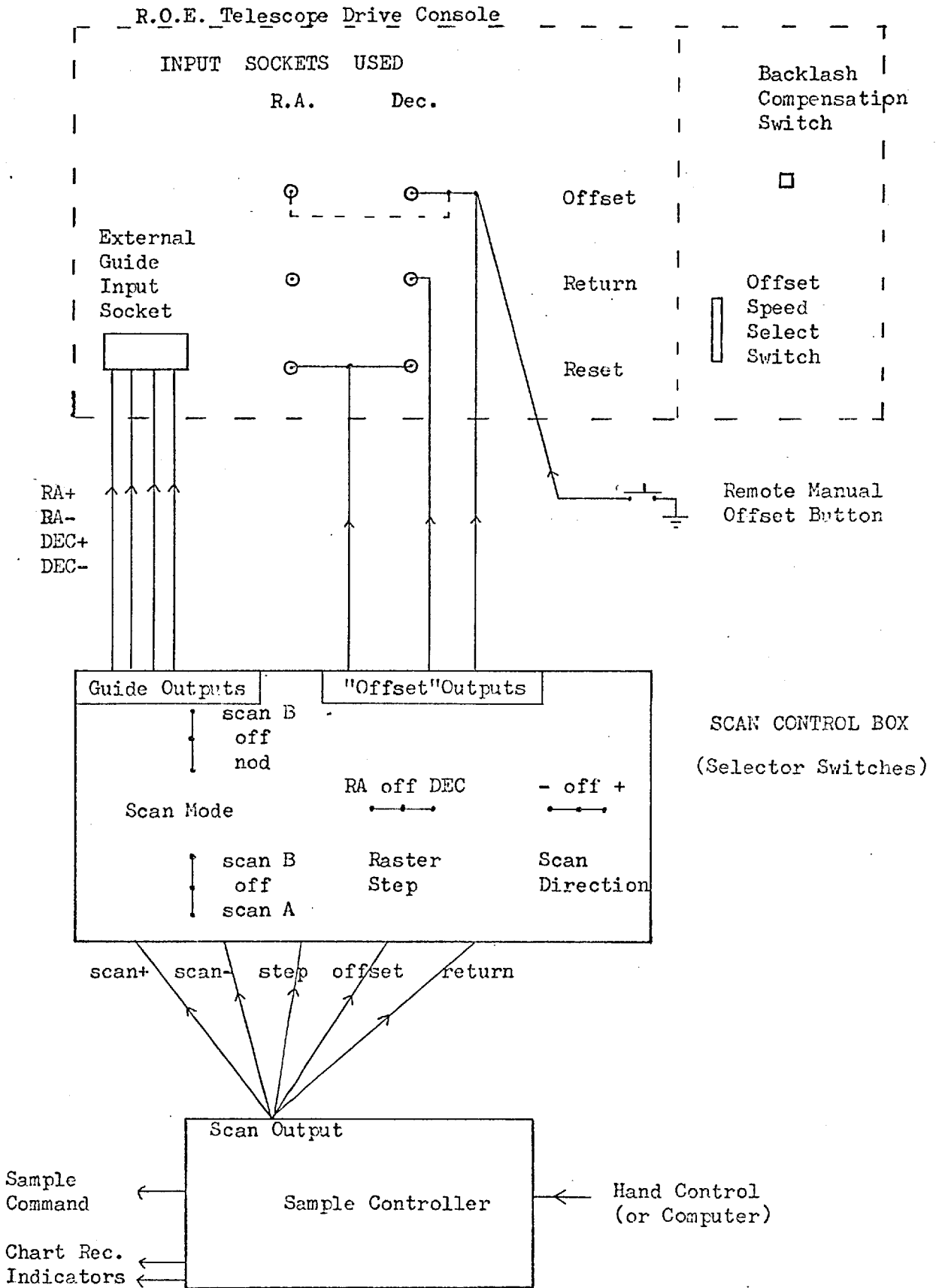
Figure 3.5

Photometry

For photometry the control is relatively simple since we only require that the telescope alternately "nods" between two positions as required for standard beam-switching. At the end of a sequence of recordings in one beam position my control box generates a nod pulse which causes an offset motion of the telescope by a pre-set amount (often $10''$). The next sequence of recording in this position is performed, and at its completion, a second nod pulse causes a return motion to the other beam position.

A pre-set pause allows settling before recording recommences. This process could be performed by using the drive rack's automatic "offsat-dwell" facility, but this is, in fact, less flexible and is not synchronised with our data sampling period. The ability to nod the telescope (i.e. offset or return it) from my control box and also having alternate blocks of recordings printed in different colours and spaced out is found useful when setting up or checking operation.

Scanning

When scanning or rastering a few different methods have been made available. The telescope can be scanned at the slow guide rate in +/- RA or DEC., and this is done semi-automatically by my control box providing relay closures which cause these motions whilst the relays are operated. Another method of scanning which has been implemented is to cause an offset in the reqnired direction by an external pulse - the telescope then moves a pre-set distance at a rate which can be adjusted by a limited amount, as required. The telescope can also be made to return automatically to the start position and also do a step at right-angles at the end of the scan by using the appropriate pulsed control signals.

When observing, the scan is initiated at the same time as the sequence of recording samples. At the completion of the set of samples the telescope can be returned to the start position, and recording recommences automatically after a set pause, if required. The ease with which various functions can be controlled simultaneously greatly facilitates efficient use of observation time. Single scans can also be started by use of a hand-control which has enabled one observer to guide and control scans alone when necessary. More details of scanning procedures in practice are given in the following chapter.

3.4. Use of a Nova Computer

The addition of a Nova 2/10 mini computer to the telescope facilities has given the opportunity for some on-line data analysis and reduction. For more effective observing it has also been linked to the sample control system, and is used to initiate recordings when 'ready', i.e. if no error is detected and if previous analysis is completed.

3.4.1. Computer configuration

Figure 3.6 shows some of the computer interfaces to the rest of our equipment. The computer has a camac crate containing an analogue-digital converter, a pre-set counter and interrupt register; a VDU screen enables immediate display of incoming data or of partially reduced data; a teletype and set of push buttons to the interrupt register are used for instructions and manual control, and finally a paper-tape punch provides a means of directly recording either "raw" or partially analysed data. Other camac interface modules are available and, for example, the purchase of suitable input-output registers and, perhaps, a disc store could extend the use of this computer further.
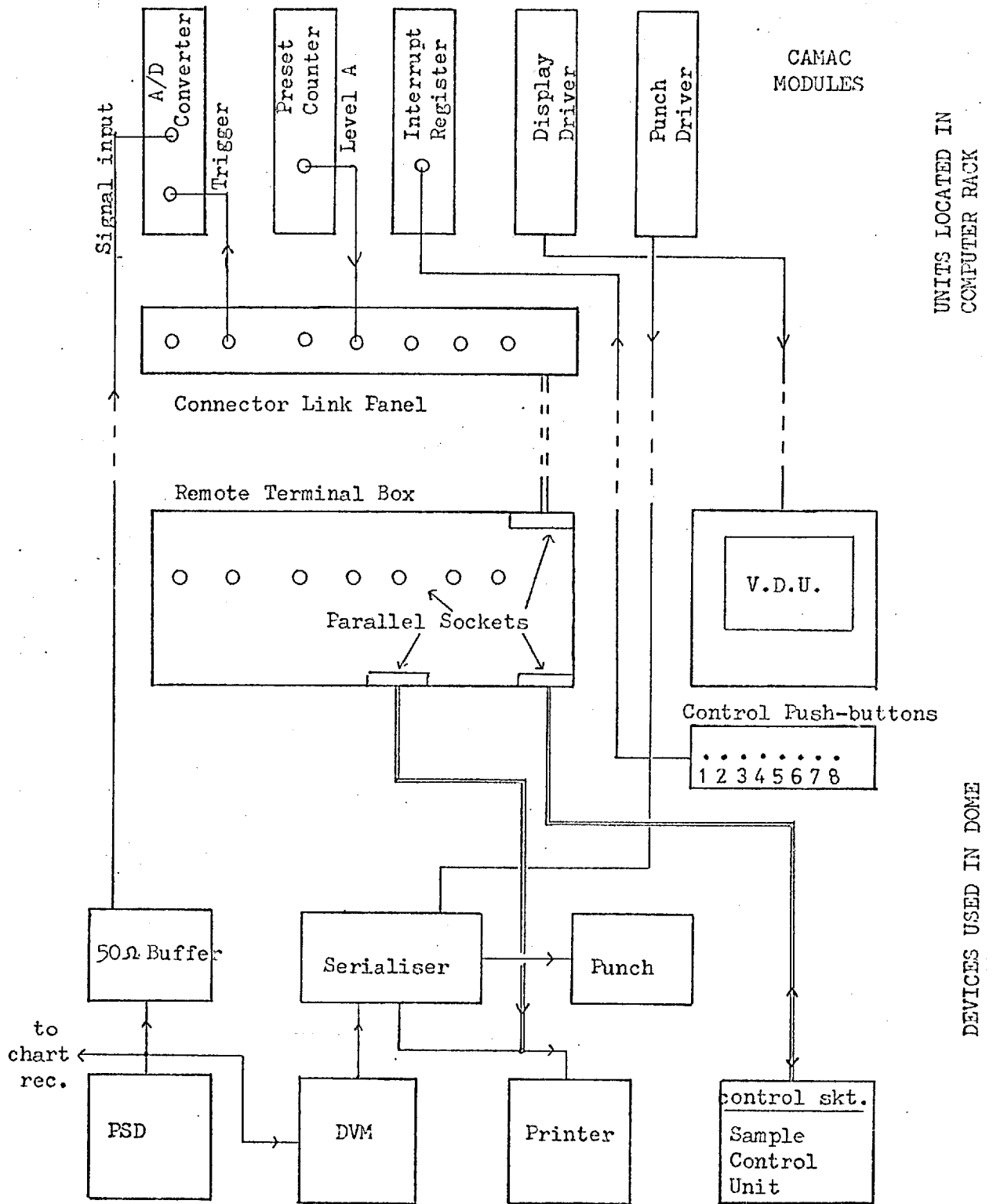
Figure 3.6

Our analogue signal (from the PSD) previously has merely been fed

to the DVM and recorded on paper-tape to be analysed at the end of an

observing period. This signal is now also sent, via a suitable buffer,

to the A/D converter and is then read directly into the computer. The

A/D receives a trigger input pulse from my control box, and thus it samples

at the same time as our DVM, which is operating in parallel as a back-up.

A set of 8 push-buttons are linked to the computer via an interrupt

register, and with their use various controls, e.g. start, stop, etc.

can be executed. The computer provides a control signal output ("level A"

from its pre-set counter module) which is taken to my control box and

used to release the pause state. This enables recording to commence in

a similar way to using the previous hand-control, which required a control

button to be pressed.

When observing, we find it convenient to have the teletype, push-

button interrupts and visual display in the dome whilst the computer and

other peripherals remain in the adjacent room. Suitable drivers and

interfaces were constructed to enable operation of parts of the system

whilst remote from the computer; these are important to ensure adequate

signal levels and to maintain noise at a low level particularly in the

signal channel. Some details of these are given in Figure 3.7.

50 OHM BUFFER (Gain= 2.0)   A/D CONVERTER INPUT

SG110   LH0041   Unity-Gain
Voltage Follower   Power Op. Amp.   Buffer
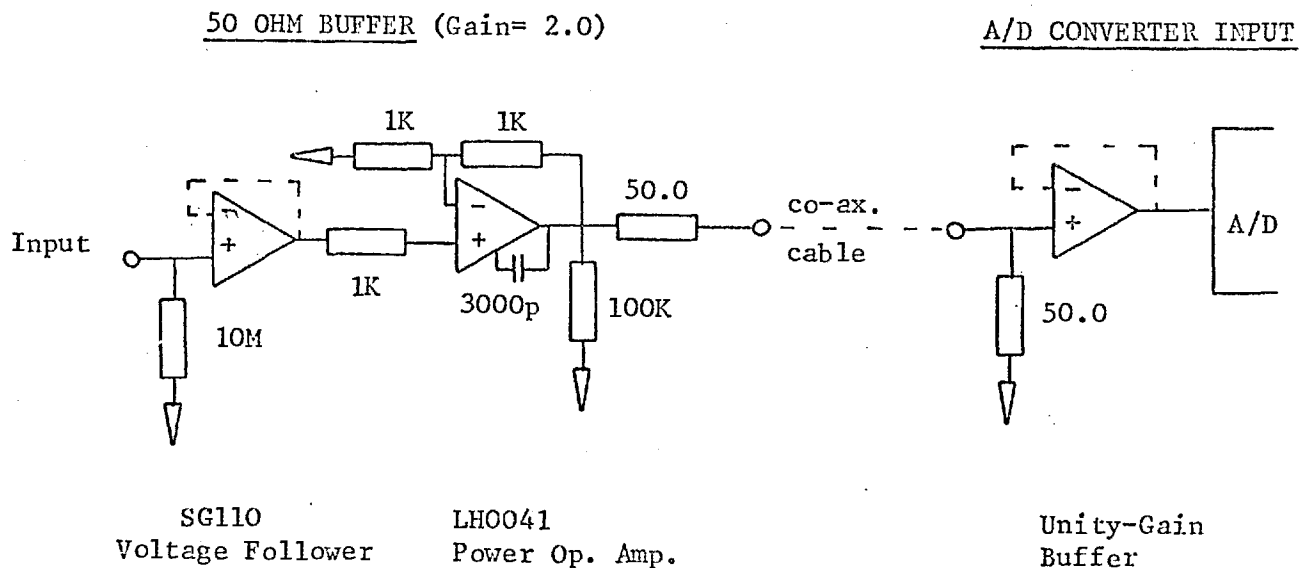
Figure 3.7

3.4.2. Computer usage

Two computer programs have been developed, mainly due to help from Nic Vine; one is used for photometry of single sources, the other is used for scan and raster work. The "photometry" program is more sophisticated in its analysis, and includes an error detection routine, whereas the "scan" program is used merely to add up points mainly to obtain a running total. Each program uses most of the available core store of 8192 words and thus, depending on the observational work intended, the appropriate program is loaded in prior to observing. The programs are recorded on paper-tape, and can be read in (via the teletype) in about 15 mins., and therefore could be exchanged in the night if necessary.

When everything is set up to begin recording the "Start" button to the computer is pressed; this indirectly causes the "level A" output to release the pause state on my control box and the sampling sequence starts. The program can be halted at any time or various other options chosen by suitable button pressing, as described below. Dialogues with the computer are performed using the teletype which receives input data about start conditions, etc. and can print out several types of information including an "end result" of an observing period.

3.4.3. Photometry program

The Photometry Program is used when sets of N sample recordings are made in alternate beams as for normal "point-source" photometry. Figure 3.8 shows an abbreviated flow chart of the program. The initial parameters, including star co-ordinates, sidereal time, number of data points, etc., are entered via the teletype. On pressing the "Continue" button the computer then allows the sampling procedure to start, i.e. my control box initiates a set of N recordings.

Photometry Program Flow Chart
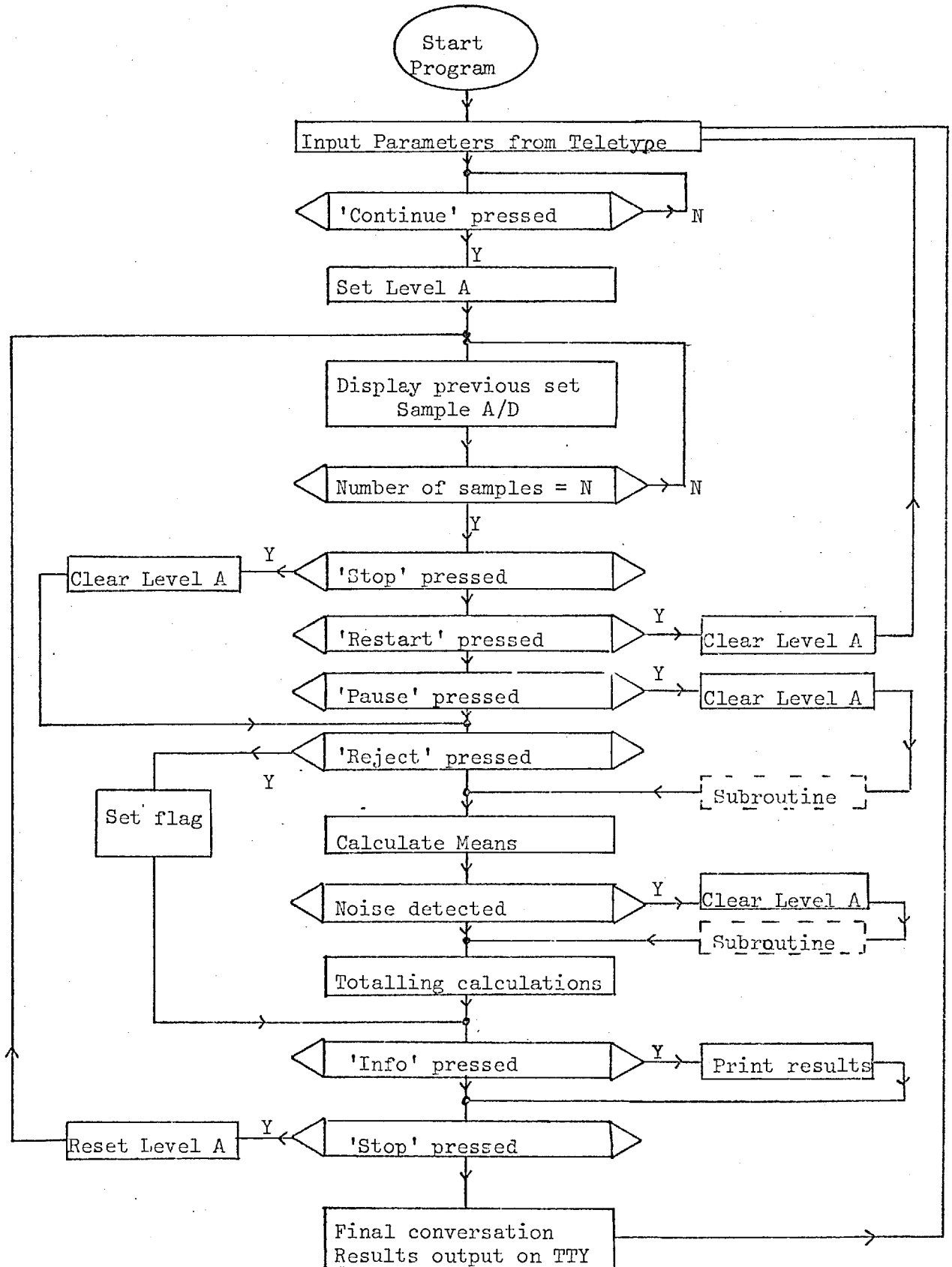
Notes: "Set Level A" - this enables sampling to commence (at control box).
The Subroutine (as above) tests the logic of the button-pressing sequence.

Y = Yes

Figure 3.8

The process of recording sets of data continues automatically, including telescope nods and pauses as required. The VDU shows a continually updated record of the previous N recorded points, this can be optionally blanked off. The program does a running calculation of the mean signal level(by substracting alternate "beams") and also of the signal to noise ratio. This information can be printed on the teletype at any time by use of the "Info" button, thus at any time we can determine whether sufficient observations have been made for an adequate S/N ratio. The recording sequence can be halted at any time by the use of the "Pause" button, the "Continue" button is used when we wish to carry on, or the "Re-start" option may be used if all previous records are to be ignored and a new start made on a given object.

The program includes an error-detection routine which halts the recording sequence and gives details of the error on the teletype if one of several faults is found. At present these include a "spike" in which the signal exceeds the normal noise level by, say, a factor of three, and a "drift" if the mean signal level changes by, say, 20%. After studying the previous data set the observer can then choose to reject the data or continue, and include it, depending on its significance.

When observations of an object are completed the "Stop" button is pressed and a final conversion with the teletype occurs. The resultant total signal is presented, an air mass ocrrection can be estimated, and a normalised intensity can then be printed out using known gain settings, etc. Comparison with similar intensities of calibration stars can be made immediately, if appropriate, and thus the magnitude of a source can be presented at once. Observations of the next object can proceed almost immediately with little delay.

3.4.4. Scan Program

The Scan Program is used when single or multiple scans are intended, but also includes a simplified point-photometry routine. A flow chart of this program is given in Figure 3.9. The program handles data sampling control for scans of the order of 200 points. The "Continue" button is pressed to initiate the recording sequence.

Many scans can be made over a single area and can be continually added to to give a running total; at the end of each scan pressing the "Continue" button starts the next scan and adds in the previous one. If the "Reject" button is used the previous scan is ignored and a new one may be started. At the end of a set of scans the summed total may be displayed on the VDU and recorded permanently on punched tape if required.

If raster scans or groups of scans in a series of areas are made the summed scan total for each area may be punched out before proceeding to the next position. The ability to keep a summed total of scans and thus see it building up as observing proceeds is, of course, particularly useful to estimate when sufficient S/N is present.

The simplified photometry section enables photometry to be performed as before but without the use of an error detection routine. Intermediate results cannot be presented as readily, but a final result is calculated; the recording sequence can still be paused and continued when required and data can be rejected if necessary.

At present both programs have been used successfully, and the transfer of some control to the computer and the data processing facilities have aided observations considerably. We still record data in parallel via a DVM and independent tape-punch and printer, but with increased reliability of the computer and the advantage of on-line processing, this may not be done in future. The extension of the computer's memory

Scan Program Flow Chart

Start

Input Parameters from TTY

Scan Selected — N → ⌐Photometry(as before)⌐

'Continue' pressed — N

Set Level A

Display Scan + Total
Sample A/D
Store Values + Total

Number of samples = N — N

Clear Level A

Display Scan + Total

'Stop' pressed — Y → Set Flag → TTY Message

'Step' pressed — Y → (Set Flag)

Display Total

'Continue' pressed — Y

'Continue' pressed — N

'Reject' pressed — N

Punch Results

Subtract Scan
TTY message

'Stop' flag set — N

Go to Start

Figure 3.9

would enable more sophisticated data analysis programs; in particular, "Least Squares" fits of profiles or Fourier analysis of scan data is envisaged.

The computer could also enable more flexible forms of data-recording, at much higher rates where necessary. By sampling more rapidly and using a shorter PSD time-constant we could obtain faster responses. The computer could perform the integration by digitally adding the recorded points to give the same reduction in noise as the analogue system. In some cases, for example, when scanning rapidly across a source, the ability to have a short response time and to record more rapidly than when limited by a mechanical punch or printer can be useful. Recording and temporary storage of many more data points gives better statistics and, with careful analysis (and perhaps noise rejection), more precise results should be possible. However, the availability of only a low resolution (8 bit) analogue-to-digital converter and small program storage ability rather limits the potential of the system at present.

3.5. More Data Recording Details

The analogue signal output from the PSD is fed into a Digital Voltmeter which presents the output in parallel BCD form at a rear connector. The analogue signal also goes to an A/D converter for the computer (as above) in the latest system. The DVM output data is recorded on a paper printer and a paper tape-punch. The first such system (see Figure 3.10) consisted of a solartron DVM ($3\frac{1}{2}$ digits) with (0 to -10V output levels), a Kienzle printer which accepted the parallel data directly, and a Creed 5-hole punch with input drivers.

Early Set-Up Used For Data Recording Apparatus
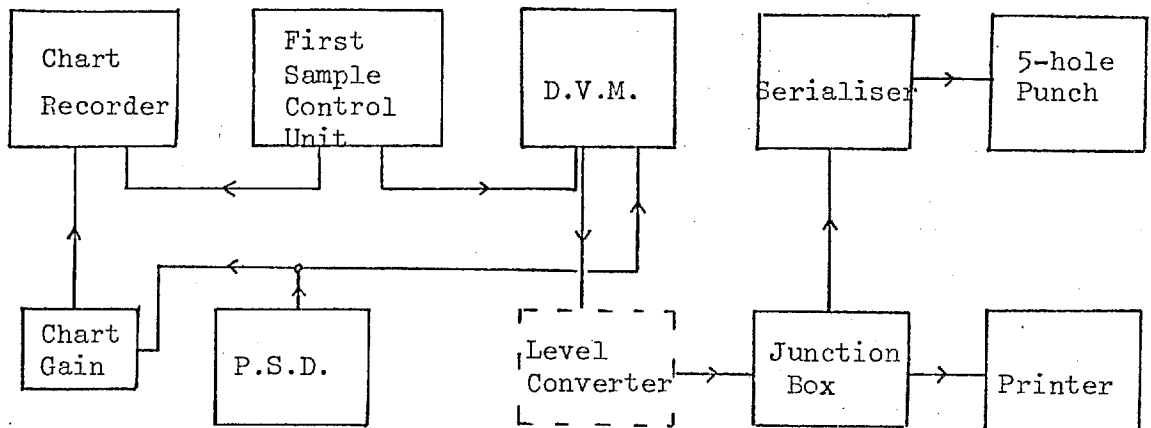
(Use of level converter depends on DVM used)

Figure 3.10

Level Converter (1 of 24 channels is shown)
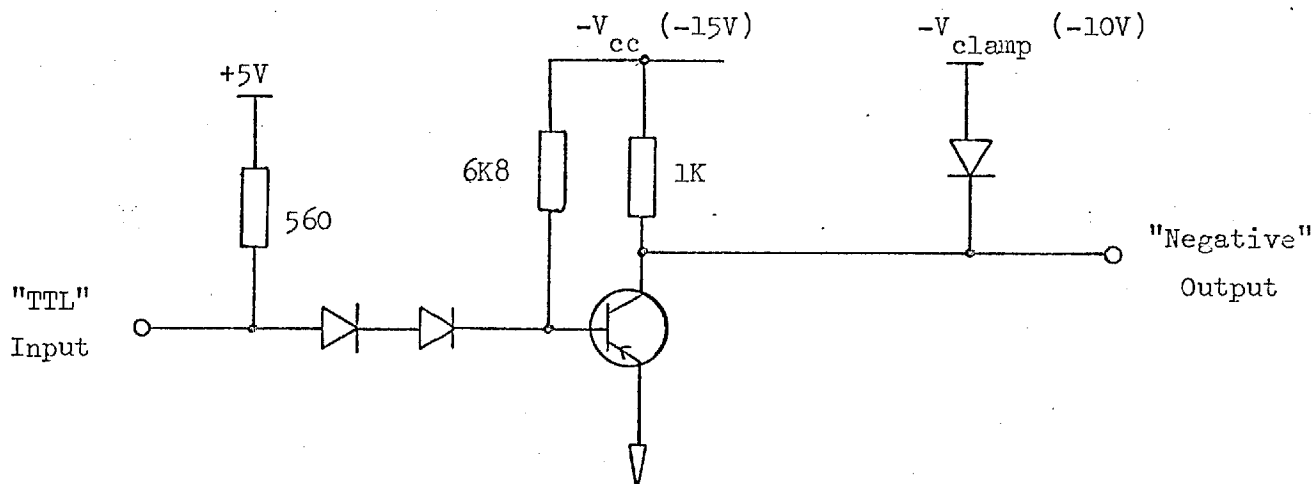
TTL Input Standard

| "LO" | V(0) = 0 - 0.4 V | O/P = 0 V. |
| "HI" | V(1) = 3.5-5.0 V | O/P = $-V_{clamp}$ |

Figure 3.12

The paper-tape punch however could only punch one decade of BCD data per cycle and so I designed and constructed a crude serialiser which read in the whole DVM output number in parallel and fed it out in suitable serial form for the punch. A manual punch option via switches and an automatic tape run-out facility were provided. The Logic diagram of this is shown in Figure 3.11.

The subsequent purchase of a more modern Hewlett-Packard DVM which had similar outputs but at TTL (0 - 5V) levels required the construction of a module of multiple level converters (see Figure 3.12) and the slight extension of the serialiser to include an extra numerical digit of data. This arrangement operated successfully but the unreliability of the old tape punch and the incompatibility of the devices caused intermittent problems.

The system was improved further by adding a modern Data Dynamics tape-punch which required the construction of a new serialiser (by Mr. J. Allen) see Figure 3.13. The new complete "modern" system operates successfully and uses TTL level signals for control and data; this enables recording of extra data such as DVM range, together with more control of the printer by my control unit.

The serialiser has also been constructed so as to be compatible with the computer camac interface. Thus data from the computer can be fed directly to our tape-punch, or alternated with our DVM Data as required. The new system wiring has been made compatible with the previous arrangement and with the use of the level converter if needed the DVM/Printer/Punch may be interchanged for flexibility, should spares be required.

SIMPLE SERIALISER – LOGIC DIAGRAM

Figure 3.11

data inputs   Camac input   OUTPUTS TO PUNCH

to Printer

Input from DVM → → to serialiser
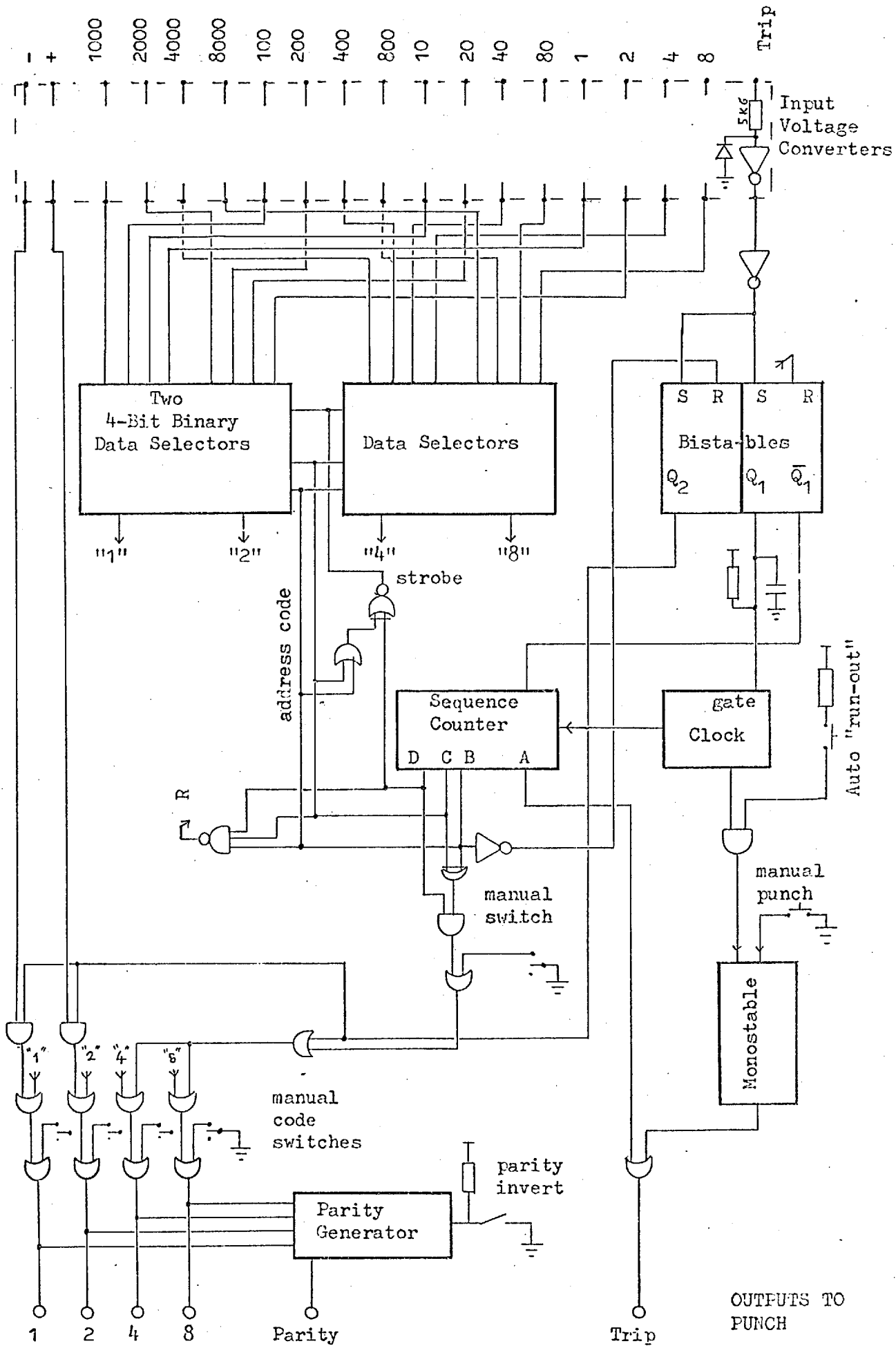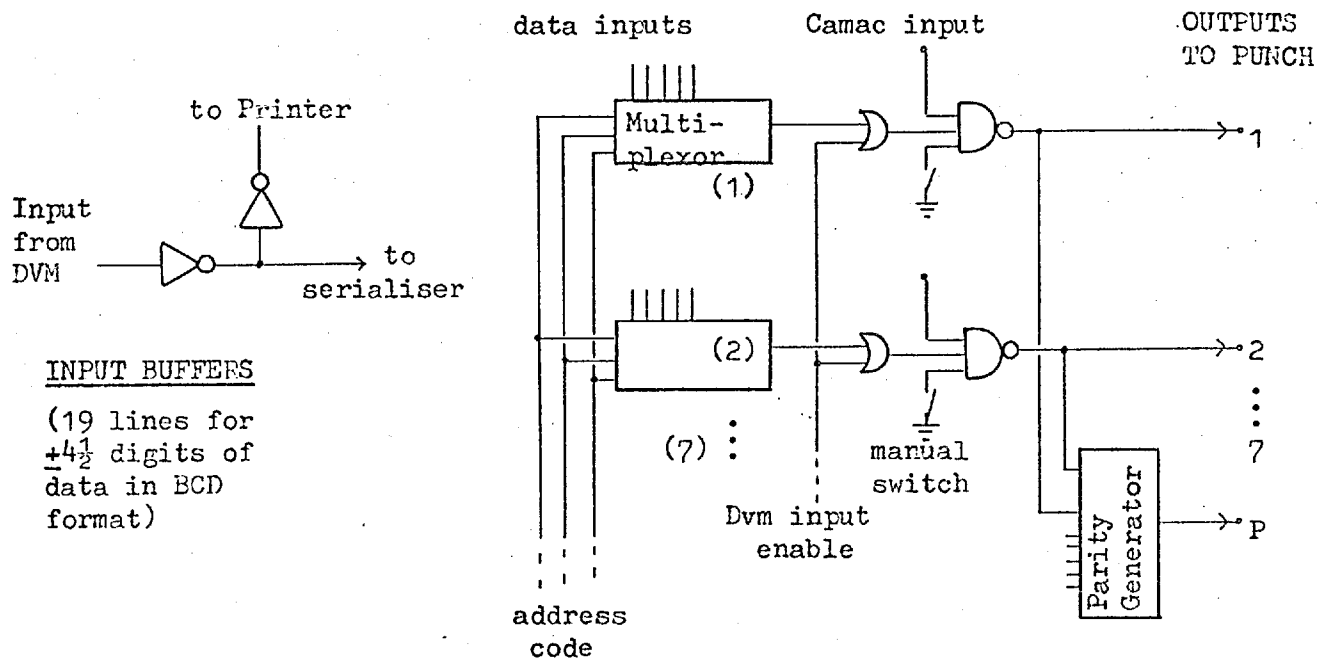
INPUT BUFFERS

(19 lines for +4½ digits of data in BCD format)

Multi-plexor (1)

(2)

(7) :

Dvm input enable

manual switch

Parity Generator

address code

1

2
:
7

P

OUTPUT MULTIPLEXERS

DVM mode select

gated Camac input

SOURCE CONTROL (i.e. punch command)

Flip-Flop S R   Monostable   manual punch switch

Binary Counter   I/P   Flip-Flop

address code

reset or count

reset

input gate

Latch R S

ACCEPTOR CONTROL (i.e. punch "ready signal)

Q Monostable   Q Monostable   Trigger Input

control gate
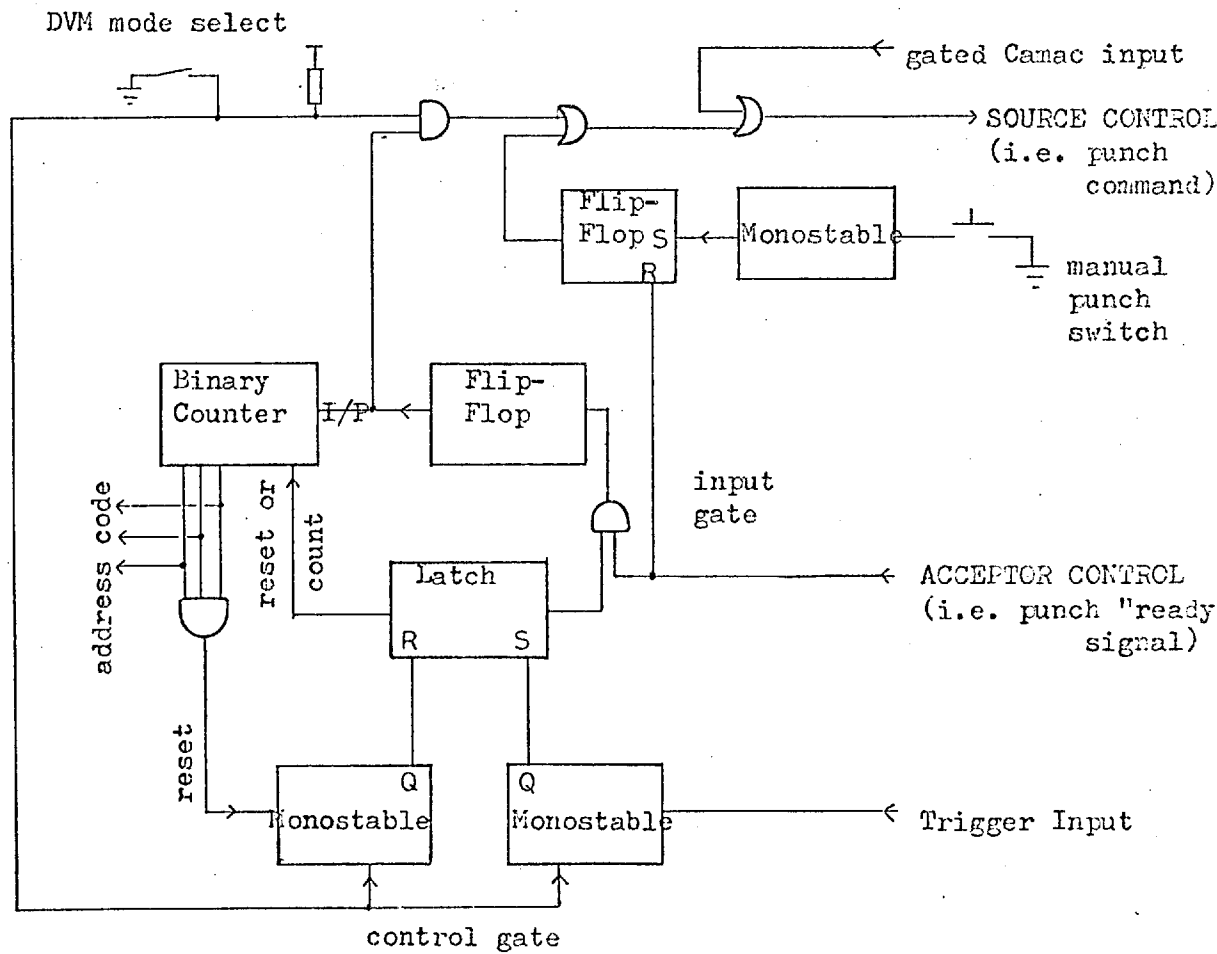
MAIN TIMING CIRCUIT

Figure 3.13

The paper-tape data is punched out in a suitable format (ASCII II)
so that it may be readily read in to the Tenerife computer or to the
I.C. system for later analysis. A chart-recorder is also used as a more
readily visible means of recording the signal and is invaluable for
this reason. It also gives timing information and extra channels when
available are useful for recording telescope "beam" position and an
event-mark corresponding to each DVM sample taken.

CHAPTER 4

RASTER SEARCHES OF H II REGIONS

4.1. Review and Objects Studied

4.1.1. Introduction

In collaboration with P.A. Whitelock, I began investigating

H II regions in 1974. We planned to search such regions for detectable

IR sources that were expected to be associated with them (this work

followed partly from an existing interest in planetary nebulae in the

I.C. Astronomy Group). At that time Wynn-Williams and Becklin (1974)

had just reviewed IR emission from H II regions and this paper gives a

useful introduction to the subject. Quite a few regions had been studied

and many more have been done since; the Orion complex has been very

extensively studied and the so-called Becklin-Neugebauer (BN) object is

an example of a possible protostar.

Compact H II regions (size < ½ pc, electron density > 10^4 cm^{-3}) have

been studied in particular. They are often optically obscured and many

emit measurable IR radiation from 2 - 100 μm. Visual extinctions in

excess of 10 magnitudes are common (e.g. see Wynn-Williams et al.1972)

and radio continuum measurements can be used to select regions for study

(examples of catalogues are Goss and Shaver, 1970 or Felli and Churchwell,

1972). In particular, high angular resolution radio telescope measure-

ments are most useful when selecting regions to study. There is no infra-

red survey of sufficient sensitivity to give information on such sources;

a considerable time is needed to search suitable areas from ground-based

telescope.

Of the sources that have been measured by others some were done at

short wave (1.6, 2.2, 3.5 μm), some more extensively from 1 - 20 μm, and

some only at 100 μm. The large variation in beam sizes (and resolution)

made correlation of different measurements more difficult.

4.1.2.   The Nature of the sources

In many cases heated dust, associated with the ionised hydrogen, can give sufficient excess IR emission. For example, the W3 complex has been studied comprehensively and such dust emission was discussed in an early paper by Wynn-Williams et al.(1972). Most of the work to date has concentrated on the near IR (1 - 10 µm) emission from H II regions.

Stars and proto-stars can be measured at wavelengths of 1 - 3 µm. Such sources are usually compact in size, i.e. < 2". Larson (1972, and earlier papers) has modelled the evolution of proto-stars and describes the characteristic dust cloud that surrounds such sources. The BN object, as well as other strong IR emitters (R Mon, R CrA, Lk Hα101, etc), can be interpreted as such protostars. The source IRS5 in W3 is also considered to be a possible protostar (Wynn-Williams et al.1972).

At wavelengths λ < 5µm free-free emission from ionised hydrogen can be strong, although extinction reduces the measured intensity of course. At wavelengths of 10 - 20 µm radiation from heated dust within the ionised region is measured. The distribution of emission is often similar to the radio emission and indicates that the dust is well mixed with the gas. Colour temperatures are $\sim$ 200K, whereas brightness temperatures are often $\sim$ 100K, indicating that the source is optically thin at 10 - 20 µm.

At wavelengths around 100 µm sources are usually found to be more extended with a lower temperature ($\sim$ 50K). Such sources are considered to be a larger surrounding dust cloud, exterior to the short wave sources within the ionised region. Of the sources discussed here, most of the energy is emitted at infra-red wavelengths and thus IR measurements are necessary to estimate the total luminosity.

The H II regions that have proved to be the most interesting to observe in the near infra-red, that have been most likely to contain protostars, have one or more of the following properties: compact areas, nearby OH/H_2O maser sources, far infra-red emission (40 - 350 µm), radio continuum flux, detection of molecules (e.g. CO,etc.).

Formaldehyde absorption has been measured and "silicate" absorption at 10 µm is also common, especially in the presence of large amounts of short wavelength (1 - 2 µm) extinction due to dust. Possible pre-main sequence objects are also detected outside the ionised region, often correlated with OH masers or H_2O sources (see Lo et al.1975).

Maps at 20 µm have proved to be closely correlated with radio maps, although lack of sufficient resolution usually prevents an exact matching of the measurements. At 2 µm sources are similarly found to be associated with the H II regions but the presence of absorbing dust affects the measurements strongly at short wavelengths. Extended low-surface brightness regions are more readily picked up by the larger beams of radio-telescopes, whereas the beam switching technique necessary for IR work makes this less sensitive to such signals.

4.1.3.   Observations

A good example of a H II region with IR sources has proved to be NGC 6334, a region of optical nebulosity which in 1973 had been detected at far IR wavelengths. The 40 - 350 µm maps (Emerson et al. 1973) corresponded roughly with Schraml and Mezger"s radio continuum map (1969); OH & H_2O sources had also been detected. It seemed that this presented a possible collapsing protostar embedded in dust and we therefore attempted to scan the region at 10 µm in 1974.

Unfortunately, due to poor sensitivity, we failed to detect this source which we also had to observe at a very low elevation in relatively bad conditions. It has since been detected by Becklin and Neugebauer (1974) and measured at 16 - 20 μm. One source in NGC 6334 they compared to another well-known one ("BN" in Orion), since it was located close to an OH source and also showed strong silicate absorption at 10 μm.

Table 4.1 lists the various regions which we have studied, mainly with negative results which were caused partly by poor sensitivity and by incomplete coverage due to guiding problems. In most cases the scan results were analysed after the end of the observing trip; bright sources would be noted on the observing night, of course. One object observed in August 1974 - "IR 45.5 + 0.1" was just detected when scan data was added and analysed some time after the trip. More details are given in Section 4.4.

Another significant detection was obtained in June 1975 near the end of the observing trip and this region, "Sharpless 54" is also discussed in more detail in Section 4.3. P.A. Whitelock (1976) has treated the subject of HII region studies in more depth and should be referred to, particularly for full details of Sharpless 54 results.

Table 4.1:   H II Regions Studied and Results Obtained

Date	Object	Search λ(μm)	Detection	References & Notes
4-74	NGC 6334	10	no	see text
4-74	L134	2	no	1
8-74	Sh 138	2,10	possible	2, 3
8-74	Sh 149	10	no	4
8-74	Sh 152	2	no	2, 3
8-74	Sh 156	2,10	no	12
8-74	Sh 191	2	no	-
8-74	Sh 194	2,10	no	-
8-74	Sh 201	2,10	no	3
8-74	W31	10	no	5, 6
8-74	OH1735-32	10	no	7
8-74	OH2019+37	10	no	8
8-74	G45.5+0.1	2	yes	see text
8-74	G24.5+0.2	10	no	5
11-74	Sh 172	2	no	9
11.74	Sh 207	2,10	no	9
11.74	Sh 222	2,10	(yes)	9,10
11-74	Sh 226	2	no	-
11-74	Sh 305	10	no	9
11-74	Sh 307	2,10	no	9,11
6-75	Sh 54	2	yes	see text

Notes: Sources marked "Sh..." come from Sharpless 1959.
1. Lynds Dark cloud number 134 (Lynds 1962). This was very hard to scan due to guiding problems in a very faint field of view.
2. Frogel & Persson (1972) have done H ,K ,L photometry to date. Sh 138 possibly detected (with $m_K \sim 8$).
3. Dickenson, Frogel & Persson (1974) have detected CO emission.
4. No published magnitudes known.
5. Shaver & Goss 1970.
6. Hoffman et al.1971, 100 μm measurement.
7. Hardebeck 1972, this is an OH/IR source in fact.
8. Hardebeck & Wilson 1971, this is an OH source associated with the H II region.
9. These objects detected by Felli & Churchwell (1972) at 1400 MHz.
10. Lk Hα101 detected strongly at 2,10 μm, we find no other sources.
11. Persson & Frogel (1974) made H, K, L measurements only.

4.1.4. Source selection

One profitable way of selecting H II regions for study could be by using the recently available Schmidt Survey I and V plates, the plate limits are 17^m and 21^m respectively. Compact H II regions can first be selected from radio observations and then a comparison of the I and V plates for the same area gives a good indication of the extent of the reddening present.

Any clusters of stars which show up on the I plate and not on the V plate would almost invariably be suffering a large amount of extinction. Only stars cooler than M6 (main sequence) stars have intrinsic values of $(V - I)_o > + 4$.

Using a standard extinction law of Van de Hulst, curve number 15 (Johnson 1968, p193) it is possible to estimate the effects of reddening on various star types. This extinction curve is shown for reference in Figure 4.1. Data on star colours is taken from Johnson (1966), stars of class AO and M5 are considered as two examples for these calculations.

For a star of given I magnitude ($\leq$ 19) its corresponding magnitude at V, K, etc. can be estimated for various degrees of reddening. The relations used are:

AO stars   - $(V-I)_o = (K-I)_o = 0$

M5 stars   - $(V-I)_o = 3.5$, $(K-I)_o = -1.7$, $(L-I)_o = -2.6$

observed colour $(I-K) = (I-K)_o + (A_I - A_K)$

colour excess $E_{IK} = A_I - A_K = 0.38A_V$

Figure 4.2 shows the expected values of m_K (for AO and M5 stars) corresponding to values of visual extinction $A_V = 0 - 30^m$. The solid part of the curves indicate the ranges of A_V that are necessary to satisfy the

The Reddening Law – Van de Hulst's Curve Number 15
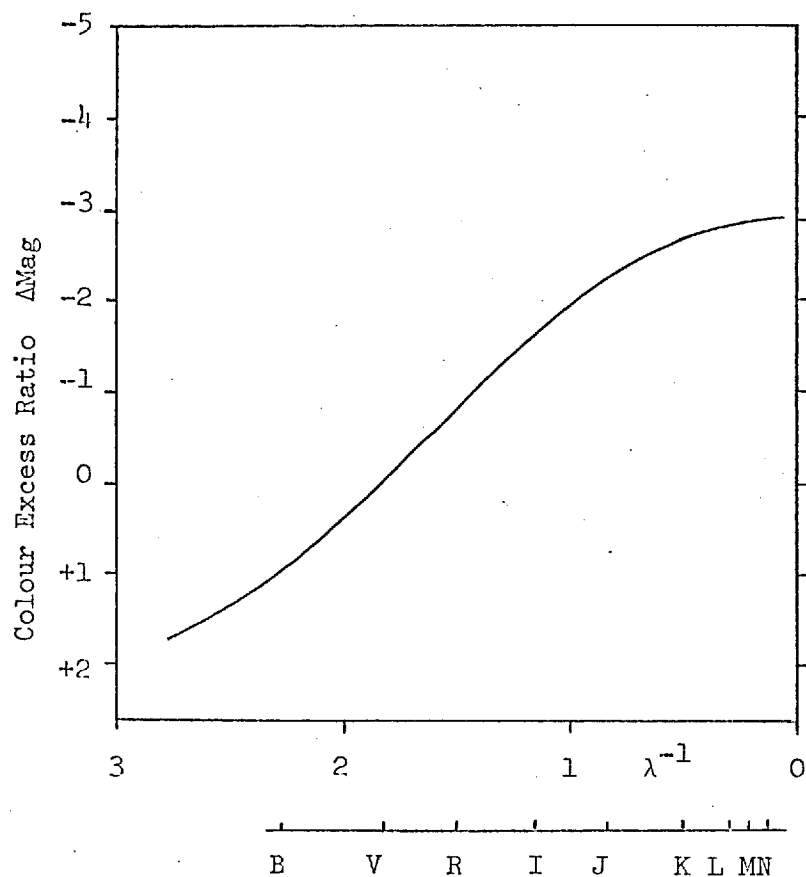
$$\Delta M = \frac{E_{\lambda V}}{E_{BV}} = \frac{A_\lambda - A_V}{A_B - A_V}$$

Wavelength Band	Extinction A_λ
U	1.561
B	1.328
V	1.00
R	0.738
I	0.470
J	0.245
H	0.15
K	0.088
L	0.046
M	0.033
N	0.013

N.B. This data is normalised to $A_V = 1.0$

Figure 4.1

2.2μm Magnitudes for Stars of known I-Magnitude
with varying degrees of extinction

($m_K = m_I - 0.38A_V$)   AO Stars

($m_K = m_I - 1.7 - 0.38A_V$)   M5 Stars
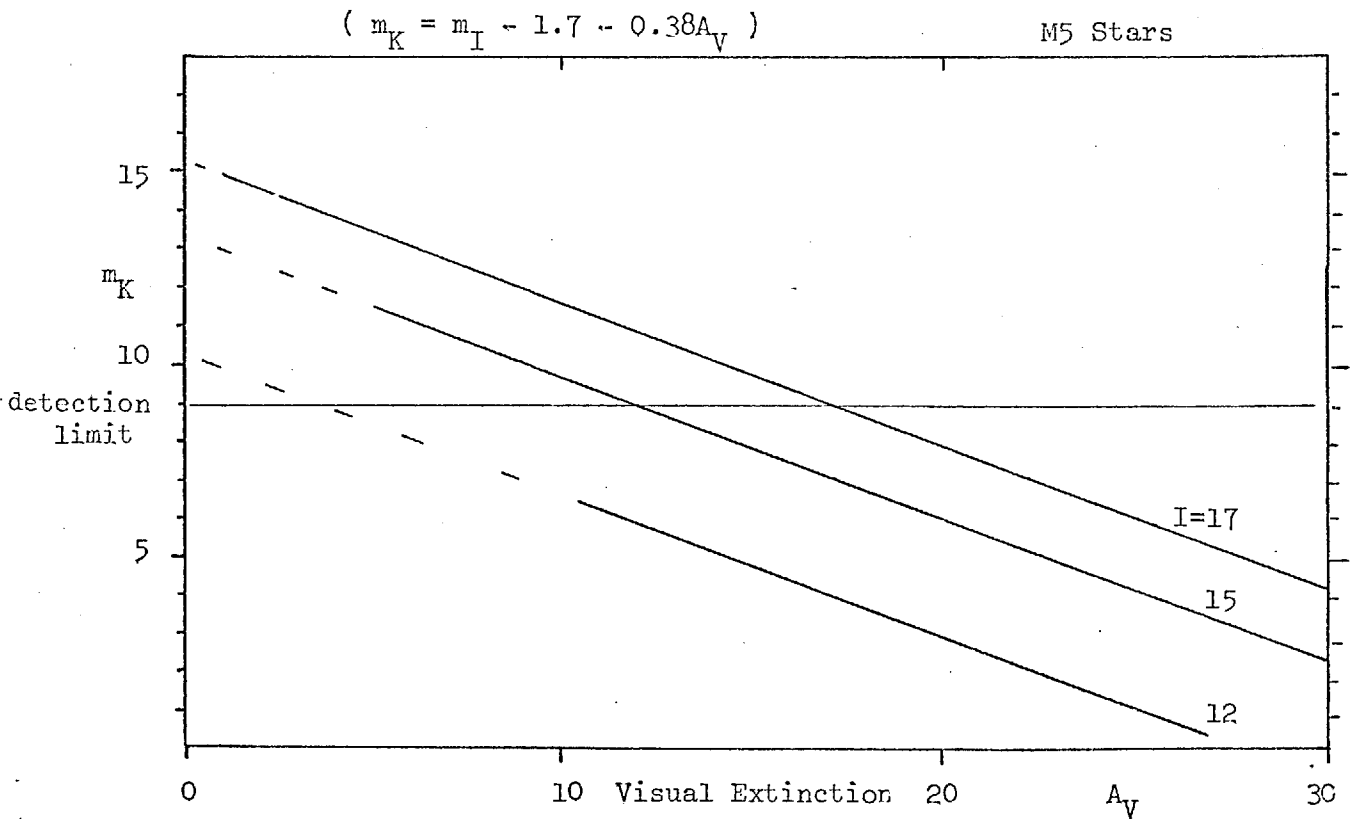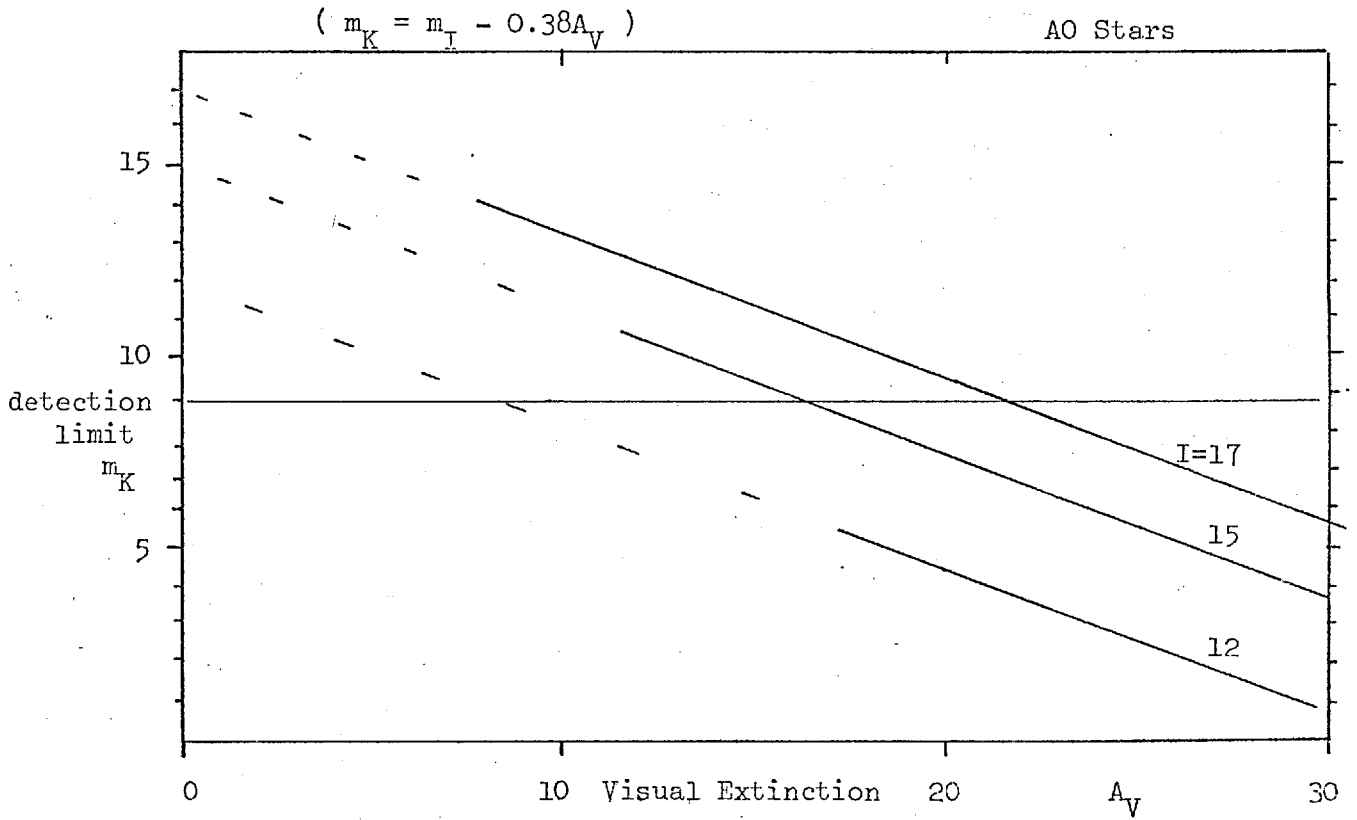
Figure 4.2

condition that $m_V > 21$. Our present detection limit of $m_K \sim 9$ is indicated, although we expect this to improve to ~ 11 in the near future. Similar curves can be readily derived to estimate m_L or other values.

It can be seen, for example, that an M5 star that is just seen on the I plate (and not on the V plate) should be readily detectable if it suffers more than $\sim 10^m$ of visual extinction. It is also evident that the I plate detection limit is superior to our 2.2 μm limit for hot stars reddened by A_V up to 20^m, and for cool stars reddened up to $A_V \sim 15^m$. Our 1.6 μm limit is the same as the 2.2 μm one and therefore work at this wavelength (H) is less useful due to larger extinction effects.

For most stars the K-L intrinsic colour differences are small and the measured values of (K-L) only exceed 1^m if the visual extinction to the source exceeds $\sim 25^m$ (with a normal reddening law). Since our detection limit at 2.2 μm is approximately 1^m better than at 3.5 μm it is clear that such stars will be detected best at 2.2 μm in general. However, any sources which are heavily reddened, or which exhibit dust emission at perhaps 600K, will be detected most strongly at 3.5 μm. This is demonstrated by the results discussed in the following sections, where most of the "interesting" sources have $m_K - m_L > 1\frac{1}{2}$.

4.2. Scanning Techniques

4.2.1. Introduction

Various different modes of scanning have been attempted as part of the H II search programme and for other purposes. Here "scanning" includes all types of IR photometric measurements which are made whilst the telescope moves as opposed to the normal "photometry" work where stationary measurements of sources in alternate beam positions only are

made. For certain measurements, e.g. of star profiles, extended source measurements, etc., a single scan or repeated scans in the same line are required. However, much of the work described here has involved raster searches by means of many scans with an offset step sideways between each one.

The sky chopper displaces the beam in declination and so all scans are normally done in declination also, this results in a "point-source" profile as in Figure 4.3. The length of scans varies between $\sim$ 40" for a star profile to about 5' when searching larger areas.

The minimum scan length of $\sim$ 40" is required in order to measure the whole of a profile together with a reasonable zero level, the maximum length is restricted by slow telescope drifts (or tracking errors) which become significant over long scans. When searching an area of sky with a 10" beam size it is necessary to do steps of only 5" in R.A. between scans to ensure detection of the faintest sources, however, if time is very short or it is desired to locate a known fairly strong source, then 10" steps are adequate.

4.2.2. Methods used

The "simplest" method of scanning would involve holding the handset "slow guide" control for the required time. However, the ROE telescope drive rack provides facilities for several methods of automatic control, and interfaces between it and the control box (Sections 3.2,3.3) have been constructed. The "slow-guide" speed of the telescope drive is set at about 1".4 sec^{-1}; this gives a reasonable scanning sensitivity. The variable offset speeds of the telescope enable faster scans to be done at the expense of reduced sensitivity and resolution.

Tracings of Measurements made on 2 stars (at 10μm in this case)

Scan through a
faint source

"Upper" beam
Centre
"Lower" beam

Photometry of
same source
for comparison

L C U

Strong
Source

ııııııııı   ıııııııı   ıııııııı   ıııı Sampling Points   ıı
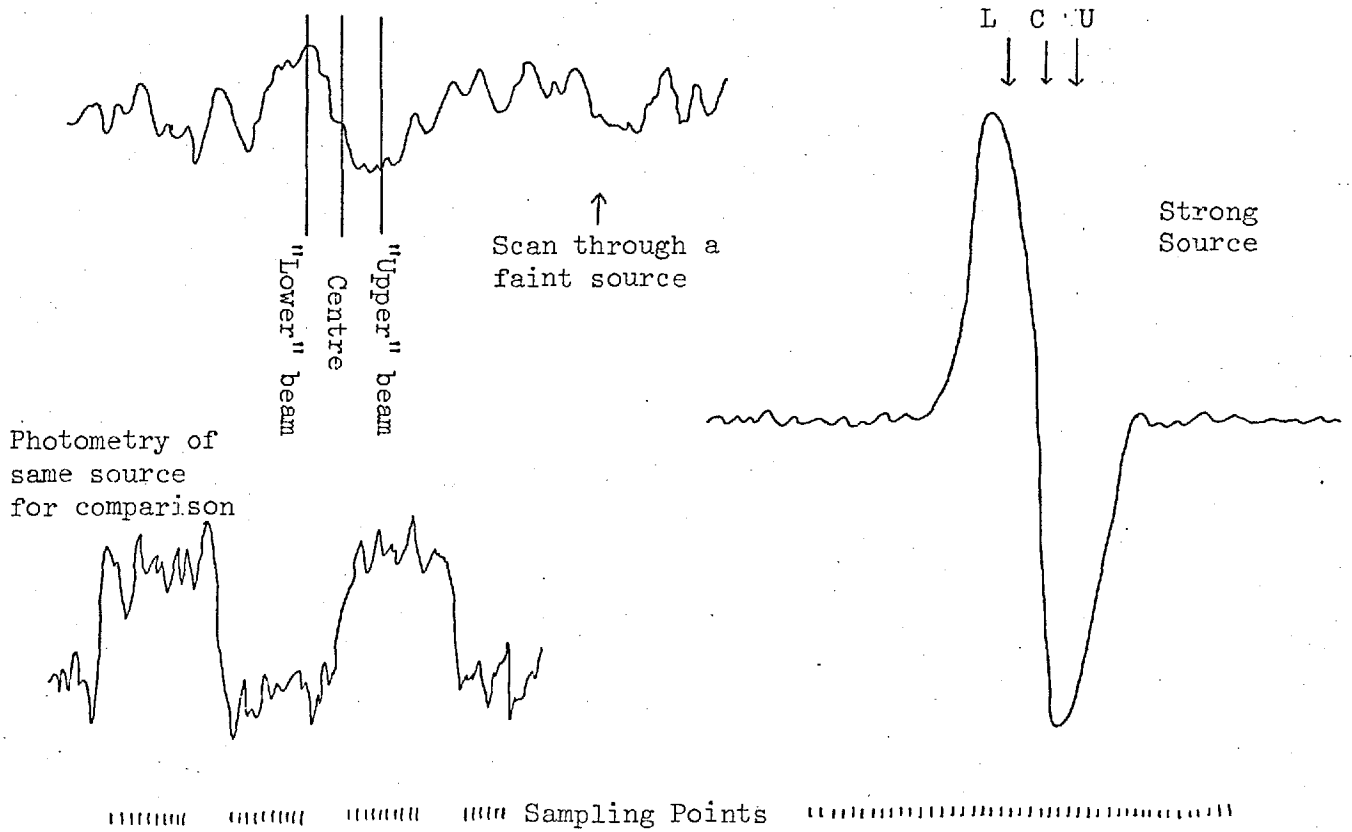
Figure 4.3

Normal Method of Raster Scanning

Motions at beginning of a raster scan

Control Sequence

+Dec. Scan (Slow Guide),with Sampling

Backlash
Compensation

-Dec. Offset & RA
Step

ıııııııııııııııı   ıııııııııııııııı   Sample Commands @ 1 sec

Guide Command &
Dec. (& RA) Reset

Dec. Offset (& RA Step)
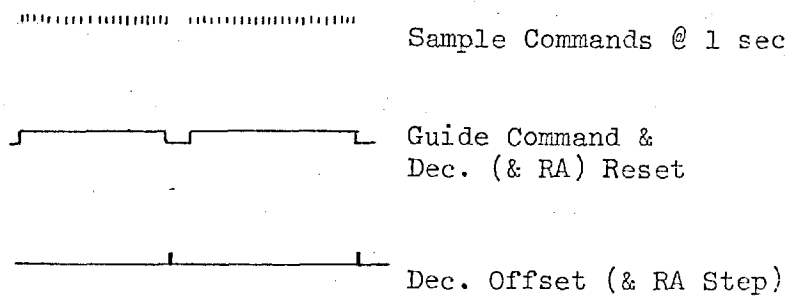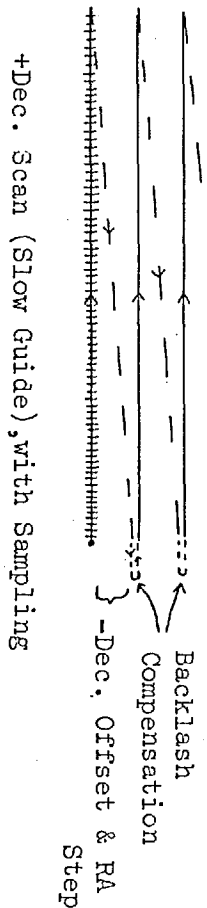
Figure 4.4

Some typical slow scan parameters are given below:

Scan length 180", declination increasing.

Scan speed 1".4 sec^{-1}, 1 sec. sample interval.

Scan time 130 seconds, return time 8 seconds.

Beam size 10", chop amplitude 10".

Detection limit at 2.2 μm, m_K = + 9 (source "just seen" on chart).

The telescope guide rate was measured to be constant in any direction, thus giving repeatable scan lengths. It has been found that a "standardised" scan procedure is useful for ease of operation and later analysis. Multiple scans can be successfully added since the start position can usually be set within 1". When starting a scan there is a 1-2 second repeatable pause, due to inertia, before motion commences.

Generally the declination motions of the telescope have been found to be very repeatable, with errors of less than 1" over a scan up to 5' in length; the position display also gives accurate values (without drift) to ± 5" for long periods. Errors in the R.A. position can occur; careful balancing,however, has given very little tracking error or drift for periods of up to 10 mins (measured after the telescope clutch has been recently improved). It is normally found necessary to correct the R.A. position after each scan or so by 1" or 2", in any case we often step by 5 or 10" in R.A. between each scan.

Raster scans of several hours have been performed and these present no problems when reasonably bright field stars are available. In many cases at least one star of magnitude m_V < 12 is to be seen in the field; this enables the start position of each scan to be set precisely and thus a complete area can be covered with certainty. In other cases the presence of only very faint stars or none at all makes the work very difficult; dark of the moon time is much better for this sort of work.

It is possible to offset from a bright star and then carry out a limited raster automatically, but its usefulness is limited by the lack of precise positional knowledge and doubt about complete coverage. R.A. drifts of ± 5" can occur during a scan and the position displays can give no information of motions < $\frac{1}{2}^s$. For scans with known field-stars the Palomar Sky Survey Red and Blue plates are often used, then the start position of each scan can be determined relative to these stars to an accuracy of about 1". The relative position of a source in the scan can be determined to at least 1-2".

Raster modes

Most raster work is performed as in Figure 4.4. This consists of a slow scan in declination with continuous recording throughout its length. At the end of the scan sampling ceases and a rapid return occurs, a small R.A. step can also be performed at this point automatically or by hand. Automatic backlash compensation occurs at the end of the return (this is a drive system option).

A new scan can then be started and a new series of data samples taken after the start position has been adjusted as required. The length of scan is defined by the time for which "slow guide" control is activated, which is proportional to the number of samples taken (at a 1 second interval). The return is by means of the faster dec. offset facility whose distance is set up on thumbwheel switches, the return distance can be matched to the scan distance to within 1".

In this mode of operation a raster to cover an area of 5 x 5' by means of a 5' dec. scan and 5" R.A. steps would take at least 4 hours, as follows:- scan time = 215 secs, return time = 13 secs, time to set start of each scan = 12 secs, therefore 60 scans x 4 mins = 240 mins total.

Other raster modes have occasionally been used. One method involves scanning in a positive dec. direction whilst sampling and then, after a preset pause, returning at the same slow speed and still sampling, then pausing and going in the alternate direction, and so on. This has the disadvantage that scans of opposite direction are less easily compared or added and also it is less easy to be certain of the start position of each scan or to correct for drifts.

Scans at faster speeds are possible by using the drive rack dec. offset facility which has 10 different speeds (in factors of 2 down from a maximum of 60"/sec.). A fine control is also available and in fact 5"/sec. has proved to be a useful speed, it gives a reduced sensitivity but is faster when searching for an expected source of moderate magnitude.

Recordings are normally taken continuously when a scan/raster is performed and then analysed later for weak sources (P.A. Whitelock has constructed computer programs for this purpose which prove very effective). It is also possible to perform a raster scan of an area and continuously monitor the chart record only, any weak sources that are seen by the "experienced" eye can then be re-examined at once or returned to later. It is proposed to use the computer at the observatory to optimally detect weak sources (see Section 4.5).

4.2.3. Choice of wavelength

The wavelength chosen for almost all of the early searches (with the PbS detector) was 2.2 µm; at this wavelength we had good detector response and many sources were expected to have strong fluxes. At shorter wavelengths extinction can reduce the signal. At 3.5 µm, although many sources emit more strongly, the detector response is poor

and sky noise is more serious. The new InSb detector is better at 3.5 μm than the PbS one. Some scans were made at 10 μm, but this has been less profitable due to low detector sensitivity.

At 2 μm sky emission is low (see Table 2.1) and its photon shot noise is less than our present detector noise. (Sky Noise $\sim 3 \times 10^{-16}$, N.E.P. $\sim 2 \times 10^{-15}$ WHz$^{-\frac{1}{2}}$). Thus it is possible to use larger apertures (and chop amplitudes) to study fields of view of $\sim 30"$ without being sky noise limited. The condition will not be valid in the near future when values of detector N.E.P. $\sim 4.10^{-16}$ WHz$^{-\frac{1}{2}}$ should be achieved (A.D.Macgregor private communication, 1977).

A field lens system can be employed in the cryostat to give a faster beam without an increase in detector size. Sources found in this way could then be re-examined with a 5 or 10" aperture to give more precise positions, and photometry at other wavelengths then performed.

Some early work was not very useful due to a very poor PbS detector response - they deteriorate with time, as mentioned earlier. We also used an excessively high chop frequency at one stage which reduced our response; we now do more careful checks to maximise our sensitivity !

4.2.4. Source density estimates

It is possible by various means to calculate the number of sources one would expect to find in a given region of sky at a certain wavelength. The 2 μm survey (Neugebauer and Leighton, 1969) catalogues IR sources brighter than $m_K = 3$. The AFCRL and AFGL surveys (Walker and Price, 1975 and Price and Walker, 1976, respectively) contain sources to a limit of $m(4.2) = 1.1$ and $m(11) = -1.2$.

If we assume a uniform distribution of sources and no significant extinction it is possible to extrapolate source counts in a given area. Neglecting extinction causes an overestimate in fact.

The relation used is $N(I) \propto I^{-3/2}$ (or, $\log N = 0.6m + c$) where N is the number of sources visible with an intensity $\geq$ I.

The assumption of a uniform source distribution and no extinction imposes a limit on the method. For example, at 2.2 μm a typical interstellar extinction is $\sim$ 0.1 mag kpc^{-1} (from Allen 1973 and Figure 4.1) and therefore we might expect a reasonable estimate of source counts out to a distance of $\sim$ 10 kpc. This corresponds to a magnitude range of $\sim 5^m$, that is we can extrapolate from the 2 μ survey roughly to a limit of + 8^m (at K) without gross errors. (The 2 μ survey measures sources out to a distance of approximately 1 kpc).

Another means of extinction is to use visual statistics of star counts to estimate infrared source distribution. This method has been discussed by P.A. Whitelock (1976 Thesis); its extrapolation over large ranges is probably less valid (because it is based on measurements of nearby stars).

All calculations of this nature are prone to systematic and statistical errors and can only give very rough estimates. It is planned to investigate source distribution and the validity of such extrapolations in the near future by using a sensitive InSb detector to search over a given area of sky. Some examples of source counts and extrapolated numbers are given in Table 4.2.

Table 4.2:   Source Count Data

2 μm Survey	Number of Sources (arcmin)$^{-2}$		
	$M_K < 3$	$M_K < 6$	$M_K < 9$
Galactic Centre	2×10^{-4}	.014	0.9
G45.5 (in galactic plane)	$.9 \times 10^{-4}$	.006	0.35

AFCRL Survey (4.2 μm)	Number of Sources (arcmin)$^{-2}$			
	$M_4 < 1.1$	$M_4 < 3$	$M_4 < 6$	$M_4 < 9$
G45.5	2×10^{-5}	3×10^{-4}	.02	1

Visible Data extended to 2.2 μm	Number of Sources (arcmin)$^{-2}$		
	$M_K < 3$	$M_K < 6$	$M_K < 9$
Galactic Plane ($b^{II} = 0$)	3×10^{-5}	8×10^{-4}	.02

4.3. Observations of Sharpless 54/W35

4.3.1. Introduction

During the June 1975·observing period one of the H II regions
we chose to search was Sharpless 54. This H II region was first listed
by Sharpless (1959) as having a size of 140 arcmin with a bright irregular
filamentary structure. It contains the cluster NGC 6604 and has been
included in the survey of Rodgers, Campbell and Whiteoak (1960) as
No. RCW167. Radio continuum maps at 1400 MHz (Felli & Churchwell 1971),
5000 MHz (Goss & Shaver 1970) and 408 MHz (Shaver & Goss 1970) have been
published.

The area that we have studied has been designated G18.7+2.0, this
being the most compact area of radio emission and also showing dense
optical nebulosity. OH absorption associated with this region has also
been reported by Goss (1967). The H II region was surveyed by Westerhout
(1958) who numbered the source as W35. It appears that G18.7+2.0 is at

a distance of 3.2 kpc and is probably at a similar distance but not related to NGC 6604 which is 30 arcmin further south.

At the end of the observing period, which was spent partly searching for possible proto-stars, we were encouraged by the detection of a bright source with a 2.2 μm magnitude of ∿ +3. We subsequently found two more fainter 2 μm sources and were able to measure the first one at 10 μm. On the final night further raster scanning produced four more 2 μm sources under relatively poor conditions; we then had to postpone further observations until a future date.

The detection of these seven sources is reported in a paper by Jorden et al.(1976) - see Appendix 1, although further work has slightly modified the results presented there.

4.3.2.   The measurements

In August 1975 a total area of almost 15 x 15' was searched (at 2 μm) and twenty-five new sources were found, with a detection limit of m_K ∿ 9; sources were noted if they appeared significant on a chart record during the scan. In the available time we were able to do J, H, K, L photometry on fourteen of these sources using our PbS detector. Subsequently in April 1976 using the new InSb detector we were able to spend some time doing J, H, K, L photometry on a few more of these sources, we also checked some of the early measurements.

In almost all cases the source magnitudes were measured with respect to calibration stars HD 169226 and ν Her. The latter is a useful "primary" standard with a 2.2 μm magnitude of 3.20; the former was chosen from a list by D. Allen (1973) since it was very close in

position to the area we were studying. On the basis of our measurements

of HD 169226 we derive some more precise estimates of its magnitude

(with respect to ν Her) than did Allen originally, these are shown below.

HD 169226: $m_J = 5.35$, $m_H = 4.81$, $m_K = 4.51$, $m_L = 4.23$, $m_M = 4.09$

Early measurements were plagued by the non-linear behaviour of the

PbS detector, whereas later work with the InSb detector has shown no such

problems and thus more accurate photometric calibration can be done.

Photometry from 1.2 to 5 μm has been done on sources 1-10, 12-15. Sources

1 and 7 have also been detected and measured at 10 μm.

Note that the numbering of sources described here is purely in order

of discovery, whereas in the paper by Jorden et al.(1976) they were listed

in order of Right Ascension. Our infra-red measurements of Sharpless 54

are shown in Table 4.3.

The Air Force Cambridge Research Laboratory Survey (Walker & Price

1975) reports a source at $18^h 15^m 05^s \pm 08^s$, $-11° 46'$ .5 ± 2. '5. The

magnitudes are given as $m_{20\mu} = -3.9$, $m_{11} = -2.15$, $m_4 > 1.1$ for this source,

number CRL 2113. In April 1976 we searched at 10 μm an area 4' in dec. x 3'

in RA centred on this position. We found no significant point source to

a limit of about 0^m.

However, the source is noted as being extended with respect to the

CRL detector size of 3.4 and thus our lack of detection is not surprising

since with a 10" or 30" chop any large sources are nullified by our

technique. Walker & Price associate it with NGC 6604 but their source may

in fact only be related to the area of the radio emission peak G.18.7÷2.0

(which is 30' away as was noted earlier).

Table 4.3:   Sharpless 54 - IR Source Magnitudes

Source No.	J	H	K	L	M	N
* 1	6.0	4.3	3.4	2.45	2.2	0.55
2	11.95	9.2	7.55	6.15	5.5	0.8
3	9.5	8.2	7.5	6.7	-	0.8
4	9.2	7.5	6.9	6.0	5.7	-
5	10.6	9.2	8.5	7.75	6.9	-
6	10.2	9.2	8.3	7.8	-	-
7	6.2	4.55	3.85	3.3	3.8	2.6
+ 8	9.5	7.95	7.15	6.5	-	-
9	8.0	7.55	7.3	6.9	-	-
10	8.6	8.55	8.3	7	-	-
12	9.5	9.1	9.0	7	-	-
13	6.8	5.9	5.65	5.3	-	-
+ 14	8.8	7.55	6.7	6.0	-	-
15	10.2	9.05	8.45	7.4	-	-
+ 18	10.5	8.6	7.7	7.05	6.2	-
27	10.65	8.7	8.2	7.45	-	-
32	9.7	7.75	6.85	6.05	4.05	-
33	-	8.45	7.95	7.95	-	-

Notes: The results are quoted to $\pm$ $0^m.05$, except where noted below.

The H, K, L errors are $\pm$ $0^m.1$, and those for J, M, N are $\pm$ $0^m.2$.

* Source 1 has given measurements differing by $\pm$ $0^m.4$ from those shown.

+ These Sources have H, K errors of $\pm$ $0^m.05$.

Source 7 has errors of $\pm$ $0^m.05$ for H, K, L.

4.3.3. Discussion

The sources occur around an area of heavy optical obscuration on the plates of Sharpless 54. Sources 1 and 2 which are nearest the centre both show (V-K) $\gtrsim 13^m$, thus the infra-red sources seem to be behind, or associated with, the H II region and dust. We assume that most are spacially co-incident and physically associated with the gas and dust. A few of the sources may be foreground objects, particularly numbers 9, 10, 12, 13 (for which we have photometry). These sources are only slightly reddened and appear equally strongly on I and V plates, whereas the more strongly reddened ones are most intense on the I plate.

The H and K magnitudes of seven sources studied to date are accurate enough to estimate colours reasonably well. However, the various errors in calibration (random and systematic) make good estimates of m_V, m_H, m_K difficult; there are also uncertainties in the reddening law, the spectral types of the sources, and in the ratio of total to selective extinction in this area. The available data can only suggest the possibility of early and late-type stars in this complex region of gas and dust. (Borgman, Koorneef & Slingerland, 1970, reported a cluster in Ara in which early and late-type supergiants were found to be present).

One source, numbered 7, was measured extensively from 1.2–10 μm and a 3200–1100 Å spectrum of it was obtained by P.A. Whitelock. This proves to be a carbon star, it is a highly evolved (cool) source, suffering less extinction than many of the other sources and is probably not associated with the main group in Sharpless 54.

Plates 4.1 and 4.2 show the I and V plates of the Sharpless 54 area, our measured sources are indicated by crosses.

Plates 4.3 and 4.4 show the Palomar Sky Survey red and blue plates of the same area.

" V "

" I "
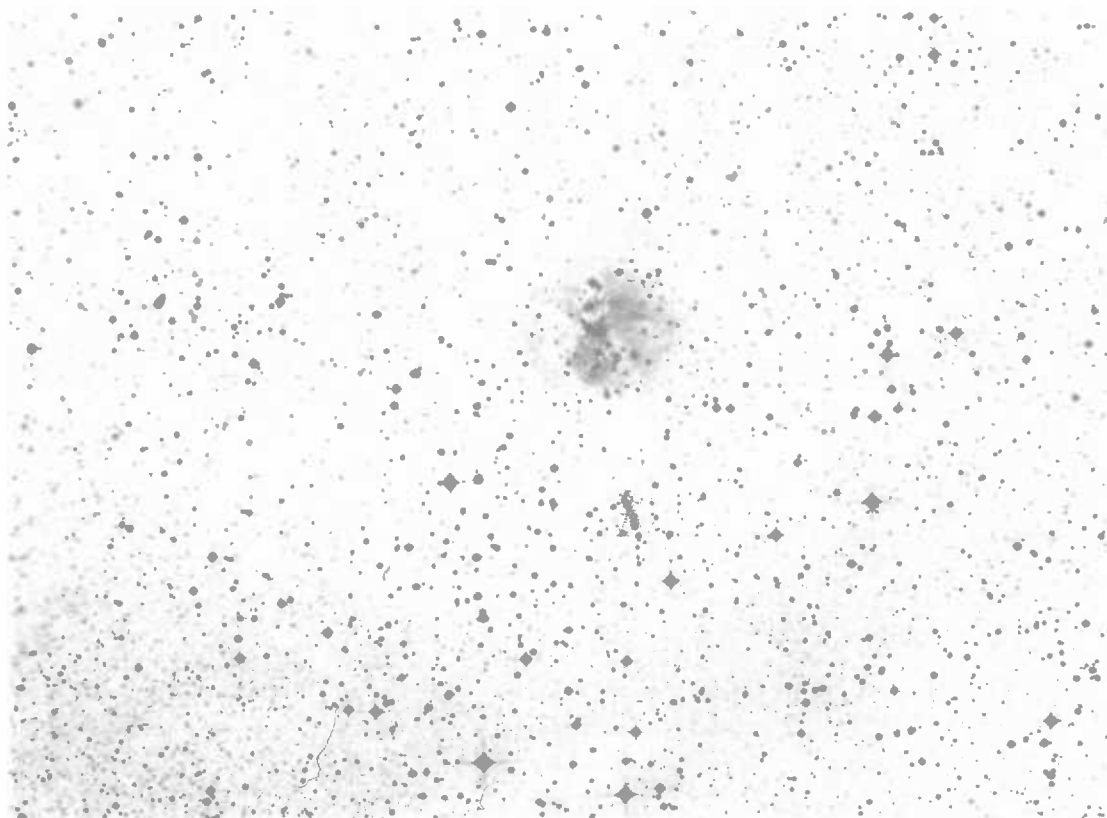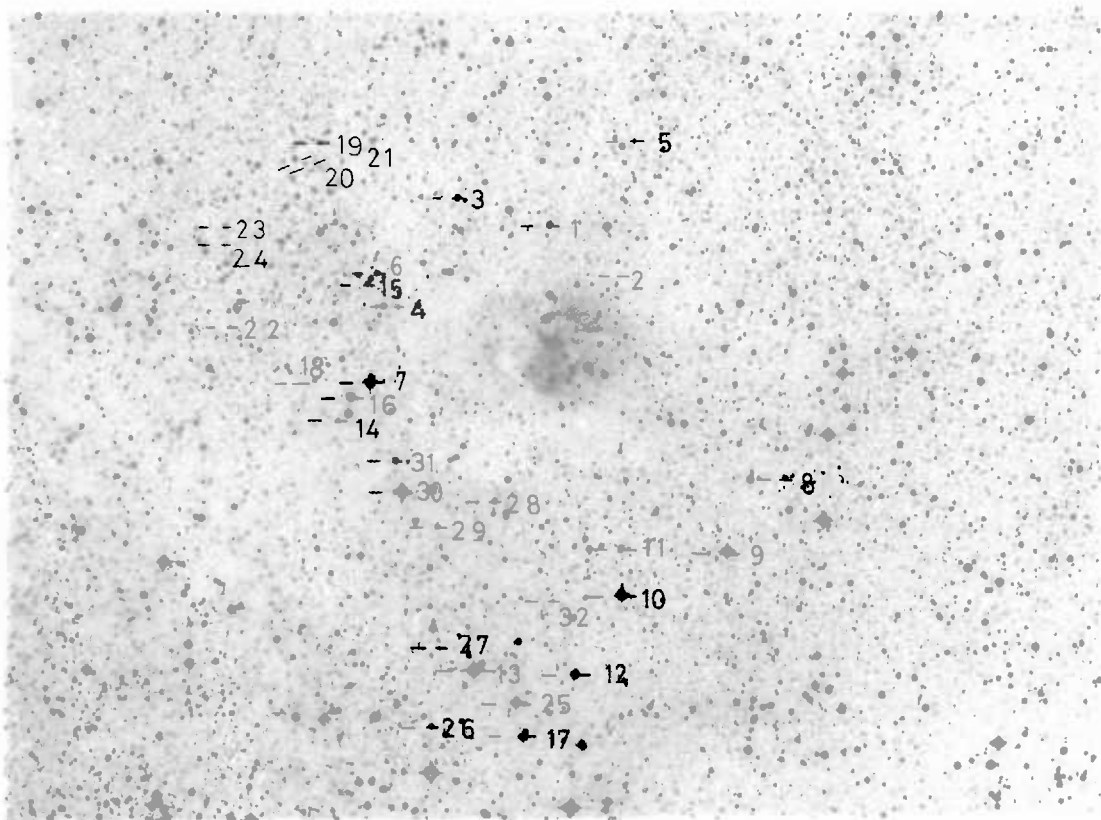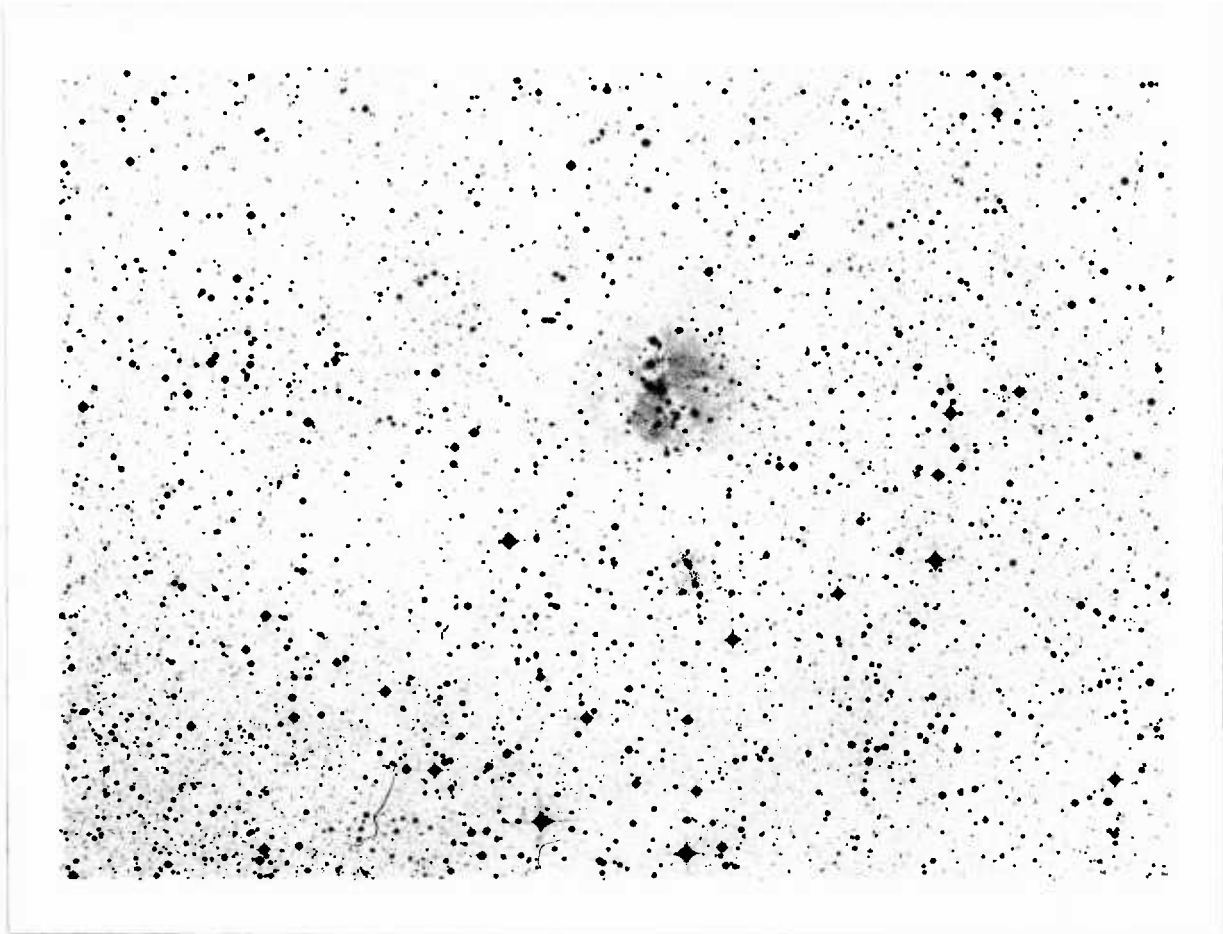
PLATE 4.1
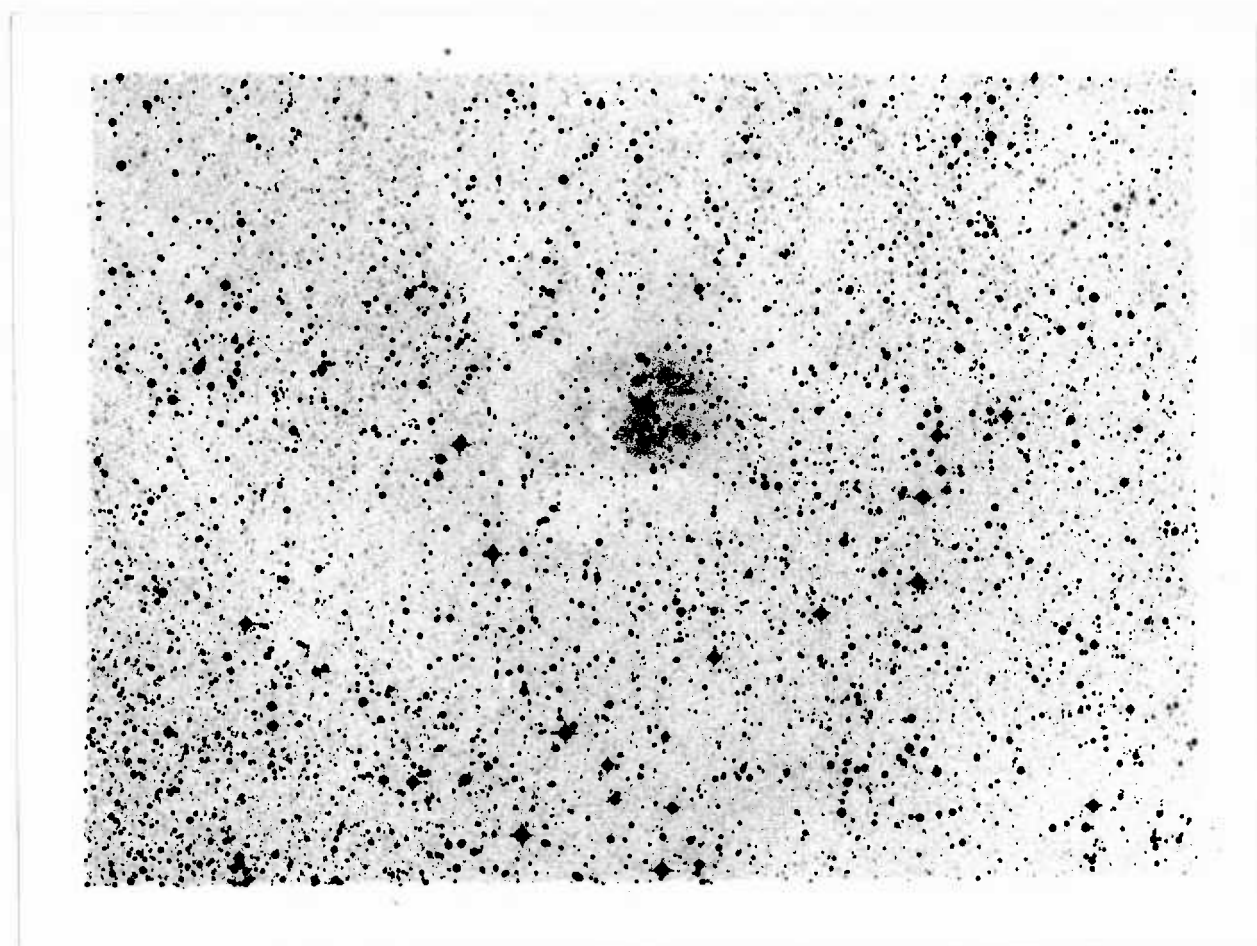
PLATE 4.2

PLATE 4.1

PLATE 4.2
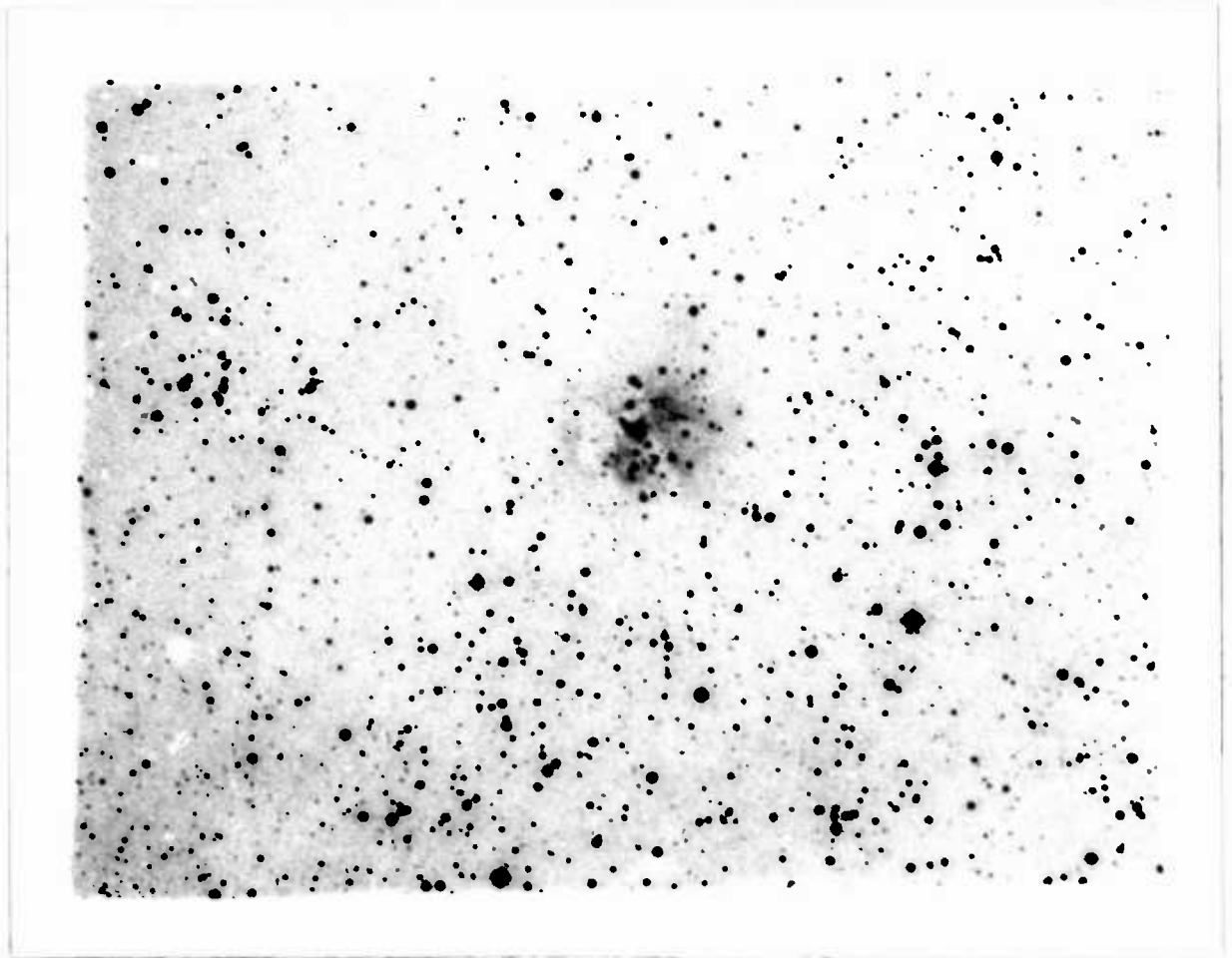
PLATE 4.3
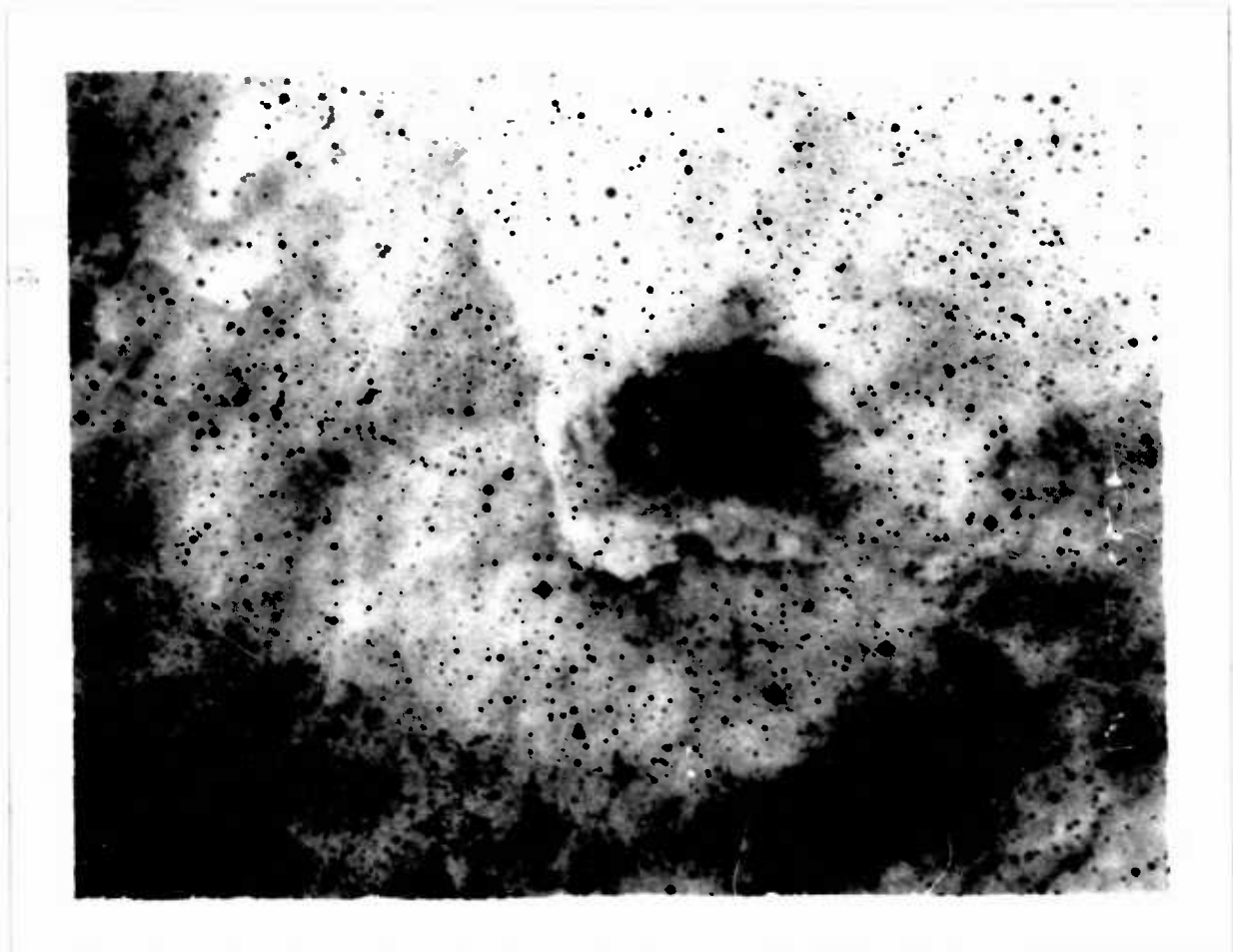
PLATE 4.4

4.4. Observations of G45.5 + 0.1 Region

4.4.1. Introduction and measurements made

This area was selected for study on the basis of known compact radio condensations (Wynn-Williams, Downes, Wilson 1971, hereafter WDW) and reported measurements of two OH sources by Goss et al.(1973). We chose to study an area of about 3 x 4 arc minutes around each of the OH sources. When scans of these areas were first made, we only detected one source of magnitude $m_K \sim 6$ near OH45.5 + 0.1 (of Goss et al); this was a result of our very poor sensitivity with a PbS detector at that time.

Figure 4.5 shows an original scan through the source, together with the data convolved with the instrumental profile in order to enhance the signal (see following section). After our initial detection, but before further measurements were made, Zeilik, Kleinmann & Wright (1975, hereafter ZKW) reported their measurements of another infra-red source near OH45.5 + 0.0, and at the centre of one radio component.

We subsequently measured this region in more detail and with the increased sensitivity of an InSb detector; four sources have been detected, including the two mentioned above. In this case we searched at 3.5 μm, which has proved to be efficient for the reddened sources discussed here. A paper discussing these measurements by Jorden et al.(1977) is in press, see Appendix 1. A 2.7 GHz Map of the region by WDW is shown in Figure 4.6, our infra-red sources and various other associated measurements are indicated.

IRS1 is the source reported by ZKW and subsequently measured by us. IRS2 is a brighter source near the boundary of the radio-continuum condensation. IRS3 is the source first detected by us near OH45.5 + 0.1 and close to the northern condensation. IRS4 is a further source first

The Detection of a new infra-red source - IR45.5+0.1

Original Scan Data
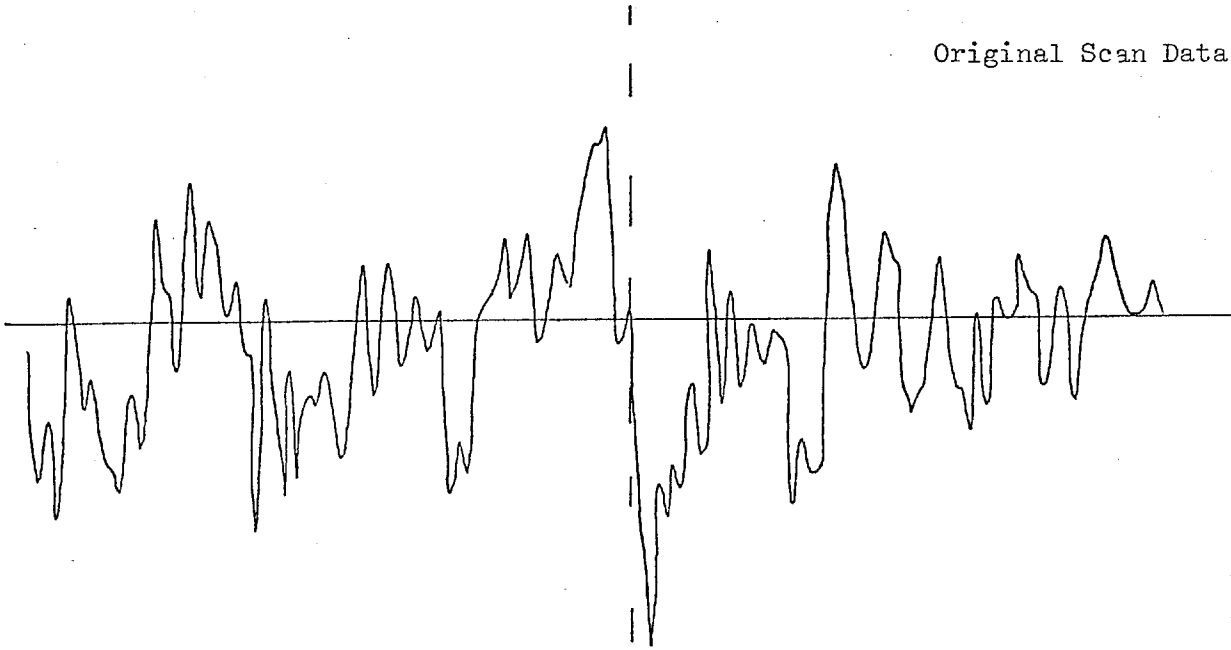
Sample
Points

Scan data convolved
with the instrumental
profile, about the
central source position
only
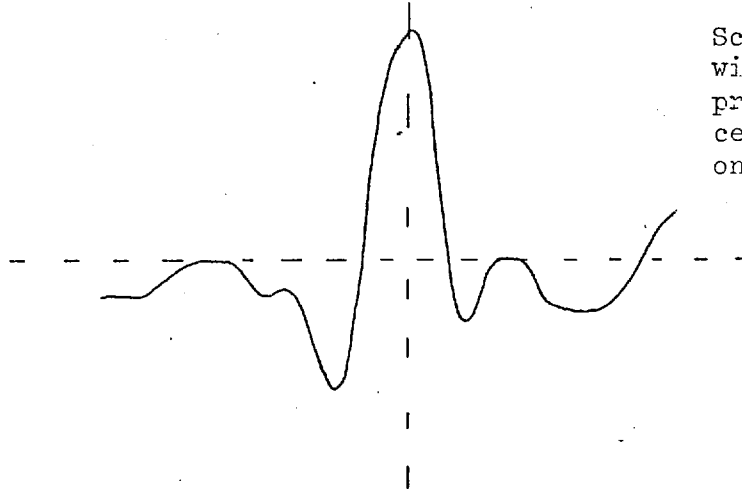
Scan Information :

Object Ref. G138

Scan Rate = 1.4" sec^{-1}

150 Samples/Scan

2 Scans in each position

Scan Length = +215"

+5" R.A. Step between positions

Wavelength 2.2μm

Source detected in scans 13,14

Source magnitude = +6.0 (2.2μm)

Position - $19^h 11^m 44.9^s$

(1950) $+11°07'34"$

Position Error (± 10")

Figure 4.5

G 45·5+0·1   1950 COORDINATES
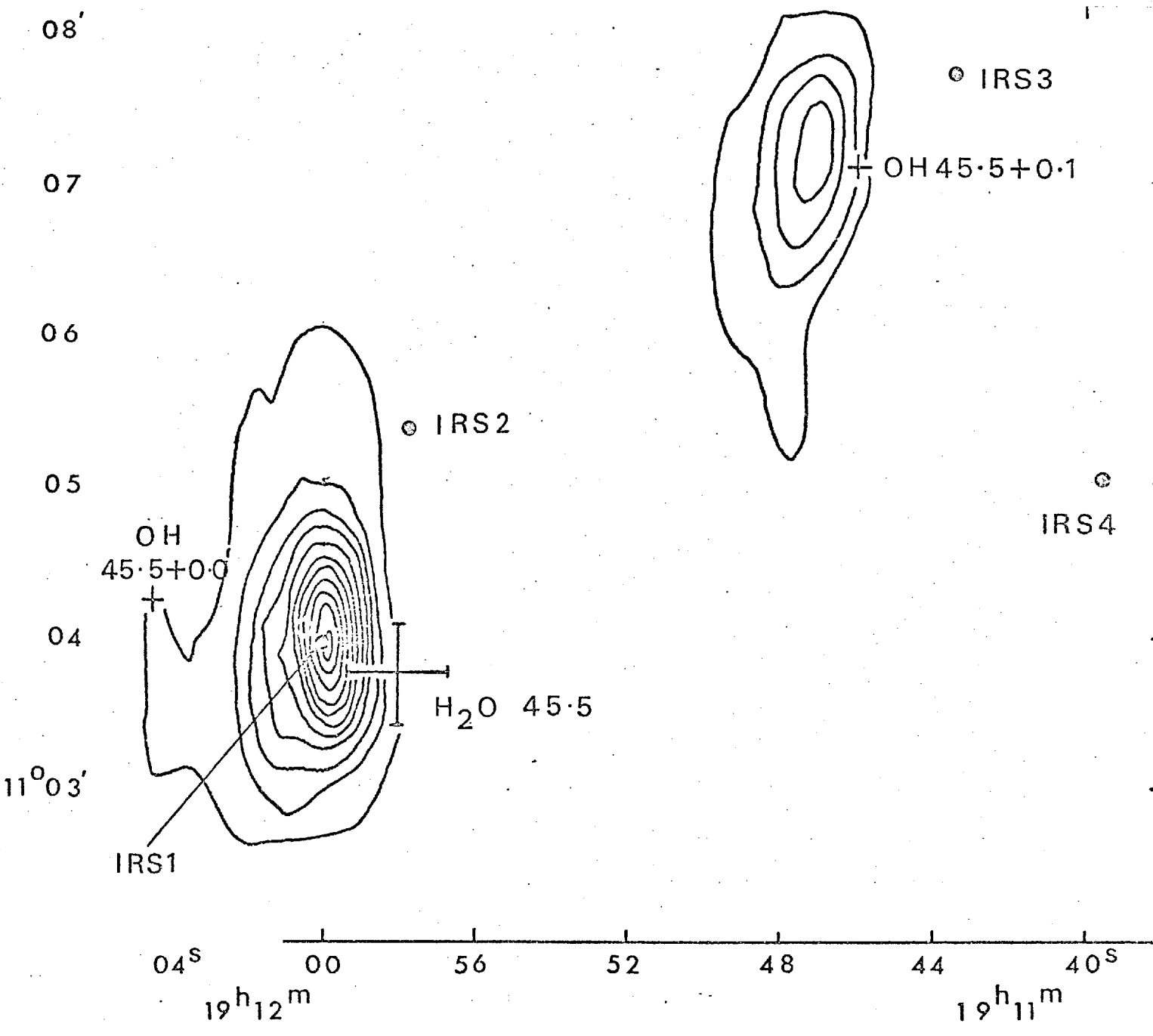
Figure 4.6

detected during our search scans but slightly further from the radio-components. Table 4.4 indicates the measurements made of these four sources.

Table 4.4:   Measurements of G45.5 + 0.1 Sources

(a) Measured Magnitudes, and PSS red plate estimates

λ(μm)	IRS1	IRS2 Aug.1976	IRS2 Oct.1976	IRS3	IRS4
0.65	20	18 (1)		20	17 (1)
1.25	13.9(.2)	10.67(.05)	11.8 (.1)	10.98(.05)	8.9 (.05)
1.65	12.3 (.1)	9.28(.05)	10.4 (.1)	7.9 (.05)	7.38(.05)
2.2	9.86(.05)	6.91(.05)	7.88(.05)	6.07(.05)	6.84(.05)
3.4	7.57(.05)	4.10(.05)	4.91(.05)	4.64(.05)	6.40(.05)
4.9	5.4 (.1)	2.68(.05)	3.28(.05)	4.25(.05)	6.3 (.6)
10.6	2.0 (.35)	0.6 (.2)	1.6 (.2)	2.7 (.5)	-

The 1σ errors are given in brackets after each measurement.

(b) Derived Fluxes, F_ν (in units of 10^{-26} W m^{-2} Hz^{-1})

Waveband	$0^m.0$ flux used	IRS1	IRS2	IRS3	IRS4
R	3200	3×10^{-5}	2×10^{-4}	3×10^{-5}	5×10^{-4}
J	1770	.005	.095	.072	.49
H	1070	.013	.21	.74	1.20
K	620	.070	1.07	2.31	1.14
L	300	.28	6.87	4.18	.83
M	180	1.2	15.2	3.59	.5
N	38	5.7	22	3	-

The 0^m flux levels are taken directly from Johnson (1966) or interpolated (for our filters) from his measurements.

Various radio continuum, OH emission, IR detections and associated measurements of the G45.5 + 0.1 region are shown in Table 4.5. Schraml and Mezger (1969) made a 1.95 cm continuum map of the area, and classed it as a compact H II region; this was followed in 1971 by the 2.7 and 5 GHz continuum maps of WDW,in which three components were identified as well as a H109α recombination line measurement.

In 1970 Downes measured 1665 MHz OH emission with 3 velocity components which were later proved by Goss et al.(1973) to be two sources (OH45.5 + 0.0 and OH45.5 + 0.1) on the outer regions of the high density H II condensation. Winnberg et al.(1973) detected a type II OH/IR source at 1612 MHz which they decided was probably not associated with the other two OH sources (classed as type I); in 1976 Schultz et al.measured this source at 4 μm.

In 1975 ZKW reported their measurements of the extended source IRS1 as above. No detections in this region are recorded in the 2 μm Sky Survey (Neugebauer & Leighton 1969), but this is to be expected since we have found no sources brighter than their detection limit of $m_K \sim 3$.

4.4.2.   Source 1

IRS1 has been fairly extensively studied by ZKW from 2.2-21 μm, our observations support theirs and also give measurements at 1.2 and 1.6 μm. The source is extended to about 20" (at 10 μm) and is at the same position and has a similar size to the 2nd radio component of WDW. Unfortunately no short wavelength scans have been done which would show whether or not it is extended for λ < 5 μm.

| | Table 4.5: | G45.5 + 0.1 Measurements | | |

Type of Measurement	Results	Source Co-ordinates		References
1.95 cm continuum	map	19^h12^m	$11°04'$	Schraml & Mezger 1969
1665 MHz OH emission	3 velocity features	see below		Downes 1970
1665 MHz OH emission	OH45.5 + 0.1, velocity = 59 km s^{-1}	$19^h11^m46^s.1$	$11°07'06''$	Goss, Lockhart, Formalont
	OH45.5 + 0.0, velocity = 65,68 km s^{-1}	$19^h12^m04^s.4$	$11°04'15''$	& Hardebeck 1973
2.7 GHz, 5 GHz continuum	map shows 3 components:	$19^h11^m47^s.2$	$11°07'08''$	Wynn-Williams, Downes
H109 recombination line	radial velocity of line = 55 km s^{-1}	$19^h12^m00^s.0$	$11°04'00''$	& Wilson 1971
		$19^h12^m01^s.3$	$11°03'55''$	
Formaldehyde absorption	–	–		Wilson 1970
CO emission	line velocity = 58 km s^{-1}	–		Wilson et al.1974
OH 1612 MHz emission	type II OH/IR source,vel.= 18,53 km s^{-1}	see Evans 1976		Winnberg, Goss, Höglund & Johannson 1973
Discussion,nature of OH source	–	–		Wallerstein 1973
OH 1612 MHz source position	–	see Evans 1976		Winnberg et al.1975
Position of 1612 MHz OH source	position to ± 5"	$19^h11^m58^s.3$	$11°05'25''$	Evans et al.1976
IR counterparts to OH sources	$m_{3.8}$ = 3.75	$19^h11^m59^s.5$	$11°05'.5$	Schultz, Kreysa & Sherwood 197
Infra-red	IRS1 photometry, see later	$19^h12^m00^s$	$11°04'00''$	Zeilik,Kleinmann & Wright 1975
Infra-red	m_{11} = 2.25, m_{20} = -5.15	$19^h11^m.9$	$10°52'$	Walker & Price 1975
H$_2$O 22 GHz maser	line velocities = 48,59 km s^{-1}	$19^h11^m58^s$	$11°03'44''$	Lo, Burke & Haschick 1975

The indications are that there is a large amount of extinction ($A_V \sim 30^m$) and this is a result of dust associated (and well mixed) with the gas in the H II region. The source OH45.5 + 0.0 is at the edge of the radio condensation associated with IRS1. See our paper in Appendix 1 for a fuller discussion of this source. Very recently (Zeilik, 1977) this source was included in a discussion on a dust model for the IR emission from compact H II regions.

4.4.3. Source 2

IRS2 is located about $1\frac{1}{2}'$ from IRS1 on the edge of the same radio continuum component. It has the brightest magnitude at L of all four sources studied, and was found to have a size of $\leq$ 2" (i.e. point-like to the limits of our resolution).

A type II OH/IR source was found by Winnberg et al. (1973) and a subsequent precise position determination (Evans et al. 1976) shows that it coincides with the position of our source IRS2. In 1976 Schultz et al., in a search for IR counterparts to 1612 MHz OH sources, measured this source at 3.8 μm and failed to detect it at 11 μm.

Their result at 3.8 μm accords with our 3.4 μm measurement and their 11 μm detection limit of $0^m.6$ is also consistent. They decide that no field star is visible on the Palomar Survey although it appears that two stars lie within 5" on the red plate. One mas a magnitude $\sim 18^m$, the other is close to the plate limit of $\sim 20^m$; nothing is seen on the blue plate.

Such OH/IR sources are usually identified as late M stars, however IRS2 has much larger colour indices than are typical for late M giants or supergiants (e.g. K-L $\sim 3^m$, compared with a more normal value of

$\sim 0.^{m}3$). This implies a large amount of reddening and/or large IR excess. Spectra of IRS2, de-reddened by various amounts from 0 to $15^{m}(A_{v})$, are shown in Figure 4.7. Various black body curves are shown for comparison.

The longwave (2 - 10 μm) measurements indicate dust emission at a temperature close to 650K. The maximum allowed $A_{v} \sim 15^{m}$ gives a short-wave flux distribution $F_{v} \alpha v^{2}$,corresponding to a hot star. However, this results in an unlikely absolute visual magnitude of $M_{v} \sim -8$, for the source at a distance of 10 kpc. The 0.7 - 1.6 μm results are, in fact, best fitted by an $A_{v} \sim 10^{m}$, which implies an M supergiant (of effective temperature $\sim$ 3500K, and absolute visual magnitude $\sim$ -4).

The variability of these OH/IR stars has been studied by Harvey et al. (1974); they gave relations between the period and the value of log (F10 μ/$F_{3.5 \mu}$) and also between the period and $\Delta V(OH)$. The flux ratio can be derived from our measurements and the velocity component difference was given by Winnberg et al. (1973); both methods give a period of $\sim$ 700 days.

The results that we obtained for this source on two dates (August and October 1976, see Table 4.4) were different by up to 1 magnitude. From Harvey's data, a period of 700 days correlates with an expected total change in 2 μm magnitude of $\Delta M_{K} \sim 2 - 2\frac{1}{2}$ magnitudes. Our measured variation of $\sim 1^{m}$ in 60 days is not inconsistent if we were measuring the source at its maximum rate of change. Further observations to check this will be made as soon as possible.

Scans were made at 3.5 μm and 5.0 μm and this source appears "point-like" in size. The procedure used was based on a least-square fit of Gaussian and "Top-Hat" model profiles to the scan data. The signal-to-noise of the scans was such that the lack of any significant "fit" to the models, over a range of sizes, indicates a size < 2".
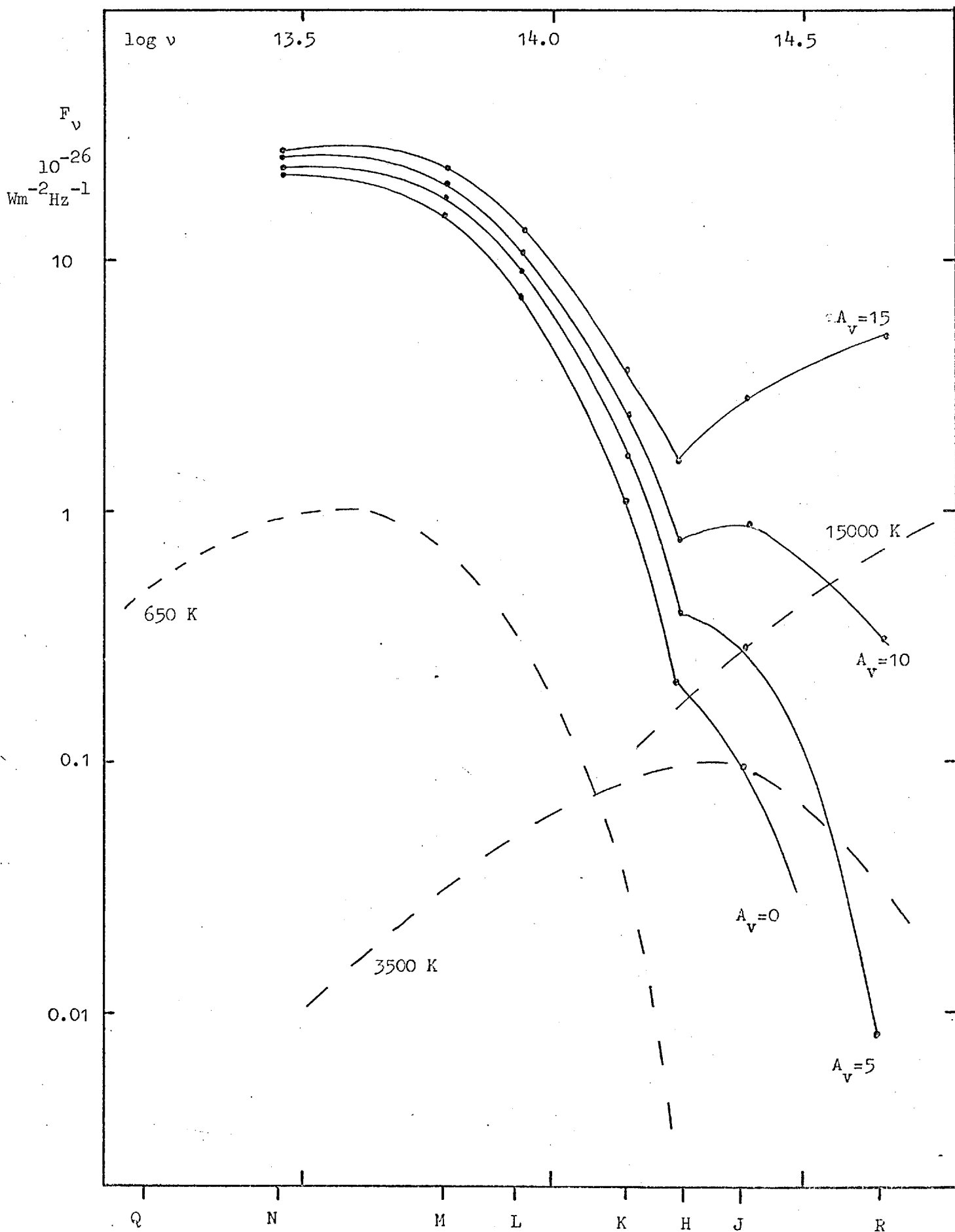
Figure 4.7

4.4.4. Sources 3 and 4

IRS3 lies near the northern radio component and about 1' from OH45.1 + 0.1. This source appears point-like according to 3.5 μm scans; no star is visible on the PSS red or blue plates. Spectra of IRS3 for various amounts of de-reddening are shown in Figure 4.8, the maximum black-body slope of $F_\nu \propto \nu^2$ is also indicated.

The highest value of $A_V \sim 30^m$, indicating an early-type star results in an excessively high intrinsic luminosity, whereas a value of $A_V \sim 20^m$ would correspond to a very cool star (T $\sim$ 2000K) and a very high luminosity. The most probable result is that the source is an M supergiant, with a visual extinction of $\sim 25^m$ and a high absolute magnitude of ~ -7. Some IR excess at $\lambda \geq 5$ μm, presumably due to heated dust, also seem to be present.

IRS4 is located about 3' from the northern radio condensation and is thus less directly associated with the radio continuum emission than the other objects. The various de-reddened spectra of IRS4 are shown in Figure 4.9, the infra-red colours are less reddened than the other three sources considered above.

The range of possible values of A_V seem to be $\sim 5 - 13^m$, and in fact the larger value implies a hot star which would have an impossibly high absolute magnitude, at a distance of 10 kpc. A value of $A_V \sim 6^m$ gives a reasonable fit to the results for an M supergiant. This value of A_V does seem rather low for an assumed distance of 10 kpc. If this object is assumed to lie in front of the G45.5 + 0.1 region at a distance of say 3 kpc (since an average visual extinction of 2^m kpc^{-1} is common), then IRS4 could be a rather less luminous M-star.
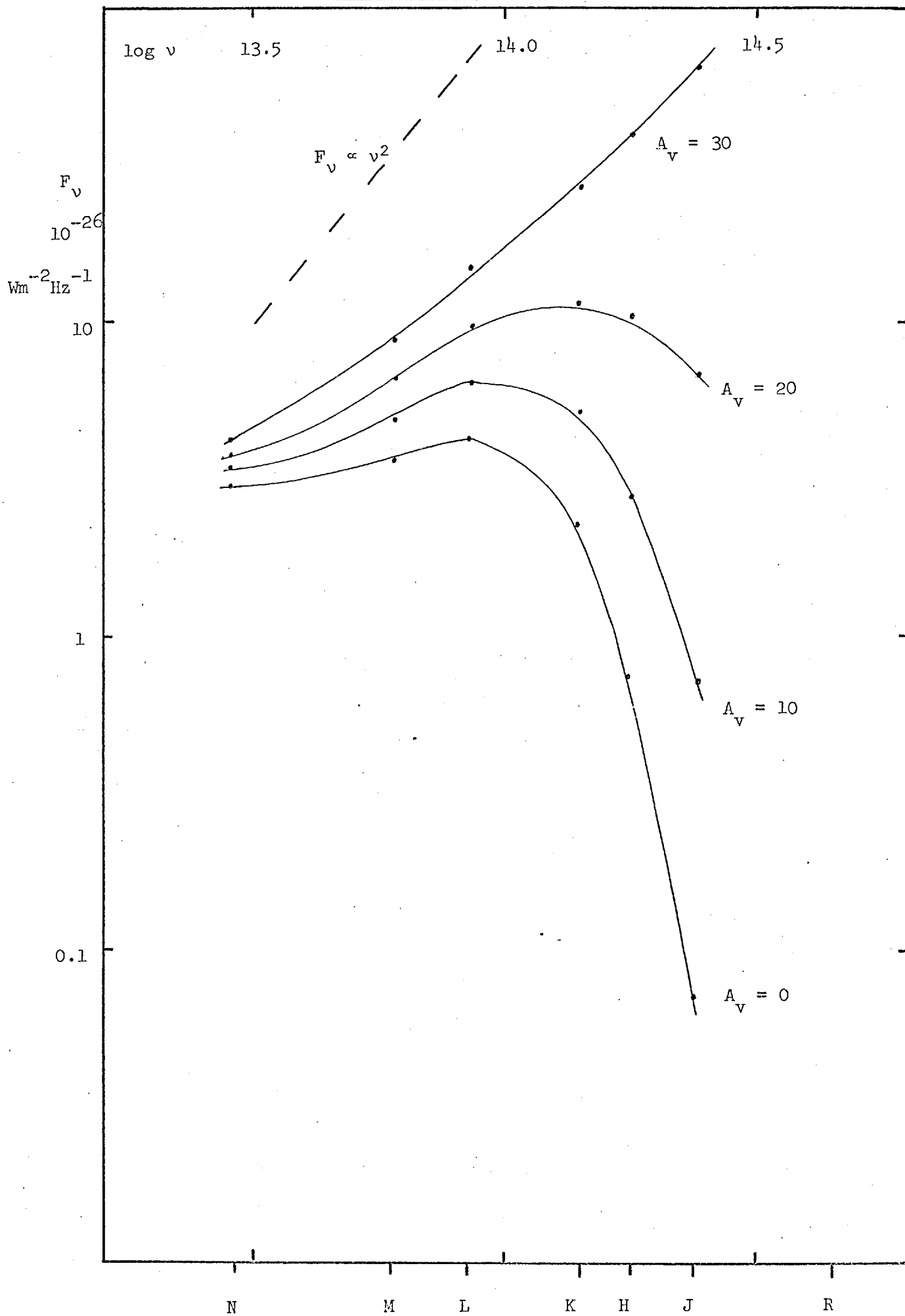
Figure 4,8
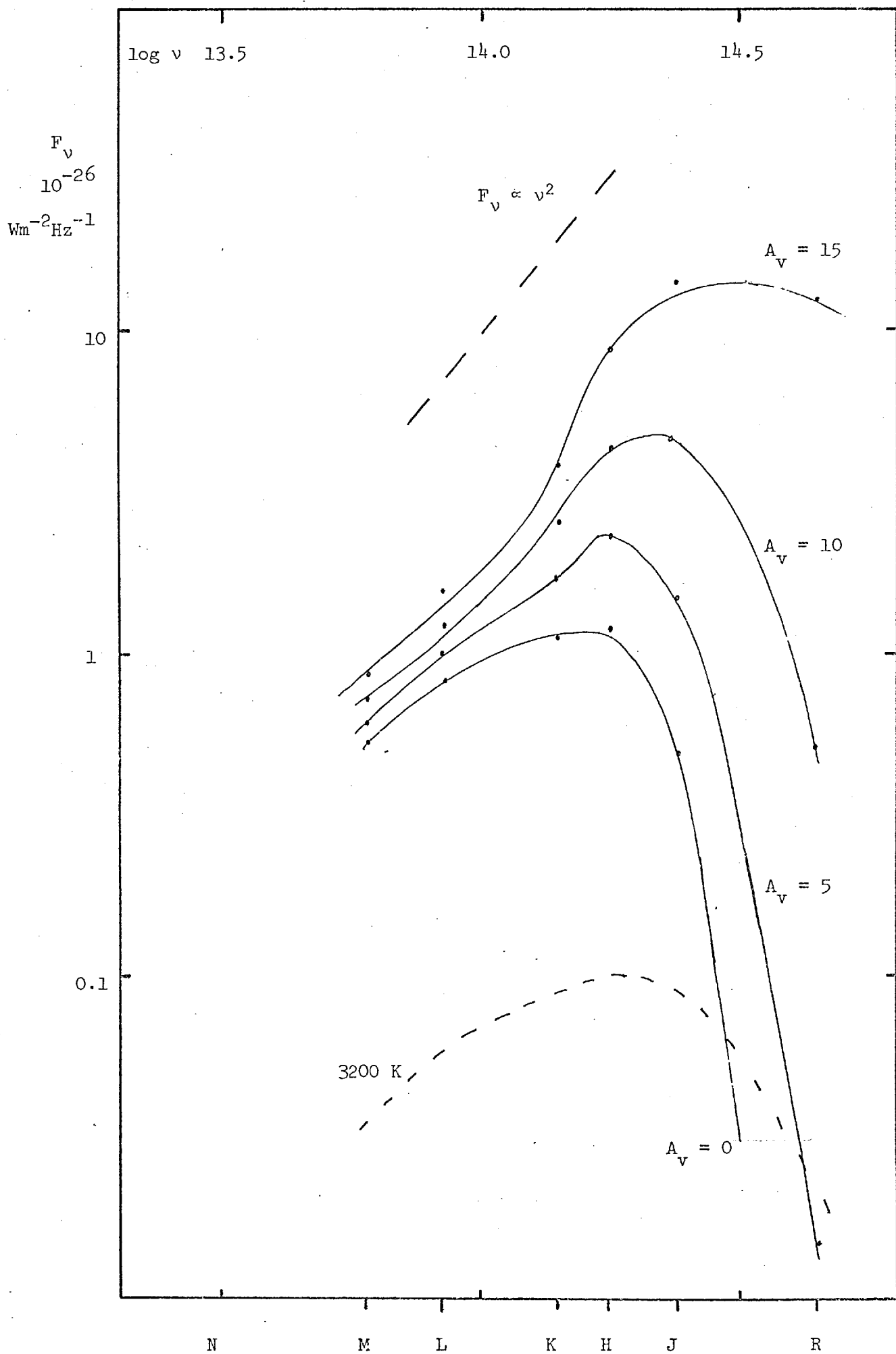
Figure 4.9

Plates 4.5 and 4.6 show the Palomar red and blue plates of the G45.5 + 0.1 area. The likely positions of two of the sources, as discussed above, are shown on the red plate. The scale is approximately 10" mm^{-1}. Note that IRS4 was too weak for useful size measurements to be made.

4.5. Computer use for Optimum Source Detection

4.5.1. Introduction

When searching for faint sources the resulting scan signal consists basically of noise with possibly a small signal superposed. Various means for identifying sources, at the limits of detection, can be used. The simplest, and probably most widely used, technique consists of observing the chart recorder either whilst the scan is in progress or at any subsequent time. A characteristic profile, whose amplitude and width represent source intensity and size, would be seen. This is very tedious and prone to errors during the course of a long raster; it is also subjective and the detection sensitivity depends on the skill of the observer.

By considering the problem as that of identifying a signal, of known form, which is buried in noise it can be shown that the best result is obtained by "matched filtering" of the data. The instrumental profile (roughly a sine-wave in shape) has a corresponding frequency spectrum; if a Fourier transformation is performed it is seen that most of the information is contained in a fairly narrow frequency band. However, in general, the noise measured covers a wider frequency range.

If the input is filtered precisely according to the frequency spectrum of the instrumental profile, i.e. that of the "expected signal", then the maximum signal/noise is obtained. In the Fourier domain this would

blue

PLATE 4.5

red

PLATE 4.6

G 45.5 + 0.1
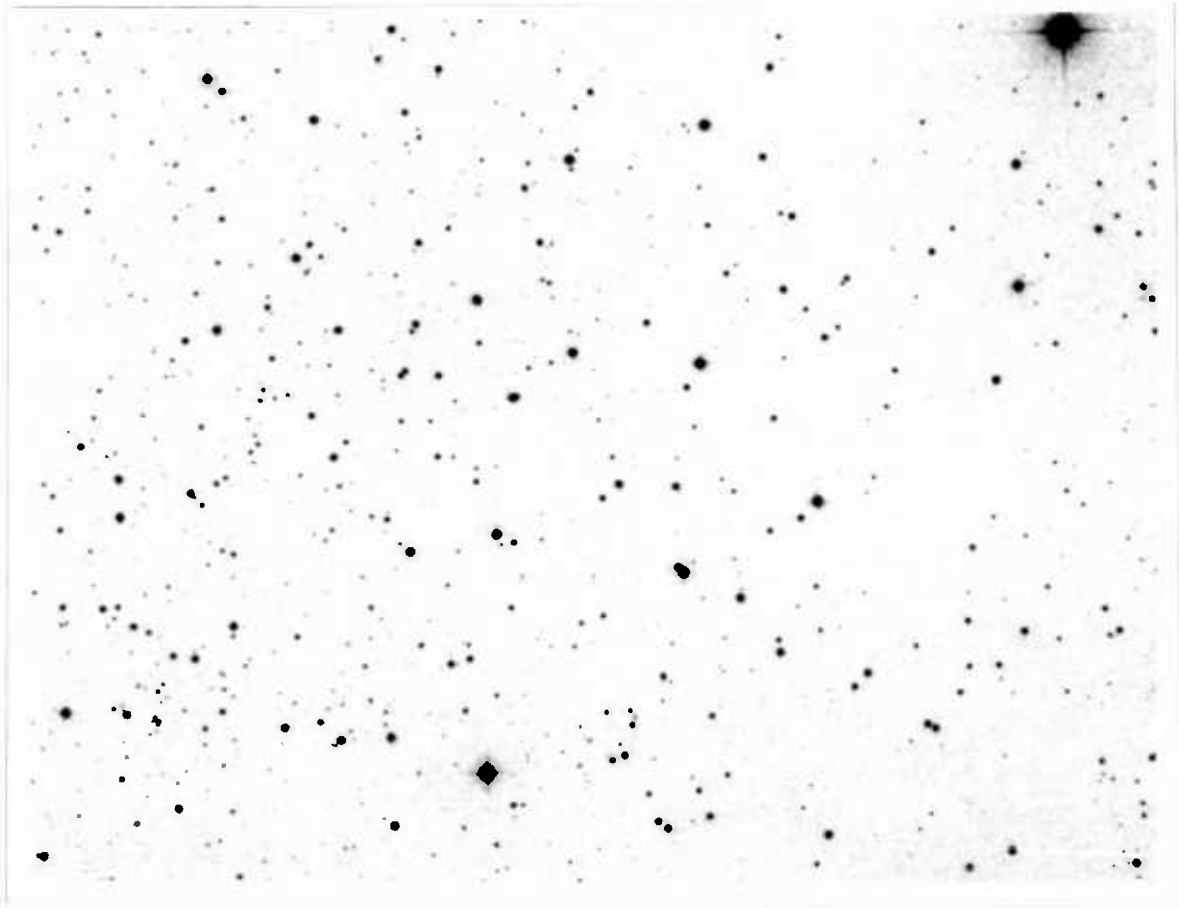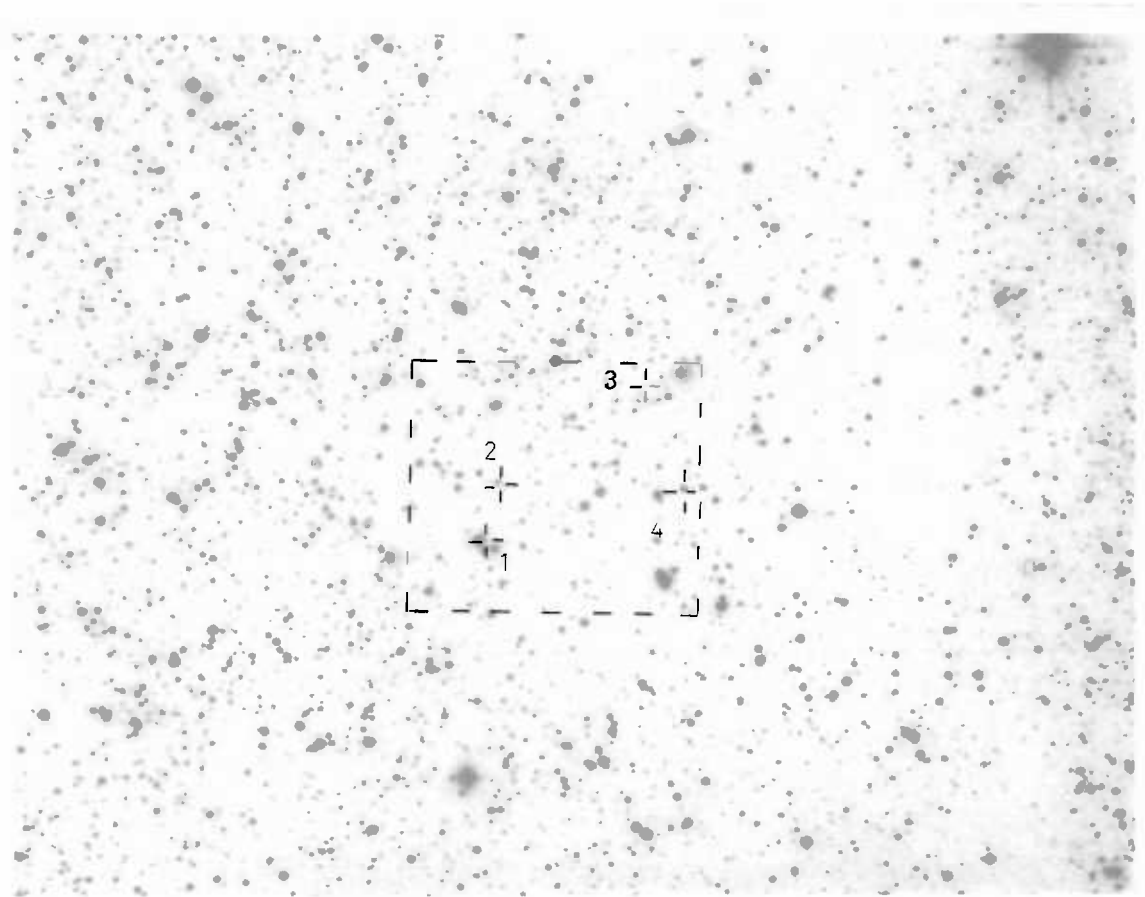
blue
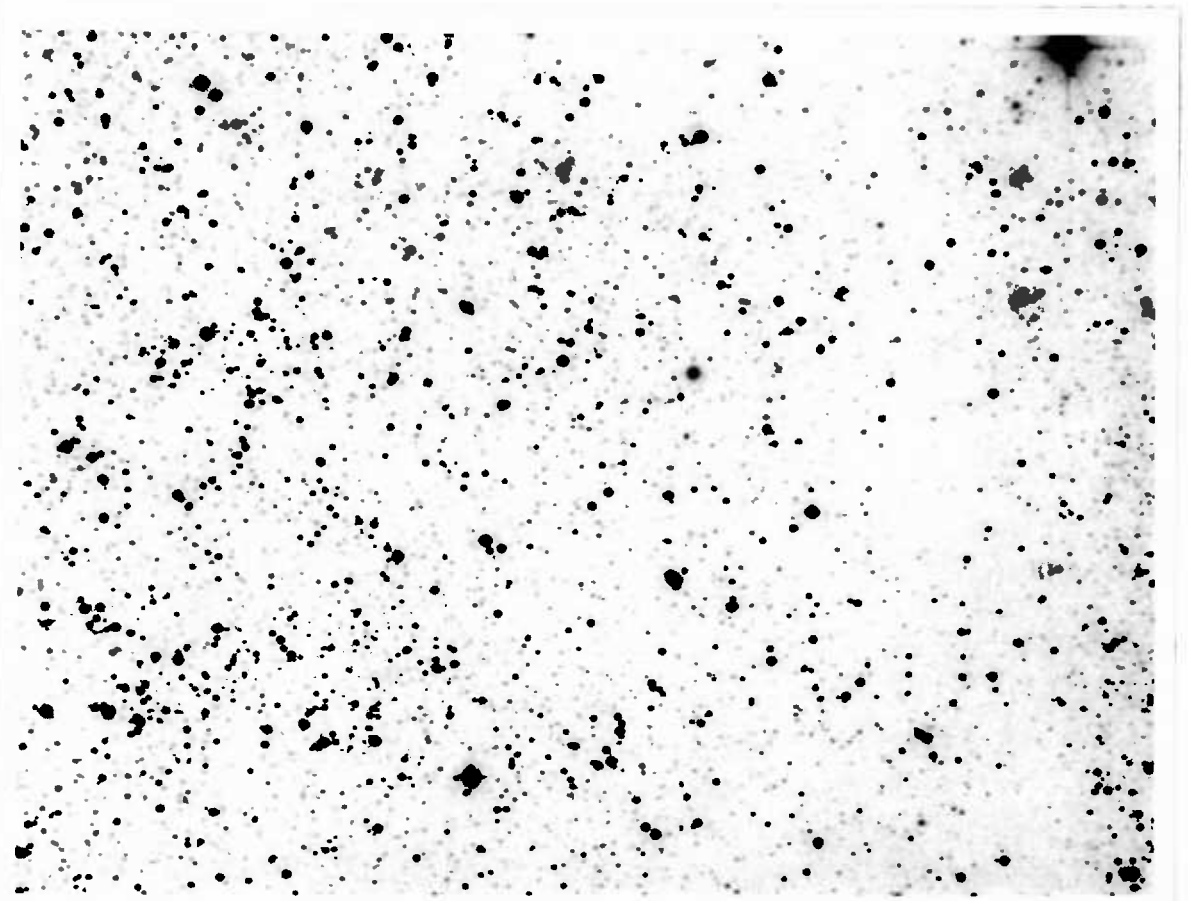
PLATE 4.5

red

PLATE 4.6

require a multiplication of the data by the frequency spectrum, the corresponding operation on the original input is to convolve it with the instrumental profile. This has the effect of enhancing those features of the original scan which are most similar to the expected source profile. A peak in this convolved scan would correspond to a source detection in the original scan.

4.5.2.   Method used

As mentioned earlier, this procedure has been used in a computer program, written by P.A. Whitelock, to analyse data in this way at the end of an observing period on return to College. It seemed feasible to attempt this on-line using the Observatory computer in Tenerife and a Basic program was written with the help of N. Vine.

During the course of a scan the values are stored in the computer, sampling occurs at a rate of 1 Hz usually. At the end of the whole scan the computer performs the required calculations and indicates if any significant sources are detected. The program is listed in Appendix 2 and is now described in more detail.

The program uses an instrumental profile that may either be kept within the program in the form of a data statement or may be read in via the teletype from a short tape. The shape of the instrumental profile will vary if the scan direction, speed, or sampling rate are changed, and the correct profile should be used, but small changes will not significantly affect the result. The number of data points must be input to the computer when the program is first run, a maximum of 200 is allowed with present storage limitations.

The search scan is initiated by pressing the "continue" button linked to the Interrupt Register. The scan then proceeds and the data

values are read from the A/D converter; the corresponding values of the previous scan are punched on tape simultaneously if required. When the required number of N points have been sampled the final calculations occur whilst the telescope is returning for the next scan.

The scan is reduced to a zero mean value. If P2 is the number of points in the stored profile (usually $\sim$ 25) then sets of P2 scan points are multiplied by this profile at each of (N - P2) positions along the scan. The total of this multiplication, for every set of points, then results in a series of values which make up the new convolved scan. (It is in fact an autocorrelation, since the profile is not reversed before use).

The standard deviation about the mean, of the values in this convolved array, is then evaluated. This is evaluated on the assumption that "most" of the original, and hence the convolved, scan consists of noise. Each point of the convolved scan is then compared with this standard deviation and any significant excess is noted as a possible detection. The original scan and the convolved scan are displayed on two halves of the computer VDU, and the positions of any signal detections are printed on the teletype as well as their detection level (S/N ratio).

The detection "threshold" can be set empirically to ensure all real sources are detected but to eliminate too many "false alarms". The program has been briefly tested in use at the telescope and performs well, a scan of sufficient length to give a realistic estimate of the "noise" level must be done. Sources which could not be reliably identified on the chart record by visual inspection were detected quite consistently

by this program and were evident in the convolved scan display. It seems
that this form of "optimal detection" is at least as good as manual
source identification and may in fact give an increase of up to 1
magnitude in the detection limit; it is also more convenient and less
tiring. More quantitative tests of the program's performance will be
performed when possible.

CHAPTER 5

A COOLED FABRY-PEROT SPECTROMETER

5.1. Introduction

A helium-cooled Fabry-Perot spectrometer has been developed for use in the 8-14 μm atmospheric window. This "FP" is sufficiently compact to fit within a relatively standard cryostat and can thus be easily used on an infra-red photometer. The design owes much to Dr. M.J. Selby, who initiated this project.

A brief paper, describing the principles of this instrument, has been published by Selby et al. (1976) and is shown in Appendix 1. The FP is used on-axis without any collimating optics and its resolution is limited to 1400 in an F/13 telescope beam. This is not a problem since we only intend to use the instrument at relatively low resolutions.

The spectrometer requires cooling below room temperature in order that it does not contribute to the radiation falling on the detector. For example, the sky emission (10% at 280K, f/13 beam, 1 mm detector) gives a background $\sim 10^{-8}$W in an 8-13 μm bandwidth. If the detector sees a 77K-cooled spectrometer (through an 8-13 μm helium-cooled filter) it would only receive 2.10^{-12}W. A 4.2K instrument therefore contributes a negligible amount to the radiation background on the detector. The photon shot-noise due to a background of $\sim 2.10^{-8}$W is $\sim 2.10^{-14}$W Hz$^{-\frac{1}{2}}$; if a bandwidth of 0.5 μm is used at 10 μm, the background falls to $\sim 2.10^{-9}$W, with a corresponding shot noise of $\sim 6.10^{-15}$W Hz$^{-\frac{1}{2}}$ – thus a detector of low NEP is required for such use.

A high sensitivity (at low resolution) should be obtained by using the cooled FP, with its high efficiency of transmission and low background noise performance. The one important use of this instrument is

to measure the so-called "silicate" feature which occurs at 9.7 μm in the spectrum of many IR sources. The construction and use of the spectrometer are described in the following chapters.

5.2. 10 μm Spectral Measurements

5.2.1. Introduction, spectrophotometry review

The FP should be useful for the measurement of several lines in the 10 μm band, but the low resolution instrument is intended particularly to study the so-called "silicate" feature at 9.7 μm. Several lines near 10 μm have been detected in planetary nebulae and may be studied in future; these lines include Ar III (8.99 μm), S IV (10.52), Ne II (12.78). (For further details see Gillett et al.1973 and references therein).

Aitken and Jones have used a grating spectrometer to obtain 8-13 μm measurements with a resolution of 0.05 μm. Their uncooled system has been used to measure Ne II emission from H II regions (Aitken and Jones, 1974) and silicate absorption at the Galactic Centre and in the possible protostar W3-IRS5 (Aitken and Jones, 1973).

Many 10 μm spectral measurements have been made by others using a circular variable filter (CVF). This device typically has a resolving power $\leq$ 100 and can be manufactured for use at various wavelength bands. Presently available CVF's cost upwards of $1000 and have a transmission in the range 20-80%, depending on the type used.

Gillett and Forrest (1973) have described a liquid nitrogen cooled filter system; they used this (at a resolution of 0.1 μm) to measure the 8-13 μm spectrum of the Orion "BN"-object. A broad 10 μm "silicate" feature, as well as a 3.1 μm "Ice"-absorption, was detected.

The presence of a 3.1 μm absorption (attributed to ice) in the interstellar medium and particularly molecular clouds has been correlated with the presence of silicate absorption (Merrill et al.1976 and Figure 5.2a). However, the optical depths of these two features do not correlate well, implying that the ratios of the two materials may vary. The ice feature will not be discussed further, although it is a candidate for future measurements with a short-wave spectrometer.

5.2.2. The "silicate" feature

The presence of absorption or emission features at 10 μm, which are attributed to silicate material, is now fairly well established. Woolf & Ney (1969) first reported excess emission from some M stars (including μ Cephei); this matched quite well with the emission observed from a silicate grain mixture. Subsequently other measurements of such emission or absorption have been reported (for example: Humphreys, 1974, excess emission from cool stars; Gillett et al.1975, absorption in the spectra of H II regions; Rieke, 1974, absorption towards a star – VI Cygni number 12).

Forrest, Gillett & Stein (1975) measured characteristic "silicate" emission from several M and S stars. This emission, from circumstellar grains, was broadly similar to the emission observed from the Orion Trapezium region, it is observed as an excess over the black body continuum (∿ 3000K).

Gillett et al.(1975) subsequently measured the 8-13 μm spectra of H II regions and found a broad absorption feature, centred at 9.7 μm. By using the spectral emission characteristics from the Trapezium region they fitted a model to their observed absorption. For the underlying continuum they used either a black body or an optically-thin Trapezium-

like emission, the latter was found to give the best fit in most cases. Figure 5.1 shows some examples of measured silicate absorption.

The observed flux could be described by an equation of the form

$$F_\lambda = \text{const.} \quad \epsilon_\lambda \cdot B_\lambda (T_d) \cdot e^{-\tau_\lambda}$$

$B_\lambda (T_d)$ is the black body function, at the dust temperature ($T_d \sim 250K$ normally), ϵ_λ is the spectral emissivity of the radiating material (hot dust), τ_λ is the optical depth of the obscuring (cool) dust. It is assumed that the obscuring dust is similar to the emitting material, which is identical with the material giving the emission features of the Trapezium.

$$\text{i.e.} \quad \tau_\lambda \sim \epsilon_\lambda \sim F_\lambda (\text{Trap})/B_\lambda (\text{Trap})$$

where, $F_\lambda(\text{Trap})$ is the observed emission from the Trapezium.

Values of τ_λ were derived, these were found to be in the range 1-3. The visual extinction (A_v) to the H II regions could be estimated from the short-wave measurements (see also Section 4.4), and hence the ratio of $A_v/\tau_{9.7}$ could be estimated. Typical values were found to be $\sim$ 10-20.

Rieke (1974) was able to measure a silicate absorption feature in a star (VI Cygni No.12) and a value of $\tau_{9.7} \sim 0.42$ was derived. (See Figure 5.2b). Direct short-wave measurements (Johnson, 1968) had indicated a value of $A_v = 10.0$, hence a ratio of $A_v/\tau_{9.7} \sim 24$ is derived. This comparison of the two values, obtained by direct measurements, is rare. Sufficient extinction to give a measureable value of $\tau_{9.7}$ usually precludes any visual measurements.

Persson et al.(1976) studied the silicate absorption feature in southern H II regions and concluded that there was insufficient evidence
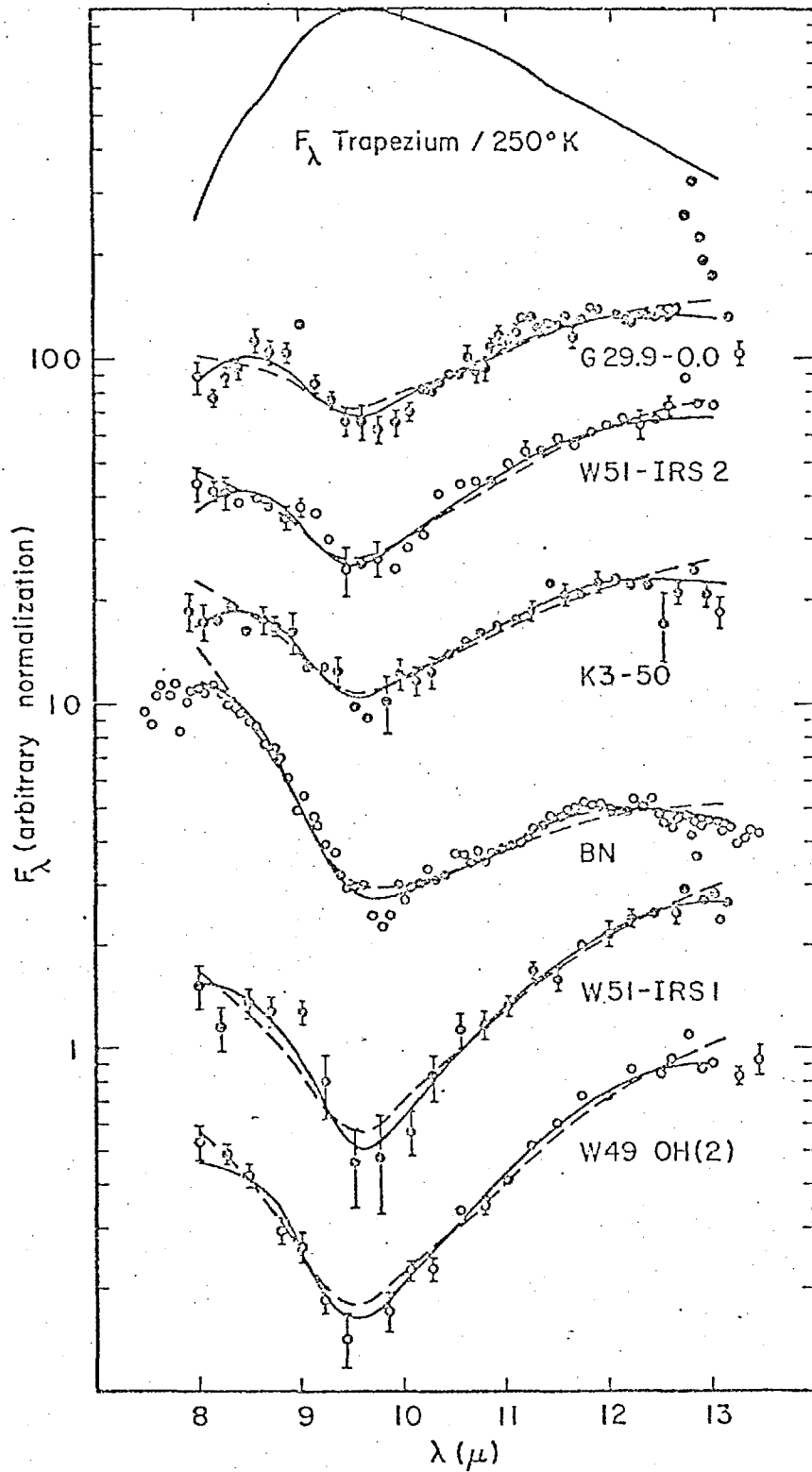
From Gillett et al , 1975. Model fits to obseved spectra of HII Regions.

The top curve shows the measured emission from the Trapezium.

The other spectra include measured points and the fitted model curves.

Figure 5.1

(a) Silicate Optical depth compared to other measures of extinction
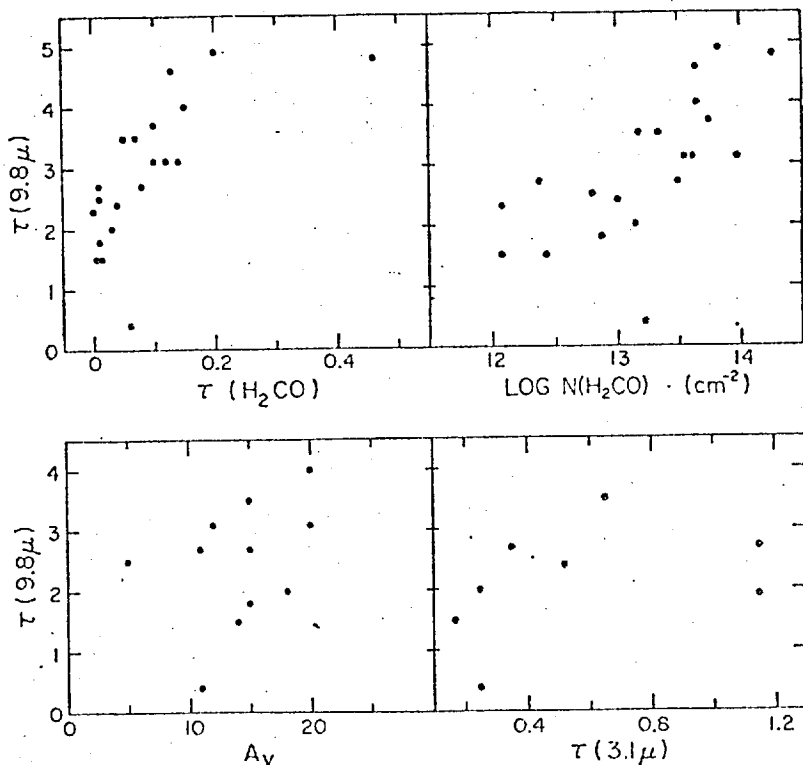
from Persson, Frogel & Aaronson 1976

(b) Measured Silicate absorption towards VI Cyg No. 12
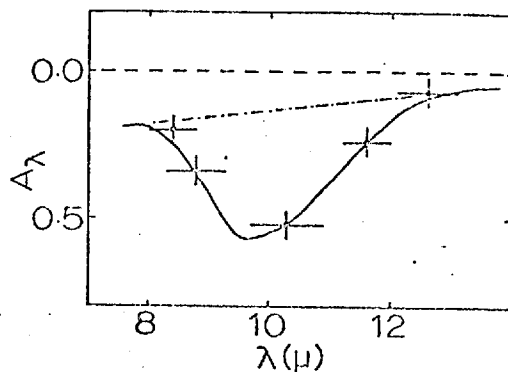
FIG. 1.—Interstellar extinction toward VI Cyg No. 12. The vertical bars on the observational points represent the rms errors, and the horizontal bars are the filter bandpasses. The dash-dot line is an extrapolation of van de Hulst's (1949) curve No. 15. The solid line shows the effect of adding a "silicate" absorption with a maximum optical depth of 0.42. The shape of the silicate feature is from the observations of Merrill and Soifer (1974).

from Rieke 1974 .

Figure 5.2

of a direct correlation between $\tau_{9.7}$ and A_v. Some examples of their measurements are shown in Figure 5.2a.

Merrill et al.(1976) have measured silicate absorption (also ice absorption) in molecular clouds. They did a similar fitting procedure to that described above, and derived values of $\tau_{9.7}$ which they were able to compare to values of τ_{ice}. The presence of silicate absorption was found to correlate with the presence of ice absorption, although the relative magnitude varied.

It is clear that much more useful knowledge could be gained from observations of "silicate" absorption. Spectra in the 8-13 μm band can indicate the shape of the feature, and the optical depth can be derived after making assumptions about the underlying emission. The ability to detect faint absorption features (small values of τ_λ) would enable a comparison with A_v measurements over a larger range than is presently possible. (Typically, $\tau_{9.7} = 0.5$, $A_v \sim 10$ are measured at present; extension to $\tau_{9.7} \sim 0.1$ would enable comparisons with $A_v \sim 2$).

5.3. Optical Theory

The Fabry-Perot spectrometer discussed here is a single etalon device, and those parts of the theory which are relevant to its use are given below. Fuller details of multiple beam interferometers can be found in standard optics texts. Basically an input beam suffers multiple reflections between two partially reflecting plates, the emergent beams can be combined and focussed by a lens to give interference fringes at its focal plane. Figure 5.3 shows a schematic interferometer.

Fabry-Perot Interferometer

Etalon

θ

Filter

Reflecting
Surfaces

Imaging
Lens

Viewing
Plane

Figure 5.3

Total
Transmission

Intensity Distribution of FP Fringes

1.0

R=.25

.50

.75

.95

2nπ

2(n+1)π

δ →
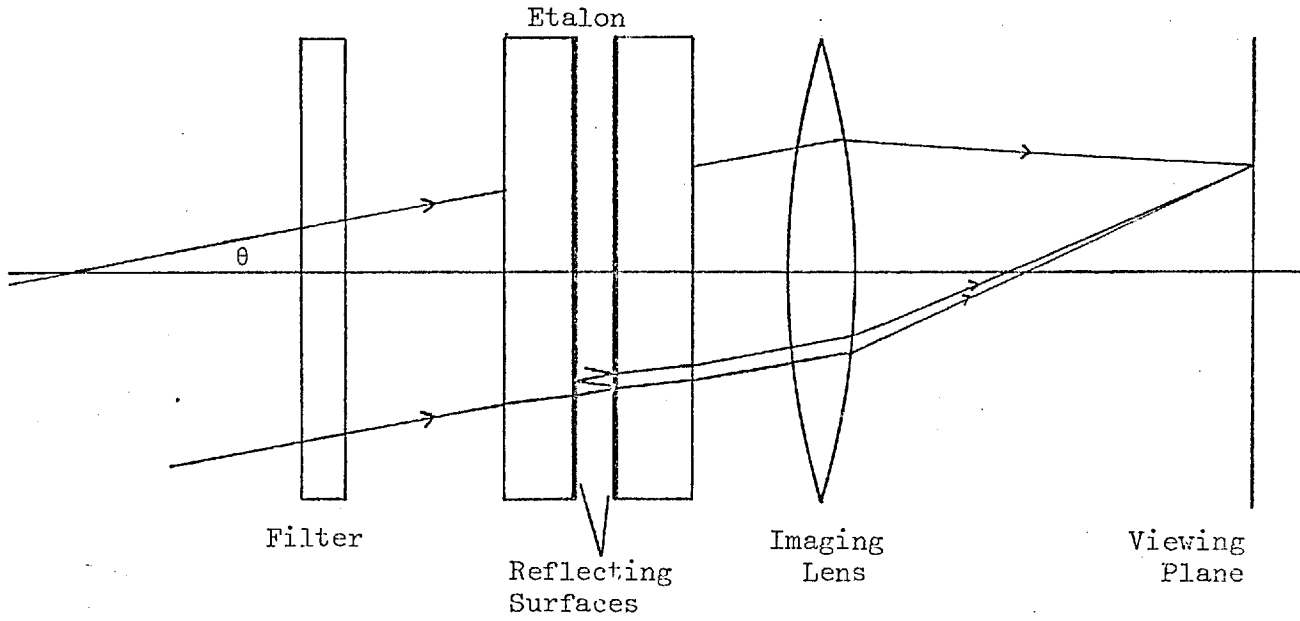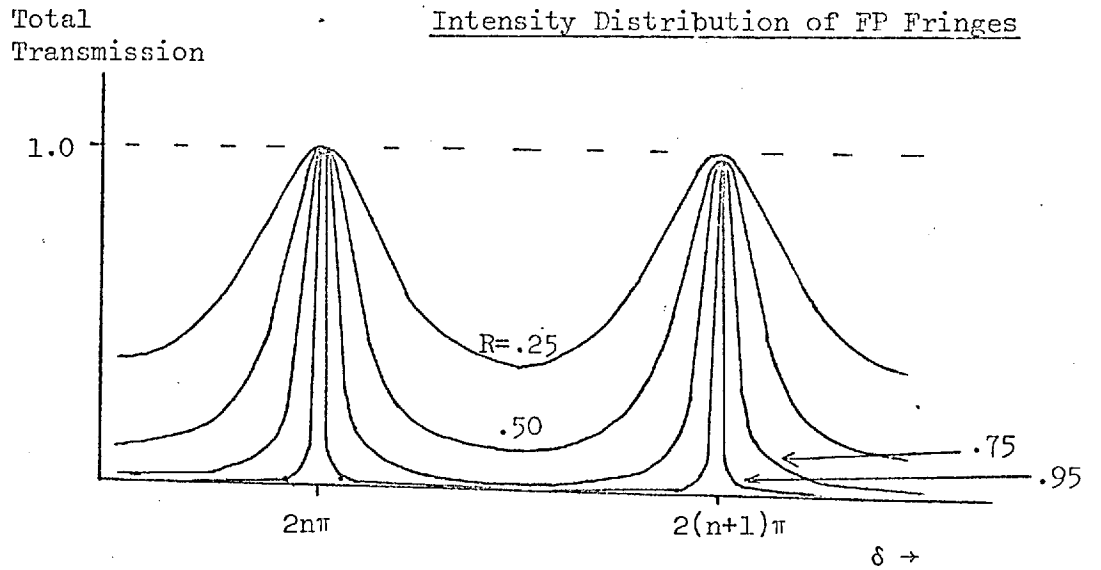
Figure 5.4

The net transmission of the etalon is given by

$$T^{I} = \frac{T^2}{(1-R)^2} \cdot \frac{1}{1 + 4R.\sin^2(\delta/2)/(1-R)^2} \qquad \ldots\ldots\ldots \quad (1)$$

where $\delta = 2\pi. \, 2 \, \mu \, t \, \cos\theta / \, \lambda$

The symbols have their usual meaning, $T = 1 - R - A$

T = transmission of the plate surface.

R = reflection coefficient of each plate.

A = absorption coefficient of each plate.

μ = refractive index of medium between the plates.

t = plate separation.

θ = angle of incidence.

Maximum transmission of the etalon is obtained when

$$2 \, \mu \, t \, \cos\theta = n\lambda \qquad \ldots\ldots\ldots \quad (2)$$

thus with $\mu = 1$ and $\theta \sim 0$ the maximum transmission is obtained for

wavelengths, $\lambda = 2 \, t/n$ $\qquad \ldots\ldots\ldots \quad (3)$

Here n is known as the order of interference.

The separation between two transmission peaks, of order n and

n + 1, can be obtained from equation (3); the free spectral range,

$$\Delta\lambda = \lambda^2/2 \, t = \lambda/n$$

The Resolving Power is given by: $\dfrac{\lambda}{\delta\lambda} = n \dfrac{\Delta\lambda}{\delta\lambda} = n \, N_T$

where $\delta\lambda$ is the smallest resolvable wavelength interval, N_T is the

total Finesse.

Finesse

The transmitted intensity of an FP is shown in Figure 5.4, it is

seen that the sharpness of the transmission fringes is determined by the

reflection (R) of the plates. A useful parameter is the Reflection

Finesse (N_R), defined as the ratio of the fringe-spacing to the half-

value width of the transmission peak. It can be shown from equation (1)

that $N_R = \pi \, R^{\frac{1}{2}}/(1-R)$.

The relations used here mainly apply only for axial incident rays, such that $\cos\theta \sim 1$. Rays at any other angles have different wavelengths of peak transmission and this results in a broadening of the fringe width. This effect is conveniently described in terms of an Aperture Finesse (N_A). It can be shown that for a beam of focal ratio F, and an order of interference n,

$$N_A = 8 \, F^2/n$$

In addition, variations in plate separation t cause a fringe broadening. Thus plates which, as a pair, are said to be "flat to $\bar{\lambda}/x$" give a corresponding Defect Finesse, $N_d = x/2$.

Similarly the effect of changes in parallelism (resulting in a change in t) can give a Parallelism Defect (N_p). For plates that are "parallel to λ/y", $N_p = y/\sqrt{3}$.

The effects of all these finesses, each of which gives a corresponding half-width to the transmission function, can be combined approximately. The total instrumental finesse is given by,

$$N_T^{-2} = N_R^{-2} + N_A^{-2} + N_d^{-2} + N_p^{-2}$$

In many optical FP's the limiting resolution is determined by the value of N_d; the problems of plate manufacture make a high value of N_d difficult to attain. For a given value of N_d, maximum transmission is obtained with $N_R = N_d$. This results in a final $N_T \sim 0.7 \, N_R$, since with a small aperture and careful alignment N_A and N_p can be ignored. In our case, at 10 μm, the defects are relatively smaller and we can have $N_T \sim N_R$ (especially at lower resolutions).

5.4. Optical Transmissions

The telescope beam passes through the outer cryostat window, through a broad-band pre-filter, and is then focussed at the etalon first surface. The FP plates consist of a Zinc Selenide substrate with a dielectric reflection coating. The transmissions of a KRS5 window, an uncoated Zn Se element, and the "8-13 μm" filter are shown in Figure 5.5.

Early tests were performed on Barium Flouride plates coated by ITT (STC Ltd) with a standard CO_2 laser coating. These had an increasing absorption for $\lambda > 12$ μm and the coatings proved not to be very durable (after repeated abrasion during tests). The plates were replaced by Zn Se - coated ones, manufactured by SPECAC Ltd. The transmission and implied reflection characteristics are shown in Figure 5.6; similar computed curves for a gold layer on Zn Se are shown for comparison.

Zinc selenide has a very low absorption at 10 μm and a refractive index of 2.4, its short-wavelength transmission limit of 5000 Å gives it an orange colour. The plates were intended to have a reflection coefficient of $75 \pm 5\%$ from 8-14 μm; this proved very difficult to manufacture and the result of the coating was shown in Figure 7.4. The very high transmission around 8 μm has necessitated the use of a wavelength band of only 9-13 μm in tests to date; an 8.5 μm cut-on filter was used for this purpose, combined with an 8-13 μm element.

Anti-reflection coatings can improve the total transmission of the KRS5 window and Zn Se plates, although the full improvement over the whole range (8-14 μm) is hardly possible. The plates were coated with an annulus of partially reflecting aluminium, outside the central 3 mm

Transmissions of three optical elements
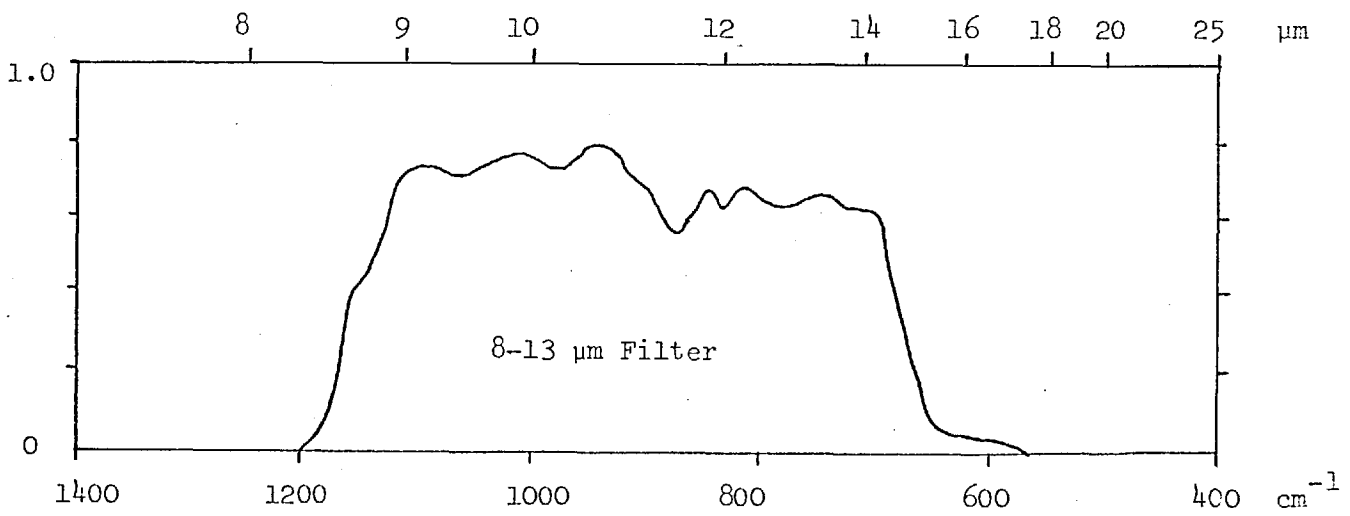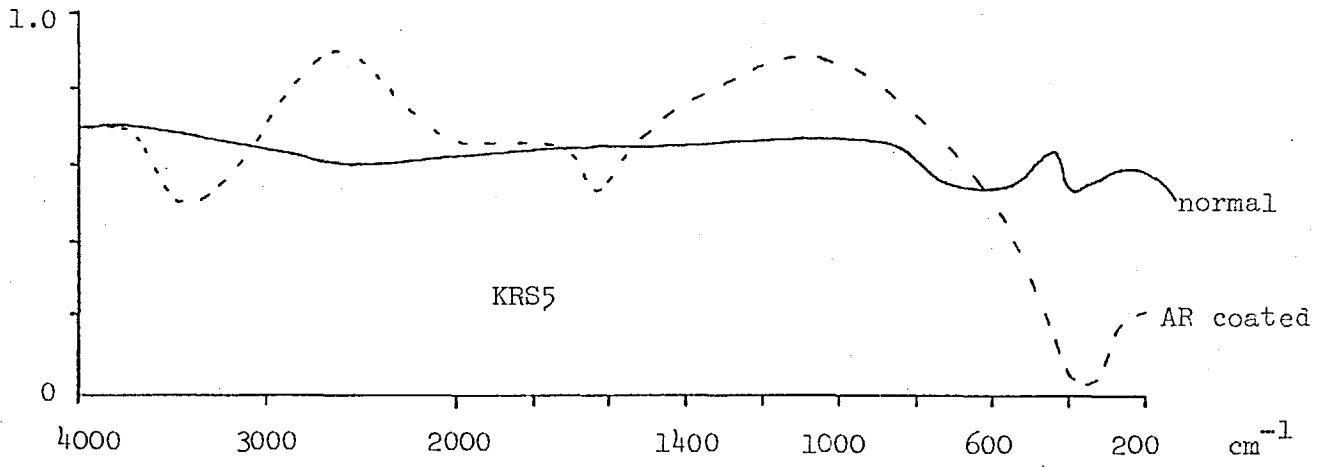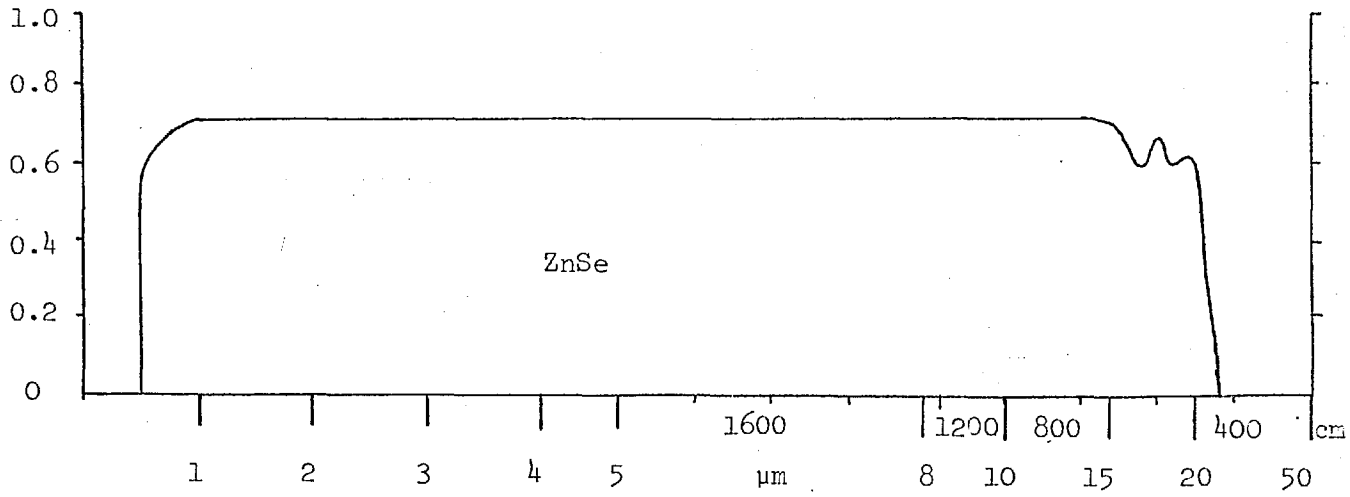
Figure 5.5

Transmission and Reflection Characteristics of FP Plates

(a) SPECAC Flats

coating thickness = .006μm
transmission @ .55μm = 0.7

(b) Gold on ZnSe
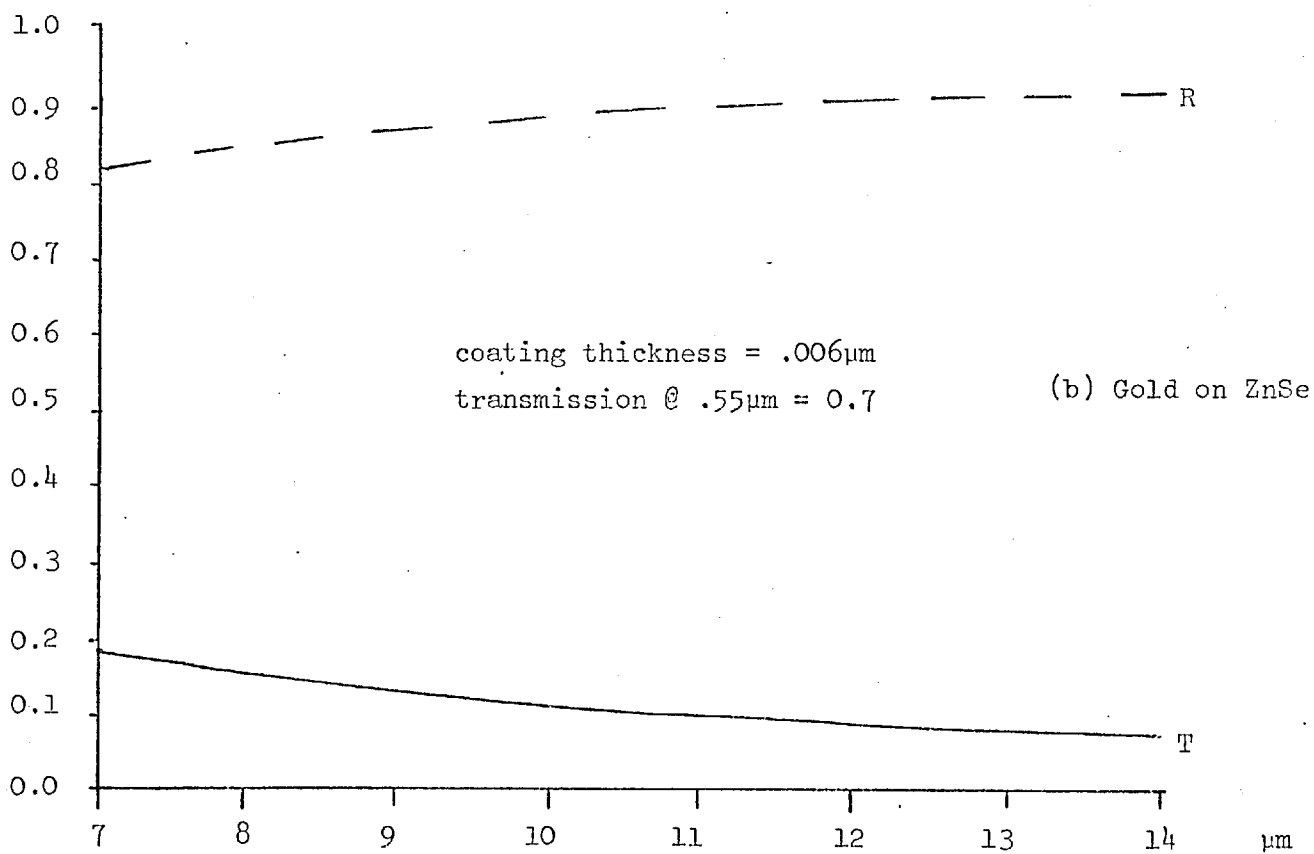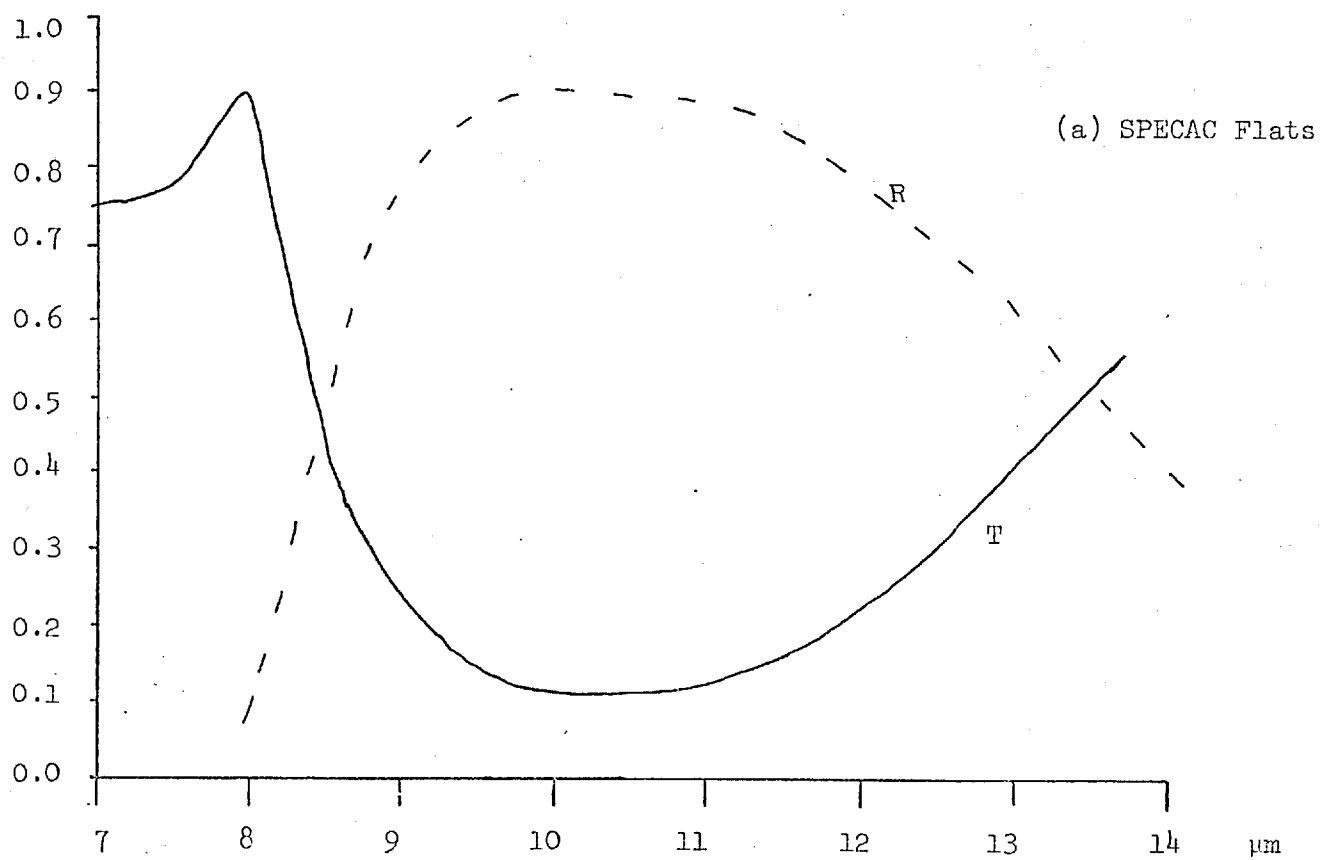
Figure 5.6

of infra-red coating. This was to aid optical alignment by observing monochromatic fringes from a mercury lamp, but it proved unnecessary because the central coating was found to transmit visible light quite well for this purpose.

The efficiency of the device depends on the optical transmission of the components and the coupling between them. The transmission of the etalon, for example, is given by

$$T^1_{max} = T^2/(T + A)^2$$

It is important that the reflection coating has minimum absorption. (If R = 90%, T = 8%, A = 2%, the efficiency is 64%; in practice dielectric coatings can have much lower absorptions and quite high efficiency.

5.5. Optical Design

This spectrometer is used inside the cooled cryostat and, since we only intend to use it at low resolution, a collimated beam is not required. The f/13 beam of the telescope is brought to a focus at the first surface of the etalon. This "nearly" parallel beam (maximum angle $\sim 2^o$) passes through the etalon and is focussed onto the detector. For convenience, and to eliminate losses caused by extra components, the exit surface of the etalon was made convex to act as a simple lens.

The complete optical system is shown in Figure 5.7. The 10" field of view of the telescope is defined by a 1 mm aperture in the field stop, which consists of a small metal insert in front of the etalon. A detector aperture of 1.5 mm is required to collect all of the radiation from the 1.5m primary. The field lens has a radius of curvature of 28 mm which gives a focal length of 20 mm (for λ = 10 µm). An intermediate baffle of diameter 1.4 mm is placed 10 mm from the detector, this tube and axial hole help reduce stray radiation falling on the detector.

FP Optical System
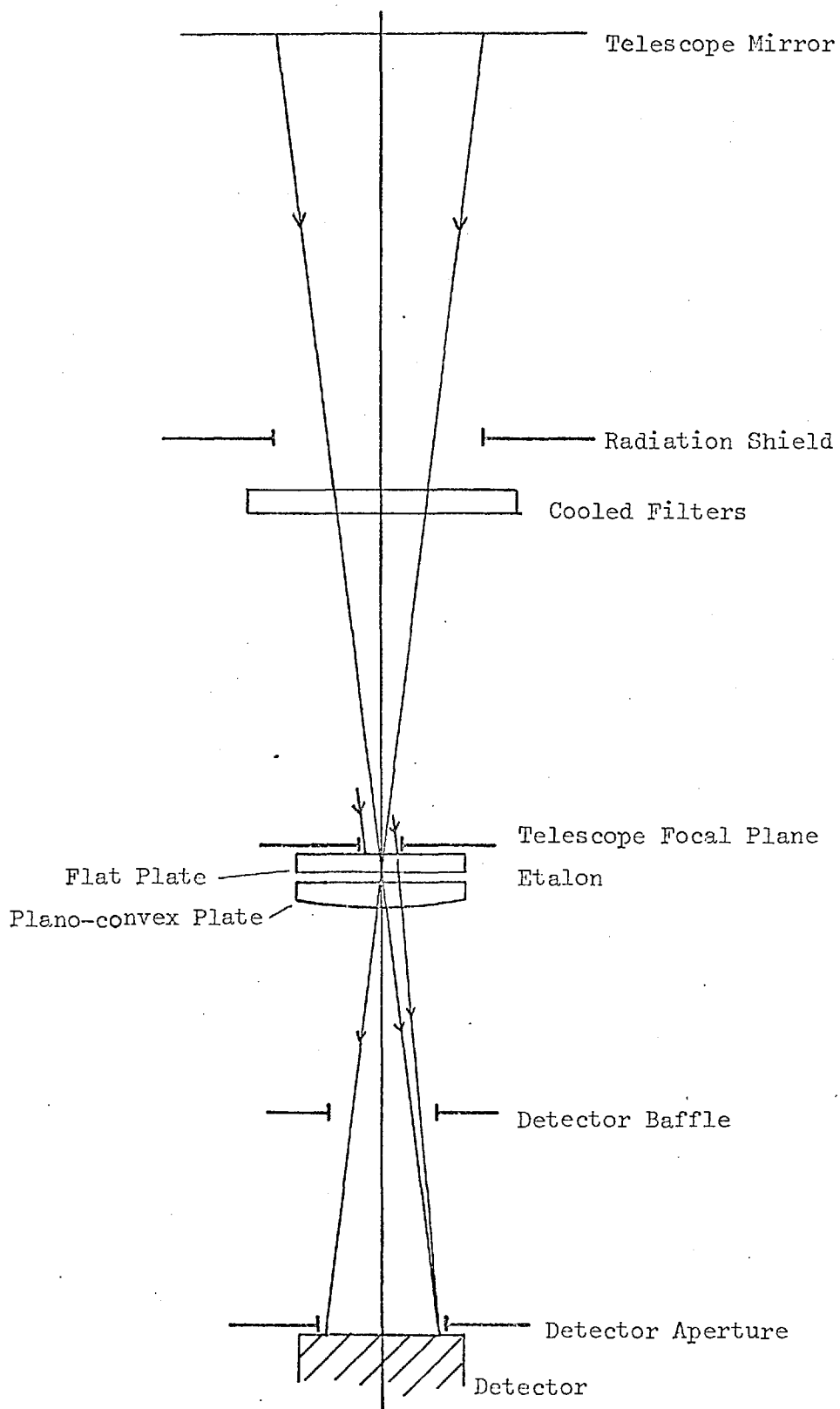
Figure 5.7

We use a single infra-red detector to measure only the centre of the fringe pattern; this is convenient to do and in effect we are using the FP etalon as a monochromator. The wavelength transmitted at normal incidence is $\lambda = 2$ t/n and we scan a range of wavelengths by varying t. A displacement of $t = \lambda/2$ (5 µm in our case) is sufficient to scan from one order to the next.

Tolerances and restrictions

The uncollimated entrance beam of the telescope results in an aperture finesse of $N_A = 8 \times (13.5)^2 \sim 1400$, in first order. It is seen that this is only a limitation if resolving powers in excess of 1400 are to be used.

The plates were manufactured to a tolerance of $\lambda/10$ in the visible, resulting in $\lambda/200$ at 10 µm, giving a defect finesse of $N_d \sim 100$. This is still much larger than the reflection finesse we use, and could probably be increased by a factor of 10 if desired.

The alignment of the etalon is performed using green light and an accuracy of $\lambda_{5500}/40$ should be attainable when observing the monochromatic rings. This results in a 10 µm accuracy of $\lambda/800$ which corresponds to a parallelism finesse of ~ 500. (The plates need to be securely held in place to ensure that alignment is maintained).

As was shown earlier, the strip-spring system should maintain parallelism to at least this order of accuracy. Thus, provided the servo-controlled plate separation is maintained (so as not to contribute to the defect finesse) the resolution obtained should primarily be defined by the reflection finesse, at a given order.

5.6. Wavelength Range

The "10 μm" Window is useful from about 8-13 μm and a broad-band filter can be used to allow only wavelengths in this range through the system. A Fabry-Perot, operating in first order, could then be used to transmit this range of wavelengths as its gap was changed from 4-6.5 μm. The resolution obtained then depends on the finesse of the etalon ($\delta\lambda = \lambda/N_T$, which gives $\delta\lambda \sim 0.5$ μm at $\lambda = 10$ μm, for $N_T = 20$ if $R \sim 86\%$).

If operation at a higher order is required then a narrow band pre-filter is necessary to prevent confusion between orders. For example, a 1 μm wide pre-filter would allow operation from 10 μm-11 μm at 9th order as the gap changed from 45-49$\frac{1}{2}$ μm. (A 10th order fringe at 9.9 μm would be outside the filter passband). This would give a resolution of .05 μm if $N_T = 20$, and could be useful for studies of spectral lines in a narrow frequency range.

A simple filter gives an easy means of limiting the spectral range of radiation and a set of four filters, each 1$\frac{1}{2}$ μm wide, would allow coverage of the whole 10 μm window at a resolving power of say 100. Most work to date has in fact involved the use of a broad-band 8-13 μm filter and operation in low orders.

The resolving power of the instrument could be greatly extended by combining it with a grating as an order-sorting filter. This is not considered here since this considerably increases the complexity and size of the spectrometer and is not appropriate for the applications discussed. The resolving power of a single etalon (at a given order) can only be increased by having a higher finesse. The limit to the finesse which is possible is partly determined by the plate defects and

partly by the reflection coating which has more significant absorption losses as R → 1 (i.e. $\frac{A}{T}$ increases). A finesse of up to 100 should be possible if the drive system maintains the plate separation to better than $\lambda/200$ and if the coatings have an absorption of < 1%. (Giving 50% total transmission when R = 97%).

A spectrometer with a resolution as low as 0.5 μm can be very useful when studying radiation from 8-13 μm. In fact a high transmission and wide bandwidth are an advantage wheh studying sources of low intensity. It seems difficult however to obtain a good reflection coating which has a nearly constant reflectivity and low absorption over a wide range.

CHAPTER 6

FABRY-PEROT SPECTROMETER : MECHANICS

The mechanical construction and assembly of the Fabry-Perot spectrometer are described in this chapter. Some details of the helium-cryostat used to contain the FP are also given.

6.1. Spectrometer Assembly

In this Fabry-Perot instrument the wavelength of peak transmission is varied by changing the physical separation of the two interferometer plates. The instrument is operated at the low pressure prevailing inside the cooled cryostat, essentially in a vacuum. The FP is mounted in the centre of a cryostat, which has a window in the middle of its base, and the radiation beam passes axially through the system until it reaches the detector.

The etalon uses two interferometer plates of 5 mm diam. x 2 mm thick, these are mounted in plate holders by means of Oxford Instruments low temperature adhesive (components M5 and M6). This epoxy resin secures the plates well and survives repeated cooling cycles with very little degradation. The plate holders consist basically of a hollow tube with a circular flange which is screwed to the main support arms of the interferometer carriage.

Most of the FP is constructed of aluminium alloy, although it is recognised that stainless steel would be a more suitable material to use for any future model in such an environment. One plate is mounted on a fixed part of the assembly and the other is secured to a moving carriage. The moving carriage is supported by four phosphor-bronze strip springs to form a parallel motion structure.

The etalon assembly and its cylindrical container is shown in Figure 6.1. The fixed side of the parallel-assembly is screwed to the side of the 5 cm diameter copper cylinder in which the whole device is housed. The moving carriage is driven by means of a screwed arm which projects through a hole in the cylinder wall.

The etalon module is contained within the copper cylinder which also has a cap which holds filters and has a beam defining aperture. This cylinder is mounted on a copper plate which is screwed to the helium reservoir, the detector mount is screwed to this plate and fits within the cylinder.

The drive mechanism employed to date has consisted of a small superconducting coil which is held on the moving arm. This coil fits within a magnet which is secured to the outer wall of the copper cylinder. The magnet was obtained from a 0.2W loudspeaker, its performance was not noticeably degraded even after many cooling cycles. The best super-conducting wire to use was found to be a niobium-titanium wire, FMA61/15. Thanks are due to Imperial Metal Industries for supplying samples.

The coil consists of 40 turns of insulated wire wound closely on a copper former and held in place by shellac lacquer. The copper coil former was to give a good heat conduction and thus ensure that a super-conducting state is maintained, a copper braid from the coil to the helium base was also used to aid this purpose. A temperature of less than 9K is required.

The plate holders are secured by means of screws to the etalon carriage. One plate holder is fixed rigidly to the moving carriage by means of three equal spacer rings. The other plate holder can be adjusted

The Fabry-Perot Assembly   Baseplate

Electrical pins

FET   Detector mount

Radiation shield lower plate

Magnet   Strip-spring

Superconducting coil   Plate holder

                                                                   Coated FP flats

Moveable carriage   Adjusting screw

                                                                   Broad-band
                                                                   filter holder

Entrance aperture
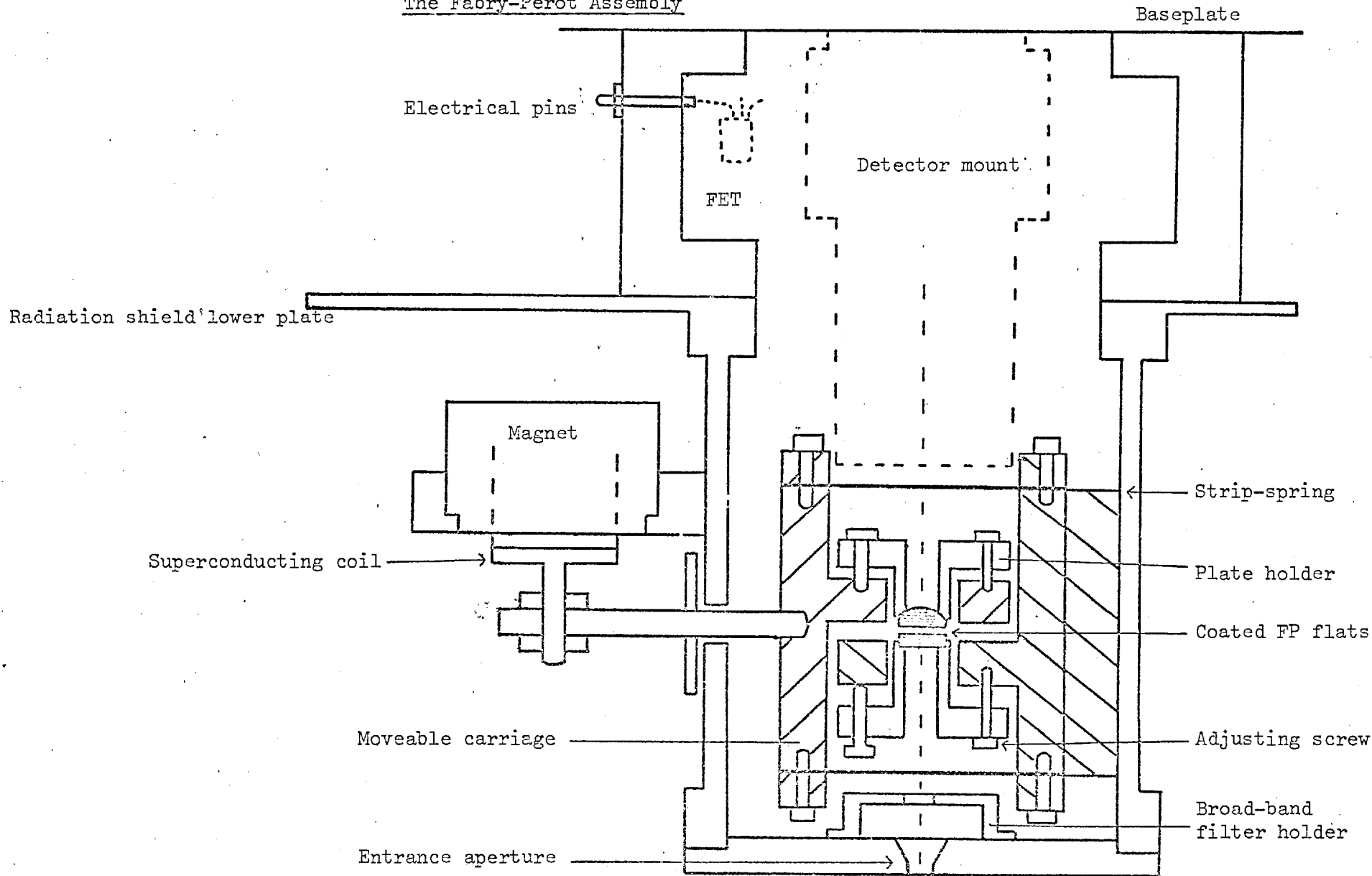
Figure 6.1

for alignment by using 3 pairs of push-pull screws; 3 single screws and springs could not be relied on to lock the plate position during the cooling process. All parts are constructed of aluminium and the symmetrical construction gives equal contraction and thus plate alignment is maintained after cooling from 300-4.2K.

6.2. Etalon Mechanical Performance

The parallel strip-spring assembly for the etalon was chosen because of its simplicity in producing an adequate parallel motion, and it also has good long-term stability provided the springs are not over-stressed. The structure has a mechanical resonance whose frequency is determined by the mass of the carriage and the stiffness of the springs used.

Parallel-spring movements are now well known and Jones has discussed them in some detail in two papers in 1951 and 1956. It can be shown that for the FP constructed here the deviation from parallel motion is very small for the range of movement required.

$$a \sim 4 \text{ cm}$$
$$b \sim 2 \text{ cm}$$
$$1 \sim 2 \text{ cm}$$
$$t \sim \tfrac{1}{4} \text{ mm}$$
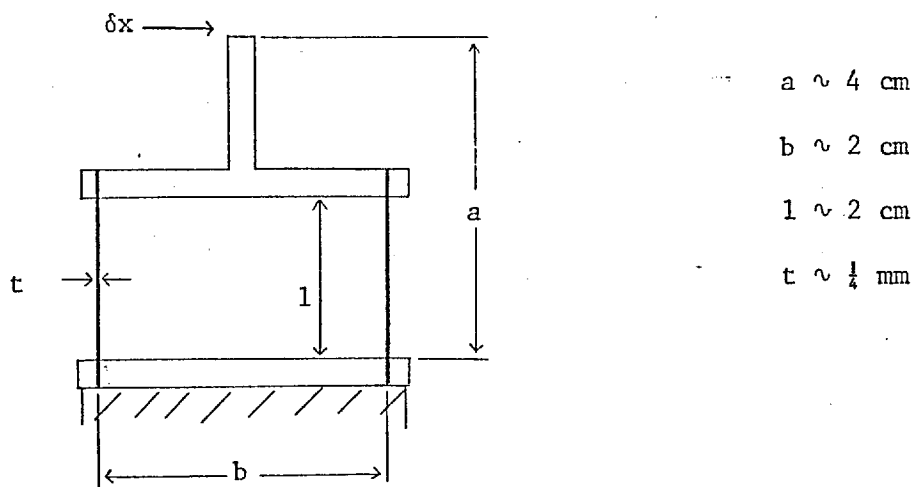
The departure from parallelism for a displacement δx is given by

$$\theta \sim \frac{2(1 - 2a).t^2.\delta x}{b^2.1^2}$$

which, for $\delta x = 50\,\mu m$, gives $\theta \sim 0.2$ arc sec. That is, a deviation of $\sim .005\,\mu m$ across a 5 mm aperture, this corresponds to an error of $\lambda/2000$.

The aluminium carriage has a mass of about 25 grams and the phosphor-bronze springs have dimensions of 0.38 mm thick x 0.5 cm wide. Classical formulae for the deflection of such a cantilever can be used to derive the expected motion which agrees quite well with that obtained in practice. Tipping the etalon from horizontal to vertical gives a deflection due to the weight of the carriage.

An effective stiffness constant can be calculated and the resulting frequency of the "simple" mechanical oscillator can be deduced from the known mass. The resonant frequency of the system can actually be measured readily by driving the coil at various frequencies until a maximum amplitude motion is detected. The measured resonant frequency is in agreement with the expected value.

Finally by measuring the "$\frac{1}{2}$-power" resonant points on either side of the peak frequency the Q-factor can be derived. This gives an indication of the total resistive damping of the system. Ideally a minimally resonant system would be most desired, as discussed later. The extent of unwanted vibrationally-induced motion can be reduced by using stiff springs but then more drive force is required to change the gap. The final parameters are a compromise which seem to give the best results. Various properties of this system are now given.

The following quantities are approximate figures for tests made with springs of thickness 0.38 mm, although a thicker set is used in practice (0.58 mm). The behaviour is similar to a classical oscillator with an equation of motion of the form $m\ddot{x} + r\dot{x} + sx = F$. m is the mass of the carriage, r is the damping term, s is the spring stiffness, F is the applied force and x is the resulting displacement.

If $r^2 < 4sm$ (little damping) then the resonant frequency $\omega_o = (s/m)^{\frac{1}{2}}$.

mass $m = 25$ gms, measured resonance $\rightarrow \omega_o = 2\pi \times 120$ Hz

hence $s = 1.4 \times 10^4$ kg s^{-2}.

The measured displacement, $x = 20$ μm, due to gravity acting on the carriage, gives $s = \frac{mg}{x} = 1.2 \times 10^4$ kg s^{-2} in good agreement.

The Q factor at resonance has been measured to be $\sim$ 5-10 $(Q = \frac{\omega_o}{\Delta\omega})$. Since $Q = \frac{\omega_o m}{r}$ this gives $r \sim 4$ kg s^{-1}.

This should be compared to $r \sim 40$ kg s^{-1} which is required for a critically damped system (when $r^2/4m^2 = s/m$).

The change in position due to the gravitational force has the form $x - x_o = \frac{mg}{s} (1 - \cos\alpha)$, where α is the angle that the etalon is tipped from the vertical. In practice the maximum $\alpha = 60^\circ$ gives a maximum $x - x_o = \frac{mg}{2s}$. Differentiating the above equation indicates that

$\frac{\delta x}{\delta \alpha} = \frac{mg}{s} \sin\alpha$, and that a minimum rate of change of plate gap occurs near the zenith when $\alpha = 0$.

6.3. The FP and Cryostat

The FP has been designed as a compact instrument so as to fit readily into an infra-red cryostat. It was first intended to be used within a filter chamber (containing four pre-monochromating filters of $\Delta\lambda \sim 1$ μm in the 10 μm window). This structure was fitted in a BOC helium cryostat which was used for preliminary tests but was changed because of repeated cooling problems.

The FP is now used in an Oxford Instruments cryostat with a four-inch working cavity and an axial base window. The helium chamber is supported at one end by its filling tube and at its base by means of

four stainless steel wires held in tension from the copper nitrogen shield. The nitrogen reservoir is similarly supported by its three fill tubes at one end, and by means of two nylon pegs at the radiation shield, which locate securely into the cryostat base.

The outer KRS5 window consists of a 2.5 cm disc held in a screwed aluminium ring by means of Oxford Instruments M5/M6 adhesive. Two electrical plugs are fitted in the "side-window" positions of the cryostat, with corresponding fittings on the nitrogen shield. The FP is shown within the cryostat in Figure 6.2.

The cryostat has a nitrogen capacity of 1.7 ℓ and a hold time of about 18 hours. The helium capacity is 1.4 ℓ with a hold time of 25-50 hours depending on use. About 3 ℓ of helium are required for a fill, after initial pre-cooling with nitrogen. The cryostat has an aluminium outer case with stainless steel liquid reservoirs and copper radiation shield and helium base. The total weight is about 15 kg, not inconveniently heavy.

For access purposes the baseplate of the cryostat can be removed; when the endplate of the nitrogen shield is unscrewed the whole of the working cavity is accessible. It is also possible to remove the outer wall and then the sides of the nitrogen shield, this gives more complete access to the instrument mounted on the helium baseplate.

The rigidity of the nitrogen cooled chamber is ensured by means of the three fill tubes at one end and by the two nylon locating pins at the radiation shield endplate. The inner helium chamber has a long thin neck which is quite flexible, lateral location is maintained by

Helium
fill
tube

1 of 3 nitrogen
fill tubes

Evacuuation
port

Nitrogen
reservoir

Outer wall

Helium chamber

Nitrogen-cooled
radiation shield

Helium-
cooled
radiation
shield

FP
chamber

Electrical
plug

Baseplate
& Window
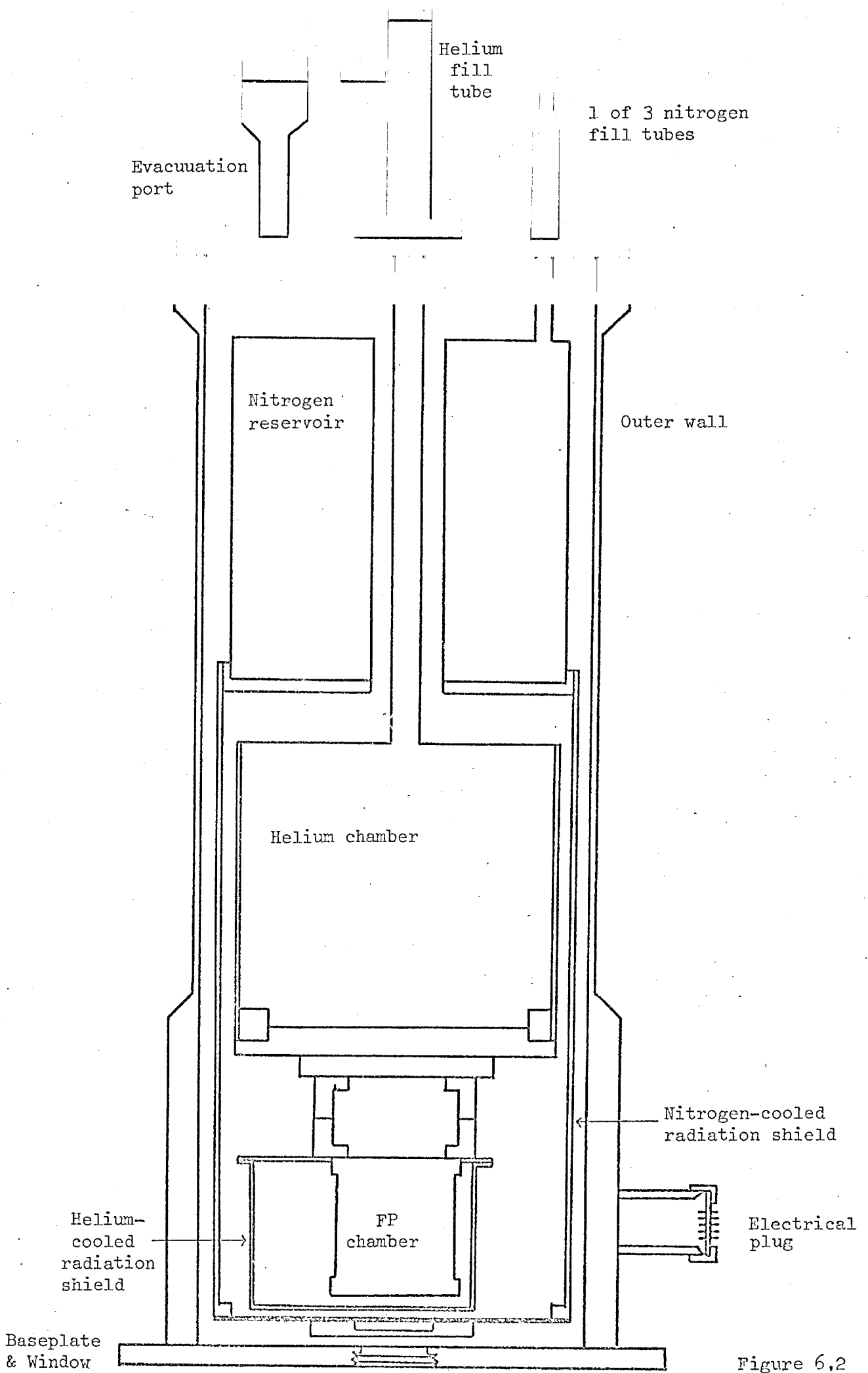
Figure 6,2

means of four taut wires which can be adjusted to align the centre of the vessel with the cryostat axis. It is found that a much more secure arrangement is needed for transport purposes, the inside is packed with polystyrene foam and metal location pins are used for this purpose.

The copper cylinder containing the Fabry-Perot etalon is enclosed within a gold coated copper radiation shield, this shields from 10 μm radiation leaks and helps to maintain the superconducting coil and other elements at a low temperature. This shield has one aperture for the signal beam, most parts of the assembly within the shield are painted with Nextel 101 - C10 black coating.

6.4. Heat Inputs

The heat inputs which result in evaporation of coolants are mainly due to radiation exchange and thermal conduction, very little gaseous conduction occurs since the cryostat is usually pumped to $\sim 10^{-5}$ torr and then cryopumping occurs after cooling. Various heat inputs to the cryostat are shown schematically in Figure 6.3. All inner surfaces (that can exchange radiation with others at a different temperature) are polished and have emissivities that vary from ~ 0.1 for stainless steel at room temperature to ~ 0.005 for copper at 4.2K.

The nitrogen vessel receives radiation from the surrounding 300K area of the outer walls, this is minimised by using polished surfaces and some layers of superinsulation on the nitrogen reservoir. It receives heat that is conducted down its three stainless steel fill tubes and also from the top section of the helium tube which is heat-sunk to it by a copper clamp. There is a further input from the two nylon location pins. The various electrical connection wires are made of stainless steel (sleeved in PTFE) as well as two of 40 gauge copper, for the coil current.

Heat Inputs to Cryostat

300 K radiation

Neck conduction

Neck conduction

300 K radiation

77 K radiation

Stainless Steel wire conduction

Electrical wire conduction

Copper & Stainless Steel wires

Nylon pin conduction

300 K radiation (direct to helium)
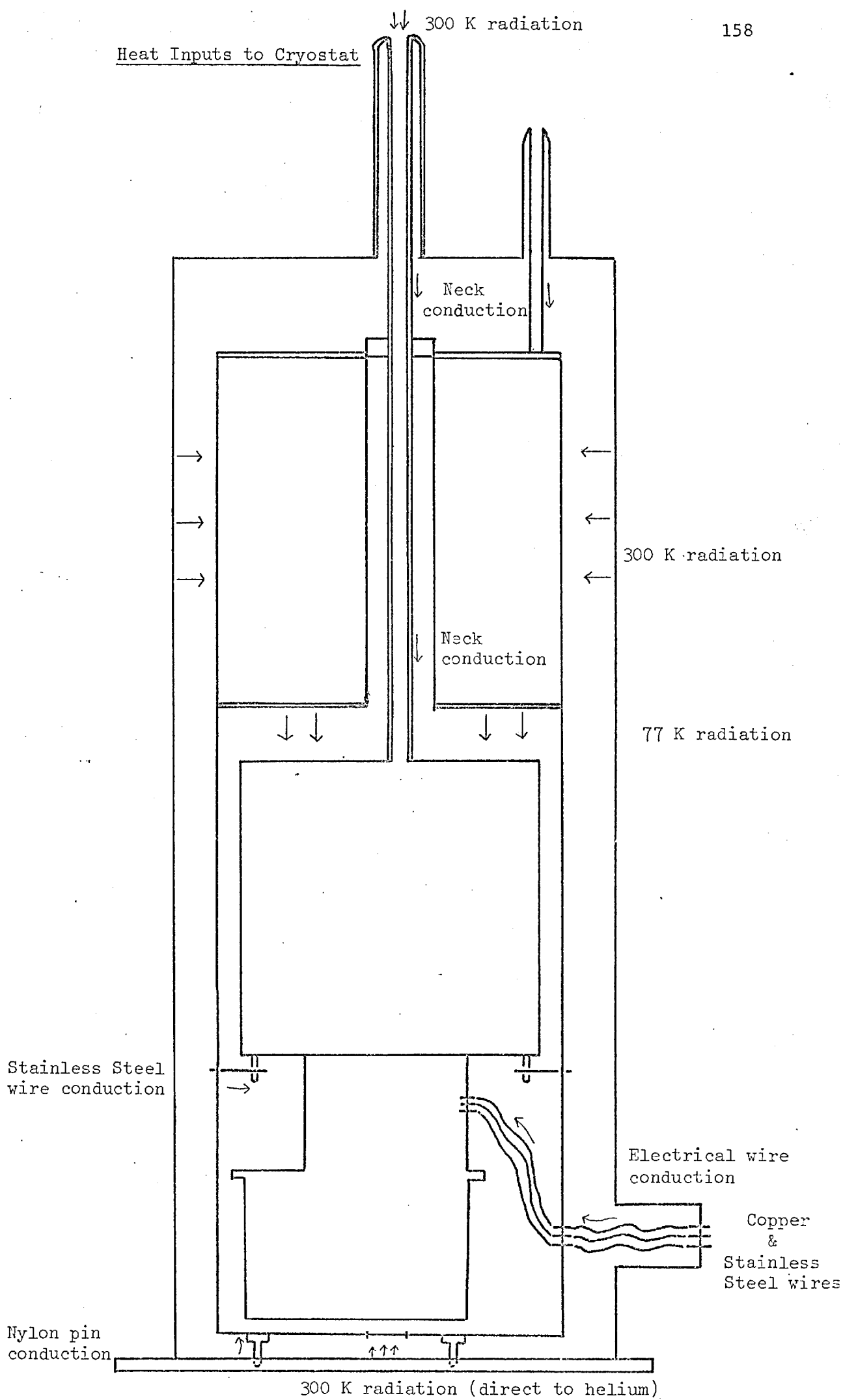
Figure 6.3

The helium chamber receives radiation from the surrounding nitrogen-cooled vessel and shield, this is minimised by using polished surfaces and keeping the surface area of cooled elements as little as possible. There is also a small amount of 300K radiation received from the fill tube (reduced by a baffle), and also some radiation is received via the beam entrance aperture. Heat is conducted down the neck, from the nitrogen heat-clamp, and also from the four stainless steel support wires. The electrical connection wires (6 to the detector and 4 for the Fabry-Perot) also contribute to the heat input.

The nitrogen heat inputs evaporate the liquid at a rate of $\sim$ 23 cc/hour for a 1 Watt input, this can be reduced somewhat if efficient gas cooling occurs in the fill tube so that the enthalpy extracts some more heat. Heat inputs to the helium reservoir evaporate it at the rate of $\sim$ 1.4 ℓ/hour for a 1 Watt input, although baffles in the neck can enable the high gas enthalpy to minimise the neck conduction loss.

These various sources of heat input are summarised in Table 6.1. The calculated heat inputs and their resultant coolant loss rates agree quite well with those obtained in practice. There can be a considerable uncertainty in the effective areas and emissivities of radiating surfaces, as well as doubt about the efficiency of heat-sinking at intermediate points of connecting wires. The actual amount of nitrogen and helium used to cool the instrument down has been minimised by keeping all items as light as possible.

Table 6.1:   Cryostat Heat Inputs

(A)   Nitrogen Reservoir Inputs

1)   300K radiation, area of inner and outer surfaces $\sim$ 2000 cm^2
     $\epsilon \sim$ .05 for each surface. $\therefore$ Radiation Transfer $= 2\frac{1}{2}$ W.

2)   Conduction down 3 N$_2$ and 1 He neck $\leq$ 2 W.

3)   10 stainless steel wires, 38 gauge x 10 cm, contribute $\sim$ 5m W.

4)   2 copper 38 gauge wires also contribute $\sim$ 40m W.

5)   2 nylon pins, $\frac{1}{8}$" hollow tubes, give $\sim$ 0.1 W.

                Total $\leq$ 5 Watts

(B)   Helium Reservoir Inputs

1)   77K radiation, area $\sim$ 1000 cm^2, $\epsilon \sim$.05 $\therefore$ radiation $= 5$m W.

2)   300K radiation from $4\frac{1}{2}$ mm aperture, radiation $\leq$ 7m W.

3)   Cryostat neck conduction $= 1$-10m W.

4)   4 stainless steel support wires (28 gauge) give $\sim$ 4m W.

5)   10 stainless steel electrical wires (38 gauge) give $<$ 1m W.

6)   2 copper, 40 gauge wires give 15m W.

                Total $=$ 30-40m W

6.5. The Detector Mount

A detector column for an Arsenic-doped-Silicon photoconductor has been designed and constructed for use with the FP. Copper has been used for this assembly, to ensure good thermal conductivity, and a single disc of saphire (2 cm diam. x 2 mm thick) was used for electrical isolation. The mount is shown in Figure 6.4.

The Santa Barbara detector consists of a rectangle of As:Si soldered to a copper 5 mm cube as a heat sink. The detector area is 2 x 2 mm and has a depth of 4 mm. This block is screwed into the top of a copper column, which has an oblique face at about 10°. This copper column slides into a base sleeve which is secured to the helium chamber via the saphire disc, the column can thus be adjusted for height and then clamped by screws to the sleeve.

A top cap with an aperture of ∿ 1.5 mm is screwed in place over the detector column and forms an enclosed cavity. The inner surface has been machined to produce a hemi-spherical reflector, with the detector surface at its centre of curvature. The combination of the inclined detector and this reflection should ensure that much of the radiation passing through the detector aperture is finally absorbed despite the initial reflection of 30%. The cap is extended above the aperture to help baffle any stray radiation. One electrical connection is made by screwing a thick copper wire directly on the detector column and taking this to the gate of the nearby FET. The second connection consists firstly of a short, thin wire from the side of the As:Si block. This detector wire is soldered to another wire, within the cavity, which is then led out through a hole drilled in the column. This wire, of 40 gauge enamelled copper, is sealed at its exit from the hole by means of Emerson and Cummings Stycast 2850 resin.

Optical
Axis

Aperture cap

Hemi-spherical
reflecting surface

Detector on
copper block

Detector cavity

screw for
electrical →
terminal

support
column

2nd electrical
connecting wire

column clamp
screw

nylon bush

saphire disc

Helium cooled baseplate

Figure 6.4

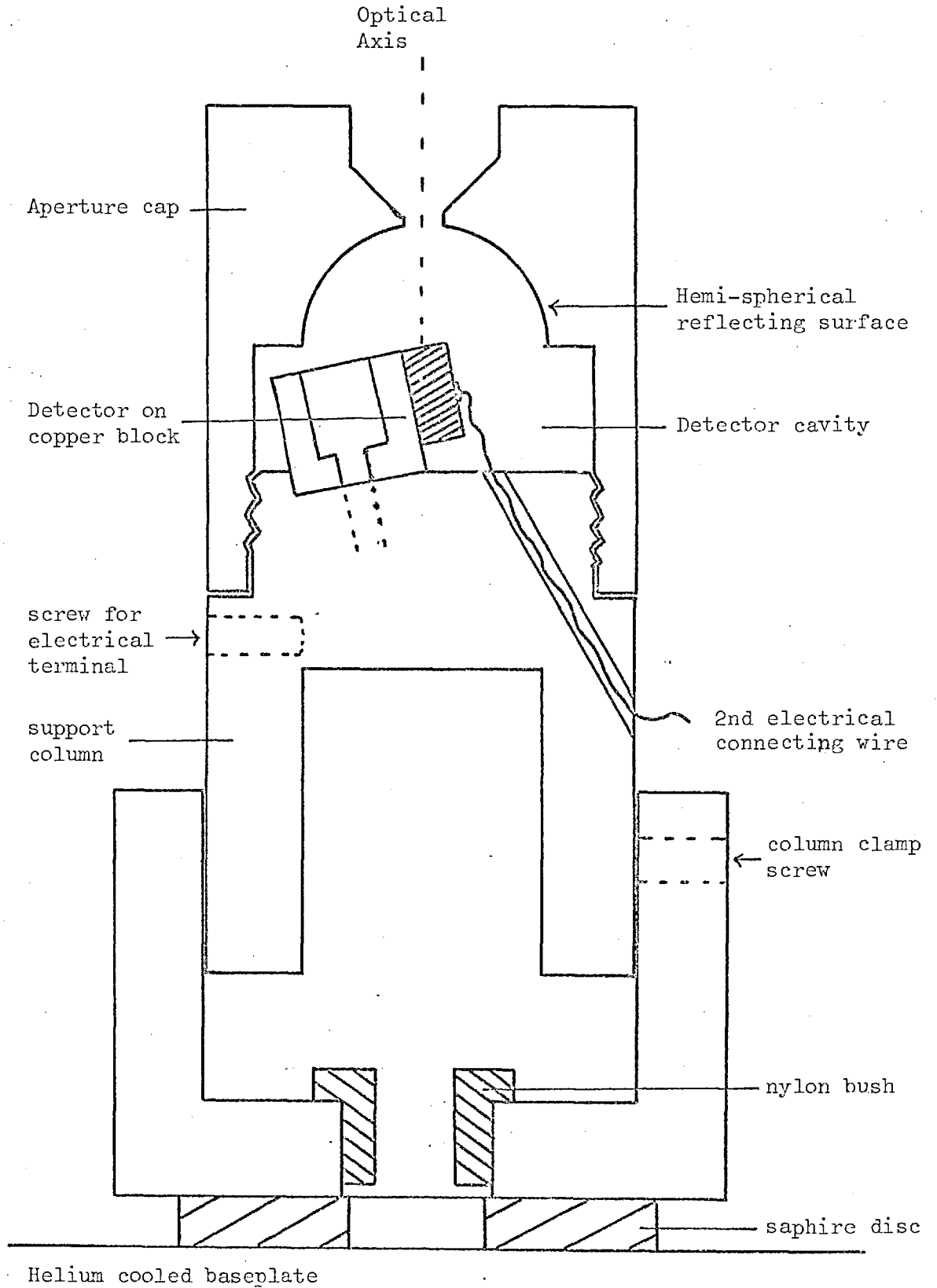The cooled FET and load/feedback resistor are held within the cavity formed by the Fabry-Perot cylinder and are close to the detector column. Ceramic lead-through pins are fixed in the wall of the support cylinder and the FET is soldered directly to these. A small multi-way connector socket fits onto these pins, and stainless steel wires are taken to a lead-through plug which is mounted in the nitrogen shield.

CHAPTER 7

FABRY-PEROT ELECTRONICS

7.1. Detector Circuitry

The FP is used with a helium-cooled As:Si detector; this detector and the pre-amplifier were described in Chapter 2. The circuit used, and wiring arrangement, are shown in Figure 7.1. A MOX-type 4000 MΩ feedback resistor has been used with reasonable results; it has a Johnson noise of $\sim$ 1 μV, which is similar to the MOSFET noise at present. A wire-wound (uncooled) 20 kΩ resistor is used as the source load for the M103 MOSFET.

An adjustable voltage is fed into the non-inverting input as a compensation for the MOSFET gate-source offset voltage; this is initially trimmed after cooling, with a zero detector bias being applied. A variable detector bias voltage is applied directly (from a potentiometer across a battery). The operational amplifier used is an OP05, this has a low input noise of 10 nV Hz$^{-\frac{1}{2}}$ from 10-1000 Hz.

The feedback resistor (of value 4000 MΩ) with its shunt capacitance $\leq$ 0.2 pF allows operation up to $\sim$ 200 Hz with this circuit. The frequency compensation components (R_c, C_c) have not been used .

The detector had an NEP $\sim$ 10^{-13}W Hz$^{-\frac{1}{2}}$ in most of the tests made with the FP to date, this being due to excess pre-amplifier noise mainly. Recent tests have given an NEP value of $\sim$ 2.10^{-14}W Hz$^{-\frac{1}{2}}$ and lower values are expected in the near future when lower-background tests are made.

7.2. FP Capacitance Sensor

For the successful operation of the scanning etalon it is necessary to have an accurate means of measuring the separation of the plates.

Fabry-Perot Detector Pre-amplifier

4.2 K   Room Temp.

R_c

C_c

C_f R_f

MOSFET

D

OP. AMP.

mode B

G   SS   +18V

Normal
Output

S

Output B

C_T Detector

20K

+18V

+18V

100K

+18V

+30V

Detector
Bias

Detector Wiring

Nitrogen
Shield

Detector
Column R_f

Pre-amp.
box

FET

Stainless
Steel wires

Outer wall
& hermetic plug

Helium
Cavity
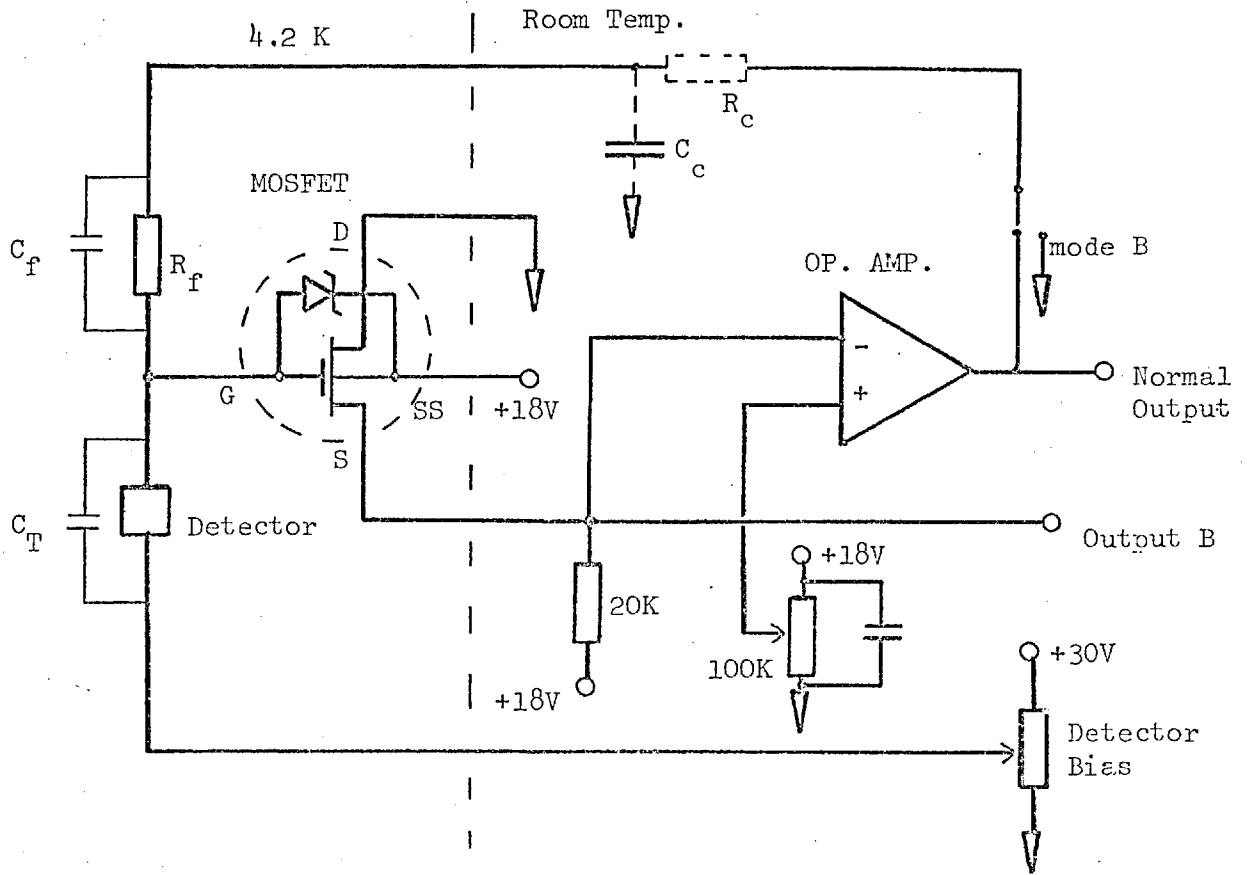
Figure 7.1

The method used must be sensitive (to detect changes < 0.01 μm), reliable, and compact for use within the cryostat. The method adopted has been the use of a capacitance sensing system based on work of Jones & Richards (1973) and further adaptations by Hicks (1974). T.R. Hicks has built and operated a capacitance-sensed, servo controlled optical Fabry-Perot and his helpful comments are acknowledged here.
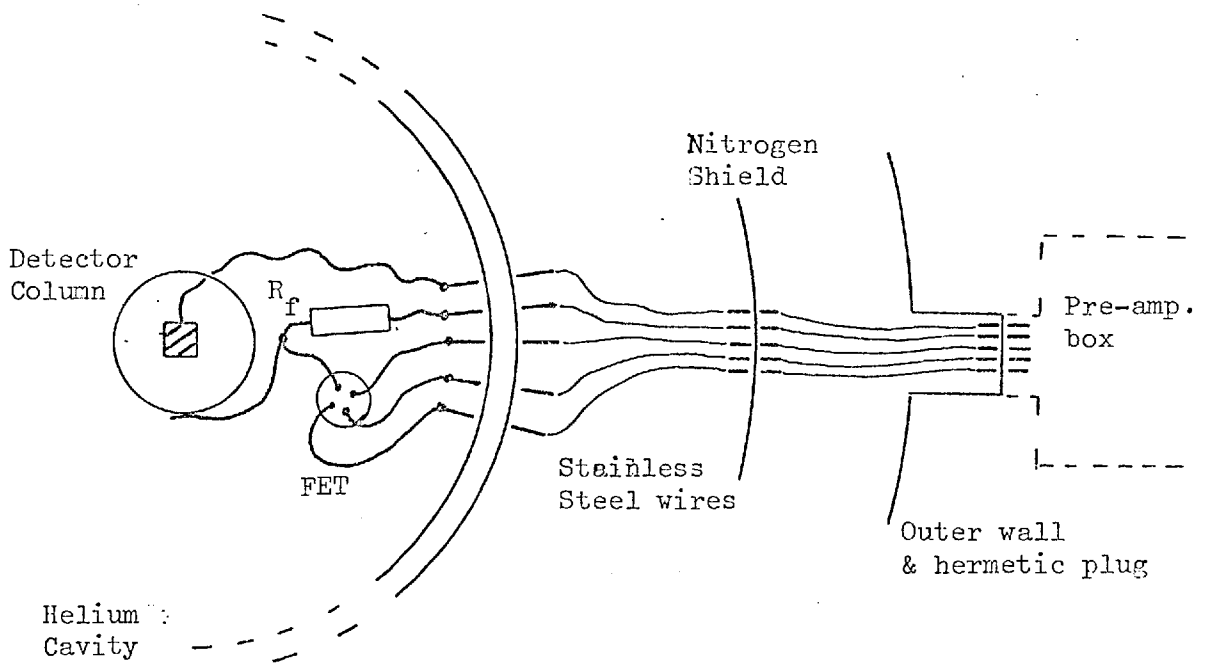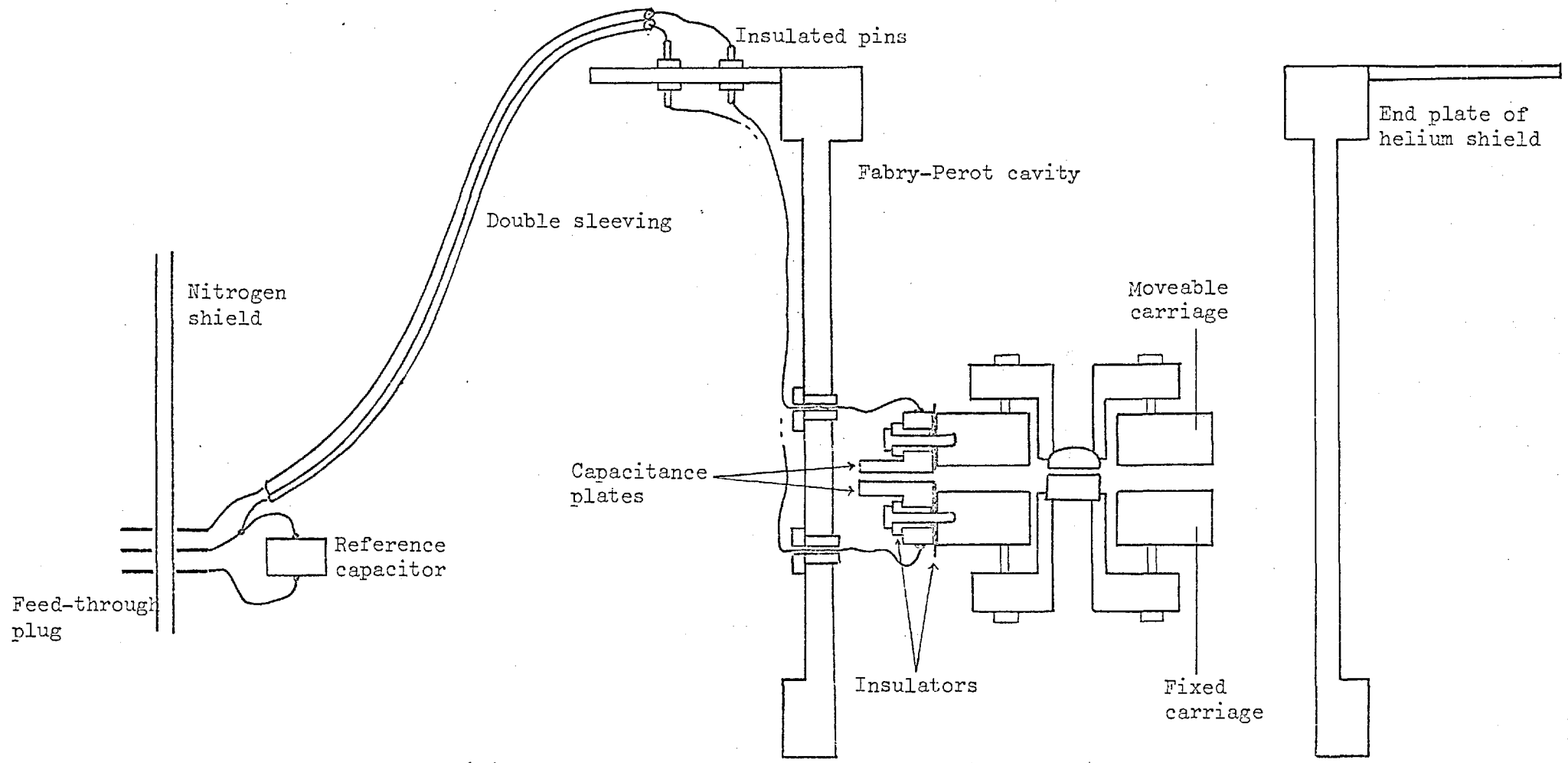
A simple capacitor is constructed by screwing two metal plates, via insulated spacers, onto the etalon structure. One of the plates is fixed and the other moves as the carriage is moved. They sit within the FP chamber and small enamelled copper wires are led out through holes in the wall. Two stainless steel wires in a double insulating sleeve are then taken to the nitrogen shield, where a fixed reference capacitance is positioned. See Figure 7.2.

The sensing capacitor is set up so as to have a gap of about 100 μm which results in a capacitance of close to 5 pF. The reference capacitor used is a flat mica capacitor of similar value, very little change is noted on cooling and the stability of the environment then ensures a constant reference. However, it is extremely important that the connecting wires are securely taped down, since any relative movement results in a change in capacitance. The requirement of low heat conduction does not allow thick, rigidly secured connections but a satisfactory solution is obtained by running the wires in parallel insulating sleeves and fixing these in place as much as possible.

The sensor capacitance is measured with respect to the reference by means of a transformer ratio bridge, a system discussed fully by Hicks (1974). The circuit diagram of the capacitance detector and amplifier system is shown in Figure 7.3. A stable oscillator supplies a 16 kHz signal to the bridge arrangement, the output of the bridge measures the difference between the two capacitances. This is amplified

Insulated pins

Fabry-Perot cavity

Double sleeving

Nitrogen
shield

Moveable
carriage

Capacitance
plates

Reference
capacitor

Feed-through
plug

Insulators

Fixed
carriage

End plate of
helium shield

Capacitor Plate Assembly & Wiring

167
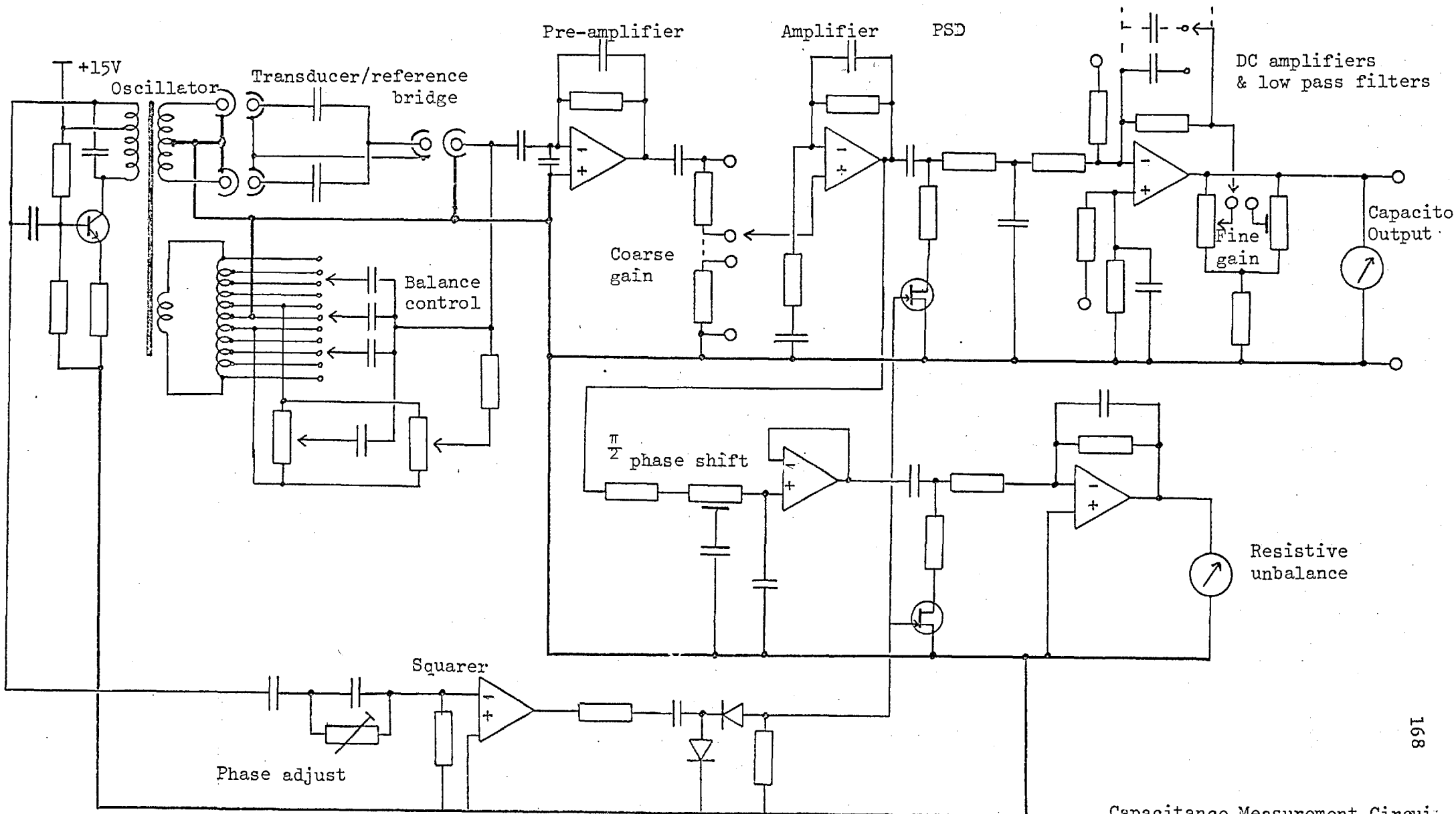
Figure 7.2

Capacitance Measurement Circuit

Figure 7.3

168

and then passes to a phase sensitive detector, with a coherent reference
from the oscillator, so that a DC output proportional to the capacitance
difference is obtained.

A 90° phase-shifted output also indicates any resistive unbalance.
Various switched capacitors at the input allow the bridge to be
balanced so that zero output is obtained for various sensor values, as
required. The sensitivity of the circuit can be adjusted, and low pass
filters are provided to change the measurement bandwidth. This circuit
is adequately sensitive and an output voltage of 5 volts for a change
in gap of 1 μm is typically used.

The capacitance arrangement used is such that the measured
capacitance $C = \frac{kA}{t}$ and changes in this give $\frac{\delta c}{\delta t} = \frac{-kA}{t^2}$. If the movement
to be measured, $\delta t \ll t$ then a constant sensitivity is obtained. In our
case $t \sim 100$ μm and $\delta t = 2\frac{1}{2}$ μm (for a scan range of 8-13 μm), and thus
the departure from linearity is $\sim \pm 1\%$, not serious for our use although
allowance is necessary if test scans over a wide range are made.

7.3. Servo Control of the Etalon

The drive system to change the gap, combined with the capacitance
sensor, gives a means of servo control for the etalon. Feedback can
be used to give a fixed, or variable plate separation control that
should be superior to a simple uncompensated drive arrangement. A servo
mechanism can compensate for the gravitational scanning that occurs as
the orientation of the etalon changes, long term drifts can be corrected
and also it should be possible to reduce short term or higher frequency
plate motions.

In an ideal system the output of the capacitance sensor would be amplified and then fed into a control input for the drive system so as to give negative feedback. Any changes in plate position then give an error signal which, after amplification, produces a strong correction drive signal, and thus the plates are maintained at a fixed gap which gives a zero, or small error signal. Deliberate changes in the etalon gap can be produced by introducing an offset voltage into the servo loop which can then only be cancelled by a plate movement which generates an "error" signal so as to nullify the offset.

A generalised diagram of the servo loop system is given in Figure 7.4. It can be shown that an offset to cause a "scan" of the plate gap is best introduced at an early stage of the servo loop. The resultant motion is then more stable and less susceptible to changes in amplifier gain which may occur after the offset point, and a smaller offset is also required.

In practice with the Fabry-Perot assembly there are limitations to the advantages which one would theoretically expect. The resonance of the system typically occurs at 100-200 Hz and is not very strongly damped. We obtain a resonant frequency of 180 Hz, and a Q factor of 10, with springs of thickness 0.58 mm. (Damping techniques are discussed in Section 8.3.3.).

This resonant motion has the effect of limiting the maximum gain that can be applied in the servo loop. Too high a gain gives positive feedback near the resonant frequency and self-sustaining oscillations are the result. By careful design it is possible to use various filters in the servo loop to give high gain at low frequency and a useful gain

Fabry-Perot Servo Loop
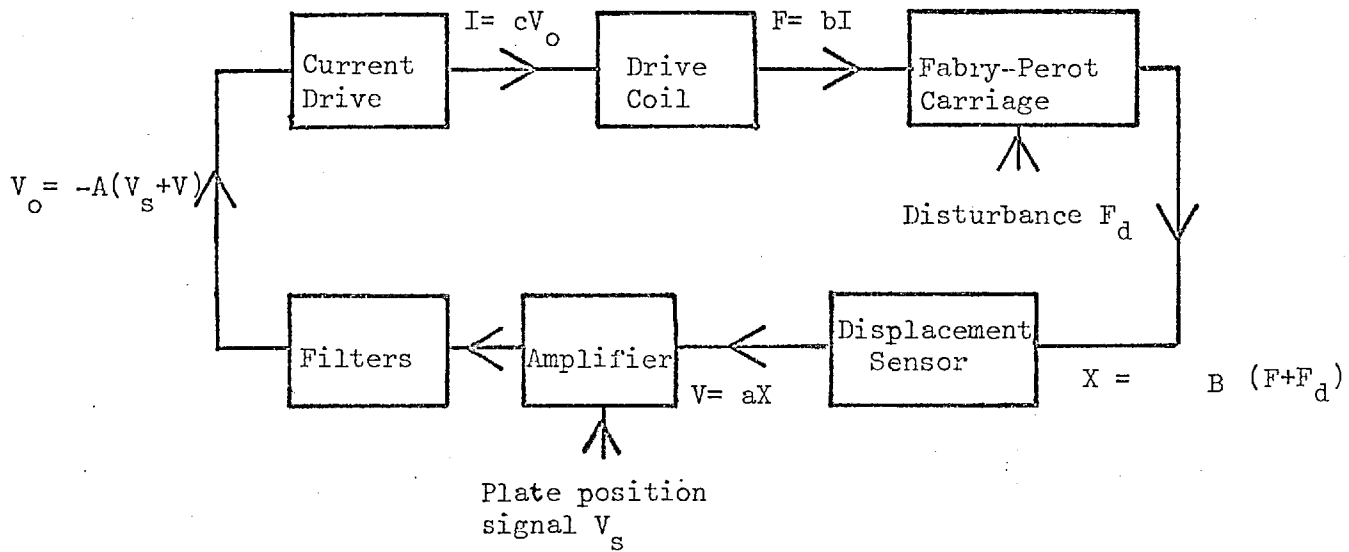
Notes.   a,b,c are constants , A,B are more complex functions
The displacement X is a function of the forces F and F_d , it varies
with frequency. The control voltage V_o is similarly a function of
frequency. The effect of the disturbing force F_d is reduced by the
total "gain" of the system .

Figure 7.4
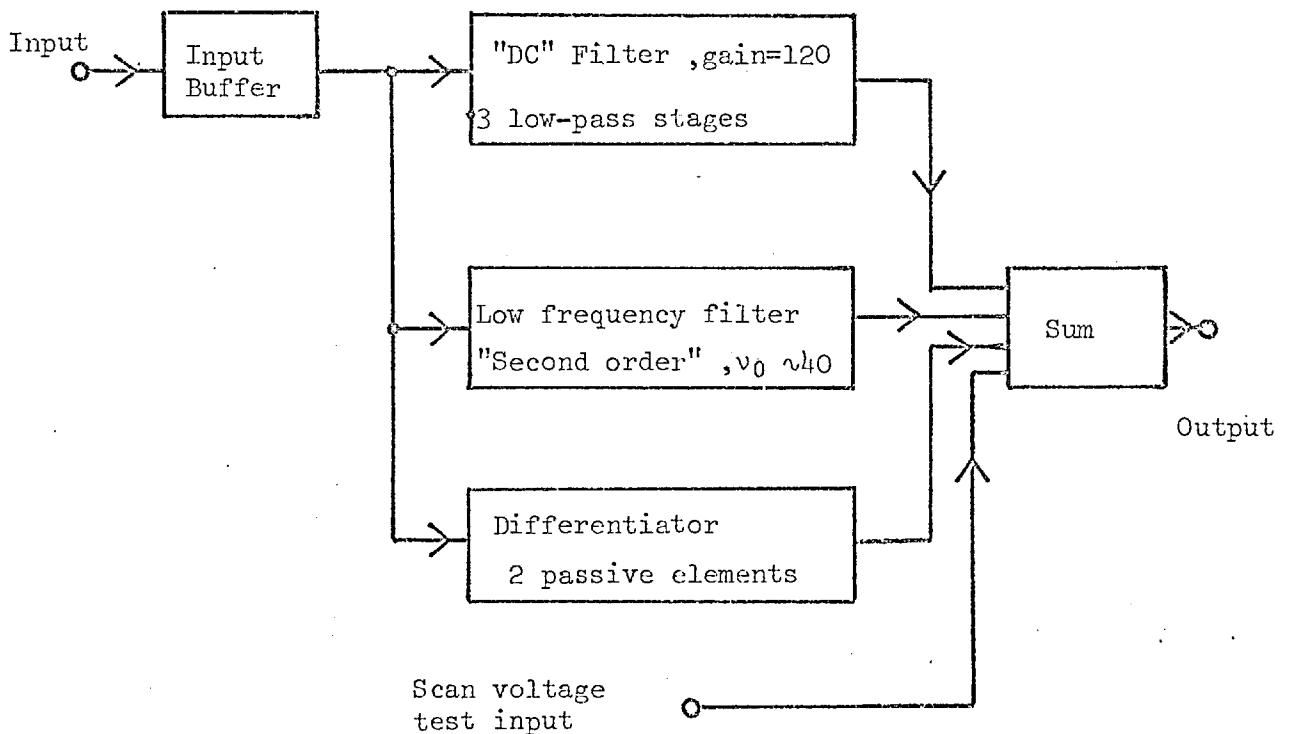
Servo Filters

Figure 7.5

at other frequencies. Figure 7.5 shows the type of filters used in the servo loop and Figure 7.6 gives the full circuit details.

A high DC gain is useful for long term stability and to compensate for gravitational scanning. As much gain as possible is required in the 5-20 Hz range to reduce any plate-motions which might be induced by the focal plane chopper. It is then necessary to damp or reduce the resonance as much as possible since these motions can potentially be large and are readily excited by telescope vibration. Compensation at frequencies about say 300 Hz is less important because the available excitation energy is rather small.

The "DC" filter has a total effective gain of 500 at DC, it has two primary low pass stages which reduce the gain so that it is much less than 1 as the resonant frequency is approached (where the phase changes can give positive feedback). The low frequency filter is used with a gain of 1-2 at frequencies less than 40 Hz, to help reduce chopper induced motion. The Differentiator has been carefully tuned to give an optimum amount of differential feedback near the resonant frequency (180 Hz in the design shown).

The use of a tuned circuit which had the same characteristics as the response of the FP assembly was investigated. However, it was found that the parameters had to be very critically matched for it to be useful near the resonant frequency, and any changes in the mechanical or electronic elements made the resultant servo behaviour very poor. Also, a single tuned circuit was found to make the plate vibrations much worse at frequencies above the resonance, this being due to more complex mechanical effects and further phase changes. The final design of the servo system was designed and empirically found to be the best readily available solution.
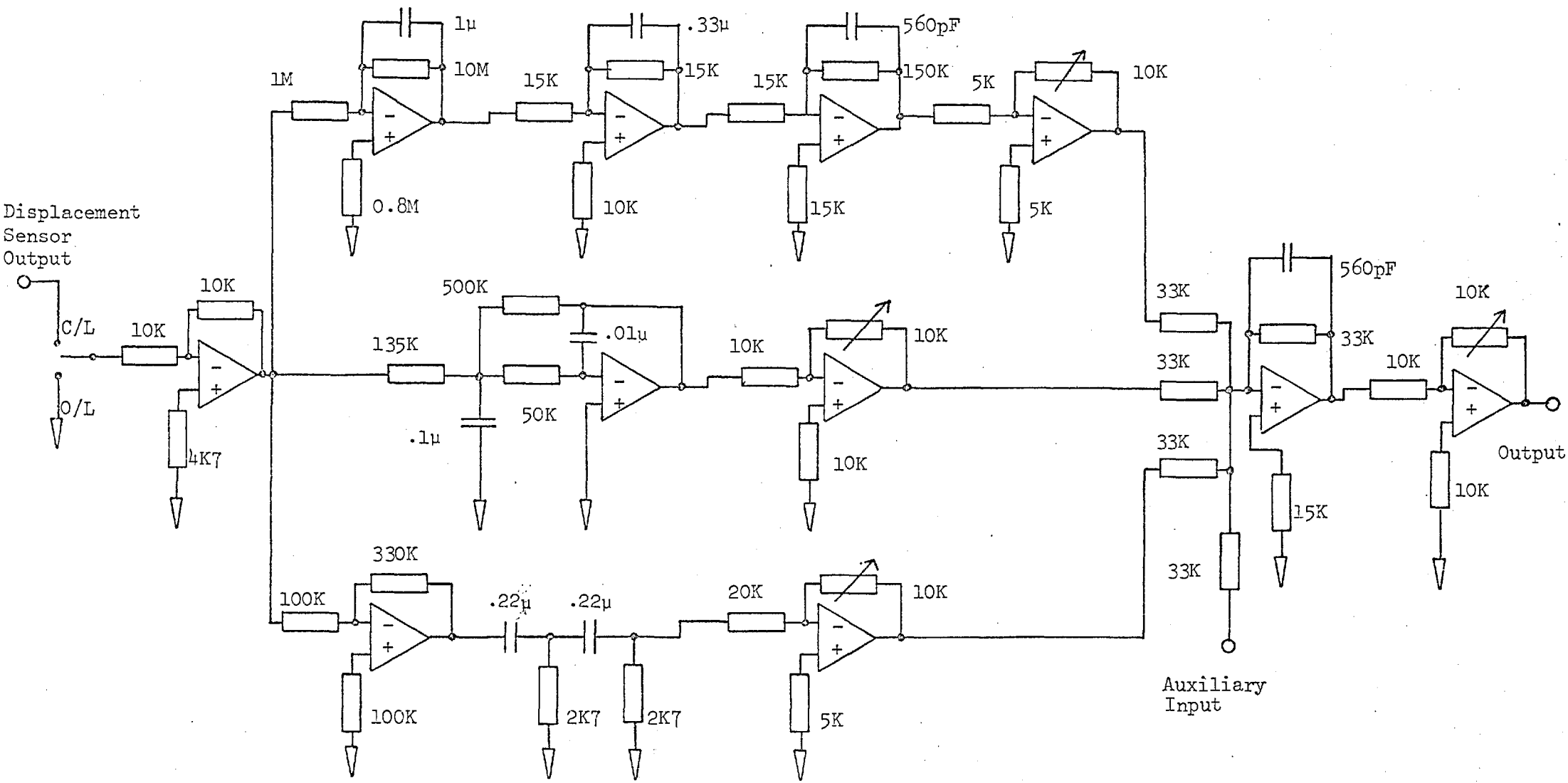
Circuit Diagram of Servo Filters

Figure 7.6

173

The transfer function of the system (i.e. the mechanical displacement versus frequency for a constant force) is indicated in Figure 7.7. The motions of the etalon with no servo control (open-loop), and then the motions with the servo on, are shown. The strong phase changes that occur are also shown. It is seen that the primary resonance can only be reduced at the expense of slightly increased movement at other frequencies. The very strong servo action at frequencies less than 1 Hz is not indicated in this figure.

7.4. The Coil Drive Unit

A constant-current programmable drive unit has been built for use with the etalon superconducting coil. The output current is directly proportional to the input control voltage and is not dependent on the load resistance within reason. The circuit uses a National Semiconductor LH 0021 CK power operational amplifier which has a bipolar output current of up to ± 1 Amp.

Details of the circuit are shown in Figure 7.8. A "normal" input, a "X2" input and a variable offset input are provided. The gain may be pre-set or varied with a fine control from -20 to -70 mA/Volt (for the normal input). A meter is provided to indicate the output current. For minimum output drift and high gain stability 1% thick-film resistors are used in the critical positions. The circuit operates from a 1 Amp, ± 15v supply.

The frequency response of the circuit is flat from DC to $\sim$ 1 kHz (a low-pass filter gives a 3 dB point of 1.3 kHz). Crossover distortion is not noticeable for frequencies below 100 Hz, and only occurs when the output current is zero, not normally the case. A trim control at the

Mechanical Response of Fabry-Perot Etalon

FP vertical

mechanical
displacement

(arbitrary
scale)

FP horizontal

mechanical
displacement

frequency
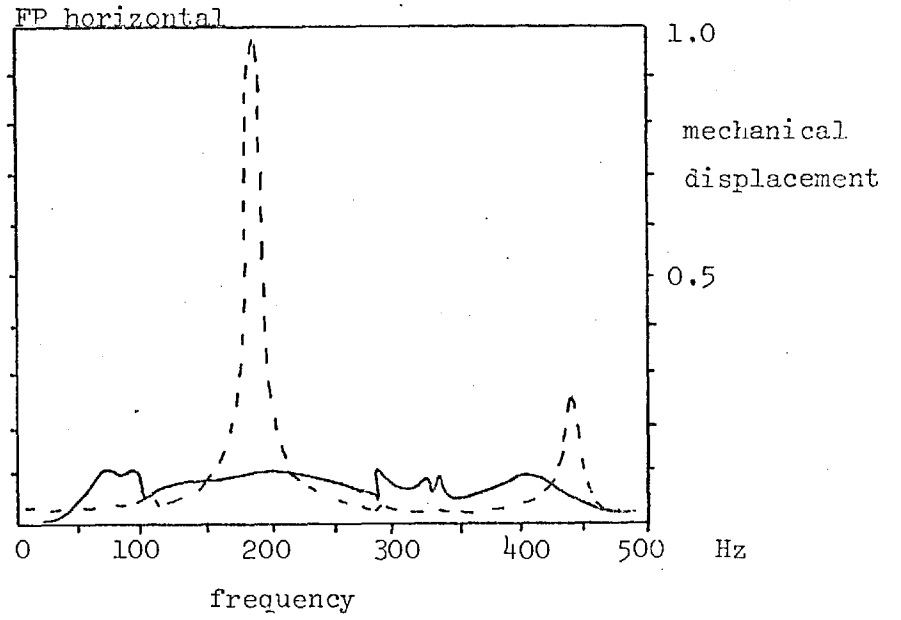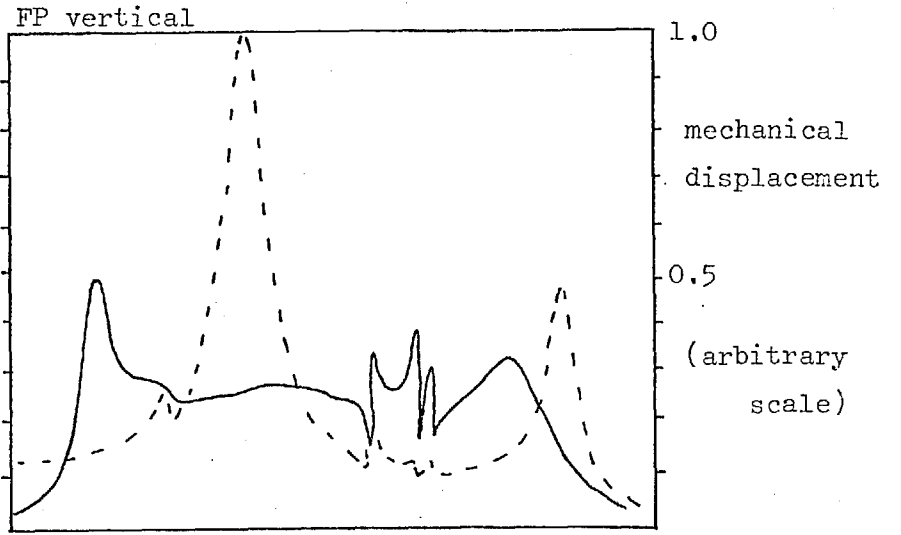
N.B.   dotted line = servo off , solid line = servo on

phase
change

frequency

Figure 7.7

Current Drive Unit

Figure 7.8

$$I_{out} = \frac{V_{in} \cdot R2}{R5 \cdot R1}$$

176

input buffer (a 741 Op. Amp) is used to reduce the output offset current to less than 1 mA, when the inputs are at zero volts.

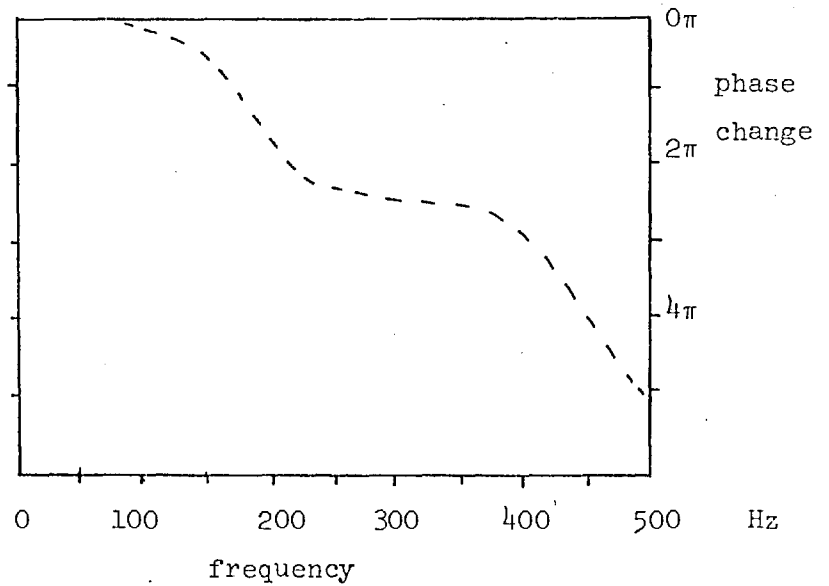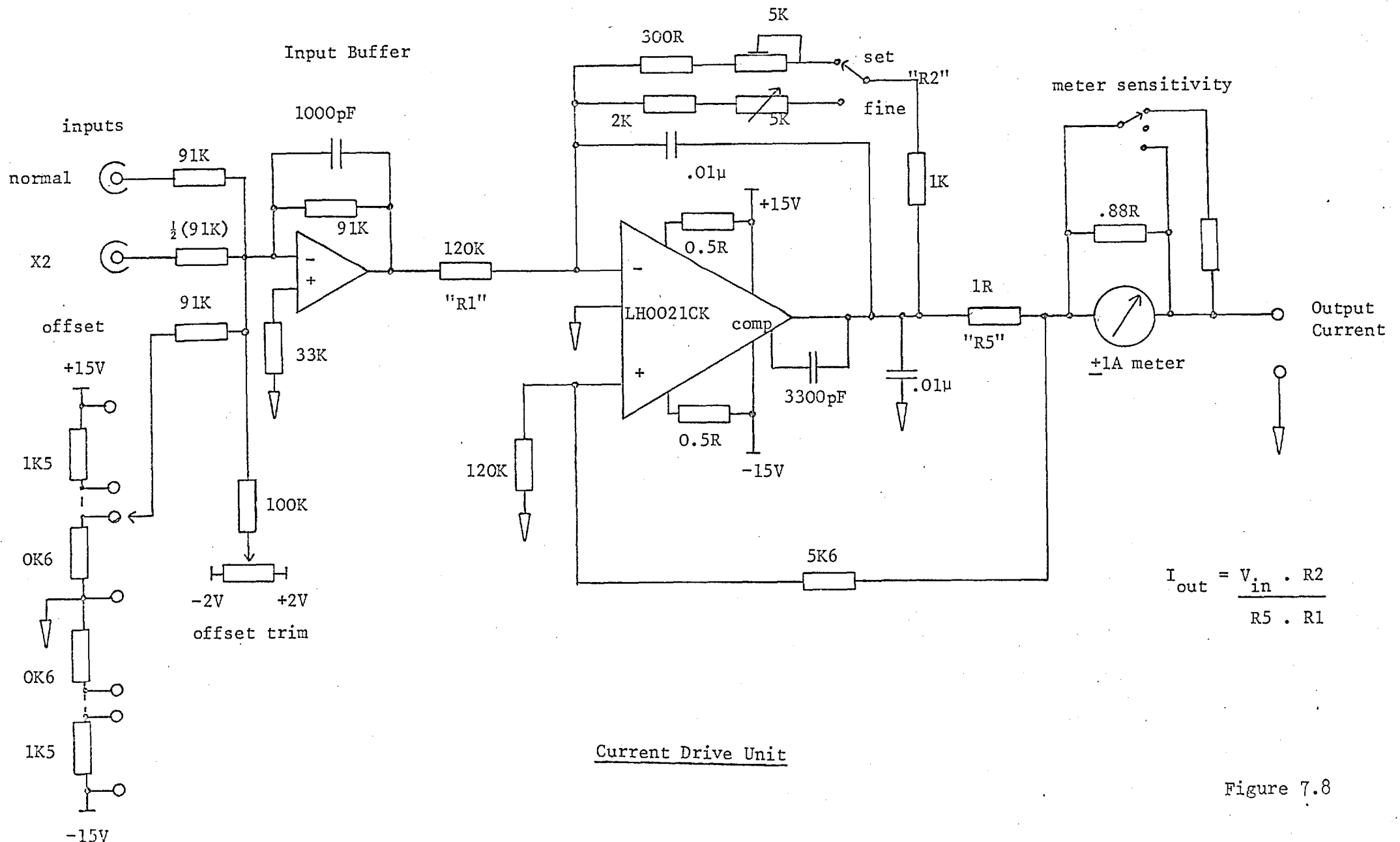The maximum drive current obtainable is ± 0.9 A, limiting resistors are included in the circuit, and with the maximum gain and full input voltage of 15 V this current is reached. The unit will successfully drive a "normal" 4Ω coil, or a superconducting coil of lower resistance, and has good linearity.

7.5. The Analogue Scan Controller

In order to provide a means of scanning the plate gap of the FP a simple analogue controller has been constructed, and incorporated into the coil drive module for convenience. The main need was to provide a flexible ramp voltage whose slope, direction and amplitude could be adjusted.

The circuit is shown in Figure 7.9, four "741" operational amplifiers have been used with a supply of ± 15 V. The main element is an active integrator with a large time constant and an input voltage which is variable from 15-0.5 V. By careful input offset trimming the drift can be kept low, typical output drift = 10 μV/sec. The integrator can be reset, held at a fixed voltage, or allowed to integrate in either direction.

The scan output ramp voltage can readily be inverted, its amplitude can be attenuated, and an offset of ± 15 V can be applied. A further element aloows the introduction of single or multiple pulses in order to increment the scan control output in a stepped mode.

The maximum ramp rate is set at 1 Volt/sec and the minimum is $\frac{1}{32}$ V/sec. A completely linear ramp, with an error of less than 1%,
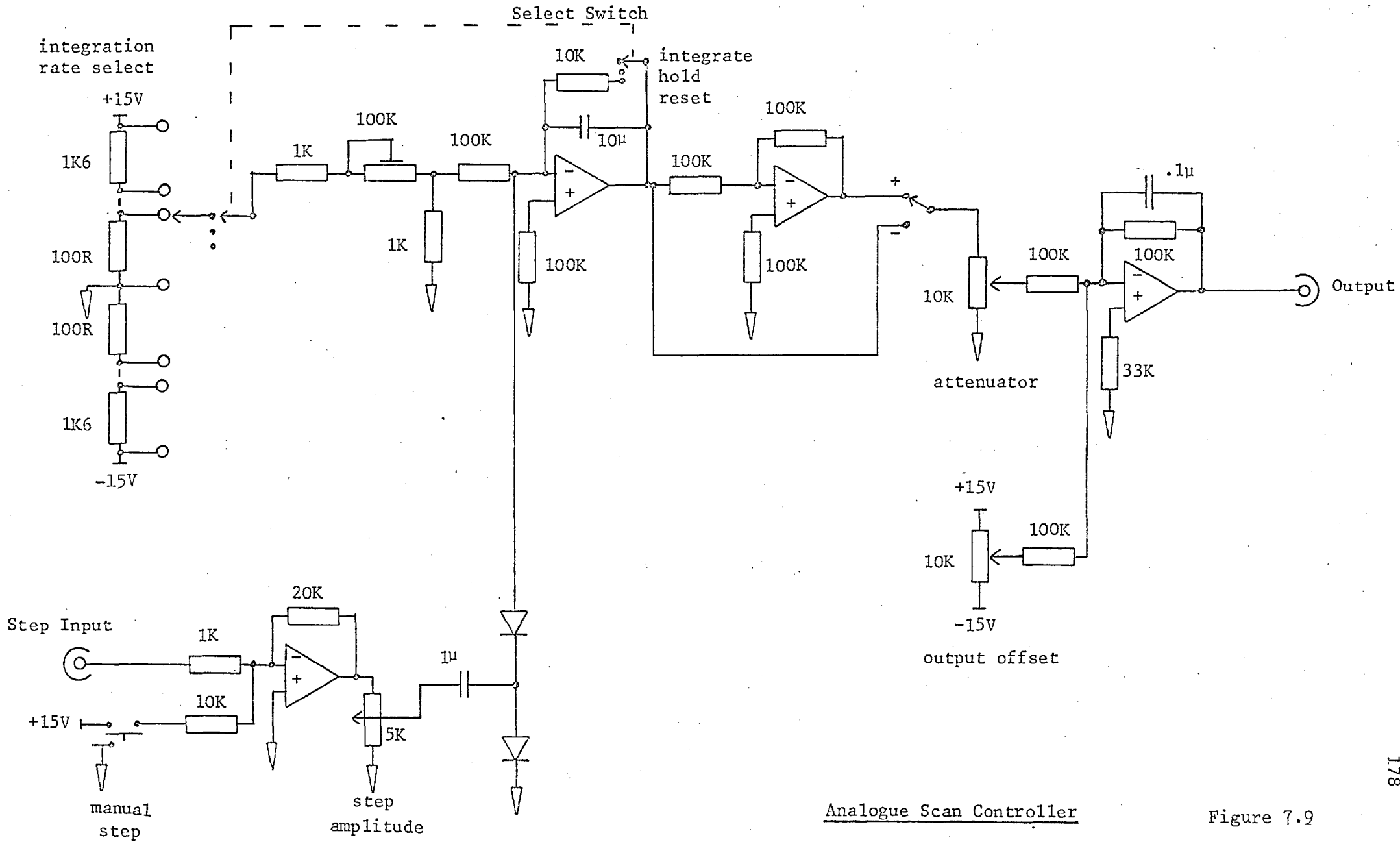
Analogue Scan Controller

Figure 7.9

178

is obtained over the output range of 0-14 Volts. This unit has performed

adequately in practice although a digital or computer control is planned

in future,

7.6. Improvements in the FP Electronics

It is possible to improve the precision of the plate gap control

by using methods other than the analogue scan control. The best place

to introduce an offset signal into the servo loop is at the input of the

first pre-amplifier of the capacitance sensor. To do this a variable

amplitude sinusoidal signal at the bridge frequency of 16 kHz must be

generated.

A constant amplitude oscillator reference is extracted and used as

one input of an analogue multiplier, the output of this unit is then

an AC signal whose amplitude is determined by a DC voltage applied to the

second input. This adjustable offset signal is fed via a switchable

attenuator, and scaling capacitor, into the pre-amplifier input in the

same way as the bridge balance controls.

The scan control voltage is now applied to the input of the

multiplier (Analog Devices Model 435 K). The planned method of control

is to use a minicomputer, via a camac crate and I/O register, to set a

D/A converter which feeds the multiplier. A 12-bit converter will give

an adequate precision of $\sim$ .001 μm over a 4 μm scan range, and the use

of a computer should enable very flexible control of the Fabry-Perot.

Figure 7.10 shows the whole arrangement and it is planned to construct

this facility in the near future.

Some improvement in sensitivity of the capacitance sensor could

be obtained by using pre-amplifiers with a lower noise, this is not
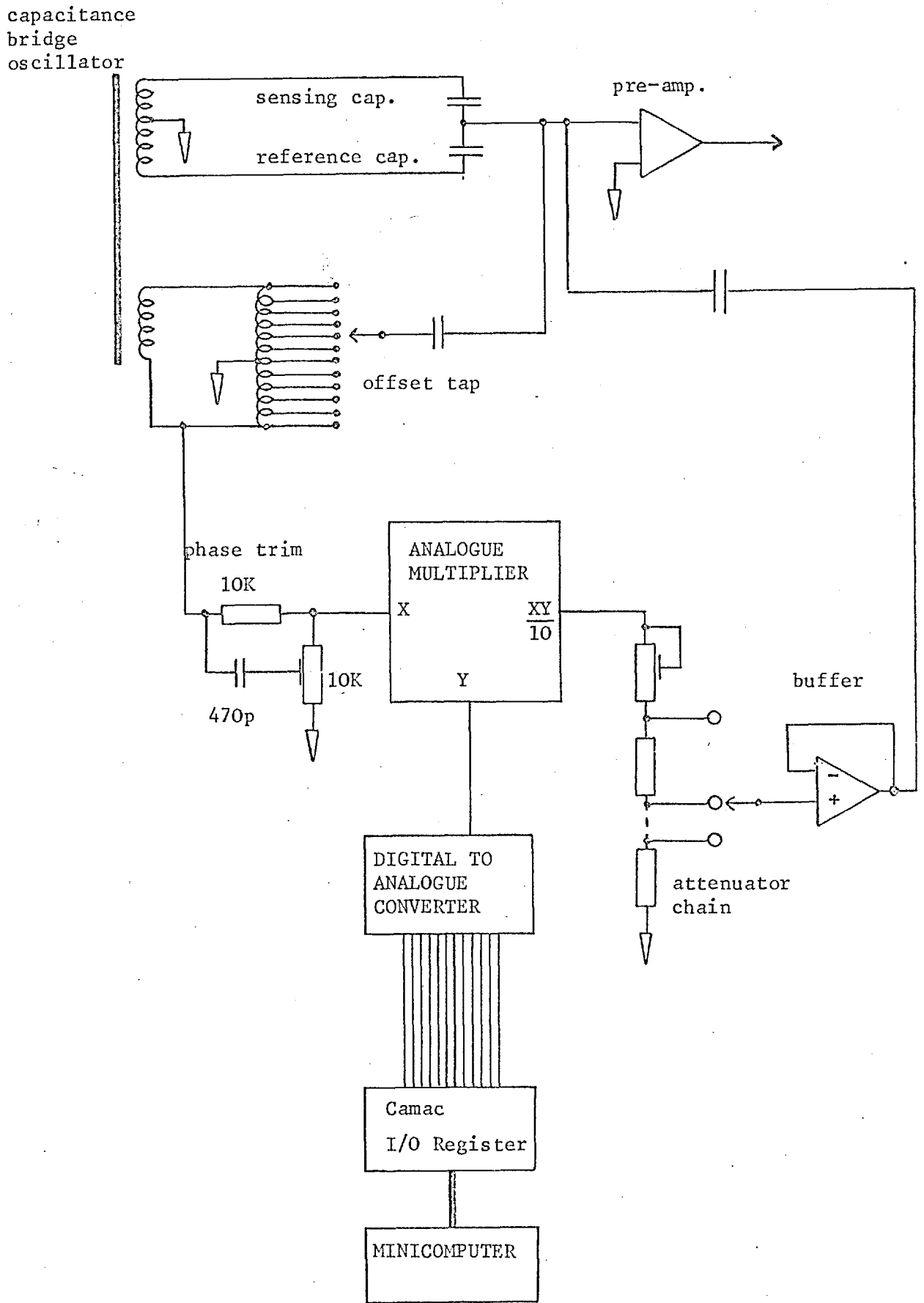
Improved Scan Control Facility

Figure 7.10

serious at present, but future developments with a higher resolution spectrometer may require a change. The capacitance connecting wires inside the cryostat prove difficult to secure rigidly and the use of special miniature coaxial cable with a low heat conduction is being investigated.

CHAPTER 8

FP USAGE AND TEST RESULTS

8.1. Wavelength Scanning

For most applications a linear scan of plate separation is useful; this results in a peak transmission which varies linearly. Successive spectral scans can be recorded and added. If the detection system PSD has a time constant of 1 second, a scan rate of 1 μm/minute allows adequate sampling at an interval of 2 seconds (with a resolution of ∿ 0.5 μm).

Sky cancellation, using the usual chopping system, can be performed simultaneously; the spectral scan is performed in either beam. Alternate scans are best performed in opposite beams and then algebraically added.

The FP can be used as a monochromator with ($\Delta\lambda$ ∿ 0.5 μm) whose transmission wavelength varies from 8-13 μm. Good wavelength stability is possible with the servo control and integration on a source at one wavelength could be performed. However, the advantages of the instrument really lie in its ability to scan or operate at different resolutions in a flexible way.

"Spectral Chopping"

For measuring the strengh of a particular spectral feature the rapid mechanical response of the etalon allows "spectral-chopping" to be performed. This consists of supplying a drive signal (at 5-100 Hz) so as to cause the plate separation to oscillate between two values. The drive is set so that transmission wavelength moves from the centre of the spectral line to a comparison point in or near the continuum.

The amplitude of the resulting change in signal should be a good measure of the line strength. If a PSD is used, with a reference from the λ-drive oscillator, then the output gives a very sensitive means of determining the strength of a feature. In particular, if the field of view of the instrument were changed (by rastering the telescope), then the strength of a "silicate" feature would be mapped across a region of sky (see Section 5.2.2.).

It is possible to perform sky cancellation, by chopping, at the same time as wavelength oscillation, provided different frequencies are used. For example, sky chopping could be performed at 300 Hz and the signal passes into a first PSD (with a corresponding 300 Hz reference). This PSD output, with a time constant of 0.1 second, then goes into a second PSD (which has a reference from the λ-oscillation at 5 Hz). The output of this PSD, with a time constant of 1-3 seconds, would then be a direct measure of the spectral line strength.

This technique is indicated in Figure 8.1. It is possible to beam-switch on the sky, although this is not essential because the second PSD ignores any slow DC level changes which may occur as a result of sky background fluctuations.

The wavelength oscillation can be performed from the central wavelength to either side; the final output could be taken as the difference of these two measurements (in Figure 8.1, line strength α (a-b) - (c-a)). In fact, this process can be done in one step by using a wavelength oscillation of twice the amplitude and a reference at a double frequency; the final PSD output then indicates the line strength above the mean continuum level.

The Spectral Chopping Technique

FP Drive
Signal
(PSD$_2$ ref.)

Sky-
Chopper
Drive
(PSD$_1$ ref.)

Spectral
Chopping

Spatial
Chopping

λ

c   a   b

sky
beam

source
beam

Sky-chop ref.

λ-chop ref.

Detector

PSD$_1$

PSD$_2$

OUTPUT

(a-b)

(c-a)
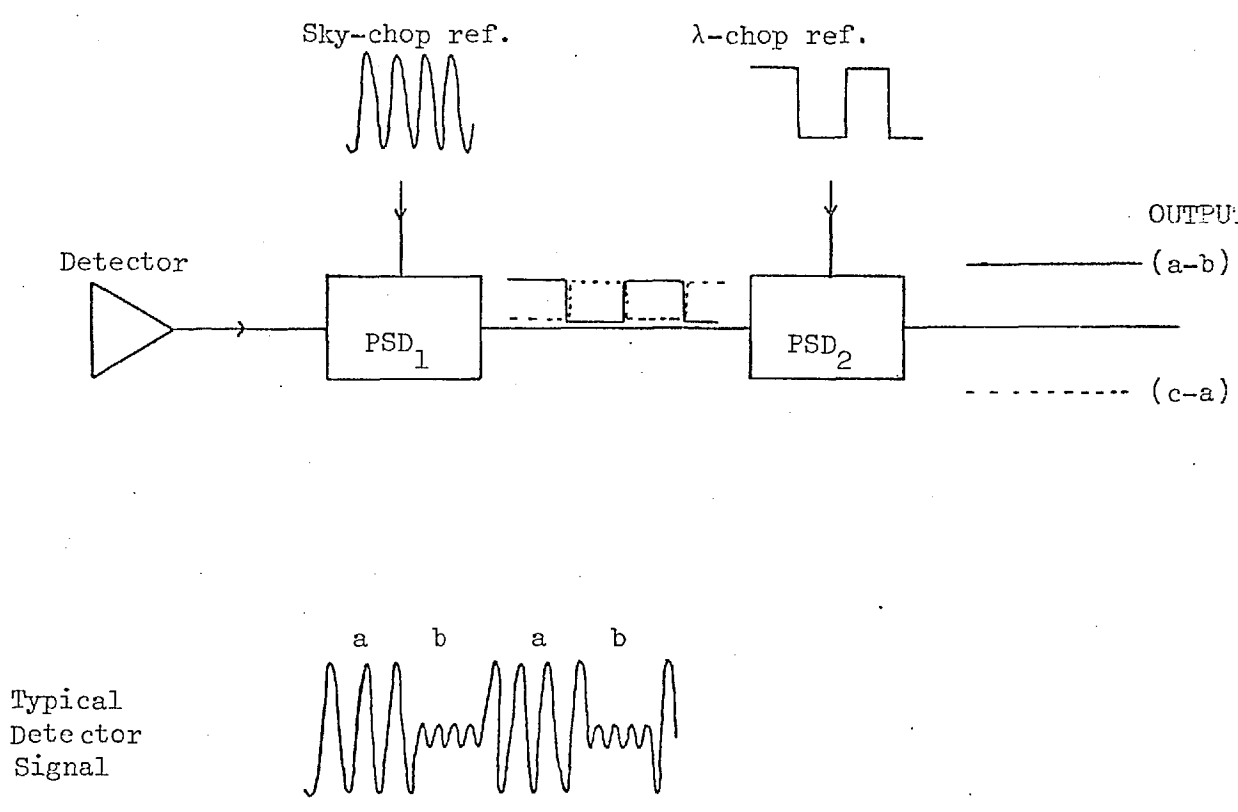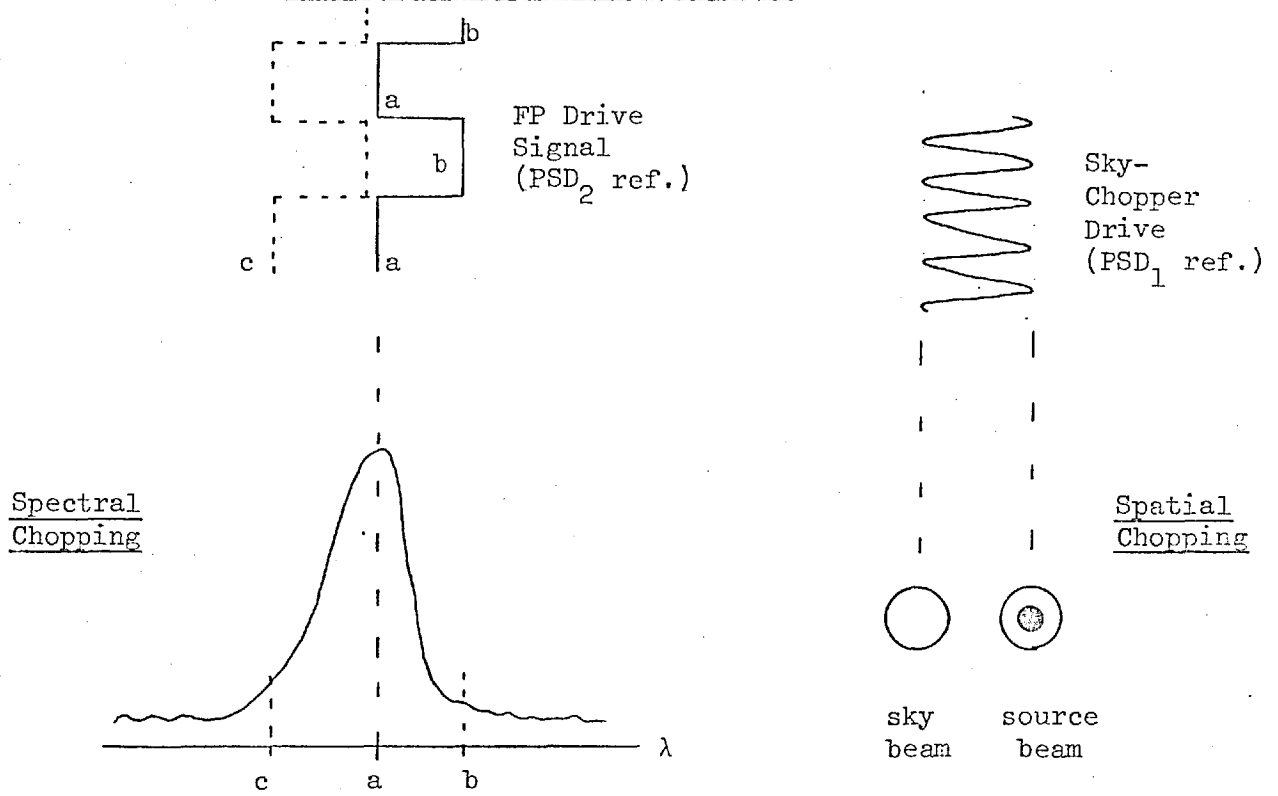
Typical
Detector
Signal

a   b   a   b

Figure 8.1

In principle it is possible to use the wavelength oscillation technique alone, without using a sky chopper. This only works well if the sky emission (or other dominant background) is fairly constant across the wavelength band. This is not the case and a large (and possibly variable) output offset makes sky cancellation necessary.

8.2. Laboratory Performance Tests

8.2.1. The test arrangement

The transmission properties of the FP have been measured on a test set-up similar to that shown in Figure 2.9. A hot source, consisting of a 1000 C black-body or a "Nernst" filament (temperature = 1500-2000K), has normally been used. For room temperature tests the FP is placed vertically or horizontally at the focal position of the test bench and a Golay cell is used as a detector. For cool tests the FP is fully assembled within a cryostat with a helium-cooled detector.

The black-body source was more convenient to use and had a well stabilised temperature, howeve, the Nernst filament was used for many of the tests because of its stronger intensity which gave a better signal/noise for the tests described here. A grating monochromator, with a bandwidth variable from $\sim$ 0.01 - 0.3 μm at 10 μm, was used extensively for tests - it had a wavelength resolution of $\sim$ 0.02 μm.

Prior to any measurements, the FP would be optically aligned (at room temperature) by observing fringes with the aid of a mercury lamp. The 1 mm "focal plane" aperture would then be inserted at the outer surface of the first plate. The plate gap is varied by controlling the current to the drive coil and the position of the carriage is determined by means of the capacitance sensor output.

The displacement drive is best calibrated in practice by determining the current required to scan the etalon through 1 or more orders. The monochromator is set to pass only a narrow line at say 10.0 µm and the difference in current between two transmission peaks would correspond to one order (or a total displacement of 5 µm). The displacement produced by a given current is found to be linear over a wide range. The capacitance sensor can be calibrated similarly, but as described earlier, it is only approximately linear over a limited range.

8.2.2. "Optical" tests

Figure 8.2 shows the result of applying a scanning current to the FP coil. The monochromator was set to transmit at 10.0 µm with a bandwidth of 0.1 µm. Various transmission peaks were obtained at each order as the plates were moved from "contact" to the end of the drive range. The finesse could be measured directly since it is defined as the ratio of the peak separation to the full half-width. A finesse of ~ 13 was measured in this example.

The fringe width can be broadened by the PSD time constant and chart recorder response if the scan is performed too fast. The mono-chromator bandwidth should also be sufficiently low so as not to contribute to the final peak widths. (The effect can be crudely calculated, assuming a Gaussian-like shape : $d\lambda^2_{Total} = d\lambda^2_{mono} + d\lambda^2_{FP}$).

The transmission profile of the FP at a fixed plate separation is shown in Figure 8.3. The plates were set to transmit at 10.0 µm (with a gap ~ 5 µm from the "contact" position). The monochromator was scanned from 8-12 µm and the resulting signal was recorded on the chart.

Fabry-Perot Transmission versus Plate Separation $\lambda = 10.0\mu m$
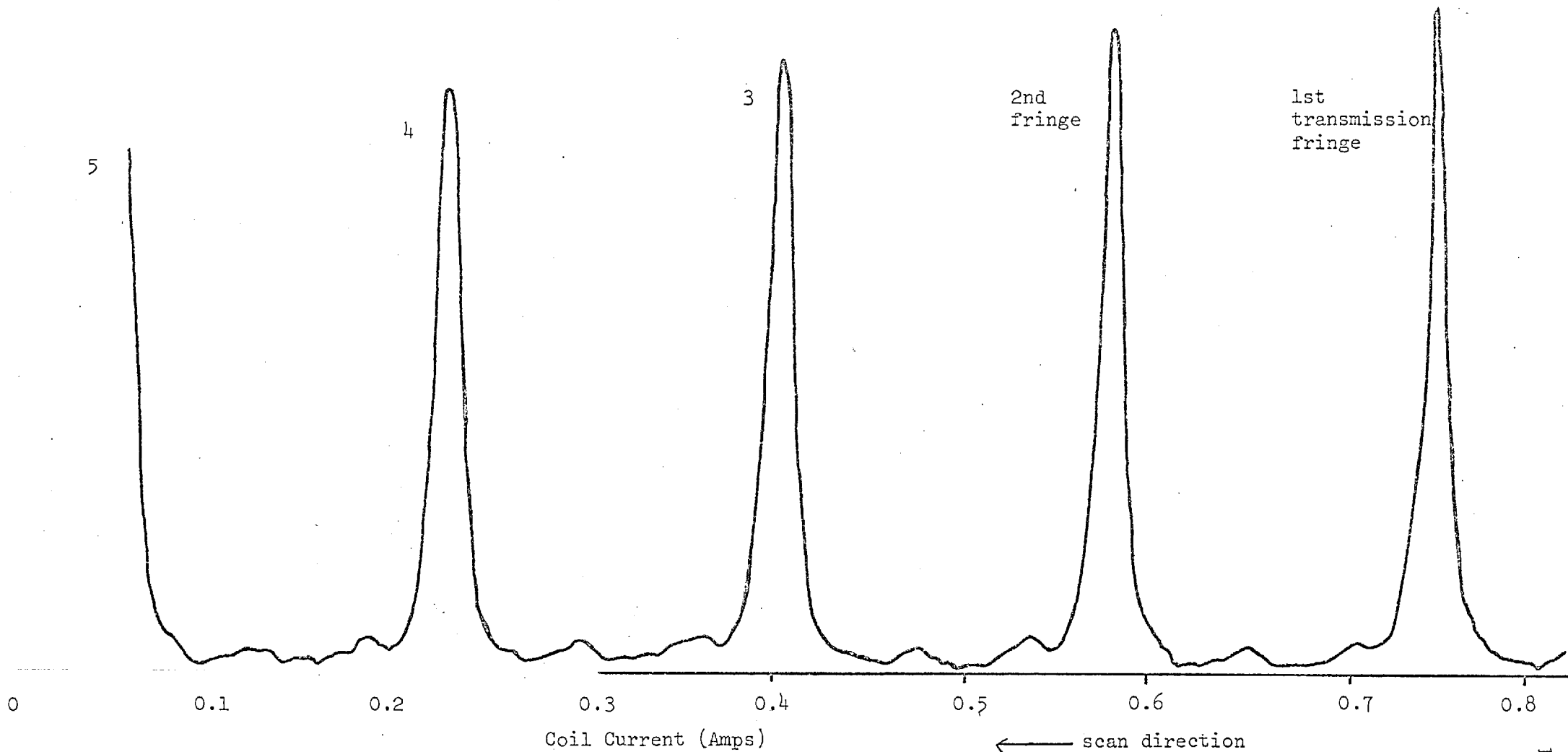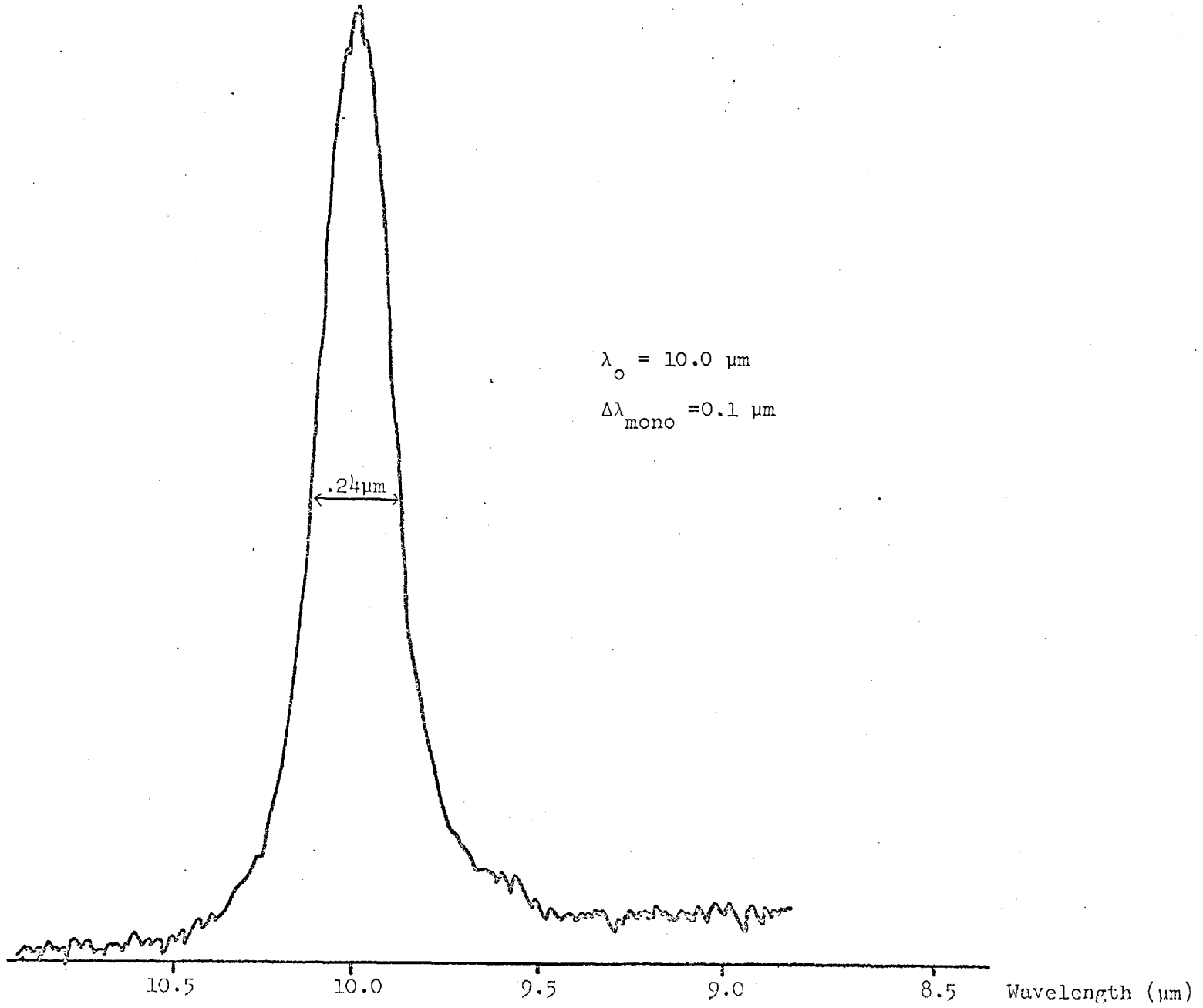
Coil Current (Amps)   ⟵ scan direction

187

Figure 8.2

Transmission Profile of FP

λ_o = 10.0 μm

$\Delta\lambda_{mono}$ =0.1 μm

.24μm

10.5 10.0 9.5 9.0 8.5 Wavelength (μm)

In this case the half-width of the transmission peak represents the wavelength resolution, which depends on the finesse and the order. The strong transmission peak occurs at 10 μm but some leakage around 8.5 μm is seen - as a result of the high plate transmission for $\lambda < 9$ μm.

The effect of vibrations on the etalon stability are readily examined on the test bench. A magnetic coil on the cryostat stand can be driven to produce vibrations at frequencies from about 10-10 kHz. The reduction in transmitted intensity or changes in the fringe width due to various vibration amplitudes and frequencies can be observed although the exact effects of telescope motion cannot be predicted.

The position of the FP plates remains stable for long periods, the separation has been measured to be constant within 0.02 μm over an 8-hour period. The above test was made with the FP within the cryostat which ensures a stable environment; the un-servoed stability at room temperature in the laboratory is rather worse - although variations $\lesssim 0.1$ μm in 1 hour are typical.

8.3. Telescope and Laboratory Performance of FP

8.3.1. Vibration tests

The performance of the FP interferometer depends very much on the stability of the plate separation. Any vibration of the system can cause changes in the spacing which result in a broadening of the transmission profile; the finesse is effectively reduced by the changes in etalon spacing. The resonant characteristics of the FP carriage, as described in Section 6.2, make this problem worse.

Laboratory tests were performed in which the change in plate gap was measured as a function of vibration frequency. Strong vibrations

(when the cryostat base could be felt to move) caused a plate movement of ∿ 1 μm at 10 Hz – without the servo control. With the servo on, the motions were kept < 0.1 μm for all vibration levels that were likely to be found in practice. With a bandwidth ∿ 0.5-1 μm no serious degradation of the instrument's transmission profile is obtained.

Another, more serious, effect is the change in transmission wavelength due to vibration. Because the background is the dominant radiation at 10 μm, any changes in transmission cause a lot of "noise" at the detector. This problem was not fully recognised in laboratory tests because the signal levels were high and low background noise measurements were less readily made in a laboratory environment.

8.3.2. Telescope measurements

The FP has been taken to Tenerife but no spectral scans have been possible yet. Early attempts were plagued by cryostat damage in transit and subsequent leaks (it appears tha only hand carriage, or extreme padding for air freight, prevent damage by rough handling). The most recent trip was unsuccessful due to very poor weather, although some test measurements are presented here.

The cryostat, containing the cooled FP and As Si detector, was mounted on the photometer (with the telescope pointing near the zenith). The sky condition at the time was cloudy (during the day). The vibrational motion of the etalon was measured under various conditions; the detector noise level was also estimated (directly on the oscilloscope, pk-pk Volts). See Table 8.1.

Table 8.1 :   Etalon Vibrational Motion

Conditions		Measured Motions	Detector Noise
a)	Chopper off, telescope drive off	.005 μm	5 mV
b)	Sidereal drive on	.01 μm	8 mV
c)	15 Hz sine wave chop on	.01 μm	8 mV
d)	Telescope slow δ guide on	.07 μm	50 mV
e)	15 Hz square wave chop	.2 μm	100 mV

NOTES: i) FP set at 10.0 μm ($\Delta\lambda \sim 0.5$ μm).

ii) The DC pre-amp offset at the time was 4V. Therefore maximum noise level was ~ 5 mV/4V $\sim 0.1\%$ of background level.

iii) The servo reduced b) and c) by 30%, but did not change d) or e) appreciably.

Vibrational motion can significantly increase the noise; sidereal telescope motion plus sinusoidal chopping approximately double the noise level. Guide motions of the telescope give serious noise levels which cannot be reduced by the servo (because of the broad spectrum of vibration input). Similarly, the use of a square wave chop excites vibration of the FP at various harmonic frequencies, these are not reduced much by the servo.

The use of a more rigid FP carriage assembly should alleviate these problems. Thicker springs in the parallel motion structure will reduce motion and the servo improves matters further. The very strong vibration generated by a low frequency (single mirror) square-wave chopper is not readily removed but good operation is possible with a sine wave chop. (The use of the new double-mirror chopper, of Section 1.5.3, may be possible in a square-wave mode).

Some very short measurements of a star, α Tau, were made under cloudy conditions (low altitude, blowing over the observatory). Observations at 10 μm in two beam positions are shown in Figure 8.4a, the chart record shows the signal and noise levels that were obtained. Figure 8.4b shows two spectral scans from 9-11 μm (at first order), these were performed in both beams. The two scans can be subtracted to obtain the net signal; however the sky noise was too large for any meaningful results. Further observations are planned as soon as possible.
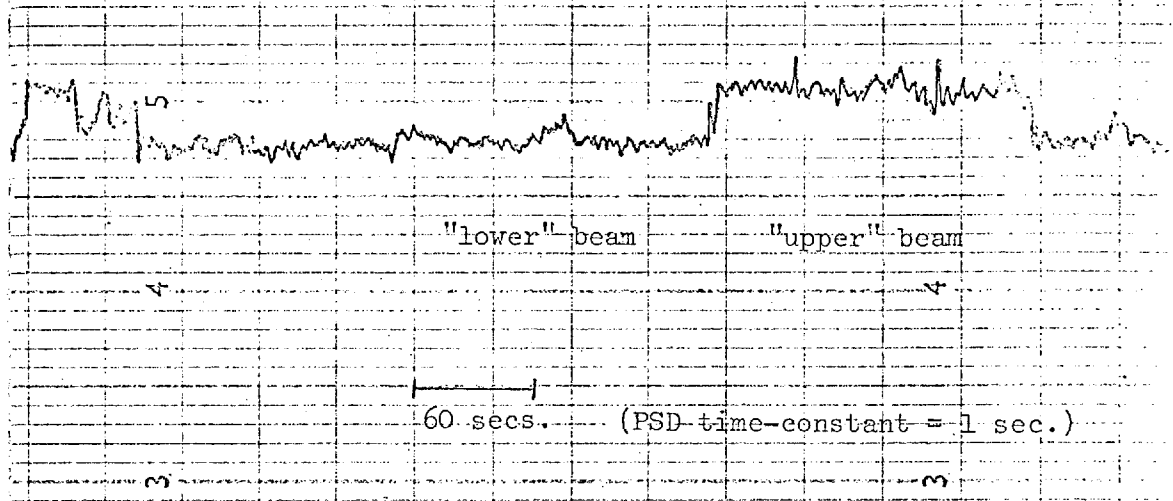
8.3.3. <u>Vibration damping techniques</u>

Various means of reducing the vibrational motion of the FP carriage, particularly the resonant motion, have been considered. No mechanical damping method seems applicable in the helium-cooled vacuum environment, especially since motions << 1 μm need to be absorbed. However, damping can be produced by electrical or magnetic means.

Damping by the use of a (superconducting) coil moving in a magnetic field has been considered, as shown in Figure 8.5. The coil (or probably a single loop) would be in series with a resistor and attached to the moving FP carriage. Any motion generates a current and a resistive force can be generated when the current is dissipated in the resistor. Rough calculations have shown that for any reasonably simple configuration (magnetic field strength < 1 W m^{-2}, coil size ~ 1 cm, etc) the force produced is likely to be 100X too small.

As discussed in Section 7.3, an electronic damping technique has been adopted. The capacitance sensor and servo system give differential feedback which effectively increases the resistive damping. That is, for a displacing force F_D (e.g. vibration input), an etalon displacement x is produced. With negligible intrinsic damping and no

(a) "Photometry" Measurements on α Tau , at 10μm (1st order)

"lower" beam   "upper" beam

60 secs.   (PSD time-constant = 1 sec.)

(N.B. Both measurements were made in very cloudy conditions)

(b) Spectral Scans of α Tau , from 9-11 μm , in 1st order

"lower" beam   "upper" beam

11μm   9μm

11μm   9μm

120 secs./scan   (PSD time-const. = 3s.)
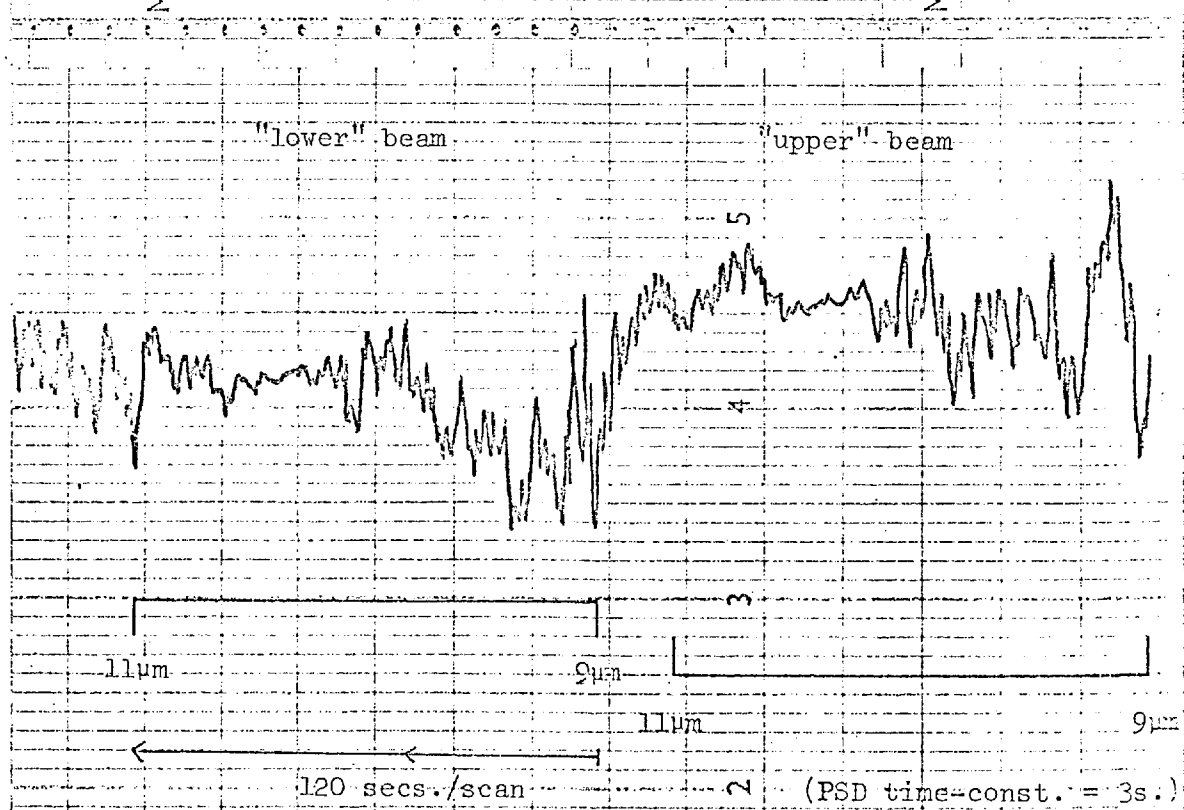
Figure 8.4

A Magnetic Damping Technique

$$B \qquad \frac{dB}{dx}$$

Figure 8.5
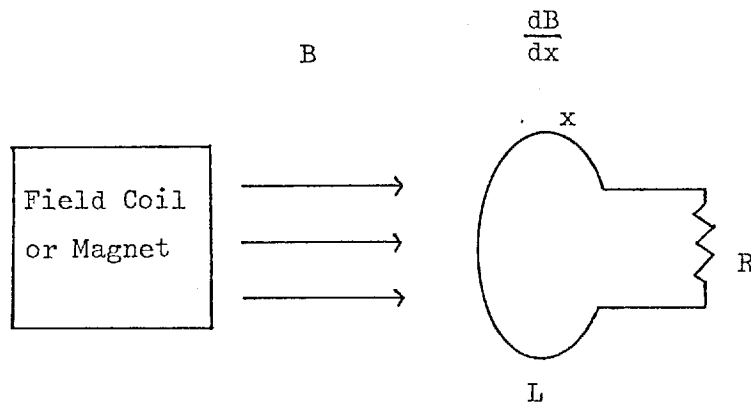
Induced Voltage(due to coil motion in a field gradient),

$$V \propto \frac{d\phi}{dt} \propto \frac{dB}{dx} \cdot \frac{dx}{dt}$$

hence, Induced Current $I = V/(R+j\omega L)$

Force generated, $F \propto I \cdot B \propto B \cdot \frac{dB}{dx} \cdot \frac{1}{(R+j\omega L)} \cdot \frac{dx}{dt}$

i.e. Resistive Force $F \propto \frac{dx}{dt}$, if $R \gg \omega L$

a force proportional to the velocity can be obtained under certain conditions , as shown above.

(typically for a 1cm. radius single loop $L \sim 10^{-6}$ H , this requires that $R \sim 10^{-2} \Omega$, for resistive damping up to frequencies 1000 Hz .)

Figure 8.5

servo control, the displacement $x = F_D/(m\omega^2 + s)$. (The terminology is the same as in Section 6.2; m = mass, s = stiffness, ω = frequency).

The servo generates a compensating force of the form,

$$F = -(Ax + R\dot{x}) = -Ax - R\omega x$$

where A = proportional gain , R = differential gain.

Thus the equation of motion of the etalon becomes,

$$m\omega^2 x + sx = F_D + F = F_D - Ax - R\dot{x}$$

or, $x = F_D/(m\omega^2 + R\omega + s + A)$

The effective stiffness constant is increased to $s' = s + A$, and a resistive term R has been introduced. The application of such feedback is limited by the phase changes that occur in practice. The servo electronics are designed so that when a phase change $\sim 180^\circ$ occurs the gain is very low and therefore very little positive feedback occurs.

8.4. Piezo-Electric Drive Systems

The use of a piezo-electric element to provide a drive for the etalon has been investigated. The advantages of a piezo-electric transducer (PZT) are high rigidity and adequate force, the disadvantages are that it has only a small movement and high voltages are required. The most convenient PZT element is a hollow cylinder, as shown in Figure 8.6a; a radial electric field (between inner and outer walls) produces an extension/Volt which is proportional to (L/t).

One possible PZT drive system is shown schematically in Figure 8.6b. Two PZT's are used so that the contraction, on cooling from 300-4.2K, is compensated and does not significantly displace the FP carriage. The polarity of the applied voltage on one tube is the opposite of the other and so one tube contracts whilst the other expands.

Piezoelectric Elements

(a) Expansion of a PZT Tube
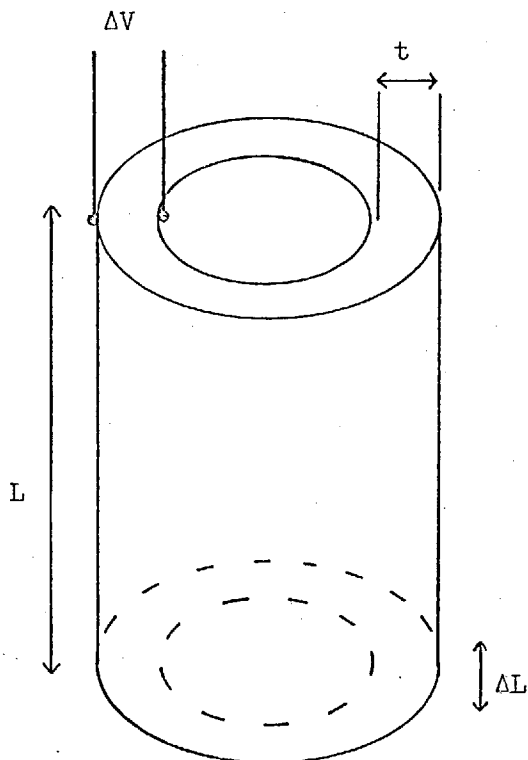
$$\Delta L = (L/t).d_{31}.\Delta V$$

where ΔL is the change in length produced by an applied voltage ΔV

L = cylinder length
t = wall thickness
d_{31} = PZT constant

(b) A Simple Drive System

one tube contracts & the other expands , the net motion is $2\Delta L$.

Figure 8.6

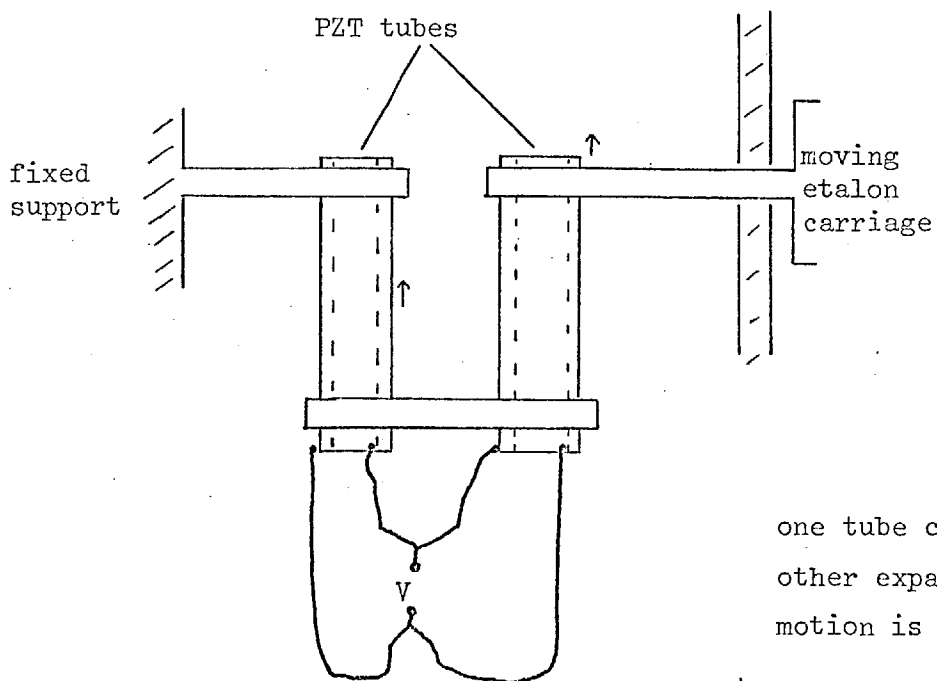Cylinders of length 2.5 cm, wall thickness 0.08 cm, and $d_{31} =$ 270 x 10^{-12} m V^{-1} were obtained from Vernitron Ltd. The expansion is given by,

$$\Delta L = (L/t)d_{31} \quad \Delta V \rightarrow 8 \ \mu m \ kV^{-1}. \quad (PZT - 5H \ material)$$

Tests were performed to determine the change in the parameter d_{31} as a result of cooling. The following results were obtained (relative to room temperature);

$$d_{31} = 1 : 0.56 : 0.32 , \quad T = 300 : 77 : 4.2K$$

The tests were, in fact, performed on a sample of another PZT material (G1500) from Gulton Industries Inc.

Subsequent data from Vernitron confirmed that a reduction in the coefficient d_{31}, by a factor of 3, is obtained on cooling from 300-4.2K. It appears that different grades of PZT reduce to the same value of d_{31} at 4.2K (i.e. $\sim$ 50 x 10^{-12} V m^{-2}). Thus, materials with high values of d_{31} at room temperature are not necessarily an advantage when cooled.

For two cylinders we therefore expect an expansion of $\sim$ 1.6 μm/100V at room temperature, and about 0.3 μm/100V at 4.2K; the former value has been obtained during tests. It was decided that an applied voltage that did not exceed $\pm$ 400V could be used within the cryostat with few problems.

For the PZT tubes (0.79 mm wall) the maximum recommended field is 0.6 kV mm $^{-1}$, and therefore 400V is almost the most that can be applied without risks of depoling the PZT. Higher voltages, up to at least 1 kV, have been used in a cooled cryostat (A. Betz, private communication 1977); this needs the use of thicker-walled PZT's which also have greater physical strength.

A high voltage power supply was constructed, as shown in Figure 8.7a. This provides a regulated +400V DC supply, at 20 mA if required. The PZT elements are driven from a programmable controller, as shown in Figure 8.7b. A differential voltage of ± 400V can be applied to PZT elements that are electrically isolated from earth. The PZT elements can therefore be controlled by a voltage which ranges from −400V to +400V; this output voltage is linearly proportional to the input, with a gain of 1000.

A lever system has been considered as a means of amplifying the PZT motion; however the compact and very rigid structure that is required is not easily achieved. A simple direct assembly (Fig. 8.6b) should give a range of motion of 2.5 μm, which covers half of the free-spectral range. This is useful at first order ($\Delta t = 4-6.5$ μm $\rightarrow \lambda = 8-13$ μm), but does not give any degree of flexibility or allow scanning of multiple orders.

A further possibility is the use of an external drive from a micrometer (or similar) device, this could be reduced by means of a lever. A better alternative would be a single differential screw at helium-temperature, with a PZT element in series to give fine control. This method is being investigated for future use.

(a) H.T. Supply

(transistors: BUY71)
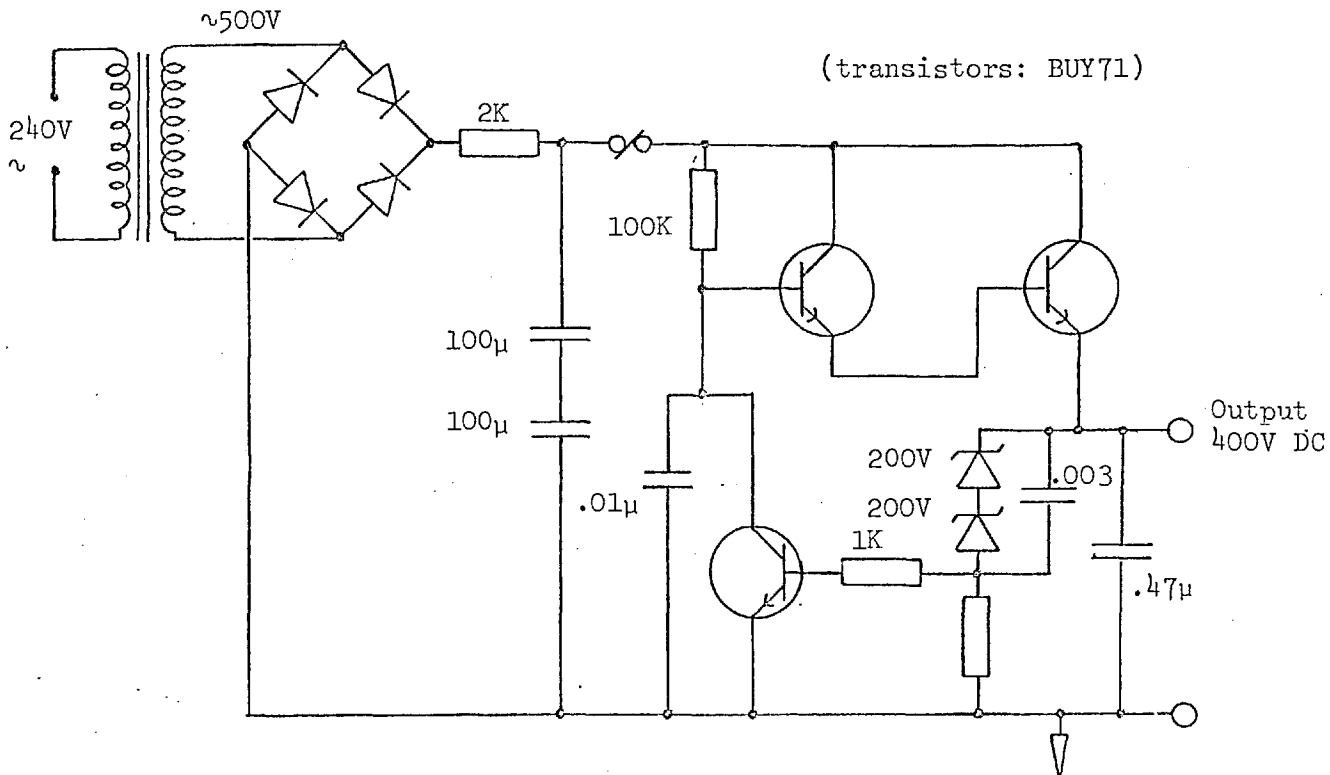
(b) Programmable Controller
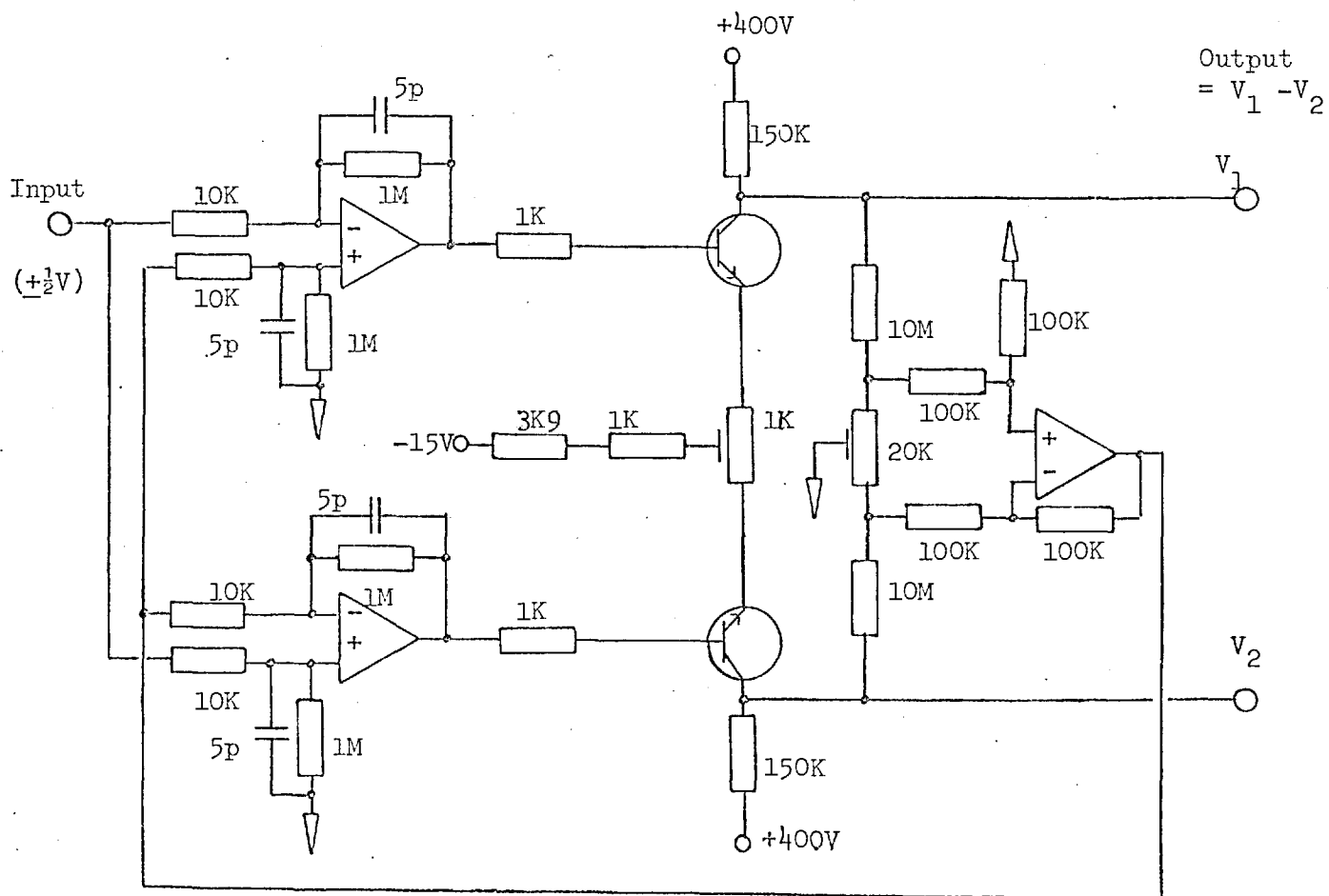
(when input= 0V. , $V_1 = V_2 = 200V$)

Figure 8.7

REFERENCES

Aitken, D.K. and Jones, B. 1973, Astrophys.J., 184, 127.

Aitken, D.K. and Jones, B. 1974, Mon.Not.R.astr.Soc., 167, 11P.

Allen, C.W. 1973, Astrophysical Quantities, 3rd Ed., Athlone Press,London.

Allen, D.A. 1973, Mon.Not.R.astr.Soc., 161, 145.

Becklin, E.E. and Neugebauer, G. 1974, H II Regions and the Galactic
    Centre, Proc. 8th ESLAB Symposium (ESRO SP-105), p.39.

Blair, D.P. and Sydenham, P.H. 1975, J.Phys.E., 8, 621.

Borgmann, J., Koorneef, J. and Slingerland, J. 1970, Astr.Astrophys.,4, 248.

Dickenson, D.F., Frogel, J.A. and Persson, S.E. 1974, Astrophys.J., 192, 347.

Downes, D. 1970, Astrophys.Lett., 5, 53.

Emerson, J.P., Jennings, R.E. and Moorwood, A.F.M. 1973, Astrophys.J.,
    184, 401.

Evans, N.J., Crutcher, R.M. and Wilson, W.J. 1976, Astrophys.J., 206, 440.

Fahrbach, U., Haussecker, K. and Lemke, D. 1974, Astr.Astrophys., 33, 265.

Felli, M. and Churchwell, E. 1972, Astr.Astrophys.Suppl., 5, 369.

Forrest, W.J., Gillett, F.C. and Stein, W.A. 1975, Astrophys.J., 195, 423.

Frogel, J.A. and Persson, S.E. 1972, Astrophys.J., 178, 667.

Gillett, F.C. and Forrest, W.J. 1973, Astrophys.J., 179, 483.

Gillett, F.C., Forrest, W.J. and Merrill, K.M. 1973, Astrophys.J., 183, 87.

Gillett, F.C., Forrest, W.J., Merrill, K.M., Capps, R.W. and Soifer, B.T.
    1975, Astrophys.J., 200, 609.

Goss, W.M. 1967, Astrophys.J.Suppl., 15, 131.

Goss, W.M. and Shaver, P.A. 1970, Austr.J.Phys.Astrophys.Suppl., 14, 1.

Goss, W.M., Lockhart, I.A., Formalont, E.B. and Hardebeck, E.G. 1973,
    Astrophys.J., 183, 843.

Hall, D.W.B., Aikens, R.S., Joyce, R. and McCurnin, T.W. 1975,
    Applied Optics, 14, 450.

Hardebeck, E.G. 1972, Astrophys.J., 172, 583.

Hardebeck, E.G. and Wilson, W.J. 1971, Astrophys.J.Lett., 169, L123.

Harvey, P.M., Beckis, K.P., Wilson, W.J. and Ball, J.A. 1974,
    Astrophys.J.Suppl., 248, 331.

Hicks, T.R.   1974, Thesis, University of London.

Hoffman, W.F., Frederick, C.L. and Emery, R.J.   1971, Astrophys.J.Lett.,
    170, L89.

Humphreys, R.M.   1974, Astrophys.J., 188, 75.

Johnson, H.L.   1966, A.Rev.Astr.Astrophys., 4, 193.

Johnson, H.L.   1968, Nebulae and Interstellar Matter, Ed. Middlehurst,
    B.M. and Aller, L.H., Univ. of Chicago Press,Chicago, p.167.

Jones, R.V.   1951, J.Sci.Instrum., 28, 38.

Jones, R.V. and Young, I.R.   1956, J.Sci.Instrum., 33, 11.

Jones, R.V. and Richards, J.C.S.   1973, J.Phys.E., 6, 589.

Larson, R.B.   1972, Mon.Not.R.astr.Soc., 157, 121.

Lo, K.Y., Burke, B.F. and Haschick, A.D. 1975, Astrophys.J., 202, 81.

Low, F.J. and Rieke, G.H.   1974, Methods of Experimental Physics, 12A,
    Academic Press, London, p.415.

Lynds, B.T.   1962, Astrophys.J.Suppl., 7, 1.

MacGregor, A.D.   1974, Thesis, University of London.

Merrill, K.M., Russell, R.W. and Soifer, B.T.   1976, Astrophys.J., 207, 763.

Neugebauer, G. and Leighton, R.B.   1969, Two Micron Sky Survey,
    NASA SP-3047, Washington, D.C.

Persson, S.E. and Frogel, J.A.   1974, Publ.astr.Soc.Pacific, 86, 985.

Persson, S.E. Frogel, J.A. and Aaronson, M.   1976, Astrophys.J., 208, 753.

Price, S.D. and Walker, R.G.   1976, The AFGL Four Colour Infra-Red Sky
    Survey, AFGL-TR-76-0208, Massachusetts.

Ridgway, S.T. and Capps, R.W.   1974, Rev.Sci.Instrum., 45, 676.

Rieke, G.H.   1974, Astrophys.J., 193, L81.

Rodgers, A.W., Campbell, C.T. and Whiteoak, J.B.   1960, Mon.Not.R.astr.Soc.,
    121, 103.

Schultz, G.V., Kreysa, E. and Sherwood, W.A.   1976, Astr.Astrophys., 50, 171.

Schraml, J. and Mezger, P.G.   1969, Astrophys.J., 156, 269.

Sharpless, S.   1959, Astrophys.J.Suppl., 4, 257.

Shaver, P.A. and Goss, W.M.   1970, Austr.J.Phys.Astrophys.Suppl., 14, 77.

Walker, R.G. and Price, S.D.   1975, AFCRL Infra-Red Sky Survey, 1, AFCRL-TR-75-0373, Massachusetts.

Wallerstein, G.   1973, Astrophys.Lett., 15, 83.

Westerhout, G.   1958, Bull.Astr.Inst.Neth., 14, 215.

Whitelock, P.A.   1976, Thesis, University of London.

Wilson, T.L.   1970, Astrophys.Lett., 7, 95.

Wilson, W.J., Schwartz, P.R., Epstein, E.E., Johnson, W.A., Etcheverry, R.D., Mori, T.T., Berry, G.G. and Dyson, H.B.   1974, Astrophys.J., 191, 357.

Winnberg, A., Goss, W.M., Höglund, B. and Johansson, L.E.B. 1973, Astrophys.Lett., 13, 125.

Winnberg, A., Nguyen-Q-Rieu,Johansson,L.E.B. and Goss, W.M.   1975, Astr.Astrophys., 38, 145.

Wolfe, W.L.   1965, Handbook of Military Infra-Red Technology, U.S. Office of Naval Research.

Woolf, N.J. and Ney, E.P.   1969, Astrophys.J., 155, L181.

Wyatt, C.L., Baker, D.J. and Frodsham, D.G.   1974, Infra-Red Phys., 14, 165.

Wynn-Williams, C.G. and Becklin, E.E.   1974, Publ.Astr.Soc.Pacific, 86, 5.

Wynn-Williams, C.G., Becklin, E.E. and Neugebauer, G.   1972, Mon.Not.R. astr.Soc., 160, 1.

Wynn-Williams, C.G., Downes, D. and Wilson, T.L.   1971, Astrophys.Lett., 9, 113.

Zeilik II, M., Kleinmann, D.E. and Wright, E.L.   1975, Astrophys.J., 199, 401.

Zeilik II, M.   1977, Astrophys.J., 213, 58.

A New Two-mirror Focal Plane Chopper for Infrared Astronomy

P. R. Jorden, J. F. Long, A. D. MacGregor and M. J. Selby

Astronomy Group, The Blackett Laboratory, Imperial College

Summary. A new focal plane chopper is described which uses two mirrors oscillating in phase to give an action equivalent to a single mirror chopper undergoing parallel motion. A sinusoidal image displacement is achieved which can be maintained at high frequencies using small power dissipation; the resultant detector microphonics are many times lower than those of a conventional chopper for the same image displacement.

Key words: infrared photometry — modulation techniques

1. Introduction

In the infrared, typical sky and telescope background radiations, through broadband filters centred on the atmospheric windows, can be many orders of magnitude more intense than the majority of astronomical sources. Sky cancellation is normally achieved by either wobbling the secondary mirror of a Cassegrain telescope (Low and Rieke, 1974), or by the use of a focal plane chopper. To avoid unwanted chopped radiation signals from the telescope and surrounds, the chopper should allow the detector to receive radiation alternately from adjacent areas of sky whilst viewing nearly constant telescope geometry. Of the focal plane choppers, either the rotating segment type (Becklin and Neugebauer, 1968), or the vibrating single mirror type (Glass, 1972; Fahrbach et al., 1974), are commonly used; in these it is very important to maintain a parallel mirror motion in order to avoid excessive movement of the beams across the telescope mirrors. In cases where the chopping frequency is required to be in excess of 150 Hz or with large throws of over 1 mm, the excessive mechanical powers may be required even for sinusoidal motions; this can lead to microphonic problems at the detector.

The two-mirror type described here is a new approach to focal plane chopping which overcomes these problems being capable of operating to frequencies above 1 kHz, with large throws, using low mechanical power. It has the further advantage that the optical path length of the beams remain virtually constant during the chopping so that large throws can be used without focussing errors. It may possibly have other applications apart from infrared astronomy.

2. Principle

Figure 1 illustrates the principle used by the two-mirror system; the two mirrors are vibrated in phase with the same angular amplitude. It is easily seen that the combined motion produces a "throw" of distance d ($=4.\delta\theta.D$. See Fig. 1) which is equivalent to that produced by the parallel movement of a single mirror over the same distance. The angle between the mirrors, shown as 90° in Fig. 1, remains constant during the motion and so the system may be considered as a two-mirror retro-reflector. The chopper would also give the same parallel displacement of the chopped beam for any other set angle between the two mirrors; twice this set angle determines the total angular deviation of the beam.

The motions of the two-mirror type may be compared with the single mirror type for the same frequency and chop amplitude; the ratio of their average kinetic energies is given by $E(\text{two-mirror})/E(\text{single-mirror}) \simeq \frac{1}{12}(S/D)^2$, where D is the mirror separation and S is the mirror length (see Fig. 1). Assuming the power required to overcome air damping is proportional to the air displacement volume squared (this is a lower limit), the ratio $P(\text{two-mirror})/P(\text{single mirror}) \simeq \frac{1}{8}(S/D)^2$; it is easily possible to achieve a ratio of 1:100.

The optical path change of the two-mirror chopper, with a throw d, is of order $\delta\theta.d$ which is negligibly small; whereas the optical path change for the single mirror or segment type giving the same throw would be equal to d.

3. Mechanical and Electrical Design

Figure 2 shows a photograph of the complete assembly, in which each mirror is vibrated sinusoidally on rotation axes defined by torsion bars. Figure 3 gives more details of the assembly in which four light aluminium tubes with associated springs, forming a parallel strip spring
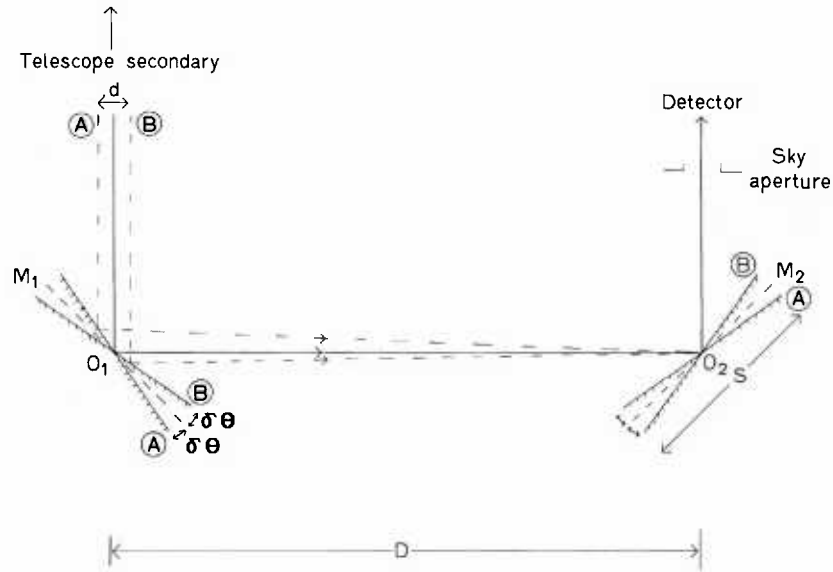
P. R. Jorden *et al.*

Fig. 1. Diagram to illustrate the principle used by the two mirror chopper. The mirrors M_1 and M_2, at separation D, are oscillated $\pm\delta\theta$ on rotation axes O_1 and O_2. This gives a parallel beam displacement, or throw, $d = 4.\delta\theta.D$

module, are used to couple the two mirrors so that they are accurately constrained to vibrate in phase at the same amplitude. The stiffness constants of the torsion bars and the parallel strip springs combine to determine the resonant frequency of the harmonic oscillator; a quality factor of $Q \simeq 40$ was measured. The system is driven at resonance by eight small loudspeaker drives;

both coil and magnet are allowed to move so that torques and momentum are balanced about the four supports, and hence vibrations transmitted to the main photometer box are small. Positive feedback is used to drive the chopper as an electromechanical oscillator constrained to stay on the peak of the mechanical resonance.
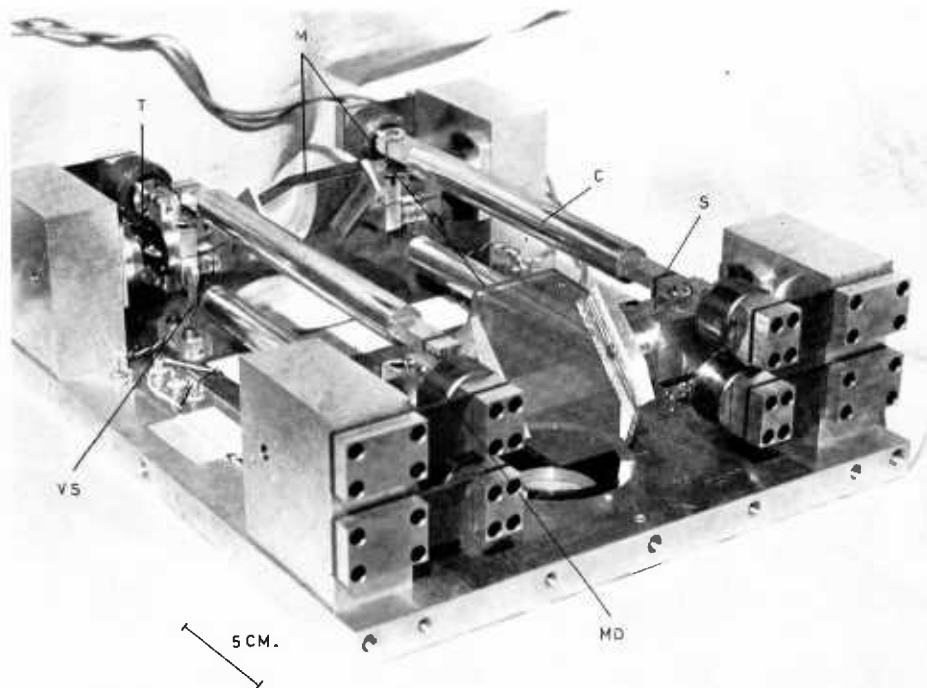

Fig. 2. The two mirror focal plane chopper. Vibration sensor VS, Torsion bar T, Connecting aluminium tube C, Spring strip S, Magnetic coil drive MD, Mirrors (beam splitters) M. The Mirror separation is 15 cm, the mirror length is 6 cm
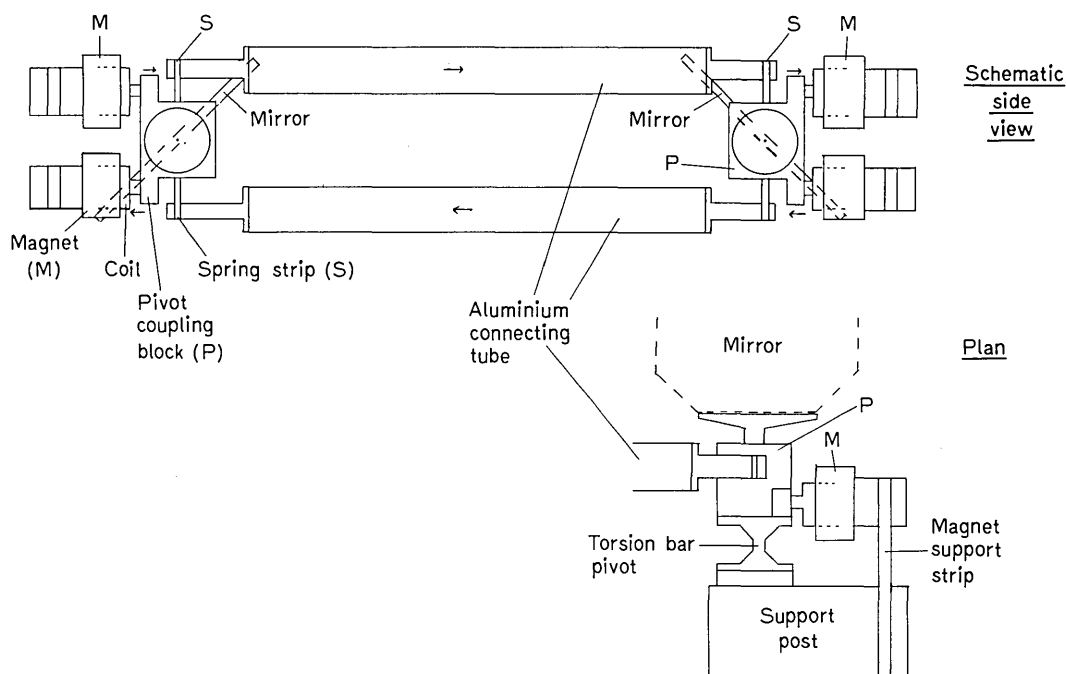
Fig. 3. Schematic side view and partial plan view of chopper assembly. In the side view the support posts are not shown for clarity, similarly many details of clamp screws etc. are omitted. The arrow indicate directions of movements during one phase of its motion. The chopper, as shown in Figs. 2 and 3, is inverted when used on the photometer
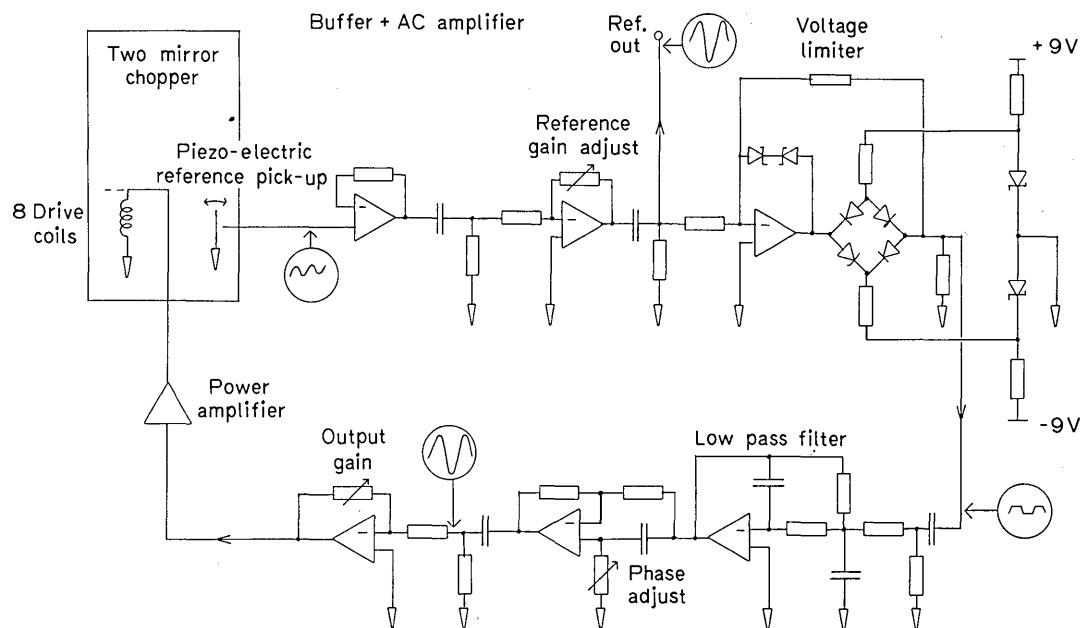
Fig. 4. Electronic control loop of the electromechanical oscillator. The phase is adjusted to maximise the oscillation amplitude; the output gain is adjusted to set the chop amplitude. The reference gain may be adjusted without changing the chop amplitude

The control system is shown in Fig. 4. A piezoelectric strip[1]) is used as a displacement sensor and the phase of the signal in the feedback loop is adjusted to give a maximum chop amplitude. Possible variations in the gain of the sensor, which would alter the chop amplitude, are removed by the use of a voltage limiter.

The gain of the output amplifier is used to alter the chop amplitude; the quality of the stages following the voltage limiter determines the amplitude stability. If the frequency of the drive were allowed to drift off the resonance in a high Q system such as this, then large phase and amplitude changes would occur; the feedback prevents such drifts by locking on the peak of the mechanical resonance.

---

[1]) Bimorph Element, Vernitron Ltd., Southampton.

4. Chopper Performance

The two-mirror chopper has been used successfully during the past two years on a photometer attached to the 1.5 m Flux Collector on Tenerife, Canary Islands, for work in the N(10 μm) and Q(20 μm) bands. A Cu:Ge 4.2 K photoconductive detector was used with wide band filters, and tests showed optimum performance at chopping frequencies around 400 Hz. Using the same set of springs and torsion rods we were able to set the chopper resonance between 500 and 100 Hz by clamping suitable weights onto the aluminium connecting tubes.

Both mirrors were coated with thin gold films to act as dichroic mirrors, and both of the transmitted beams in the visible were used to provide images. The coatings were produced to give a 50% transmission at 0.5 μm and were measured at 10 μm to have a reflectivity which was 98% of a thick gold coating. Careful cleaning of the substrate and a very thin underlayer of evaporated chromium resulted in good hard gold coatings which later could be cleaned with alcohol. The unchopped image was used for guiding, and the chopped image was conveniently used to visually monitor the chop amplitude.

The errors in the mirror motions were assessed with a laser on the telescope and were found to give a beam deviation of less than 10^{-4} radians for a 1 mm chop amplitude, corresponding to an extra displacement of less than 0.5 mm at the telescope secondary mirror. Laboratory tests indicated similar small deviations for throws up to 10 mm. We found it possible to achieve a chop amplitude of at least 10 mm in the focal plane at 400 Hz; we felt that any increase in this value might result in failure of the torsion bars. We now believe that replacement by cross-spring hinges[2] would safely allow bigger chops if desired. We found that less than 0.1 Watt of electrical power was required to achieve a chop amplitude of 1 mm at 400 Hz, and that the chop amplitude and position were stable to better than 2% for all

[2] Bendix Flexural Pivots, from Field. Tech. Ltd., Heathrow Airport, London.

orientations of the telescope; a servoed position control was considered unnecessary since the beam displacement was insensitive to orientation.

Compared with the single mirror chopper, the beam in the two-mirror type moves across one of the mirrors during the chopping, which is a minor disadvantage (see Fig. 1); however the mirrors are small and can be kept clean more easily than the telescope mirrors, which are more likely to produce radiation signals. When we compared the performance of our two-mirror chopper with our previous single mirror type, the radiation signals, from the telescope and the chopper, were similar for both choppers, and less than the r.m.s. detector noise; however, the microphonically induced signals were dramatically reduced, being undetectable with the two-mirror chopper. Where desired, it would be possible to use this type of chopper at much higher frequency and/or larger throws than we used, simply by changing the factor D/S (see Sec. 3).

References

Becklin, E. E., Neugebauer, G. 1968, *Astrophys. J.* **151**, 145
Fahrbach, M., Haussecker, K., Lemke, D. 1974, *Astron. & Astrophys.* **33**, 265
Glass, I. S. 1972, *Observatory* **92**, 140
Low, F. J., Rieke, G. 1974, The instrumentation and techniques of Infrared Photometry in Methods of Experimental Physics, Vol. 12, Pt. A, Ed. N. Carleton, Academic Press, New York and London

P. R. Jorden
J. F. Long
A. D. MacGregor
M. J. Selby
Astronomy Group,
Physics Dept.,
The Blackett Laboratory,
Imperial College,
Prince Consort Road,
London SW 7 2 BZ, England

Note Added in Proof

In principle, it is possible to ensure that the beam from the detector always "sees" the same part of the primary mirror. This can be done by changing the mirror assembly slightly so that one mirror has a different amplitude to the other. The small angular change produced can exactly compensate for the parallel displacement d on the primary. This technique is also considered in a recent paper describing another chopper: J. Koornneef, J. van Overbeeke 1976, *Astron. & Astrophys.* **48**, 33.

INFRARED PHOTOMETRY OF A HEAVILY REDDENED ASSOCIATION IN W35

P. R. Jorden, A. D. MacGregor, M. J. Selby and Patricia A. Whitelock

Astronomy Group, Physics Department, Imperial College, London SW7

SUMMARY

Seven new 2-μm point-like sources associated with the W35 H II region have been discovered and are interpreted as an association of late-type giants and supergiants seen through about 10 mag of optical extinction. Their positions and H, K and L magnitudes are reported here.

1. INTRODUCTION

W35 is a large complex H II region with a kinematic distance of $3 \cdot 2 \pm 0 \cdot 9$ kpc determined by Reifenstein *et al.* (1970). The area has been mapped at 1400 MHz by Felli & Churchwell (1972) and by Tovmassian & Nersessian (1973). The radio continuum peaks about 5′ south of a dense knot of optical nebulosity which is to the north of the main region of observable Hα emission (Sharpless 54). Radio observations of hydrogen line emission by Tovmassian & Nersessian (1973) suggest that there are two nebulae present; one, with weaker emission associated with the early-type cluster NGC 6604, the other, which is stronger, associated with the continuum emission to the north. It was around this northern area that the infrared sources were found. OH absorption associated with the same region has been reported by Goss (1967) but Wilson (1972) failed to detect formaldehyde.

Far-infrared measurements of W35 have been reported by Olthof (1974). This emission is possibly associated with cool dust around the infrared sources; however, no positions are given for the far-infrared source, so the connection is only speculative.

2. OBSERVATIONS

The observations were obtained over a period of four nights (1975 June 4/5–7/8) on the 60-in. flux-collector in Tenerife. H (1·65 μm), K (2·2 μm) and L (3·5 μm) observations were made using a PbS detector cooled to 77 K and N (10 μm) observations using a Cu:Ge photoconductor cooled to 4 K. A 10″ sky beam and a 12″ chop amplitude were used throughout.

A total area of 7′ × 7′ centred on the knot of optical nebulosity was searched, using the K filter, by scanning in declination at a rate of 4″ per second and making 5″ steps, in right ascension, between scans. The detection limit at this scan rate was nearly +8^m for visual inspection of the chart record. Following the detection of a source, photometry was performed using H, K and L filters.

The observations at N were made after the discovery of sources 2, 3 and 4 only. Sources 2 and 4 were not detected to a limit of 0^m·8. The observations of

source 3 consisted of declination scans through the object at a rate of $1''\cdot5$ per second. These were subsequently added together, a magnitude derived, and comparisons made with scans of a point source calibration star. This determined the size of the object at 10 μm to be less than $4''$.

The magnitudes of the sources are given in columns 4, 5 and 6 of Table I. The large errors are due to calibration uncertainties, and the lack of precision in centring the sources on the detector.

The positions of the infrared sources were determined relative to nearby stars and are given in the second and third columns of Table I. They are accurate to about $\pm 10''$. Source No. 7 has been identified with a very red star which appears

TABLE I

Infrared photometry and positions of sources discovered in this survey. The photometry for sources 3 and 7 is accurate to $\pm 0^{m}\cdot 1$. For the fainter sources, H magnitudes are accurate to $0^{m}\cdot 5$, K and L magnitudes to $\pm 0^{m}\cdot 3$. Estimates of the visual extinction A_V and absolute magnitude M_V are given for the two strongest sources

Source No.	α(1950) h m s	δ(1950) $\circ$ $'$ $''$	H (1·65 μm)	K (2·2 μm)	L (3·5 μm)	N (10 μm)	A_V	M_V
1	18 14 57	−11 40 04	7·3	7·0	6·8			
2	18 14 58	−11 43 34	8·2	6·5	6·0	>0·8		
3	18 15 06	−11 42 14	4·0	3·0	2·3	0·2	12	−7
4	18 15 16	−11 41 29	7·3	6·5	6·4	>0·8		
5	18 15 21	−11 44 31	6·2	5·9	5·7			
6	18 15 23	−11 44 18	7·7	7·0	6·9			
7	18 15 25	−11 46 29	4·5	3·9	3·3		7	−5

on both the red and blue plates of the Palomar Sky Survey. None of the other objects may be unambiguously identified with anything on the Palomar Sky Survey plates.

3. NATURE OF THE SOURCES

The infrared magnitudes provide insufficient information for the precise determination of luminosities and spectral types; however, if we assume the value determined by Reifenstein *et al.* (1970) to be a good estimate of the distance of the infrared objects (distance modulus $12^{m}\cdot 5$) then the absolute magnitudes of the sources may be calculated for various assumptions of luminosity type and spectral class. For the brightest source, No. 3, we find the luminosity to be unreasonably large, by comparison with the absolute magnitude values tabulated by Allen (1973), unless it is a supergiant of spectral type later than about K4. Alternatively if the distance were in error by at least an order of magnitude then the source might be explained as an early-type supergiant. It is, however, unlikely that the distance is in error by such a large quantity. For the other sources an early spectral type would not seem unreasonable as regards their absolute magnitudes, but the colour differences are comparable to or larger than those of source 3. It is therefore assumed that these are supergiants or, in the case of the lower luminosity objects, bright giants of late spectral type.

Using the above assumption and the colour differences tabulated by Lee (1970), the final column in Table I gives a very rough estimate of the absolute visual magnitudes (M_V) after correction for extinction.

4. INTERSTELLAR EXTINCTION

Using the assumption that the intrinsic H–K and K–L colour differences are those characteristic of Mo giants, the colour excesses are given by:

$$E_{HK} = (H\text{-}K) - 0\cdot17$$

$$E_{KL} = (K\text{-}L) - 0\cdot15.$$

We may deduce the visual extinction (A_v) in front of each of the objects by assuming the extinction obeys the standard reddening law described by van de Hulst (1949) (curve No. 15). From the reddening curve we have:

$$A_v = 14\cdot5\,E_{HK} = 23\cdot5\,E_{KL}.$$

The E_{KL} colour excesses can be substantially modified by any long-wave infrared excess caused by thermal dust emission. Thus the visual extinction A_v is calculated (for sources 3 and 7) from E_{HK}. For the five faintest sources the large magnitude errors preclude any reliable estimate of colour excesses or visual extinctions. These errors are not statistical but are due to a non-linear detector response which made it difficult to calibrate faint sources against the standard bright calibration sources. Unfortunately, this problem was noted too late to allow a precise correction curve to be evaluated.

Fig. 1 shows the spectra of the two brightest infrared sources after correction for extinction using the following relations:

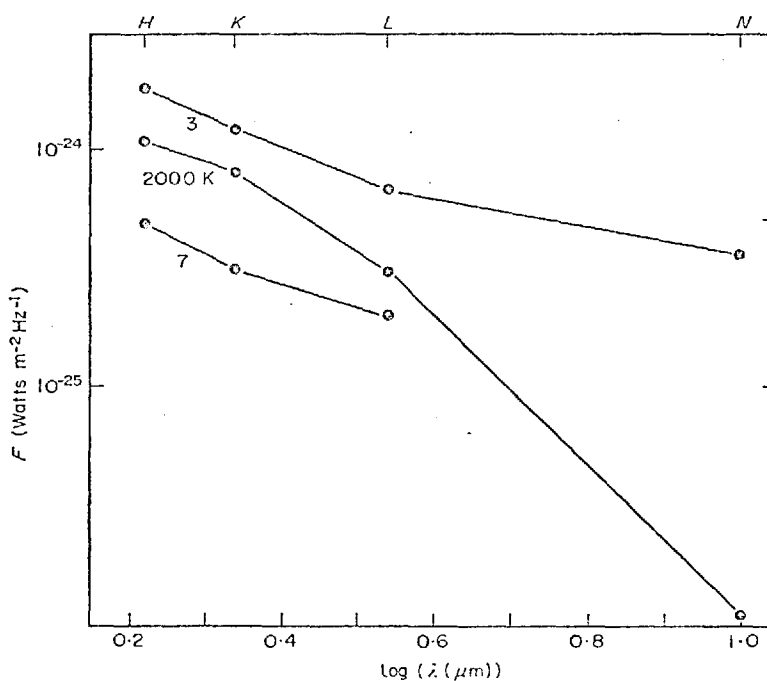$$A_L = 0\cdot06\,A_v, \quad A_K = 0\cdot1\,A_v, \quad A_H = 0\cdot17\,A_v.$$

Fig. 1. *Spectra of infrared sources (3 and 7) after correction for extinction. A 2000 K blackbody spectrum is included for comparison.*

5. CONCLUSIONS

We conclude that the most likely explanation for these new infrared sources is that they are very young giants and supergiants with late-type spectra showing a considerable amount of visual extinction. A similar cluster in Ara has been discussed by Borgman, Koornneef & Slingerland (1970) who find both early- and late-type supergiants behind about 12^m of visual extinction. We note that if there are early-type giants present in the W35 association, of a luminosity comparable to that of the late-type objects, we would expect them to be 4–5 mag fainter at K than the late-type objects and hence they would not be detected by our fast scanning search method. We are currently pursuing a more detailed survey of the area to better magnitude limits.

ACKNOWLEDGMENTS

REFERENCES

Allen, C. W., 1973. *Astrophysical quantities*, 3rd edition, Athlone Press, London, 200.
Borgman, J., Koornneef, J. & Slingerland, J., 1970. *Astr. Astrophys.*, **4**, 248.
Felli, M. & Churchwell, E., 1972. *Astr. Astrophys. Suppl.*, **5**, 369.
Goss, W. Miller, 1967. *Astrophys. J. Suppl.*, **15**, 131.
Hulst, H. C. van de, 1949. *Rech. Obs. Utrecht*, **11**, Part 1, 1.
Lee, Thomas A., 1970. *Astrophys. J.*, **162**, 217.
Olthof, H., 1974. *Astr. Astrophys.*, **33**, 471.
Reifenstein, E. C., Wilson, T. L., Burke, B. F., Mezger, P. G. & Altenhoff, W. J., 1970. *Astr. Astrophys.*, **4**, 357.
Tovmassian, V. & Nersessian, S. E., 1973. *Austr. J. Phys.*, **26**, 861.
Wilson, T. L., 1972. *Astr. Astrophys.*, **19**, 354.

INFRARED SOURCES IN THE COMPACT HII REGION G45.5+0.1

P R Jorden, A D MacGregor, M J Selby
Astronomy Group, Blackett Laboratory, Imperial College,
Prince Consort Road, London SW7 2BZ

Patricia A Whitelock
Dept of Physics and Astronomy, University College,
Gower Street, London WC1E 6BT

C Sánchez Magro
I A C, Universidad de La Laguna,
Tenerife, Canary Islands

Summary

Infrared photometric observations (1.25 - 10µm) of the compact HII region G45.5+0.1 are reported. Three new sources, which appear point-like in nature, are discussed; two of them are possibly identified with faint stars on the Palomar Sky Survey red plate. Evidence is given which indicates that they lie behind cool dust clouds with an extinction Av $\sim$ 13-30 magnitudes. These sources appear to be M stars, possibly associated with the HII region, and at least one of them is known to be a type II OH/IR source.

Introduction

G45.5+0.1 is a heavily obscured compact HII region situated in the Sagittarius arm of the Galaxy; Zeilik, Kleinmann and Wright (1975, hereafter referred to as ZKW) gave the distance as 9.7 ±1 kpc. In addition to the molecular emissions referenced by ZKW, CO emission has been measured by Wilson et al (1974) and an H_2O maser at 22 GHz has been detected near one radio component by Lo et al (1975).

An infrared source (IRS1, see figure 1) was discovered by ZKW near one of the OH sources (of Goss et al 1973). They deduced that the dust was well mixed with the gas and that the source was optically thin from 10 to 20µm. A second infrared source (IRS2) is associated with a type II OH/IR object (Schultz et al 1976).

Observations

The infrared observations reported here were made on the 1.5m telescope at Tenerife, Canary Islands. Photometric measurements were made between 1.25μm and 10μm with 77K InSb and 4.2K Cu:Ge detectors. A 10 arc second sky aperture and a focal plane chopper with a 15 arc second beam separation were used.

In August 1975 an attempt to detect infrared radiation at the OH maser positions of Goss et al (1973) was unsuccessful; a new source (IRS3) was subsequently discovered near G45.5+0.1 when some 2.2μm scans were scrutinized. During August 1976 a more extensive search was performed around two of the components of G45.5+0.1 as shown in Figure 1. Areas of approximately 3x4 arc minutes, centred on each component, were covered by declination scans at 3.5μm. Four infrared sources were measured, including the extended source IRS1 of ZKW and the OH/IR source, IRS2. We find 3.5μm to be the optimum search wavelength for such sources, when using an InSb detector.

Photometry was performed on these sources after positioning on the 3.5μm peak, and their absolute positions were found by reference to several faint field stars, see Table 1. No visual images were observed in the telescope at the infrared positions. Each infrared source was measured at least twice on different nights; α Lyr was used for calibration and extinction measurements, the absolute flux was taken from Johnson (1966) and we have adopted $1.18 \times 10^{-13} W \ cm^{-2} \mu m^{-1}$ for the $0^m.0$ flux at 1.65μm. Table 2 gives the measured magnitudes (after correction for atmospheric extinction).

Figure 2 shows the plotted spectra, and includes the ZKW measurements of IRS1. There is good agreement between the two measurements, including 10μm, when allowance is made for the different beam sizes and chop amplitudes. We scanned IRS2 and IRS3 several times in declination at 3.5 and 5.0μm and by comparing them to calibration stars we find them to be "point-like" within the limit of our spatial resolution. We noted two possible identifications on the PSS red plate (see Plate 1). A faint star of $m_R \sim 17$ lies within 5 arcseconds of IRS4; either of two faint stars of $m_R \gtrsim 18$ could be tentatively identified with IRS2 (within 5 arcseconds).

Discussion

The infrared luminosity of the extended source IRS1 was estimated by ZKW to be L_{IR} (2-21μm) $\sim 4.5 \times 10^4 L_\odot$ in a 12 arcsecond beam and using their size measurements gives a total luminosity of L_{IR} (2-21μm) $= 1.2 \times 10^5 L_\odot$. The Lα luminosity in the HII region was calculated as $1.4 \times 10^5 L_\odot$ from the radio flux. However, the infrared luminosity will increase by nearly a factor of two for an assumed extinction of $A_V \sim 30^m$ and by another 50% if the luminosity for $\lambda > 20$μm is included. It appears that the dust will absorb most of the Lα photons and possibly some of the ionising photons in addition.

Although the optical depth at 10μm within IRS1 is small, there is clearly a large extinction due to cooler dust in front of the source. ZKW found that the observed flux was less than the expected emission from the ionised gas for wavelengths $\lambda \lesssim 5$μm; this enables us to calculate the extinction as described by Wynn-Williams et al (1972). We derive values of $A_V \sim 26$, 31, 30 and 24^m for wavelengths 3.5, 2.2, 1.6 and 1.25μm

respectively; Van de Hulst's curve 15 (Johnson 1968) is the assumed

extinction law. Observations of interstellar reddening in the galactic

plane (Greenberg and Hong 1974, Allen 1973) give a visual absorption of

$\sim 2^m$ kpc^{-1}, which predicts $A_V \sim 20^m$ at the distance of G45.5+0.1; a

significant amount of the reddening caused by cooler dust is probably

local to IRS1. Following Soifer and Pipher (1975) we can deduce a lower

limit to the visual extinction of $A_V \sim 17^m$ from the lack of optical

nebulosity at the source position on the Palomar red plate.

The point-like sources IRS2, IRS3 and IRS4 clearly exhibit different

spectra (Figure 2) to that of IRS1, indicating that they are different

in nature. IRS2 is a type II OH maser source first reported by Winnberg

et al (1973) and with an accurate position subsequently determined by

Evans et al (1976). Schultz et al (1976) measured it at 3.8μm but did not

detect it at 11μm . Our measurements

show that the visual extinction must be limited to $A_V \leqslant 15^m$ if the

shortwave spectrum is to fit a Rayleigh-Jeans distribution; and in fact

an $A_V \sim 10^m$ is indicated if the source is an M-type star, in common with

other such type II OH/IR objects. The spectrum from 1.6 - 10μm shows the

presence of a dust cloud at a temperature of $\sim$ 650K. The apparent

luminosity of IRS2 is L(0.7 - 10μm) $\sim 3.10^4 L_\odot$, which increases to

$\sim 4.10^4 L_\odot$ after correcting for an $A_V = 10^m$, similar to the average value

of $10^4 L_\odot$ for such sources (Harvey et al 1974).

IRS3, which has a similar spectrum to IRS2, is located near the

northern condensation of this HII region. Depending on the adopted value

of A_V, it can be explained as either a hot or cool star, surrounded by

a hot dust cloud of colour temperature $T_c \sim$ 1000K. The shortwave spectrum

can only be fitted to that of a black-body if the visual extinction is

limited to $A_V \stackrel{<}{\sim} 25^m$. By a similar argument the visual extinction in front

of IRS4 is restricted to $A_V \lesssim 13^m$, the colour temperature T_c (5 - 3.5μm) ~ 3000K and this source appears to be a good candidate for a cool M star. The observed infrared luminosities for IRS3 and IRS4 are L(1.25 - 10μm) $\sim 1.3 \times 10^4 L_\odot$ and L(0.7 - 5μm) $\sim 5 \times 10^3 L_\odot$ respectively, assuming both objects are associated with G45.5+0.1 at a distance of $\sim$ 10 kpc.

Some evidence for an association of the sources can be obtained as follows. Following Becklin et al (1977) we have extrapolated the source counts from the 2μm survey (Neugebauer and Leighton 1969) in the direction of G45.5+0.1. Using a $^3/_2$ power law (which can only indicate an upper limit in the presence of a presumed $A_K \sim 1 - 2^m$ at 10 kpc) we would expect to detect $\lesssim 0.5$ sources with $m_K < 7$ in our search area. We in fact have at least 3 sources with $m_K \lesssim 7$. Our scan detection of four sources with $m_L < 7.5$ similarly leads us to expect ~ 0.1 sources with $m_L < 5$, whereas we find two such sources. The probability of two independent objects (with $m_L < 5$) would seem to be $(0.1)^2$ or 1%. It should be emphasized that the above calculations can only give an approximate, but nevertheless useful, estimate of the source counts in a given direction.

We consider that the above argument and the close physical proximity of the sources to G45.5+0.1 suggest a possible association. Near infrared spectra would help to clarify the nature of the sources, and measurements of any "silicate" absorption at 9.7μm would help to resolve the uncertainty in the extinction and confirm an association with IRS1. Molecular emissions (H_2O and type I OH masers) are often associated with pre-stellar activity (Lo et al 1975); the possible association of hot and cool objects makes this a region of considerable interest.

Acknowledgements

References

Allen, C.W., 1973. Astrophysical Quantities, 3rd edition, The Athlone Press London.

Becklin, E.E., Matthews, K., Neugebauer, G., Wynn-Williams, C.G., 1977. Astr.Astrophys., 55, 19.

Evans, N.J., Crutcher, R.M., & Wilson, W.J., 1976. Astrophys.J., 206, 440.

Goss, W.M., Lockhart, I.A., Formalont, E.B. & Hardebeck, E.G., 1973. Astrophys.J., 183, 843.

Greenberg, J.M. & Hong, S.S., 1974. Proc. IAU Symposium No.60, Galactic and Radio Astronomy, ed. F.J. Kerr and S.C. Simonson III (Reidel, Dordrecht and Boston).

Harvey, P.M., Beckis, K.P., Wilson, W.J., Ball, J.A., 1974. Astrophys.J., Suppl., 27, 331.

Johnson, H.L., 1966. A.Rev.Astr.Astrophys., 4, 193.

Johnson, H.L., 1968. Nebulae and Interstellar Matter, ed. B.M. Middlehurst and L.H. Aller, University of Chicago Press, Chicago, p.167.

Lo, K.Y., Burke, B.F. & Haschik, A.D., 1975. Astrophys.J., 202, 81.

Neugebauer, G. & Leighton, R.B., 1969. Two Micron Sky Survey - a Preliminary Catalog (NASA SP-3047).

Schultz, G.V., Kreysa, E. & Sherwood, W.A., 1976. Astr.Astrophys., 50, 171.

Soifer, B.T. & Pipher, J.L., 1975. Astrophys.J., 199, 663.

Wilson, W.J., Schwartz, P.R., Epstein, E.E., Johnson, W.A., ETcheverry, R.D., Mori, T.T., Berry, G.G. & Dyson, H.B., 1974. Astrophys.J., 191, 357.

Winnberg, A., Goss, W.M., Höglund, B., Johansson, L.E.B., 1973, Astrophys.Lett. 13, 125.

Wynn-Williams, C.G., Becklin, E.E. & Neugebauer, G., 1972. Mon.Not.R.Astr.Soc., 160, 1.

References - cont'd.

Wynn-Williams, C.G., Downes, D. & Wilson, T.L., 1971. Astrophys.Lett., 9, 113.

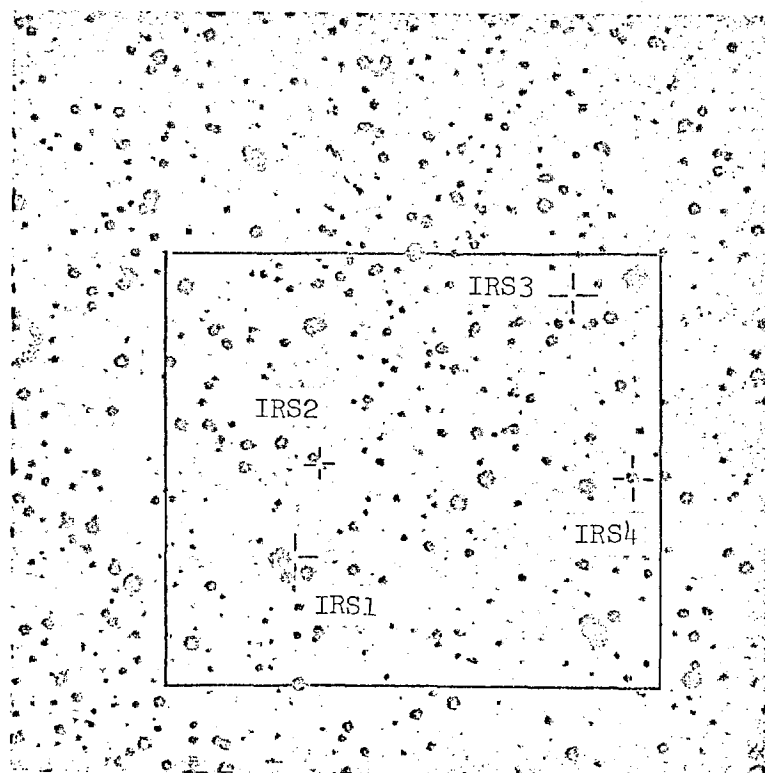Zeilik II, M., Kleinmann, D.E. & Wright, E.L., 1975. Astrophys.J., 199, 401.

PLATE 1

Table 1

SOURCE POSITIONS

	R.A.			DEC		
IRS1	19^h	12^m	$00^s.2$	$+11°$	$04'$	$06''$
IRS2	19	11	57.8	11	05	24
IRS3	19	11	43.6	11	07	45
IRS4	19	11	39.5	11	05	03

1950.0 coordinates. Estimated error $\pm 0^s.3$, $\pm 5''$

Table 2

INFRARED OBSERVATIONS

WAVELENGTH		FILTER BANDPASS	MEASURED MAGNITUDES			
λ (µm)		$\Delta\lambda$ (µm)	IRS1	IRS2	IRS3	IRS4
0.65	R	–	>20	∿18	>20	∿17
1.25	J	0.24	13.9*	10.67	10.98	8.90
1.65	H	0.30	12.3*	9.28	7.90	7.38
2.22	K	0.41	9.86	6.91	6.07	6.84
3.45	L	0.57	7.57	4.10	4.64	6.40
4.95	M	0.8	5.4*	2.68	4.25	6.3 †
10.6	N	5	2.0 †	0.6*	2.7 †	–

Notes to Table 2

1) The 0.65µm magnitudes are estimated from the PSS red plate, with an error of $\pm 1^m$.

2) The errors in the IR magnitudes are $\pm 0^m.05$ in general, except that measurements marked * have an error of $\pm 0^m.2$ and those marked † an error of $\pm 0^m.5$.

3) The quoted magnitude errors include statistical errors and uncertainties in atmospheric extinction.

4) All infrared measurements were made with a 10 arcsec beam.

Figure 1.   The 2.7 GHz map of Wynn-Williams et al (1971) with infrared

and other sources superimposed.

⊙   infrared sources of this paper

⊹   OH sources of Goss et al (1973)

⊢╤�┤   H$_2$O source of Lo et al (1975)

Figure 2.   The energy distributions of the four sources IRS1, IRS2, IRS3

and IRS4 from 0.65 - 10µm. The two R (0.65µm) magnitudes were

estimated from the PSS red plate. The flux measurements reporter

in this paper were made in a 10 arcsec beam, those of ZKW (also

plotted) were made in a 12 arcsec beam. Errors in the infrared

fluxes are about 10%, as a result of uncertainties in absolute

calibration.

Plate 1.   Palomar Sky Survey red plate showing sources IRS1 - IRS4 in the

G45.5+0.1 area. Sources IRS2 and IRS4 are seen to "coincide" with

visible (red) stars - see text. The area covered by Figure 1

is indicated on the plate.

G 45·5+0·1 1950 COORDINATES

08'

07

06

05

OH
45·5+0·0

04

1°03'

04^s

00

56

52

48

44

40^s

19^{h}12^m

19^{h}11^m

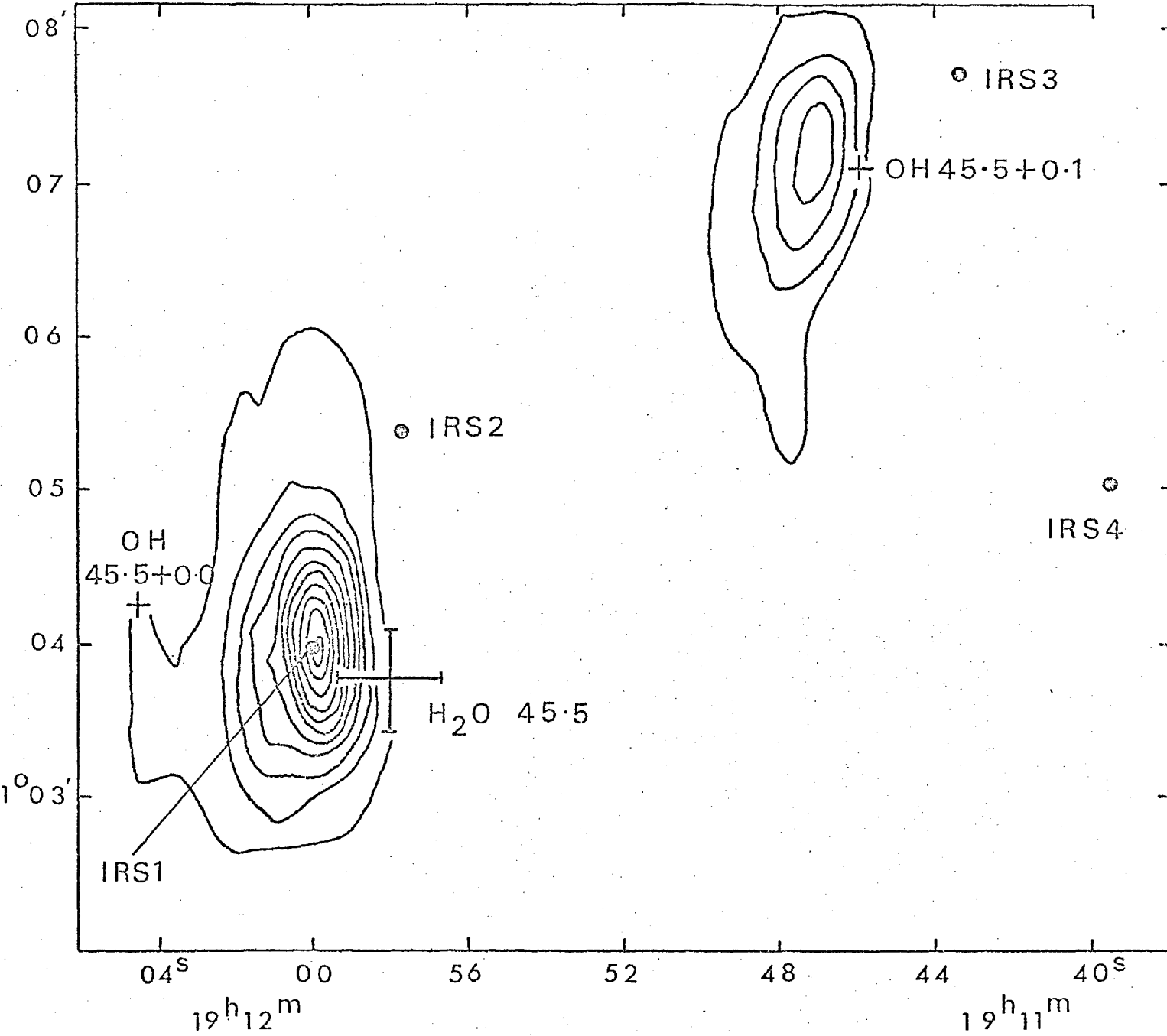IRS3

OH 45·5+0·1

IRS2

IRS4

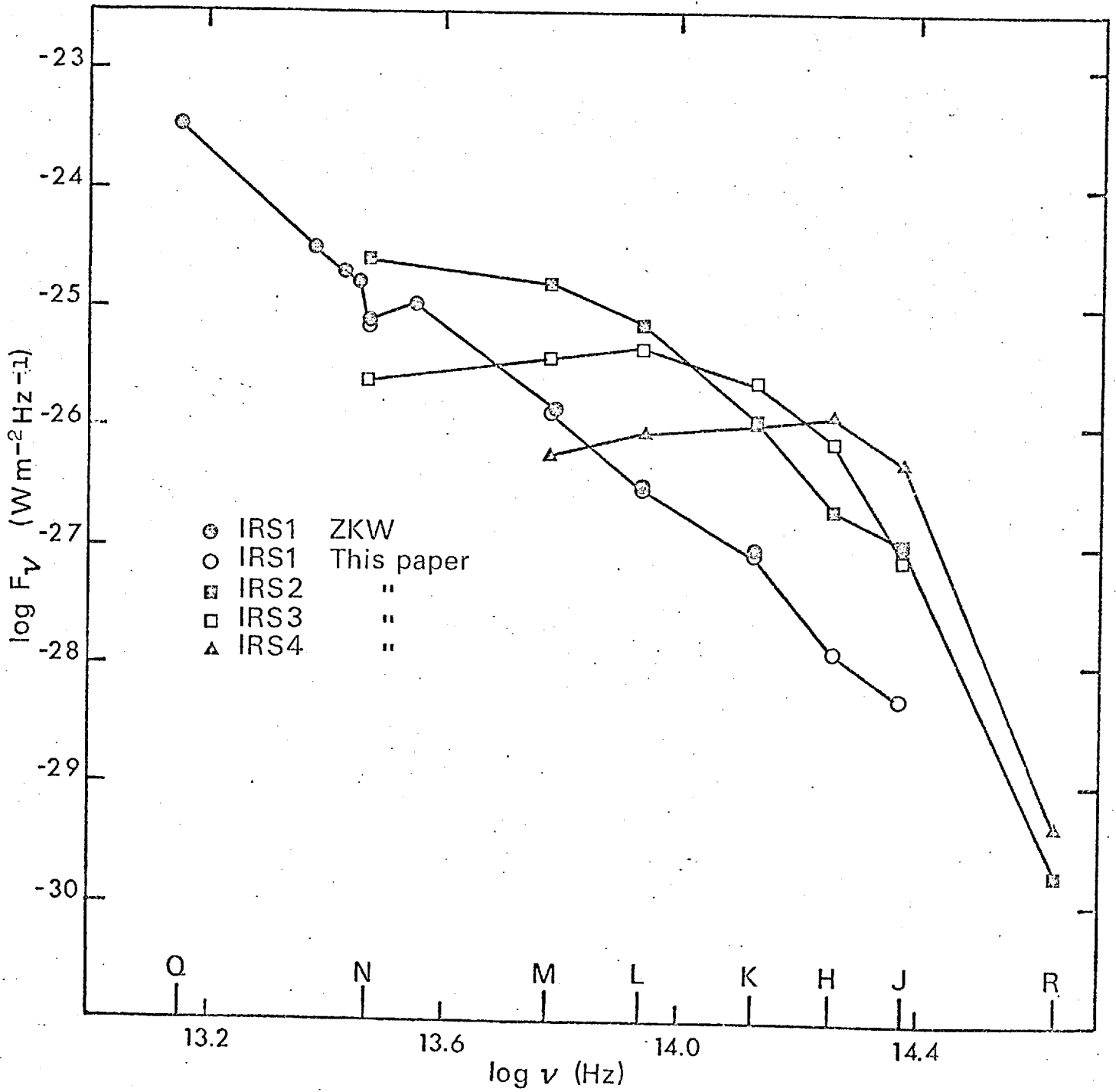H$_2$O 45·5

IRS1

Figure 1

Figure 2

A HELIUM COOLED FABRY–PEROT INTERFEROMETER FOR INFRARED ASTRONOMICAL SPECTROSCOPY

M. J. Selby, P. R. Jorden and A. D. MacGregor

Astronomy Group, Blackett Laboratory, Imperial College, Prince Consort Road,
London, SW7 2BZ

Abstract—We have built a cooled, scanning Fabry-Perot interferometer for astronomical spectroscopy in the ten micron atmospheric window. The reasons for choosing this approach are discussed, and details are given of the construction and performance of the prototype instrument.

1. INTRODUCTION

Infrared astronomical spectroscopy requires spectral resolving power $\mathscr{R}$ ($= \lambda/\delta\lambda$) of 10–10^6 in the 10 and $20\,\mu$m atmospheric windows. Specifically, resolving powers of 10–200 have proved useful for observations of broadband 'silicate' and similar features; higher powers are desirable for observations of line features, and 10^3–10^4 is optimum for measuring total line intensity, while higher resolutions would give line shape. The development of low background photon shot noise limited helium cooled photoconductors for this wavelength region (HgGe, CuGe, AsSi with reported N.E.P.'s of 10^{-15} to a few $\times\ 10^{-17}$W.Hz$^{-1/2}$) gives new scope for spectrometry.

2. BACKGROUND RADIATION AND CHOICE OF SPECTROMETER

2.1 *Background radiation*

In the 8–13 μm window the ground-based atmospheric background is typically taken to average that of a 10% emissivity 280 K black body, giving a background of $\sim 10^{-8}$ W and a photon shot noise of $\sim 1.5.10^{-14}$ W.Hz$^{-1/2}$ $10''$ aperture, F/13, 1.5 m telescope); background varies as $\mathscr{R}^{-1}$ and shot noise as $\mathscr{R}^{-1/2}$. A clean, low emissivity telescope is assumed. The large ($\times 3$) variations in atmospheric emissivity in this window are ignored. At 18–23 μm the atmospheric emissivity is higher. The spectrometer should contribute less background than this onto the detector, an impossible task for an ambient temperature spectrometer. The detector sees a 77 K spectrometer as $1.2.10^{-11}$ W background (5.10^{-16} W.Hz$^{-1/2}$ shot noise) if it sees it through a 4.2 K 8–13 μm filter. Utilising a 4.2 K post-monochromating rotatable circular filter of resolution fifty, the backgrounds at 8, 10, and 13 μm are 2.10^{-16}, 6.10^{-15} and $1.2.10^{-13}$ W and the shot noises are 2.10^{-18}, 1.10^{-17} and 5.10^{-17} W.Hz$^{-1/2}$.

2.2 *Choice of spectrometer*

Dielectric filters (either discrete elements or circular filters) are limited to $\mathscr{R} \simeq 50$–100; future advances may enable the development of high resolution line filters at reasonable prices. We know of no relevant work with prisms. At high resolution ($\gtrsim 10^5$) heterodyne spectrometry will dominate in the foreseeable future, though the theoretical minimum effective temperature of such a system, 1450 K ($= \frac{hv}{k}$) at 10 μm limits its sensitivity for lower resolutions. The choice between Fourier spectrometers (e.g. Michelsons), diffraction gratings and Fabry-Perot interferometers is less clear cut.

For a typical $10''$ ($= \alpha$ sr) aperture on an F/13, 1.5 m ($= Dm$) telescope, optimum echelle grating spectrometers lose out on resolution-luminosity product compared with

317

Michelsons and Fabry–Perots at resolving powers greater than $10^2 d$ ($= 8.10^{-3}$ $d/\alpha D$) (where d mm is the effective grating width $= W \sec\theta_{Blaze}$ where W is actual grating width).[1]

It appears difficult to construct a cooled Michelson with a folded path length much in excess of 10 cm ($\mathcal{R} = 10^4$) and the mechanical and computational problems are not trivial. If N.E.P.'s of 10^{-16} W.Hz$^{-1/2}$ can be achieved, then there is no multiplex advantage at such resolution, except when searching for unknown lines of indeterminate wavelengths. A Fabry–Perot interferometer was therefore constructed, having the advantages of a small axial instrument requiring no ancillary optics, with a resolving power controlled by the plate coating reflection coefficient and the plate spacing. It may also be excited to perform spectral chopping to give improved sensitivity for the detection of small spectral differences, (see section 3.5). Carleton[2] and James and Sternberg[3] have more detailed discussions on the relative merits of various spectrometers.

3. THE INSTRUMENT

3.1 The Fabry–Perot equations

For a full description consult the aforementioned texts or Longhurst.[4] The relevant equations for this discussion are:

The Airy equation:

$$I(\delta) = \frac{I(0)}{1 + 4R \sin^2(\delta/2)/(1 - R)^2} \tag{3.1}$$

where $I(0)$ = incident intensity

$\quad I(\delta)$ = output intensity at δ
$\quad R$ = plate reflection coefficient
$\quad \delta = 2\pi/\lambda \; 2t \cos\theta$ at wavelength λ, plate separation t, exit angle θ.

$$\text{Order } p = \frac{2t}{\lambda} \tag{3.2}$$

$$\text{Free spectral range } \Delta\lambda = \frac{\lambda}{p}$$

$$\text{Resolving power } \mathcal{R} = p \times N_T = \frac{\lambda}{\delta\lambda}.$$

Total finesse $\quad N_T = \dfrac{\Delta\lambda}{\delta\lambda}$

where $\quad \dfrac{1}{N_T^2} = \dfrac{1}{N_R^2} + \dfrac{1}{N_D^2} + \dfrac{1}{N_p^2} + \dfrac{1}{N_A^2}.$

Reflection finesse $\quad N_R = \dfrac{\pi\sqrt{R}}{1 - R}.$

Defect finesse $\quad N_D = \dfrac{x}{2\sqrt{2}}$ for 'plates good to λ/x'.

Parallelism finesse $\quad N_p = \dfrac{y}{\sqrt{3}}$ for 'plates parallel to λ/Y'

Aperture finesse $\quad N_A = \dfrac{8F^2}{p}$ for a beam of focal ratio F at order p.

The telescope beam impinges directly on the plates, so at F/13.5 $p.N_A \simeq 1400 = \mathcal{R}_A$. With collimating optics $\mathcal{R}_A = 1400 d^2$ for a used plate diameter d mm [Roesler[1]]. Plates good to $\lambda/150$ at 0.5 μm are now available, therefore $x = 3000$ at 10 μm and $N_D \gtrsim 1000$.
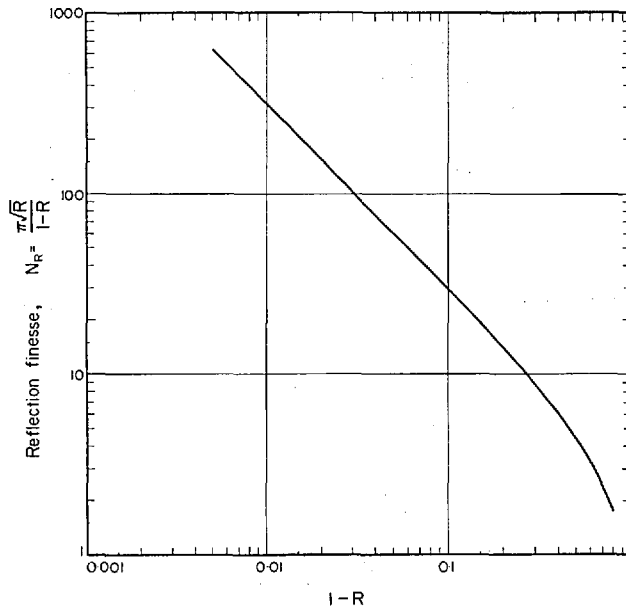
Fig. 1. The variation of reflection finesse, N_R, with the coating reflection coefficient R.

Plate parallelism is a function of mounting sophistication but $y = 150$ has been achieved at 0.5 μm with servoed etalons.[5]

It is possible at 10 μm to have N_R controlling N_T for $N_T \gtrsim 1000$. Figure 1 shows that variation of N_R with R. It is hard to get broadband high R dielectric coatings over the wide range 8–13 μm. R varies with wavelength and phase changes can change $\Delta\lambda$ at constant N_R. Figure 2 shows R, N_R and T/A computed for gold coatings. If such thin uniform gold coatings can be laid, then these are eminently suitable. The same calculations for aluminium give $T/A < 0.01$.

Figure 3 shows loci of the transmission peaks vs t, p, and λ. If N_R approaches 100 ($R \simeq 0.97$) then high resolution is available at low orders with minimal premonochromation.

3.2 Optical and mechanical details

Central spot scanning is achieved in the normal way by scanning one plate. Figure 4 shows the mechanical and optical configuration. The central millimetre of 5 mm dia plates is used. The central 3 mm is dielectric coated ($R \simeq 0.65$). The outer annulus
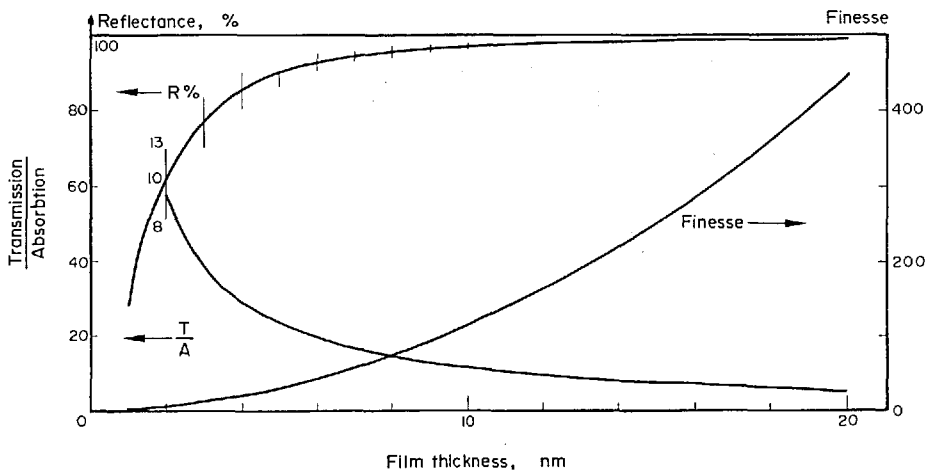

Fig. 2. The computed properties of gold coatings on Barium Fluoride at 10 μm. The bars on some of the R values show the values of R at 8 μm (lower) and 13 μm (upper).
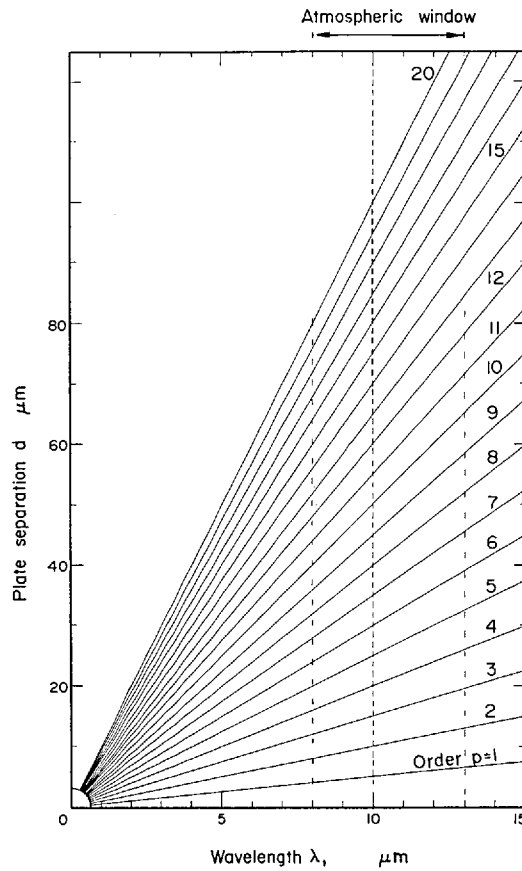
Fig. 3. The transmission peaks of an etalon plotted as a function of order, wavelength and plate separation. The sharpness of the peaks is controlled by the total etalon finesse.

is aluminium coated ($R \simeq 90\%$, $T \simeq 5\%$) enabling lining up in the visible using Mercury light. The first barium flouride plate is 2 mm thick; the second is 2 mm at the edge, with an 8 mm radius of curvature on the second surface, localizing the fringes coincident with the primary mirror and sky images onto an aperture immediately preceding the detector. The aperture diameter $b = f(8/\mathscr{R})^{1/2}$ where f is the second surface focal length.

The moving plate is mounted in a holder on a strip spring carriage which provides the parallel scanning motion. Originally bimorph piezoelectric strips provided both the
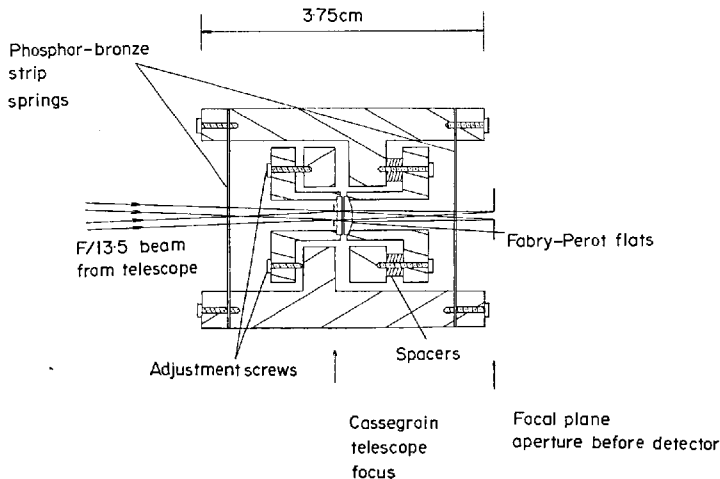

Fig. 4. An axial cross-section of the etalon, showing the mechanical and optical configurations.
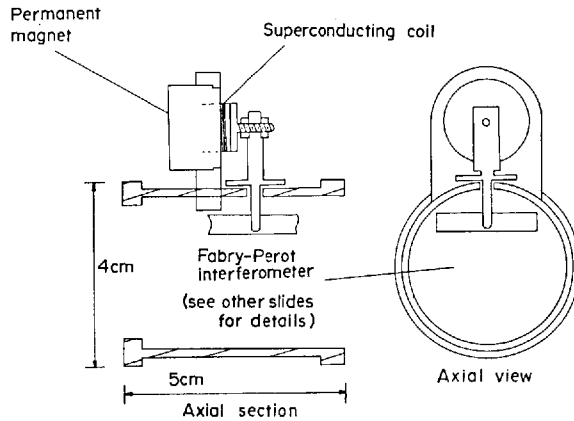
Fig. 5. Two views of the superconducting drive to the moving plate.

four strip elements and the scanning force, but these did not operate well at low temperatures. The present instrument is driven by a superconducting coil, Fig. 5. The phosphor bronze spring element thickness is a compromise between mechanical rigidity and gravitational scanning of the carriage with changing cryostat orientation. The present instrument has an open loop Q of 5 at a resonant frequency of 120 Hz and scans 10 μm from zenith angles 0–60°. A current of ± 300 mA scans the instrument 45 μm (9 orders at 10 μm). The ability to scan a large number of orders at low orders enables one to change the resolution used on any particular object simply by changing order and field stop. Following useful discussions during the conference we are re-investigating piezoelectric drives, though these have limited range.

3.3 Servo electronics

In order to give the positional accuracy necessary for scanning, the moving plate's position is servoed with respect to that of the fixed plate. Fig. 6 shows the electronic configuration employed. The position sensor is one arm of a transformer ratio arm bridge capacitive sensor. The reference capacitor is mounted adjacent to the interferometer. Scanning one order ($\Delta t = 5$ μm) gives a capacitance change $\Delta C \simeq 0.02$ pF where $C \simeq 7$ pF. The equivalent transducer noise level is ± 0.02 μm, – a positional finesse of ~ 250. The bridge concept and circuits are from James and Richards.[6] The four parallel stages of the servo amplifier include: (a) A high gain d.c. amplifier reducing δt due to gravitational scanning by 500; (b) A low pass filter to reduce drifts in plate scanning; (c) A tuned filter (~ 300 Hz) to reduce chopper-induced microphonics by 10; (d) A differentiator to reduce resonant motion by about 20. In accordance with
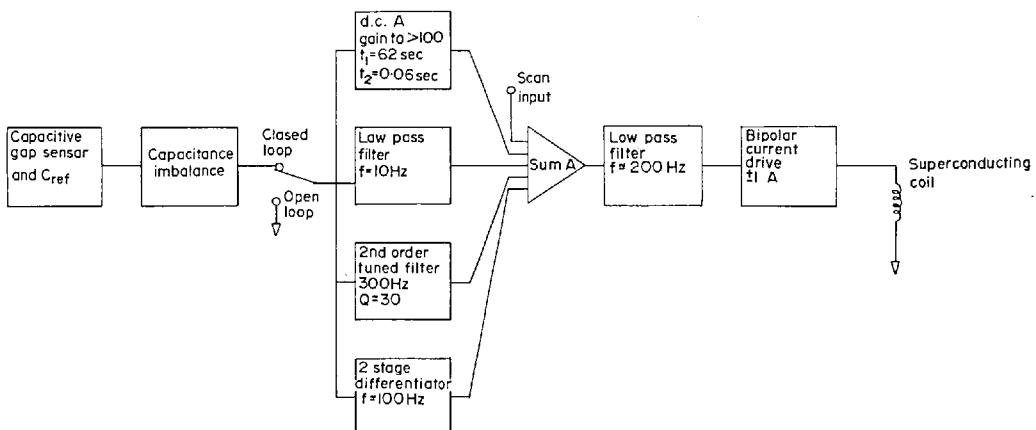

Fig. 6. A block diagram of the plate position servo system electronics.

good servo practise we are modifying the circuits to feed scan offsets into the first stage of the servo.[5]

To further reduce microphonic effects, both on the Fabry–Perot and on the detector, a two mirror focal plane chopper is employed for sky cancellation. The input beam reflects off a 45° mirror oscillating $\pm \theta$, to hit a second 45° mirror at distance c, also oscillating $\pm \theta$ in a coupled manner such that the two mirror planes are always at 90° to one another. The output beam is always at 180° to the input beam and is displaced $c \pm \theta c$ in an oscillating motion. This resonant system gives high displacements and negligible microphonics at frequencies up to 400 Hz.

3.4 Detector

A CuGe element has been employed. In order to preserve detector linearity under the varying background conditions of spectrometry, we use a modified version of the circuit of Wyatt et al.[7] in which the detector works at constant bias into a virtual earth, reducing the effective amplifier input impedance, and thus reducing the microphonic and time constant effects of high impedance circuits. Figure 7 shows the simplified circuit and the version employed. Though we believe we are presently background-limited at very low resolution, we have as yet no reliable figures on the low background performance of this detector—an important factor in the instrumental design.

3.5 Spectral scanning and chopping

Fast or slow spectral scans may be co-added and displayed in real time by the observatory's computer. We are soon interfacing the electronics to enable computer-controlled scanning of the instrument. Spectral chopping will be achieved by exciting the scan to place the transmission peak on and off the line in an oscillating manner. This sensitive technique enables us to minimize the effects of changing atmospheric transmission and emission.

At present the sky signal is subtracted by means of a focal plane chopper and phase sensitive detection at 300 Hz; telescope emission and sky emission gradients are subtracted by 'nodding' the telescope, changing the beam in which the source appears, every 30 sec; all this is conventional technique. If the Fabry–Perot performs a spectral chop at an intermediate frequency (say 7 Hz) then it may be shown that phase sensitive detection of the spectral chop gives a spectral difference which changes sign with the nod, and a similar signal, related to total source intensity averaged over the chop range, may be extracted at the sky chop frequency.

3.6 Operation and conclusions

The cooled spectrometer has been laboratory-tested and Fig. 8 shows the result of scanning the instrument with monochromatic radiation; $R \simeq 40$ is observed in eighth
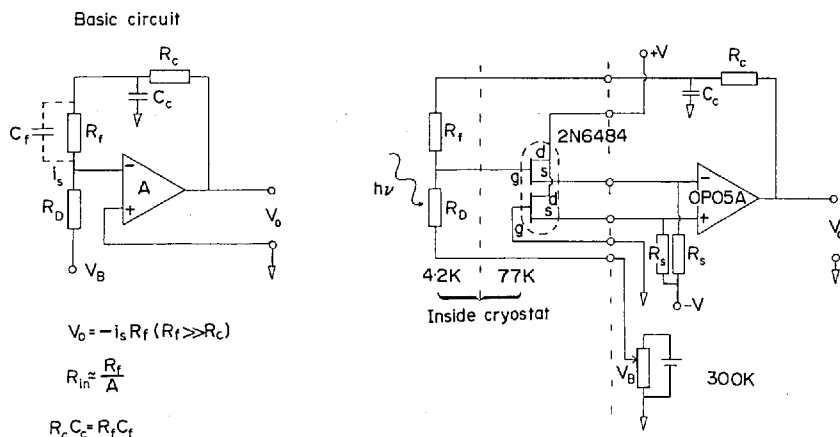

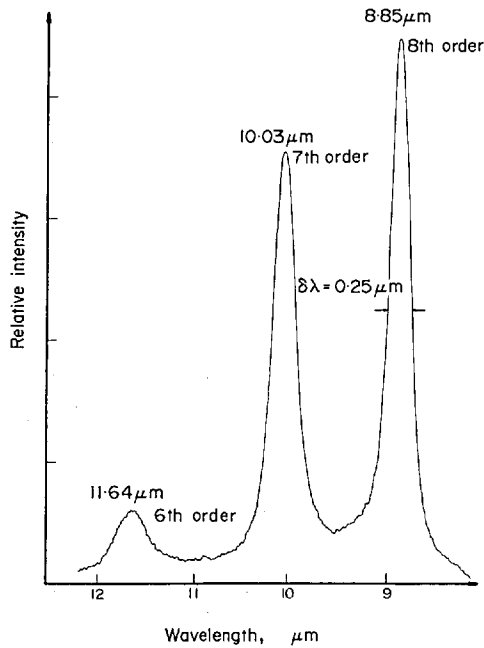Fig. 7. The cooled, current-mode, frequency compensated preamplifier used with the CuGe detectors.

Fig. 8. The 4.2 K etalon transmission at a fixed plate spacing as a function of wavelength.
The monochromator band width was 0.1 μm.

order, commensurate with the plate reflectivity. The etalon transmission is $\simeq 25\%$. Unfortunately no astronomical tests are presented here, due to cryostat damage in transmit to the observatory.

We feel the instrument to be presently limited by the plate coatings and poor plates; a resolving power of 200 seems likely when these are improved. A second instrument has been designed and resolving powers in excess of one thousand are anticipated.

REFERENCES

1. ROESLER, F. L., *Methods of Experimental Physics.* Vol. 12, Part A, Chapter 12. Academic Press, New York and London (1974).
2. CARLETON, N. Editor, *Methods of Experimental Physics.* Chapters 10–12. Academic Press, New York and London (1974).
3. JAMES, J. F. & R. S. STERNBERG, *The Design of Optical Spectrometers.* Chapman and Hall, London (1969).
4. LONGHURST, R. S. *Geometrical and Physical Optics.* Chapter 9, 2nd Edition. Longmans, London (1967).
5. HICKS, T. R., N. K. REAY & R. J. SCADDAN, *J. Phys. E* **7**, 27 (1974).
6. JONES, R. V. & J. C. S. RICHARDS, *J. Phys. E* **6**, 589 (1973).
7. WYATT, C. L., D. J. BAKER & D. G. FRODSHAM, *Infrared Phys.* **14**, 165 (1974).

```
2000 REM                                    SOURCE DETECTION IN SINGLE SCANS
2010 REM
2020 REM                           ************
2030 REM                                 ONCE-ONLY INITIALISE
2040 REM                        I.R.  STATION NO.
2050 LET N1=6
2060 REM                        P.C.  STATION NO.
2070 LET N2=7
2080 REM                        A/D  STATION NO.
2090 LET N3=4
2100 REM                        P.D.  STATION NO.
2110 LET N4=5
2120 DIM R(1,160),P(31)
2130 LET O=0
2140 LET P1=0
2150 LET S1=0
2160 LET S2=1
2170 LET F1=0
2180 DATA 0
2190 REM                                INITIALISE MODULES
2200 CALL 1,0
2210 CALL 1,3
2220 CALL 2,N1,0,26
2230 CALL 2,N3,0,26
2240 REM
2250 REM                           ************
2260 REM                                 INPUT THE PARAMETERS
2270 ;
2280 ;"ENTER NO. OF PTS"
2290 INPUT N
2300 ;
2310 REM                          ***** 'NEW PROFILE' COMES HERE *****
2320 ;"ENTER NO. FOR PROFILE"
2330 INPUT Z2
2340 ;
2350 REM                    -VE ENTERED USES VALUES IN ARRAY
2360 IF Z2<0 GOTO 2590
2370 REM              0 ENTERED PUTS VALUES IN DATA STATEMENT INTO ARRAY
2380 IF Z2=0 GOTO 2470
2390 REM           +VE ENTERED READS THAT MANY VALUES FROM TTY INTO ARRAY
2400 GOSUB 4270
2410 LET P1=Z2
2420 FOR Z1=1 TO P1
2430 INPUT P(Z1)
2440 NEXT Z1
2450 GOTO 2620
2460 REM
2470 RESTORE
2480 READ Z2
2490 IF Z2>0 GOTO 2520
2500 ;"NO PROFILE IN DATA STATEMENT"
2510 GOTO 2320
2520 GOSUB 4270
2530 LET P1=Z2
2540 FOR Z1=1 TO P1
2550 READ P(Z1)
2560 NEXT Z1
2570 GOTO 2620
2580 REM
```

```
2590 IF P1>0 GOTO 2620
2600 ;"NO PROFILE IN ARRAY"
2610 GOTO 2320
2620 REM                          CHECK PROFILE MEAN IS 0
2630 LET Z2=0
2640 FOR Z1=1 TO P1
2650 LET Z2=Z2+P(Z1)
2660 NEXT Z1
2670 IF Z2=0 GOTO 2690
2680 ;"PROFILE TOTAL IS ";Z2;", SHOULD BE 0"
2690 ;"PRESS CONT WHEN READY"
2700 REM                          WAIT FOR 'CONTINUE' BEFORE FIRST SCAN
2710 CALL 4,N1,0,0,D
2720 IF D<>4 GOTO 2710
2730 LET F2=0
2740 REM
2750 REM                                *********
2760 REM                                PRE-SAMPLING INITIALISE
2770 REM                          ***** 'CONTINUE' COMES HERE *****
2780 REM                          ***** 'ADD NEXT' COMES HERE *****
2790 CALL 2,N1,0,9
2800 REM                                SET UP SCAN ARRAY FOR DISPLAY
2810 FOR Z1=1 TO N
2820 LET R(S1,Z1)=0
2830 NEXT Z1
2840 IF F1=0 GOTO 2910
2850 REM                          PUNCH PARAMETERS FOR PREVIOUS SCAN
2860 CALL 200,O
2870 LET F2=F2+1
2880 CALL 200,F2
2890 LET F2=F2-1
2900 CALL 200,N
2910 LET O=O+1
2920 ;
2930 ;"SCAN ";O
2940 CALL 3,N2,2,17,2
2950 LET Z2=1
2960 REM
2970 REM                                *********
2980 REM                                DATA SAMPLING LOOP
2990 CALL 100,R(S1,1),N,0
3000 CALL 2,N3,0,8
3010 CALL 5,0,X
3020 IF O=0 GOTO 2990
3030 CALL 4,N3,0,0,R(S1,Z2)
3040 IF O=1 GOTO 3130
3050 REM                 DE-SCALE PREVIOUS SCAN
3060 LET M3=(R(S2,Z2)-785)*M4/235+M5
3070 IF F1=0 GOTO 3100
3080 REM                 PUNCH PREVIOUS SCAN
3090 CALL 200,M3
3100 IF F2=0 GOTO 3130
3110 REM                 ADD IN PREVIOUS SCAN
3120 LET R(S1,Z2)=(R(S1,Z2)+M3*F2)/(F2+1)
3130 LET Z2=Z2+1
3140 FOR Z1=0 TO 80
3150 NEXT Z1
3160 CALL 2,N3,0,10
```

```
3170 IF Z2<=N GOTO 2990
3180 IF P1=0 GOTO 3200
3190 GOSUB 4380
3200 REM
3210 REM                                      **********
3220 REM                               .      END OF SET CALCULATIONS
3230 CALL 3,N2,2,17,1
3240 ; ""
3250 LET M5=0
3260 FOR Z1=1 TO N
3270 REM                        ZEROISE CONVOLVED ARRAY
3280 LET R(S2,Z1)=0
3290 REM                        TOTAL SCAN VALUES INTO M5
3300 LET M5=M5+R(S1,Z1)
3310 NEXT Z1
3320 REM                        M5 BECOMES MEAN
3330 LET M5=M5/N
3340 LET M4=0
3350 REM                        ADJUST SCAN VALUES TO 0 MEAN
3360 FOR Z1=1 TO N
3370 LET R(S1,Z1)=R(S1,Z1)-M5
3380 REM                  PUT MAX. SCAN VALUE IN M4 FOR DISPLAY SCALING
3390 IF M4>=ABS(R(S1,Z1)) GOTO 3410
3400 LET M4=ABS(R(S1,Z1))
3410 NEXT Z1
3420 REM                        P2 IS MIDDLE POSITION IN PROFILE ARRAY P
3430 LET P2=INT(P1/2)+1
3440 LET M1=0
3450 LET M2=0
3460 LET M3=0
3470 REM        Z1 IS FIRST POINT OF EACH MAPPING OF PROFILE ONTO SCAN
3480 FOR Z1=0 TO N-P1
3490 LET M=0
3500 REM                        Z2 IS EACH POINT OF PROFILE
3510 FOR Z2=1 TO P1
3520 LET M=M+P(Z2)*R(S1,Z1+Z2)
3530 NEXT Z2
3540 REM              M IS SUM OF PROFILE*SCAN, STORED IN CONVOLVED ARRAY
3550 LET R(S2,Z1+P2)=M
3560 REM                        SUMS FOR S.D. AND SIGNAL DETECTION
3570 LET M1=M1+M
3580 LET M2=M2+M*M
3590 NEXT Z1
3600 LET M=N-P1+1
3610 LET S=SQR((M2-(M1*M1/M))/(M-1))
3620 REM                        M1 BECOMES MEAN OF CONVOLVED ARRAY
3630 LET M1=M1/M
3640 REM                                S = STANDARD DEVIATION
3650 REM                                M = NO. OF S.D.S FOR SIGNAL
3660 LET M=3*S
3670 REM
3680 REM                        TEST FOR SIGNAL
3690 FOR Z1=P2 TO N-P2+1
3700 REM              ADJUST CONVOLVED VALUES TO 0 MEAN
3710 LET R(S2,Z1)=R(S2,Z1)-M1
3720 REM          PUT MAX. CONVOLVED VALUE IN M3 FOR DISPLAY SCALING
3730 IF M3>=ABS(R(S2,Z1)) GOTO 3750
3740 LET M3=ABS(R(S2,Z1))
3750 IF R(S2,Z1)<M GOTO 3770
```

```
3760 ;"SIGNAL AT POINT ";Z1;" OF ";(R(S2,Z1)-M1)/S;" S.D.S"
3770 NEXT Z1.
3780 REM                        SCALE TO FILL EACH HALF OF DISPLAY
3790 FOR Z1=1 TO N
3800 LET R(S1,Z1)=R(S1,Z1)*235/M4+785
3810 LET R(S2,Z1)=R(S2,Z1)*235/M3+235
3820 NEXT Z1
3830 REM                        SWOP ARRAYS
3840 LET M3=S1.
3850 LET S1=S2
3860 LET S2=M3
3870 LET F1=0
3880 CALL 2,N1,0,9
3890 REM
3900 REM                                **********
3910 REM                                DISPLAY AND TEST BUTTONS LOOP
3920 CALL 4,N1,0,0,D
3930 CALL 100,R(S1,1),N,0
3940 CALL 100,R(S2,1),N,0
3950 REM                                TEST 'STOP'
3960 IF D=64 GOTO 4150
3970 REM                                TEST 'NEW PROFILE'
3980 IF D=16 GOTO 2320
3990 REM                                TEST 'ADD NEXT'
4000 IF D<>8 GOTO 4050
4010 LET F2=F2+1
4020 ;"SCAN ADD"
4030 GOTO 2790
4040 REM                                TEST 'CONTINUE'
4050 IF D<>4 GOTO 4090
4060 LET F2=0
4070 GOTO 2790
4080 REM                                TEST 'PUNCH'
4090 IF D<>1 GOTO 3920
4100 LET F1=1
4110 ;"PUNCHED"
4120 GOTO 3920
4130 REM
4140 REM                        ****** 'STOP' COMES HERE ******
4150 IF F1=0 GOTO 4260
4160 ;"PUNCHING FINAL SCAN"
4170 CALL 200,0
4180 LET F2=F2+1
4190 CALL 200,F2
4200 CALL 200,N
4210 FOR Z1=1 TO N
4220 LET Z2=(R(S2,Z1)-785)*M4/235+M5
4230 CALL 200,Z2
4240 NEXT Z1
4250 GOSUB 4380
4260 GOTO 2140
4270 REM                                SUBR VALIDATES NO. PROFILE PTS
4280 REM                                CHECK NO. IS < 32
4290 IF Z2<32 GOTO 4340
4300 ;"MUST BE < 32"
4310 GOTO 2320
4320 REM                        CHECK NO. IS ODD
4330 REM              0.1 IS ADDED TO COMBAT POSSIBLE ROUNDING ERROR
4340 IF INT(Z2/2+.1)*2<>Z2 GOTO 4370
```

```
4350 ; "MUST BE ODD"
4360 GOTO 2320
4370 RETURN
4380 REM              SUBR TO PUNCH BLANK TAPE
4390 REM                   AND POWER DOWN
4400 LET D=0
4410 FOR Z1=1 TO 20
4420 CALL 2,N4,0,8
4430 CALL 5,0,X
4440 IF Q=1 GOTO 4550
4450 CALL 2,N4,2,27
4460 CALL 5,0,X
4470 IF Q=0 GOTO 4420
4480 CALL 2,N4,0,24
4490 CALL 2,N4,0,26
4500 FOR Z2=1 TO 30
4510 NEXT Z2
4520 CALL 2,N4,0,8
4530 CALL 5,0,X
4540 IF Q=0 GOTO 4480
4550 CALL 3,N4,0,16,D
4560 NEXT Z1
4570 CALL 2,N4,0,24
4580 RETURN
4590 END
```